STUDIES ON THE PROGRESSIVE MATURATION OF THYMIC EPITHELIAL PROGENITORS

by

SONG BAIK

A thesis submitted to the University of Birmingham

For the degree of DOCTOR OF PHILOSOPHY

Department of Anatomy
School of Immunity and Infection
College of Medical and Dental Science
University of Birmingham

April 2014

UNIVERSITY OF
BIRMINGHAM

University of Birmingham Research Archive

e-theses repository

This unpublished thesis/dissertation is copyright of the author and/or third parties. The intellectual property rights of the author or third parties in respect of this work are as defined by The Copyright Designs and Patents Act 1988 or as modified by any successor legislation.

Any use made of information contained in this thesis/dissertation must be in accordance with that legislation and must be properly acknowledged. Further distribution or reproduction in any format is prohibited without the permission of the copyright holder.

ABSTRACT

The thymus is essential for T-cell development and is histologically divided into two specialized microenvironments: cortex and medulla. The cortex selects functional T cells and the medulla removes potentially auto-reactive T cells. Both selection events are mainly driven by thymic epithelial cells (TECs). However, ageing causes a loss of TECs, consequently resulting in a reduction of thymic function. Several studies have sought to reconstitute thymus function by regenerating TECs, with limited success.

We aim to generate thymic tissues from defined sources that may ultimately be transplanted to improve immune function. Moreover, this study seeks to identify TEC progenitors and define distinct TEC developmental pathways, which will ultimately be helpful in understanding both thymic atrophy and thymic regeneration.

We show that induced pluripotent stem (iPS) cells can generate functional TECs in vivo. Moreover, our data suggest a serial link between cTEC and mTEC lineage development. Specifically, we find that $Aire^{+}$ mTEC can develop from progenitors expressing the cTEC marker CD205, and $CD205^{+}$ progenitors acquire the expression of mTEC regulator Receptor Activator of NF-κB (RANK) before losing their cTEC phenotype. Collectively, our data help clarify potential cellular targets for the re-establishment of functional thymus tissue.

ACKNOWLEDGEMENT

I would firstly like to thank God for giving me this wonderful opportunity. I would also like to thank Professor Graham Anderson and for his support and guidance. I feel really privileged to be his PhD student and I have learned a lot from him. I couldn't finish my PhD without his support.

I would like to thank my second supervisor, Dr William Jenkinson, for his insight and input. I would like to acknowledge everyone in Anderson Lab past and present: Sonia Parnell, Andrea White, Kyoko Nakamura, Guiliaume Desanti, Amanda Holland, Jennifer Cowan, Nick McCarthy, and Kieran James.

Special thanks to everyone on the 4th Floor of IBR for all the cakes and support!
Thank you Jenny for EVERYTHING! I would also like to acknowledge Saeeda Bobat and Pete Hart for their kindness and friendship!

Finally, I would like to thank my parents and brother who were there for all the ups and downs during my PhD. I can't thank you all enough for praying for me! Love you!

TABLE OF CONTENTS

CHAPTER 1. GENERAL INTRODUCTION 10
1.1. OVERVIEW OF IMMUNE SYSTEM 11
1.1.1. Immune System 11
1.1.2. Adaptive Immune Response 12
1.1.3. T Lymphocytes 14
1.1.3.1. $CD4^+$ Helper T cells 15
1.1.3.2. $CD8^+$ Cytotoxic T Cells 16
1.1.3.3. Structure Of The T Cell Receptor And CD3 Complex 17
1.1.3.4. TCR And CD3 Signaling 18
1.1.3.5. Microenvironments For T-cell Mediated Immune Response 22
1.2. T-CELL DEVELOPMENT 24
1.2.1. Structure And Function Of Thymus 24
1.2.2. Thymus Colonization By T-cell Progenitors 24
1.2.3. Early T-cell Development In The Cortex 26
1.2.3.1. T-Cell Lineage Commitment 26
1.2.3.2. Early Intra-thymic T-cell Development 27
1.2.3.3. Thymocyte Migration In Early Stages Of T-cell Development 30
1.2.4. Positive Selection And Central Tolerance Induction 34
1.2.4.1. Positive Selection 34
1.2.4.2. Negative Selection 37
1.2.5. Emigration To Periphery 40
1.2.6. Non-conventional T Lineage Development In Thymus 40
1.3. DEVELOPMENT OF THE THYMUS 42
1.3.1. Thymus Organogenesis 42
1.3.1.1. Origin Of The Thymus 42
1.3.1.2. Molecular Regulation In Thymus Organogenesis 45
1.3.1.3. Cellular Regulation In Thymus Organogenesis 47
1.3.2. TEC Development 51
1.3.2.1. Identification Of TEC Progenitors 51
1.3.2.2. cTEC Development And Their Role In Positive Selection 53
1.3.2.3. Development Of mTEC And Their Role In Central Tolerance 56
1.3.3. Thymic Atrophy 61
1.3.3.1. Ageing And Thymic Atrophy 61
1.3.3.2. Harnessing TEC Progenitors For Thymus Regeneration 63

CHAPTER 2. GENERAL METHODS AND MATERIALS 66
2.1. MICE 67
2.2. MEDIUM AND ADDITIVES 69
2.3. TISSUE ISOLATION AND SINGLE CELL SUSPENSION ISOLATION 70
2.3.1. Tissue Isolation 70
2.3.2. Isolation Of Thymocytes Or Peripheral T-Cells 70
2.3.3. Isolation Of Thymic Stromal Cells 70
2.3.3.1. Isolation Of Embryonic Thymic Stromal Cells 70
2.3.3.2. Isolation Of Adult Thymic Stromal Cells 71
2.3.4. Bead Coating And Immunomagnetic Separation Techniques 72
2.3.4.1. Immunomagnetic Separation Of Embryonic Stromal Cells 72
2.4. IMMUNOLABELING AND FLOW CYTOMETRY 72

2.4.1. Immunolabeling For Flow Cytometric Analysis 72
2.4.2. Intracellular Immunolabeling For Flow Cytometric Analysis 73
2.4.3. Flow Cytometric Analysis 74
2.5. FETAL THYMIC ORGAN CULTURE (FTOC) AND 2-DEOXYGUANOSINE TREATED FTOC 77
2.6. FETAL THYMIC ORGAN CULTURE (FTOC) FOR RANK STIMULATION 77
2.7. HIGH SPEED SORTING AND REAGGREGATE THYMIC ORGAN CULTURE (RTOC) 78
2.7.1. Preparation Of Cells For High Speed Sorting 78
2.7.2. RTOC And Ectopic Tissue Transplantation 78
2.8. IMMUNOHISTOLOGY TECHNIQUES 79
2.9. PREPARATION OF SAMPLES FOR GENE EXPRESSION ANALYSIS 82
2.9.1. Snap Freezing Of Cell Populations 82
2.9.2. mRNA Extraction 82
2.9.3. Quantitative RT-PCR 83
2.10. ANALYSIS OF Vγ5$^+$ DETCS IN EAR 86
2.10.1. Immunolabeling And Flow Cytometry 86
2.10.2. Immunohistology Techniques 86
2.11. STATISTICAL ANALYSIS 86
2.12. GENERATION OF IPS CHIMERA 87

CHAPTER 3. DEFINING TEC PROGENITORS AND TOWARDS RESTORING THYMIC FUNCTION 88
3.1. INTRODUCTION 89
3.2. RESULTS 90
3.2.1. Defining TEC Progenitors 90
3.2.1.1. Analysis Of Embryonic TEC Development In Wild Type Mice 90
3.2.1.2. Mechanical Separation Of Thymus And Parathyroid (Wild Type) 99
3.2.1.3. Phenotypical Analysis Of Parathyroid Epithelial Cells In FoxN1 Deficient Mice 105
3.2.1.4. Use Of FoxN1:eGFP Transgenic Mice To Analyze TEC Development In Early Embryo 108
3.2.1.5. Phenotypical Analysis Of TECs And Parathyroid Epithelial Cells Using FoxN1:eGFP Transgenic Mice 111
3.2.1.6. Phenotypical Analysis Of TEC Progenitors Using FoxN1:eGFP Transgenic Mice 119
3.2.2. Restoring Thymic Function 136
3.2.2.1. Capability Of iPS Cells To Generate Thymic Epithelium In Vivo 136
3.2.2.2. T-Cell Development In Thymus Of iPS Chimera Mice 148
3.2.2.3. Functionality Of T cells Produced By iPS Chimeric Thymus 158
3.3. DISCUSSION 163
3.3.1. Phenotype Of TEC Progenitors 163
3.3.2. Capability Of iPS Cells To Generate Thymic Epithelium 167

CHAPTER 4. LINEAGE DEVELOPMENT OF CTEC AND MTEC 170
4.1. INTRODUCTION 171
4.2. RESULTS 172
4.2.1. Investigating The Capability Of CD205$^+$ TECs To Develop Into cTECs and mTECs 172

4.2.1.1. Ontogenetic Analysis of cTEC and mTEC Using FoxN1:eGFP Transgenic Mice 172
4.2.1.2. Induction Of Maturation Within $CD205^+$ TEC By The mTEC Regulator RANK 175
4.2.1.3. Potential Of $CD205^+$ TEC Progenitors To Differentiate Into mTEC Including $Aire^+$ Subset 183
4.2.1.4. Signals Important In $CD40^{High}CD205^-$ TEC Development..... 193
4.2.2. Role Of Wnt5a In TEC Development..... 200
4.2.2.1. Wnt5a Expression Within Embryonic Thymus Of Wild Type Mice 200
4.2.2.2. TEC Development In Wnt5a KO Mice 208
4.2.2.3. T-Cell Development In Wnt5a KO Mice..... 216
4.3. DISCUSSION 221
4.3.1. Serial Development Of cTEC And mTEC..... 221
4.3.2. Role Of Wnt5a In TEC Development..... 225
CHAPTER 5. GENERAL DISCUSSION 227
5.1. BACKGROUND AND OVERALL AIMS OF STUDY 228
5.2. SUMMARY OF TEC DEVELOPMENT 229
5.2.1. Identification of TEC Progenitors..... 229
5.2.2. Serial Model OF TEC Development..... 231
5.3. THYMUS REGENERATION 235
5.4. CONCLUDING REMARKS AND FUTURE WORKS 238
CHAPTER 6. REFERENCE 243

ABBREVIATIONS

-/-	deficient
AFE	anterior foregut endoderm
Aire	autoimmune regulator
AP-1	activator protein-1
APC	antigen presenting cell
BCR	B cell receptor
CCL	CC chemokine ligand
CCR	CC chemokine receptor
CD	cluster of differentiation
CDR	complementary determining region
cDNA	complementary DNA
Cld	claudin
CMJ	cortico- medullary junction
cTEC	cortical thymic epithelial cell
CTL	cytotoxic T lymphocyte
CTLA4	cytotoxic T lymphocyte antigen 4
CXCL	CXC chemokine ligand
CXCR	CXC chemokine receptor
DAG	diacylglycerol
DAPI	4,6-diamidino-2-phenylindole
DC	dendritic cells
DE	definitive endoderm
DL	delta like
DMEM	Dulbecco's Modified Eagle's Medium
DN	double negative
DNA	deoxyribonucleic acid
DP	double positive
EpCAM	epithelial cell adhesion molecule
ES	embryonic stem
FACS	fluorescence activated cell sorting
FCS	fetal calf serum
FGF	fibroblast growth factor
FGFR	fibroblast growth factor receptor
FoxG1	forkhead box G1
FoxN1	forkhead box N1
FoxP3	forkhead box P3
FRC	fibroblastic reticular cell
Fz2	Frizzled 2
Fz3	Frizzled 3
Fz7	Frizzled 7
Fz8	Frizzled 8
FTOC	fetal thymus organ culture
Gcm2	glial cell missing homolog 2
GFP	green fluorescent protein
GP38	glycoprotein 38
HEV	high endothelial venule

Hoxa3	homeobox A3
HSA	heat stable antigen
hESC	human embryonic stem cell
ICAM-1	intercellular adhesion molecule-1
IFN-	interferon
IL	interleukin
iNKT	invariant natural killer T cell
Int	intermediate
IP_3	inositol-triphosphate
iPSC	induced pluripotent stem cell
Isl1	islet 1
ITAM	immunoreceptor tyrosin based activation motif
K	keratin
KLF-2	kruppel-like factor 2
KO	knock out
LAT	linker for activation of T cells
LPS	lipopolysaccharide
LT	lymphotoxin
LTβR	lymphotoxin β receptor
LTi	lymphoid tissues inducer cell
MHC	major histocompatibility complex
mRNA	messenger RNA
mTEC	medullary thymic epithelial cell
NC	neural crest
NF-κB	nuclear factor kappa B
NFAT	nuclear factor of activated T cell
NK	natural killer
n.s.	not significant
PAMP	pathogen associated molecular pattern
Pax1	paired box 1
PBS	phosphate suffer saline
PCR	polymerase chain reaction
PD-1	programmed death 1
PDGFRα	platelet derived growth factor receptor alpha
PD-L1	programmed death ligand 1
PD-L2	programmed death ligand 2
PIP_2	phosphatidylinositol biphosphate
PLCγ1	phospholipase Cγ1
pMHC	peptide-MHC
pre-Tα	pre TCR alpha chain
pre-TCR	pre TCR complex
PRR	pattern recognition receptor
PSGL-1	P-selectin glycoprotein ligand 1
RAG	recombinase activating gene
RANK	receptor activator NF-κB
RANKL	Rank ligand
RF-10H	RPMI-1640 Hepes
RNA	ribonucleic acid

Ror2	receptor tyrosine kinase-like orphan receptor 2
RORγ	retinoic acid receptor-related orphan receptor gamma
RSS	recombination signal sequence
RT	reverse transcription
RTOC	reaggregate thymus organ culture
Ryk	receptor-like tyrosine kinase
Sca-1	stem cell antigen 1
SCF	stem cell factor
SCZ	subcapsular zone
Shh	sonic hedgehog
SLP-76	SH2 domain containing leukocyte protein of 76kDa
SP	single positive
S1P1	sphingosine-1-phosphate receptor-1
TCR	T cell receptor
Tbx1	T box 1
TdT	terminal deoxynucleotidyl transferase
TEC	thymic epithelia cell
TGFβ	transforming growth factor beta
Th1	T helper 1
Th2	T helper 2
Th17	T helper 17
TNF	tumor necrosis factor
TNFRSF	tumor necrosis factor receptor superfamily
TRA	tissues restricted antigens
TRAF6	TNF receptor associated factor 6
Treg	T regulatory
TSSP	thymus specific serine protease
UEA-1	ulex europaeus agglutitin 1
VCAM-1	vascular cell adhesion molecule 1
Wnt	wingless-int
WT	wild type
YFP	yellow fluorescent protein
ZAP-70	zata chain associated protein kinase 70

CHAPTER 1. GENERAL INTRODUCTION

1.1. Overview Of Immune System

1.1.1. Immune System

The immune system is a defense mechanism composed of cells and molecules to protect an organism from foreign pathogens. There are two different immune responses based on speed, specificity, and memory: the innate immune response and the adaptive immune response (Delves and Roitt, 2000a). The innate or 'natural' immune response is rapid, but not specific to a foreign pathogen and lacks immunological memory. On the contrary, the adaptive or 'acquired' immune response involves T and B lymphocytes expressing the antigen specific receptors. While immune responses are slowly developing during the first infection, memory T and B lymphocytes generated during initial infection are able to initiate more prompt and stronger protection during subsequent exposures to the same pathogen (Basset et al., 2003). T-cells can be subdivided into distinct forms based on the types of T-cell receptors (TCR) they express (αβT-cells and γδT-cells). Given that this thesis focuses on events occurring within the thymus, the primary site for αβ T-cell development, the $\alpha\beta TCR^{+}$ subset of T-cells is the focus of this introduction.

Prior to initiating the innate and adaptive immune responses, there is the mechanical defense mechanism along body surfaces to prevent microbes from infiltrating into body. The surfaces of the respiratory, gastrointestinal and urogenital tracts are the sites where the first defense against infection can occur. Epithelial cells secret mucus to prevent the attachment of pathogens to body surfaces or create an environment that is not suitable for the growth of microorganisms, like very acidic condition in stomach (Basset et al., 2003). When the pathogens successfully overcome these physiologic and anatomic barriers, the innate and adaptive immune responses are triggered (Turvey and Broide, 2010).

The innate immune response uses both cellular and molecular components. The main cellular components of the innate immune system include neutrophils, macrophages, dendritic cells (DCs), and natural killer cells (NKs). Phagocytic cells such as macrophages and neutrophils recognize non-self microbes via pattern recognition receptors (PRRs) (Basset et al., 2003). PRRs bind to pathogen-associated molecular patterns (PAMPs), which are the highly conserved structural molecules among various microbes. Ligation of PRRs with PAMPs expressed on pathogens leads to the activation of resident phagocytes resulting in the phagocytosis, and the secretion of molecules that include inflammatory chemokines and cytokines (Medzhitov and Janeway, 1997). These molecules function to recruit and activate antigen-presenting cells (APCs), including macrophages and DCs, that link between innate and adaptive immune responses as well as enhancing inflammatory responses. Moreover, the naïve lymphocytes of adaptive immune responses are plastic, and the cytokines produced during innate immune response give directions to the naïve lymphocytes, deciding which type of effector cells they will differentiate into. For example, macrophages produce IL-10 and IL-12 to help T-cell differentiation, and NK cells release IL-4 and IFN-γ for both T and B cell differentiation (Bonilla and Oettgen, 2010; Medzhitov and Janeway, 1997).

1.1.2. Adaptive Immune Response

The discrimination between self and non-self is crucial in both innate and adaptive immune systems but different ways of detecting foreign pathogens are used in each immune system. While the innate immune response is elicited by the non-specific recognition of pathogens, the adaptive immune response is specific to a given pathogen (Medzhitov and Janeway, 1997). Each individual antigen receptor of $\alpha\beta TCR^+$ T-cells can detect and mediate protection against a pathogen. To protect against a wide range of various microbial pathogens, the adaptive immune system must have a matching diversity of antigen specific αβTCRs. The

somatic recombination of gene segments allows T lymphocytes to have a diverse repertoire of antigen specific receptors (Chaplin, 2003). This mechanism of gene rearrangement is further explained in Section 1.1.3.3. (Structure Of the T-Cell Receptor). As mentioned previously, in addition to specificity and diversity, immunological memory is one of the key features in adaptive immunity. During initial exposure to a certain pathogen, long-lived memory T and B lymphocytes are produced and a more rapid and effective adaptive response is provided on a subsequent exposure to the same pathogen.

To initiate the adaptive immune response, antigen presentation to αβT-lymphocytes by the APCs of the innate immune system is required. Immature and mature subsets of DCs are classified based on phenotype, function, and the tissues where DCs reside (Banchereau and Steinman, 1998). Immature DCs are resident in peripheral tissues and their main function is to capture and process antigen. The maturation of DCs is induced by various microbial and inflammatory factors including lipopolysaccharides (LPS), TNFα, IL-1, IL-18 and GM-CSF (Banchereau and Steinman, 1998). Once DCs have undergone maturation, they up-regulate the expression of co-stimulatory molecules such as CD40, CD80, and CD86 and migrate to secondary lymphoid organs (such as the spleen and the lymph nodes) where they can interact with T and B lymphocytes. Since T cells only can recognize an antigen presented via the major histocompatibility complex (MHC) of APCs, mature DCs highly express surface peptide-MHC complex to prime naïve T cells (Banchereau and Steinman, 1998). Peripheral immature DCs have a lower efficacy in presenting antigens and a higher capability of processing antigens compared to mature DCs, explaining the high expression of intra-cellular MHC in immature DCs compared to mature DCs.

In addition to T cells, B cells play a vital role in the adaptive immune system. B cells develop from hematopoietic stem cells in bone marrow (MacLennan et al., 2003). Upon

activation, B cells differentiate into plasma cells secreting large amount of antigen-specific antibody. B cells can be activated through either T-cell independent or T-cell dependent mechanisms, and antigens such as polysaccharides and polymerized proteins can induce the T-cell independent activation. Once those antigens bind to B cell receptors (BCRs), the differentiation of the B cell into plasma cells secreting high levels of antibodies occurs. Instead of help from T cells, T-cell independent activation of B-cells still needs a second signal from cytokines or cell contact by DCs (Delves and Roitt, 2000b). There are also two steps in the T-cell dependent activation. In the first step, B cells work as APCs like DCs activating naïve T cells in the secondary lymphoid organs. In the second step, activated T cells up-regulate the expression of ligands, including CD40L, that bind to co-stimulatory molecules on the B cells. Signals provided by the activated T cells instruct B cells to differentiate into plasma and memory B cells. Antibodies or immunoglobulins produced by plasma cells specifically bind to pathogens and prepare them as better targets for phagocytosis (Bonilla and Oettgen, 2010).

1.1.3. T Lymphocytes

T and B cells are key cellular components in the adaptive immune system. Unlike B cells, bone marrow-derived lymphoid progenitor cells migrate into thymus and undergo T cell development (Goldrath and Bevan, 1999). Each mature T cell expresses both a T cell receptor (TCR) and a co-receptor for MHC. There are two types of co-receptor: CD4 and CD8. CD4 expressing ($CD4^+$) T cells recognize antigen presented by MHC class II and are known as helper T cells. In contrast, CD8 expressing T cells recognize antigen bound to MHC class I and are called as cytotoxic T lymphocytes (CTLs). The different phenotypes of $CD4^+$ helper T cells and $CD8^+$ cytotoxic T cells associates with its specialized functions of each lineage (Delves and Roitt, 2000b).

1.1.3.1. $CD4^+$ Helper T cells

Naïve $CD4^+$ helper T cells have the potential to differentiate into four different subsets, which are Th1, Th2, Th17, and regulatory T cells (Tregs) (Parkin and Cohen, 2001). Each subset has distinct roles in adaptive immunity. Th1 cells are responsible for the induction of a cell-mediated inflammatory response against intracellular pathogens. Both Th2 cells and Th17 cells are essential for the induction of immune responses against extracellular pathogens. Specifically, Th2 cells regulate immune responses against parasites including helminths, while Th17 cells play a major role in developing defenses against bacteria and fungi. However, Th17 cells are also found in autoimmune tissues such as arthritis, multiple sclerosis, and systemic lupus erythematosus, thus they have been thought to be involved in autoimmune responses (Bonilla and Oettgen, 2010). In addition, Tregs help to maintain self-tolerance and immune homeostasis (Zhu and Paul, 2008), as indicated by studies showing that the absence of Tregs causes severe autoimmune diseases and chronic inflammation (Fontenot et al., 2003; Kim et al., 2007).

Distinct lineages of effector $CD4^+$ T cells can be identified according to their cytokine production. For example, Th1 cells produce IL-2, IFN-γ, and LTα; Th2 cells secrete cytokines including IL-4, IL-5, IL-9, IL-10, IL-13, and IL-25; Th17 cells release IL-17, IL-21 and IL-22 (Parkin and Cohen, 2001; Zhu and Paul, 2008). Also, the expression of different transcription factors helps to categorize each lineage. The expression of transcription factor T-box expressed in T cells (T-bet) marks Th1 cells; the transcription factor GATA binding protein 3 (GATA3) is expressed by Th2 cells; the expression of transcription factor Retinoic acid related Orphan Receptor γt (RORγt) classifies Th17 cells. Lastly, Tregs are characterized by the expression of surface marker, CD25, and transcription factor forkhead box P3 (FoxP3) (Bonilla and Oettgen, 2010).

αβTCRs expressed by $CD4^+$ helper T cells are only able to recognize antigens specifically presented by MHC class II. The expression of MHC class II is largely limited to APCs such as DCs, B cells, and macrophages, although TECs are also MHC class II^+. For the generation of antigen/MHC class II complexes for CD4 T-cell recognition, exogenous antigens are taken up by APCs in an endocytic manner. The antigens are processed to peptides and the association of MHC class II with the antigenic peptides occurs within endosomes or lysosomes. Complexes of MHC class II and antigenic peptides are then transported to plasma membrane to induce the activation of $CD4^+$ helper T cells (Bryant and Ploegh, 2004; Guermonprez et al., 2002).

1.1.3.2. $CD8^+$ Cytotoxic T Cells

$CD8^+$ cytotoxic T cells develop to kill virally infected cells. The proliferation of viruses is dependent on the host's replication machinery without destroying host's cells, and all nucleated cells express MHC class I. Following a viral infection, the host cell processes intracellular viral protein and loads the antigens on MHC class I to mark itself as a target for $CD8^+$ T cells (Harty et al., 2000). Naïve $CD8^+$ T cells recognize an antigen bound on the MHC class I and differentiate into CTLs. There are multiple ways in which virally infected cells can be eliminated by CTLs. CTLs insert pore-forming perforin to infected cells and then use pores as passages to inject proteolytic enzymes capable of mediating target cell apoptosis. Alternatively, CTLs activate apoptosis by engaging FAS ligand with FAS on the infected cells. Moreover, CTLs secrete cytokines such as TNF-α and IFN-γ to enhance antiviral defenses rendering neighboring cells resistant to infection (Delves and Roitt, 2000b; Podack, 1995).

1.1.3.3. Structure Of The T Cell Receptor And CD3 Complex

On the majority of T-cells, the TCR is composed of α and β chains working as a heterodimer. Each α and β chain has three regions: a variable region, a constant region, and a transmembrane region. The variable region is somatically assembled from variable (V), diversity (D), and joining (J) gene segments. While all V, D, and J gene segments encode the variable region of the TCRβ chain, only V and J gene segments encode the variable region of the TCRα (Bonilla and Oettgen, 2010; Guy and Vignali, 2009). The variable region of α and β chains contains the binding site for the peptide-MHC (pMHC) complex and is known as a complementarity-determining region (CDR).

CDRs are hypervariable ensuring the diversity of adaptive immune response. Such diversity results from both combinatorial and junctional diversity. There are many different V, D and J gene segments within TCR genes and each different combination of VDJ genes allows for a single specificity (Fugmann et al., 2000). Additionally, the imprecise joining of VDJ gene segments provides further diversity. The sequential process of V(D)J gene rearrangement and recombination is highly controlled by the recombination activating genes *Rag1* and *Rag2* (Bonilla and Oettgen, 2010; Fugmann et al., 2000). As Immunoglobulin diversity also involves antigen receptor gene rearrangement, B cells as well as T cells express the *Rag1* and *Rag2* genes. In both cell types, RAG proteins firstly bind to the recombination signal sequences (RSSs) and cleave DNA into pieces. After cutting DNA, the RAG proteins randomly splice fragments together. Moreover, template independent nucleotides are inserted into junctions between coding regions by enzyme terminal deoxynucleotidyl transferase (TdT) (Bonilla and Oettgen, 2010). All of these mechanisms are orchestrated together to create a diverse repertoire of antigen specific TCRs or BCRs.

In order to induce downstream signaling, the TCR has to be associated with the CD3 complex, which consists of multiple invariant chains that form three dimers. The CD3ζζ homodimer is located in between α and β chain of TCR. CD3εδ heterodimer interacts with the TCRα chain, thus it lies next to the TCRα chain. On the opposite side, the last complex, CD3γε heterodimer, is associated with the TCRβ chain (Guy and Vignali, 2009; Wang and Reinherz, 2012). Immunoreceptor Tyrosine-based Activation Motifs (ITAMs) are crucial for downstream of TCR:CD3 signaling following interactions with peptide/MHC. There is a total of 10 ITAMs in a TCR:CD3 complex, and each of the CD3ε, CD3γ, and CD3δ subunits has a single ITAM in its cytoplasmic tail. The rest of six ITAMs are found in the cytoplasmic regions of a CD3ζζ homodimer (Guy and Vignali, 2009). A disulfide bond connects between TCRα and TCRβ chains and also a CD3ζζ homodimer is linked by another disulfide bond (Wang and Reinherz, 2012; Wucherpfennig et al., 2010).

1.1.3.4. TCR And CD3 Signaling

Upon the engagement of TCR with pMHC complex, the CD4 co-receptor on helper T cells binds to MHC class II, or the CD8 co-receptor on cytotoxic T cells binds to MHC class I for more stable interaction between TCRs and pMHC complexes to initiate downstream TCR:CD3 signaling. Following TCR ligation, co-receptor associated tyrosine kinase $p56^{Lck}$, which belongs to the Src family, phosphorylates the ITAMs of CD3 complexes (Deindl et al., 2007; Kane et al., 2000; Samelson, 2002; Smith-Garvin et al., 2009). The phosphorylation by $p56^{Lck}$ recruits and activates another tyrosine kinase, ZAP-70. ZAP-70 belongs to Syk family, and associates with CD3ζ chains. Then, the adapter proteins including linker of activated T cells (LAT) and SH2-containing leukocyte protein, 76 kd (SLP-76) are phosphorylated by ZAP-70, which leads to the hydrolysis of membrane lipid phosphatidylinositol biphosphate (PIP_2) into inositol-triphosphate (IP_3) and diacylglycerol (DAG) by phospholipase Cγ1

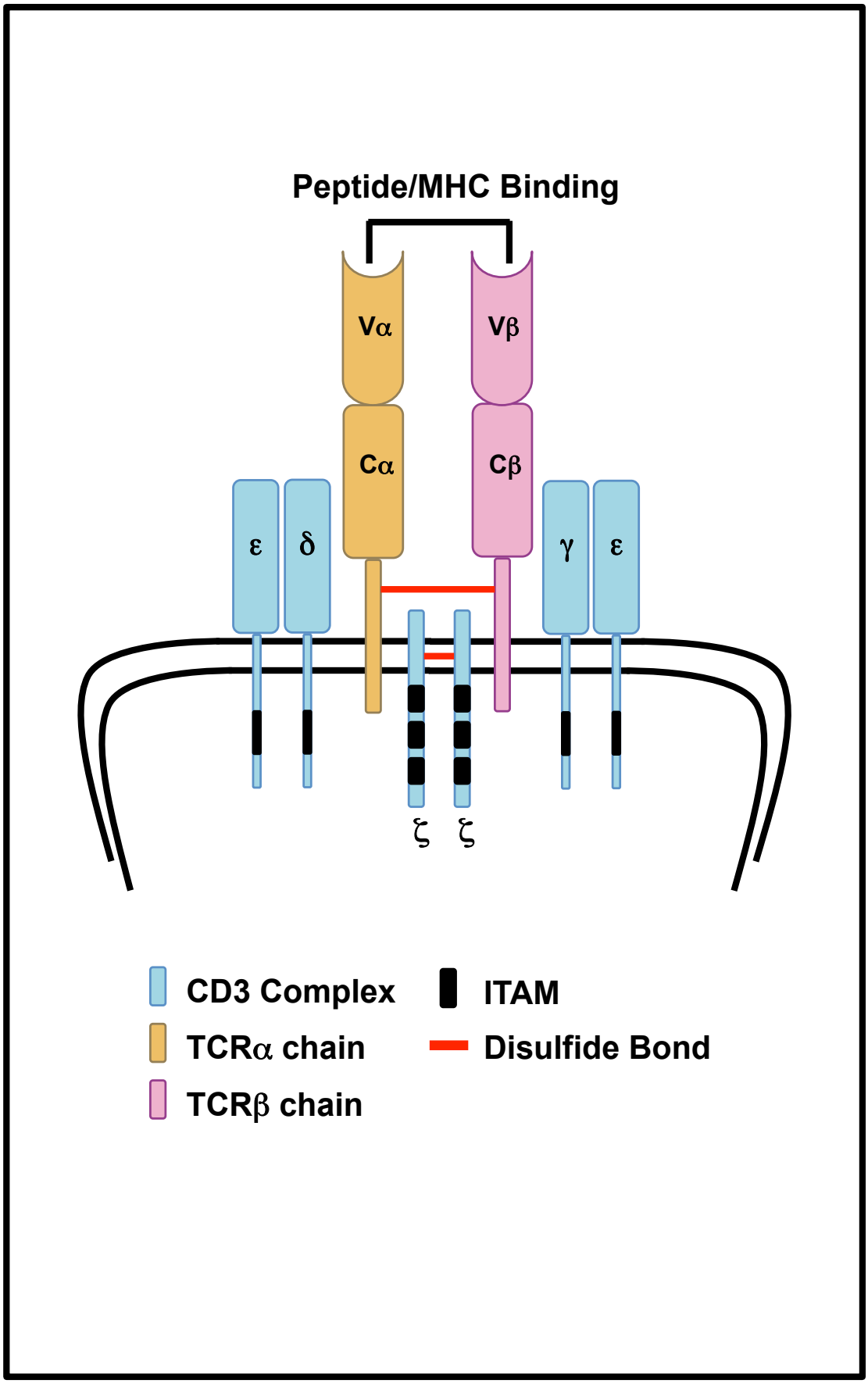

Peptide/MHC Binding
Vα
Vβ
Cα
Cβ
ε
δ
γ
ε
ζ
ζ
CD3 Complex
TCRα chain
TCRβ chain
ITAM
Disulfide Bond

Figure 1.1. Structure of T cell receptor and CD3 complex

TCR is working as a heterodimer: α and β chains. Each chain has three regions: a variable region (V), a constant region (C), and a transmembrane region. The variable region of α and β chains contains the binding site for the peptide-MHC complex and is known as a complementarity-determining region (CDR). TCR is associated with the CD3 complex, which consists of multiple invariant chains that form three dimers: CD3εδ, CD3γε, CD3ζζ. There is a total of 10 Immunoreceptor Tyrosine-based Activation Motifs (ITAMs) in a TCR:CD3 complex. There are two disulfide bonds: one in between TCRα and TCRβ chains and another in CD3ζζ homodimer.

(PLCγ1) (Bonilla and Oettgen, 2010; Smith-Garvin et al., 2009). As a result, the level of intracellular calcium increases. Collectively, the final goal of TCR:CD3 signaling is to activate transcription factors including nuclear factor of activated T cells (NFAT), nuclear factor κB (NF-κB), and activator protein 1 (AP-1), which are involved in the proliferation, differentiation and effector actions of T cells (Guy and Vignali, 2009; Samelson, 2002).

In order to enhance TCR:CD3 signaling, the additional signals mediated by co-stimulatory receptors are required. In their absence, TCR signaling fails to induce differentiation into effector T cells, production of cytokines, and T-cell proliferation, (Keir et al., 2008; Yokosuka and Saito, 2009). Co-stimulatory signals can positively or negatively affect TCR:CD3 signaling. One of the most known positive co-stimulatory receptors is CD28, which is expressed on T cells and binds to B7 stimulatory molecules expressed on APCs. Ligation of CD28 by B7-1 (CD80) or B7-2 (CD86) is essential for the activation of TCR:CD3 signaling (Yokosuka and Saito, 2009). On the other hand, B7 co-stimulation is also involved in providing inhibitory signals to activated T cells. Activated T cells express cytotoxic T-lymphocyte antigen-4 (CTLA-4), which binds to CD80 and CD86 on APCs. CTLA-4 is a negative co-stimulatory receptor. Thus, the reduction in proliferation and cytokine production is found after the binding of CTLA-4 on activated T cells with B7-1 and B7-2 on APCs (Yokosuka and Saito, 2009). Other co-stimulatory pathways include the pairs of programed cell death-1 (PD-1) on T cells with its ligands, PD-L1 (CD274, also known as B7-H1) and PD-L2 (CD273, also known as B7-DC). PD-L1 and PD-L2 are expressed on APCs. PD-1:PD-L1/PD-L2 co-stimulatory signal exerts inhibitory effects on T cell activation and it plays a major role in balancing between activation and tolerance (Guermonprez et al., 2002; Keir et al., 2008).

Collectively, it is clear that activation of αβT-cells by antigen recognition is at the center of adaptive immune responses. The development of the thymic microenvironments that control the production of these cells is the focus of this thesis.

1.1.3.5. Microenvironments For T-cell Mediated Immune Response

Since spleen and lymph nodes are the major places where the innate immune response connects to the adaptive immune response, the fine architecture of secondary lymphoid organs is essential to induce T-cell mediated immune response (Mebius and Kraal, 2005; von Andrian and Mempel, 2003). Spleen is anatomically separated into red pulp and white pulp. At the red pulp, blood gets filtered and old erythrocytes are removed. Moreover, the red pulp resident macrophages get rid of bacteria from blood. The white pulp is surrounded by the marginal zone. The marginal zone separates the white pulp from the red pulp and it is the transit area for cells emigrating from the bloodstream and immigrating into the white pulp (Mitchell, 1973). The white pulp is compartmentalized into T-cell zone (periarteriolar lymphoid sheath, PALS) and B-cell zone (B-cell follicles). Within the T-cell zone, activated APCs from periphery interact with T cells and then the activated T cells migrate into the edge of B-cell follicles. Following such T-cell migration, the activated T cells help B cells in the follicles to differentiate and secrete antibodies (Mebius and Kraal, 2005).

The histology of lymph node is similar to that of spleen but there are also differences between two tissues. The lymph node has two distinct regions: cortex and medulla. Like the spleen, the cortex is further divided into T-cell area (paracortex) and B-cell area (comprised of primary follicles and germinal centers formed after antigen challenge) (Mondino et al., 1996). The entry of circulating lymphocytes into lymph node and the interaction between T cells and DCs occur in the paracortex. The interstitial fluid enters the lymph node via afferent lymph vessels, and the lymph fluid is drained from the paracortex through a high endothelial

venule (HEV), which is located in the center of paracortex and is surrounded by the fibroblastic reticular cells (FRCs) (Mondino et al., 1996). The drained lymph travels toward trabecular sinus and then exits the lymph node by passing medullary sinus and efferent lymph vessel. The main purpose of having secondary lymphoid tissues is for T cells to efficiently encounter foreign antigens (Mitchell, 1973; Mondino et al., 1996). Thus, the organization in secondary lymphoid tissues is important for effective T-cell mediated immune responses.

1.2. T-Cell Development

1.2.1. Structure And Function Of Thymus

The Thymus is a primary lymphoid organ and its main function is to produce functional T cells. The thymus provides a specialized microenvironment for T cell development, and is histologically divided into two regions: cortex and medulla. Both regions are composed of thymic epithelial cells (TECs) and each region has its own distinctive roles in T-cell development. Bone marrow-derived lymphoid progenitors firstly migrate into thymus and then undergo T cell development involving four sequential processes: T-cell lineage commitment, β-selection, positive selection, and negative selection (Anderson et al., 2006). The crosstalk between developing thymocytes and TECs are essential for all of those four processes. The first three events occur in the cortex; cortical thymic epithelial cells (cTECs) provide signals for T-cell lineage commitment and the selection of functional T cells via β-selection and positive selection. The removal of potentially auto-reactive T cells is driven at least in part by medullary thymic epithelial cells (mTECs). Finally, the most mature thymocytes emigrate into secondary (peripheral) lymphoid tissues such as spleen and lymph nodes to induce adaptive responses (Samelson, 2002).

1.2.2. Thymus Colonization By T-cell Progenitors

The colonization of thymus by hematopoietic precursors is required for the efficient T cell production. Fetal and adult thymus colonization is different in the context of the origin of hematopoietic precursor, the entering mechanism into thymus, and the types of signal required. Liver-derived precursors initially migrate into fetal thymus at around embryonic day (E) 11.5 and bone marrow-derived precursors colonize adult thymus (Anderson et al., 2006; Kincade et al., 2002). The mechanism of thymus entry is based on whether the thymus is vascularized or not. The initial colonization of fetal thymus occurs prior to its vascularization.

Thus, progenitors exit from neighboring blood vessels, travel across the perithymic mesenchyme and enter into fetal thymus through the epithelial basement membrane (Petrie, 2003). By contrast, bone marrow-derived precursors in adult enter the thymus via blood vessels located at cortico-medullary junction (CMJ).

The colonization of early embryonic thymus is mediated by a chemotactic mechanism, because the embryonic thymus gets vascularized at around E15.5. The fetal thymus expresses chemokines including CCL21, CCL25, and CXCL12. CCL21 is a ligand for CCR7 and CCL25 binds to CCR9. Mice deficient in both or either CCR7 and CCR9 show a lower number of thymocytes in the early embryo compared to that of wild type (Liu et al., 2006). In contrast, mice lacking the expression of CXCR4, a receptor for CXCL12, display no defect in the colonization of early embryonic thymus (Ara et al., 2003). Collectively, this could suggest the redundant role of CXCR4/CXCL12 and the significance of CCL21/CCR7 and CCL25/CCR9 signal in fetal thymic colonization (Jenkinson et al., 2007; Liu et al., 2006). Recent studies show that mice with combined deficiency in CCR7, CCR9, and CXCR4 expression have a severe reduction in the number of intra-thymic progenitors confirming the redundant role of those three chemokines in the colonization of early embryonic thymus (Calderon and Boehm, 2011).

Since intra-thymic hematopoietic precursors have short-termed self-renewal capability, the continuous seeding of precursors in adult is essential for unremitting T cell production (Rossi et al., 2005). Unlike the embryonic thymus, chemokine independent signaling is required for thymic homing in the adult. P-selectin is a key mediator during adult thymus colonization and is expressed by thymic vascular endothelium. Its ligand, P-selectin glycoprotein ligand 1 (PSGL1) expressed on lymphoid progenitors in the bone marrow and thymus, binds to P-selectin on thymic endothelium resulting in extravasation (Rossi et al.,

2005). Recently, it has been shown that the correlational expression between P-selectin and CCL25 helps to maintain the levels of thymic progenitor input. In mice lacking P-selectin, higher expression of CCL25 is found, and mice deficient in CCL25 expression show elevated expression of P-selectin compared to that of wild type. Not only CCL25 expression affects the level of P-selectin expression but also extra-thymic factors such as the size of peripheral T-cell pool influence the expression level of P-selectin. Thus, the lower level of peripheral T cells leads to the up-regulation of P-selectin expression on lymphoid progenitors, consequently resulting in the higher receptivity to increase thymic progenitor input (Gossens et al., 2009).

1.2.3. Early T-cell Development In The Cortex

1.2.3.1. T-Cell Lineage Commitment

Hematopoietic stem cells in bone marrow can develop into myeloid-restricted or lymphocyte-restricted progenitors. While DC, macrophages, and granulocytes are originated from the myeloid-restricted progenitors, T and B cells are differentiated from the lymphocyte-restricted progenitors. It is controversial whether the progenitors entering thymus have already undergone through myeloid/lymphoid lineage diversification or an intra-thymic signal is required for the differentiation of thymic lymphoid cells or thymic myeloid cells from hematopoietic precursors (Ikawa et al., 2010; Schlenner et al., 2010; Schlenner and Rodewald, 2010).

Several studies have shown the importance of Notch signaling in T cell lineage commitment. Activation of Notch signaling directs the progenitor cells to the T cell lineage and inhibits the differentiation into any other lymphoid-lineage such as B cells (Sambandam et al., 2005). Notch signaling is initiated by the ligation of Notch 1 receptor on progenitors with its transmembrane bound ligand, Delta Like Ligand 4 (Dll4) expressed on cTECs.

However, it is controversial whether the Notch signal is essential for the T/B lineage choice in an extrathymic or intrathymic way. One study has demonstrated that T-cell fate specification occurs extrathymically and Notch signaling within the thymus is required for continued T-cell development of already T-cell lineage committed progenitors (Harman et al., 2005). Loss of either Notch 1 receptor or Dll4 expression leads to a complete block in T cell development accompanied by the presence of ectopic B cells within the thymus. Moreover, mice with Dll4 deficiency specifically in the thymus also have a similar cell profile with the presence of abnormal thymic B cells (Hozumi et al., 2008; Koch et al., 2008). This confirms that the intra-thymic activation of Notch signal is essential for T/B lineage choice but it is not clear where and when the initial Notch signal is required for T-cell fate decision.

1.2.3.2. Early Intra-thymic T-cell Development

The stages of T-cell development can be traced by analyzing the expression pattern of co-receptors CD4 and CD8 on developing thymocytes. The most immature thymocytes express neither CD4 nor CD8 and are called as $CD4^{-}CD8^{-}$ double negative (DN). DNs are further divided into four subsets according to the expression of CD25 (IL-2 receptor α chain), CD44 (phagocytic glycoprotein 1), CD117 (stem cell factor receptor, c-kit), and CD127 (IL-7 receptor α chain). The four DN subsets are DN1 ($CD25^{-}CD44^{+}CD117^{+}CD127^{+/-}$), DN2 ($CD25^{+}CD44^{+}CD117^{+}CD127^{+}$), DN3 ($CD25^{+}CD44^{-}CD117^{-}CD127^{-}$), and DN4 ($CD25^{-}CD44^{-}CD117^{-}CD127^{-}$) (Godfrey et al., 1993; Naito et al., 2011).

DN1 thymocytes are the most primitive thymocytes among four DN subsets and have the potential to differentiate into T cells (both αβT-cells and γδT-cells), B cell, NK cells, DCs, and macrophages. DN1 thymocytes can be even further subdivided into five distinctive populations according to the expression of CD24 and CD117. The five DN1 subsets are DN1a ($CD24^{-}CD117^{+}$), DN1b ($CD24^{Low}CD117^{+}$), DN1c ($CD24^{High}CD117^{+}$), DN1d ($CD24^{+}CD117^{-}$

), and DN1e ($CD24^{-}CD117^{-}$) (Porritt et al., 2004). DN1 thymocytes have a limited self-renewal capability but develop into mature thymocytes faster compared to hematopoietic stem cells (Zuniga-Pflucker and Lenardo, 1996). Porritt et al intravenously injected each DN1 thymocyte subset into different host mice and investigated the capability of homing to thymus and T-cell development. All five subsets could migrate into the thymus but only DN1a and DN1b were able to proliferate and undergo T-cell development. This indicates that DN1a and DN1b are more similar to progenitors and the rest are in the transition between progenitors and DN2 thymocytes (Porritt et al., 2004).

During the transition between DN1 and DN2, thymocytes up-regulate CD25 expression, lose the B-cell potential but still have other lineage potential. At the DN2 stage, the expression of *RAG* genes is up-regulated and the rearrangement of TCRγ, TCRδ, and TCRβ chains is initiated (Livak et al., 1999). Both DN1 and DN2 thymocytes require IL-7 signals for survival and differentiation. IL-7 is secreted by TECs and the engagement of IL-7 with IL-7Rα on developing thymocytes drives the differentiation of DN1 and DN2 thymocytes (Balciunaite et al., 2005; Crompton et al., 1998; Zamisch et al., 2005). However, T-cell development after the DN2 stage is independent of IL-7, as revealed by the down-regulation of IL-7Rα (CD127) expression on DN3 thymocytes.

During development to DN3 stage, there are many distinct changes. Firstly, thymocytes down-regulate the expression of CD44, CD117, and CD127, and then lose the non-T cell lineage potential. Thirdly, the rearrangement of TCRγ, TCRδ, and TCRβ chain is completed; consequently it results in the lineage diversification between αβT-cells and γδT-cells (Naito et al., 2011; Zuniga-Pflucker and Lenardo, 1996). Lastly, the pre-TCR complexes are found on the cell surface getting ready for β-selection. The rearranged TCRβ chain in the cytoplasm assembles with an invariant pre-Tα chain and CD3 components forming the pre-

TCR complex on the cell surface. The pre-Tα chain, a transmembrane protein with a single extra-cellular immunoglobulin-like structural domain and a cytoplasmic tail, is connected to the rearranged TCRβ chain by disulfide bond (von Boehmer and Fehling, 1997). The rearrangement of TCRα chain is not yet initiated at this point, thus the pre-Tα chain should be replaced with a rearranged TCRα chain so that functional αβT-cells develop at later developmental stages. The survival signal should be provided to DN3 thymocytes for further development, otherwise DN3 thymocytes would undergo the programmed cell death. Only functional TCRβ chain within the pre-TCR complex can transduce the signal for proliferation and further differentiation. This selection is termed as β-selection and it screens out DN3 thymocytes with non-functional TCRβ chain (von Boehmer and Fehling, 1997; Zuniga-Pflucker and Lenardo, 1996).

The major event in the transition between DN3 and DN4 is β-selection. Signaling during β-selection induces proliferation, stops additional rearrangement of TCRβ chain (allelic exclusion), initiates the rearrangement of TCRα chain, and up-regulates the expression of CD4 and CD8 co-receptors. In addition to those four changes, the down-regulation of CD25 expression marks the DN4 stage (Petrie and Zuniga-Pflucker, 2007). To prevent having more than one rearranged TCRβ chain in a single T-cell, allelic exclusion at the TCRβ locus occurs before the initiation of TCRα chain rearrangement. Therefore, RAG proteins can only access the TCRα gene locus. After successful TCRα chain rearrangement, the pre-Tα chain is replaced by newly generated TCRα chain. Then, the low expression of αβTCR associated with the CD3 complex on the cell surface is accompanied with the high expression of CD4 and CD8 co-receptors becoming $CD4^{+}CD8^{+}$ double positive (DP) thymocytes. About 90% of thymic cellularity is constituted with DP thymocytes due to high

proliferation in the transition between DN4 and DP stages. Before DP thymocytes are selected for further development into SP thymocytes in the cortex, they stop proliferating, although it is not clear whether there is the lack of signal inducing proliferation or it is cell-intrinsic (Naito et al., 2011; Petrie and Zuniga-Pflucker, 2007; Zuniga-Pflucker and Lenardo, 1996).

1.2.3.3. Thymocyte Migration In Early Stages Of T-cell Development

Besides the expression pattern of cell surface markers, where the developing thymocytes are resident can also discriminate stages of T-cell development. Precise localization of developing thymocytes within the thymus is important for efficient T-cell development because TECs provide distinct signals to thymocytes at each stage. Moreover, migration from one to another region in the thymus is highly controlled by chemotactic mechanisms. Thus, the differential expression of chemokine receptors on thymocytes is another indicator of developmental stages (Plotkin et al., 2003; Prockop and Petrie, 2000).

Progenitors enter the thymus via post-capillary venules located at the CMJ and migrate first into the cortex. Within the cortex, developing thymocytes spend approximately 16-18 days and undergo the early stages of T-cell development (from DN to DP). The cortex can be sub-divided into three areas: inner cortex, outer cortex, and subcapsular zone. DN1/2 thymocytes are mostly found in the inner cortex area; early DN3 thymocytes (before β-selection) are resident in the outer cortex area; late DN3 (after β-selection) and DN4 thymocytes are located in the subcapsular area. The large population of DP thymocytes is scattered out in both inner and outer cortex but not in the subcapsular zone (Ladi et al., 2006; Petrie and Zuniga-Pflucker, 2007). The direction of DN subset migration is the opposite to that of DP thymocyte migration. While DN thymocytes move across the cortex toward the subcapsular zone, DP thymocytes reverse the flow of DN thymocytes. There are three well-known combinations of chemokine and receptor playing crucial role in the intra-thymic

migration, specifically within the cortex: CCR7/(CCL19,CCL21), CXCR4/CXCL12, and CCR9/CCL25 (Misslitz et al., 2004; Petrie and Zuniga-Pflucker, 2007; Plotkin et al., 2003).

CCR7 is expressed on DN1/2 thymocytes. Additionally $CD4^{+}CD8^{-}$ single positive (SP4) and $CD4^{-}CD8^{+}$ single positive (SP8) thymocytes also express CCR7. The ligands of CCR7 are expressed not only in the medulla but also in the cortex next to CJM and by a few cTECs scattered in the mid-cortex. Mice lacking CCR7 expression show an accumulation of DN1/2 thymocytes around the CMJ and the diminution of DN2, DN3, and DN4 thymocytes in the rest of cortex except the CMJ of inner cortex zone. This confirms that (CCL19,CCL21)/CCR7 signaling mediates the migration of DN1/2 thymocytes from CMJ to the mid-cortex. Consequently, T-cell development is partially blocked at DN2 stage due to the problem of intra-thymic migration in the absence of CCR7 (Misslitz et al., 2004).

CXCR4, which is expressed on all four DN subsets, binds to CXCL12 expressed by cTECs. This engagement induces the migration of DN1 thymocytes toward the outer cortex for further development. Mice deficient in CXCR4 expression show more a severe developmental arrest at the DN2 stage than mice lacking CCR7. Collectively, CCR7 and CXCR4 have redundant roles in DN1/2 thymocyte migration toward the outer cortex but CXCR4 plays major role compared to CCR7 (Misslitz et al., 2004; Plotkin et al., 2003). Moreover, the migration of DN thymocytes to the subcapsular zone is highly regulated by CCR9, which binds to CCL25 expressed by both cTECs and mTECs. This regulation is dependent on the differential expression of CCR9 on developing thymocytes; CCR9 expression is gradually up-regulated from DN2/3 to DP thymocytes and then it is down-regulated by SP stage. Mice lacking CCR9 fail to recruit DN3/4 thymocytes to the subcapsular zone suggesting its role in homing of the DN2/3 thymocytes to the subcapsular region (Petrie and Zuniga-Pflucker, 2007; Uehara et al., 2006).

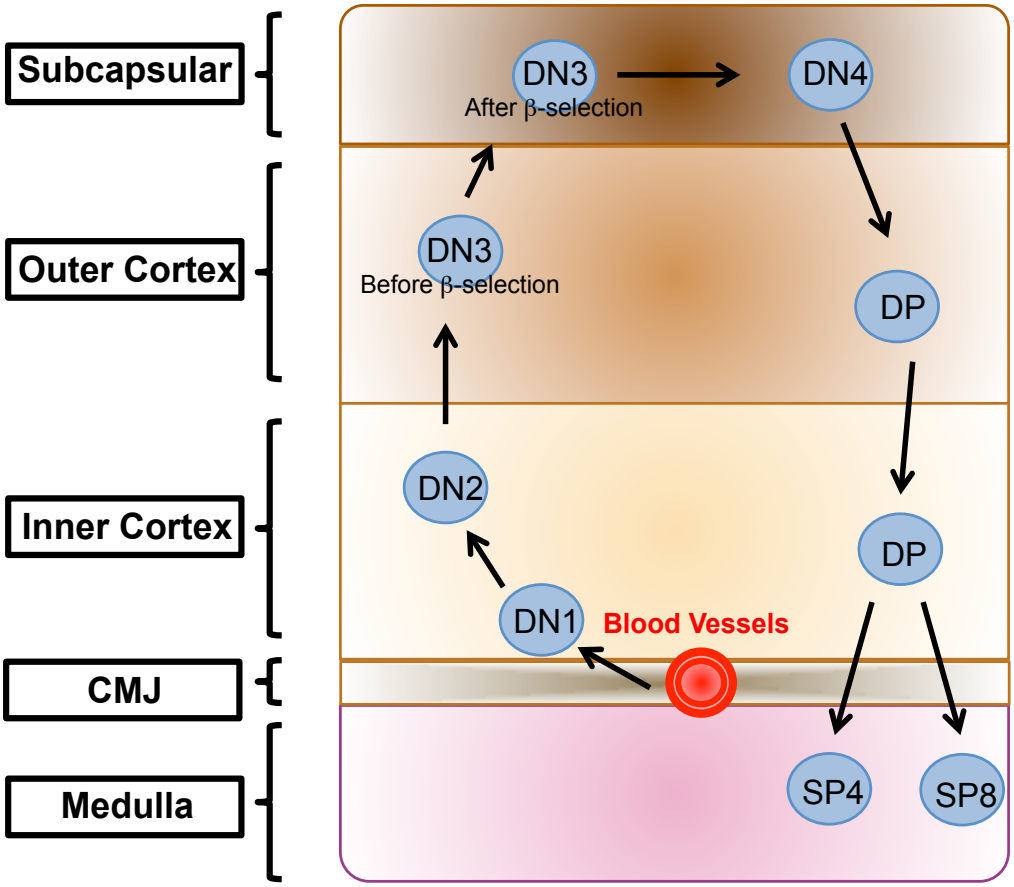

Subcapsular
Outer Cortex
Inner Cortex
CMJ
Medulla
DN3
After β-selection
DN4
DN3
Before β-selection
DP
DN2
DP
DN1
Blood Vessels
SP4
SP8

Figure 1.2. Migration of developing thymocyte during T-cell development

Progenitors enter the thymus via post-capillary venules at the CMJ and migrate first into the cortex. DN1/2 thymocytes are present in the inner cortex area; early DN3 thymocytes (before β-selection) are resident in the outer cortex area; late DN3 (after β-selection) and DN4 thymocyts are located in the subcapsular area. DP thymocytes is scattered out in both inner and outer cortex but not in the subcapsular zone. After positive selection, SP thymocytes migrated from the cortex to the medulla.

1.2.4. Positive Selection And Central Tolerance Induction

Before the most mature thymocytes emigrate from the thymus into the periphery, developing thymocytes have to pass three checkpoints: β-selection, positive and negative selection. As explained in section 1.2.3.2. (Early Intra-thymic T-cell development), the first checkpoint is β-selection. The affinity of TCR to peptide/MHC (pMHC) complexes is the key determinant for both positive and negative selection because acquiring a certain level of TCR affinity ensures the proper adaptive immune response. Too low affinity causes non-responsive adaptive immunity and high affinity may result in autoimmune disease. Thus, DP thymocytes expressing TCRs with no or too low affinity undergo apoptosis (death by neglect) and the intermediate level of TCR affinity to pMHC stimulates positive selection. Positively selected thymocytes are screened to establish self-tolerance (Klein et al., 2009).

1.2.4.1. Positive Selection

In order for successful positive selection, cTECs must efficiently process self-antigen and present the antigenic-peptide with MHC to DP thymocytes. By engaging TCRs on DP thymocytes with the self-peptide/MHC complexes on cTECs, its lineage specification into either $CD4^+$ helper T cells or $CD8^+$ cytotoxic T cells occurs simultaneously with positive selection. The failure of self-antigen presentation by cTECs results in the reduction of αβTCR repertoire. Hence, it is important to understand how self-peptides are prepared for positive selection in the cortex. Unlike peripheral APCs, both cTECs and mTECs present self-antigen. Therefore, the mechanism of antigenic-peptide preparation is different in between intra-thymic and extra-thymic APCs (Anderson et al., 2006; Klein et al., 2009).

DP thymocytes that bind to the self-peptide bound on the MHC class II of cTECs down-regulate the co-receptor CD8 expression becoming SP4 thymocytes. cTECs have unique mechanical components for antigen presentation with MHC class II that are distinct

from peripheral (hematopoietic) APCs: cathepsin L, and thymus-specific serine protease (TSSP) (Klein et al., 2009; Xing and Hogquist, 2012). The self-peptide/MHC complexes made from these two mechanisms help to positively select thymocytes with a diverse TCR repertoire. The thymus-specific proteases, cathepsin L and TSSP, process the endogenous protein for MHC class II loading. Cathepsins are lysosomal proteases and there are about 12 different kinds of cathepsin based on their structures, the type of proteins they cleave, and catalytic mechanisms. cTECs distinctively express cathepsin L whereas the peripheral APCs express cathepin S. Mice lacking cathepsin L display about 60% decrease of SP4 thymocytes resulting in a less diverse TCR repertoire (Janeway, 1999). In addition to cathepsin L and TSSP, both cTECs and mTECs have non-conventional way of self-peptide loading on MHC class II, macroautophagy. Macroautophagy is the protein degradation mechanism upon food starvation and it is found in most of tissues. However, TECs utilize the macroautophagy in a starvation-independent way. Approximately 70% of cTECs and 10% of mTECs have unusual high expression of macroautophagy (Nedjic et al., 2008). While exogenous proteins are internalized into vesicles by peripheral APCs in the endocytic manner for antigen presentation with MHC class II, the endogenously derived self-antigens are loaded on MHC class II via macroautophagy in cTECs for positive selection and in mTECs for negative selection (Aichinger et al., 2013; Klein et al., 2009).

In contrast, DP thymocytes that recognize self-peptide presented on the MHC class I of cTECs down-regulate the expression of co-receptor CD4 developing into SP8 thymocytes. The proteasome is required for peptide loading on the MHC class I. Upon the exposure to IFN-γ in the periphery, the β1i , β2i, and β5i subunits are assembled with the housekeeping proteasome turning into the immunoproteasomes. Instead of β5i subunit, β5t is incorporated into proteasome in cTECs. Thymoproteasome is a cortex-specific proteasome and its

uniqueness is known for β5t expression (de Oliveira Otto et al., 2013; Klein et al., 2009). Mice deficient for the β5t subunit have a smaller $CD8^+$ T cell pool with qualitatively altered TCR repertoire than normal mice resulted from impaired positive selection of SP8 thymocytes (Murata et al., 2007; Nitta et al., 2010).

The transition from DP to SP thymocytes during positive selection involves three stages according to the expression of CD69, a T-cell activation marker. The three steps are the pre-positive selection ($CD4^+CD8^+CD69^-$), the intermediate ($CD4^+CD8^+CD69^+$), and the post-positive selection ($CD4^+CD8^-CD69^+$ or $CD4^-CD8^+CD69^+$) (Hare et al., 1999). Right before positive selection, DP thymocytes up-regulate CD69 expression and this up-regulation requires the interaction between TCR and MHC. However, the development of $CD4^+CD8^+CD69^+$ thymocytes into SP4 or SP8 thymocytes occurs in the absence of the TCR/MHC interaction. Although continuous interaction with TECs is crucial for T-cell development, the transition of intermediate thymocytes ($CD4^+CD8^+CD69^+$) into post-positive selection SPs ($CD4^+CD8^-CD69^+$ or $CD4^-CD8^+CD69^+$) is independent on the TCR/MHC interaction (Hare et al., 1999; Wang et al., 1995; Yamashita et al., 1993).

During positive selection, there are other phenotypic changes including the expression of chemokine receptors. CCR7 expression is up-regulated in the transition from DP to SP thymocytes and its ligands are expressed in the medulla (Kurobe et al., 2006). Positively selected SP4 or SP8 thymocytes migrate into the medulla for negative selection. This migration is mediated by CCR7/(CCL19,CCL21) signaling (Petrie and Zuniga-Pflucker, 2007). In the absence of CCR7 or its ligands, positively selected thymocytes emigrate from the cortex to the periphery missing negative selection in the medulla. This indicates that the maturation and the emigration of thymocytes do not require essential signals from the medulla. However, those thymocytes fail to establish self- tolerance and causes autoimmune diseases.

Thus, the migration of SP thymocytes to the medulla is inevitable to complete T-cell development (Kurobe et al., 2006; Ueno et al., 2004).

1.2.4.2. Negative Selection

SP thymocytes spend approximately 14 days in the medulla before emigrating into the periphery. A major event during T-cell development in the medulla is the clonal deletion of potential auto-reactive T cells and this process is called negative selection (Starr et al., 2003). mTEC represent a key mediator of negative selection. During negative selection, SP thymocytes are exposed to a wide range of peripheral antigens and cells expressing TCRs with high affinity to the self-antigens undergo apoptosis. In particular, tissue-restricted antigens (TRA) are expressed by a subset of mTECs expressing the autoimmune regulator (*Aire*) gene. This $Aire^{+}$ mTEC subset is the main source of promiscuous gene expression. Therefore, the disruption in *Aire* gene causes autoimmune disease in many target organs (Klein et al., 2009; Petrie and Zuniga-Pflucker, 2007).

Newly generated SP thymocytes (pre-negative selection) and SP thymocytes resistant to tolerance induction (post-negative selection) can be discriminated by the expression of four surface markers, CD69, heat-stable antigen (HSA, also known as CD24), Qa2, and CD62L. The phenotype of less mature SP thymocytes is $CD69^{+}HSA^{+}Qa2^{-}CD62L^{-}$, and that of more mature SP thymocytes is $CD69^{-}HSA^{-}Qa2^{+}CD62L^{+}$ (Kishimoto and Sprent, 1997; Petrie and Zuniga-Pflucker, 2007). Moreover, SP thymocytes also express the ligands of tumor necrosis factor receptor superfamily (TNFRSF) such as LTα, CD40L, and RANKL. Not only do thymocytes need signals from TECs for T-cell development, but TECs also require signals from developing thymocytes. Specifically, such TNFRSF ligands are crucial to mTEC maturation and it will be more discussed in section 1.3.2.3. (mTEC development and Their Role In Central Tolerance) (Rossi et al., 2007b; White et al., 2008).

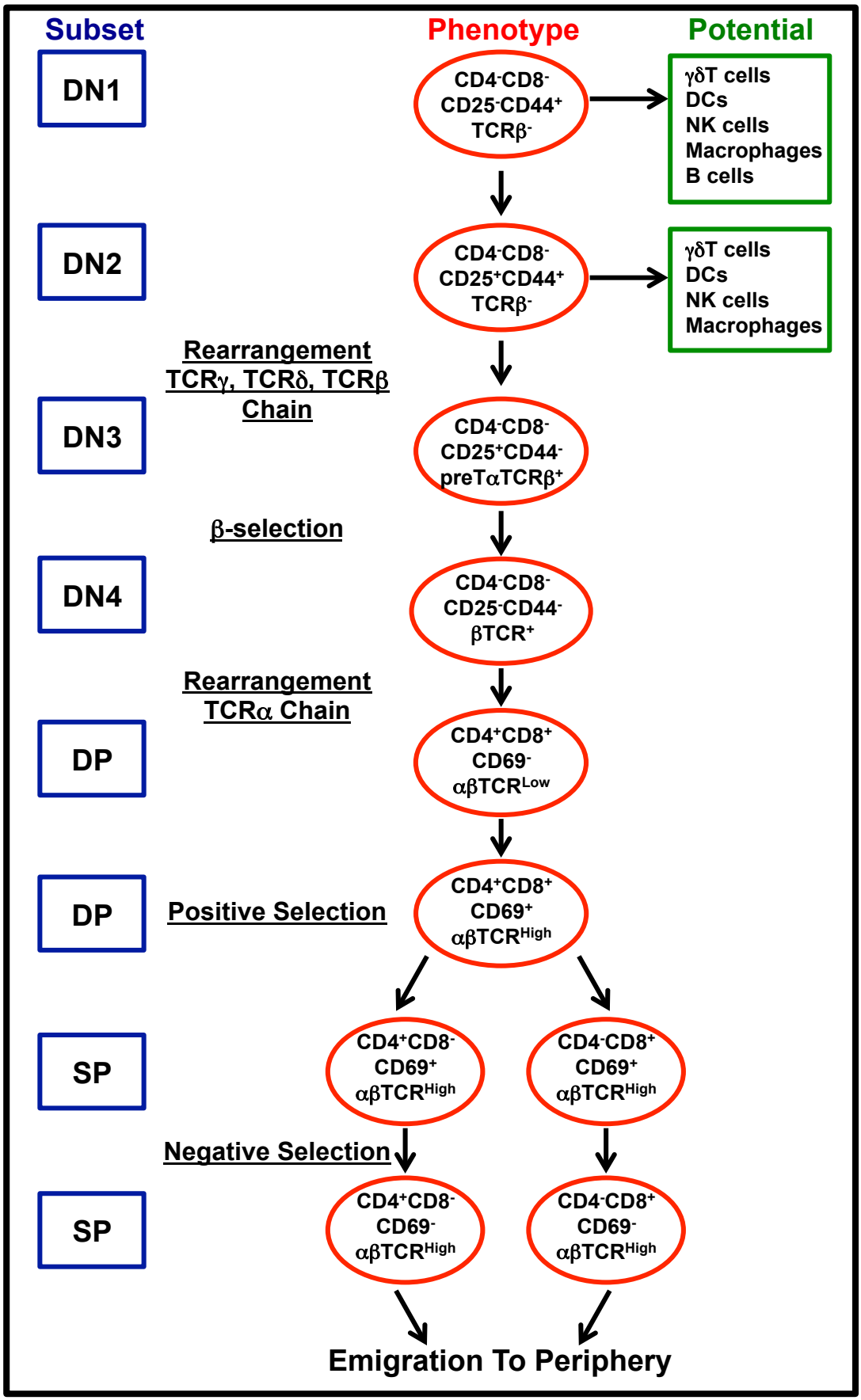

Subset
Phenotype
Potential
DN1
CD4-CD8-
CD25-CD44+
TCRβ-
γδT cells
DCs
NK cells
Macrophages
B cells
DN2
CD4-CD8-
CD25+CD44+
TCRβ-
γδT cells
DCs
NK cells
Macrophages
Rearrangement
TCRγ, TCRδ, TCRβ
Chain
DN3
CD4-CD8-
CD25+CD44-
preTαTCRβ+
β-selection
DN4
CD4-CD8-
CD25-CD44-
βTCR+
Rearrangement
TCRα Chain
DP
CD4+CD8+
CD69-
αβTCRLow
DP
Positive Selection
CD4+CD8+
CD69+
αβTCRHigh
SP
CD4+CD8-
CD69+
αβTCRHigh
CD4-CD8+
CD69+
αβTCRHigh
Negative Selection
SP
CD4+CD8-
CD69-
αβTCRHigh
CD4-CD8+
CD69-
αβTCRHigh
Emigration To Periphery

Figure 1.3. Stages of T-cell development in thymus

The phenotype of developing thymocytes defined by the expression of CD4, CD8, CD25, and CD44 is shown in red circles : DN1($CD4^-CD8^-CD25^-CD44^+$), DN2($CD4^-CD8^-CD25^+CD44^+$), DN3($CD4^-CD8^-CD25^+CD44^-$)3, DN4($CD4^-CD8^-CD25^-CD44$), DP($CD4^+CD8^+CD25^-CD44^-$), SP4($CD4^+CD8^-CD25^-CD44^-$), and SP8($CD4^-CD8^+CD25^-CD44^-$). The essential checkpoints at certain stage during T-cell development are indicated and the alterative lineage potentials are also shown in green boxes.

1.2.5. Emigration To Periphery

About 1-5% of total thymocytes pass all three selections and egress into the periphery. The mature SP thymocytes spend approximately two more days in the medulla after negative selection. During this time, up-regulation of Kruppel-like factor 2 (KLF-2) expression occurs. KLF-2 is a transcription factor that governs the expression of sphingosine-1-phosphate receptor-1 (S1P1), whose ligand is expressed on the pericytes around blood vessels at the CMJ. The lack of S1P1 expression in immature thymocytes blocks their emigration into the periphery, while enforced S1P1 expression on immature thymocytes results in the premature egress (Allende et al., 2004; Carlson et al., 2006; Matloubian et al., 2004). This confirms the importance of S1P1 expression in T cell trafficking from thymus to the secondary lymphoid tissues for adaptive immune response.

1.2.6. Non-conventional T Lineage Development In Thymus

The thymus also helps develop non-conventional T cells. Two known non-conventional T lineages, that require thymic microenvironment for generation, are invariant natural killer T cells (iNKTs) and natural regulatory T cells (nTregs). Classical iNKTs are identified by the expression of NK1.1 and the reactivity to α-galactosyl ceramide (α-GalCer) loaded on MHC class I-like molecule CD1d (Wu et al., 2009). Moreover, the majority of classical iNKTs express invariant Vα14-Jα18 TCR. Unlike conventional αβT cells, iNKTs are not positively selected by the ligation of TCR with pMHC on cTECs but are selected upon the engagement of invariant αβTCR with CD1d/glycolipid complexes on DP thymocytes in the cortex (Bendelac, 1995). The phenotype of most iNKs is similar to that of memory or activated T cells, $CD44^{+}CD62L^{-}CD69^{+}$ (Eberl et al., 1999). Newly generated iNKTs do not express NK1.1 and few immature iNKTs emigrate into the periphery and undergo further development including the stage of NK1.1 expression acquisition. In contrast, the rest of

immature iNKTs obtain the NK1.1 expression within the thymus (Benlagha et al., 2002). However, the additional requirements for later maturation of thymic resident iNKTs are not well understood.

As mentioned in section 1.1.3.1. ($CD4^+$ Helper T Cells), Tregs are important to maintain immune homeostasis and prevent autoimmune disease. nTregs are found in the medulla. Thus, the medullary mTECs and DCs are considered as key cellular components for generating nTregs. However, recent studies show the major role of mTECs in the generation of nTreg (Aschenbrenner et al., 2007; Cowan et al., 2013). Immature SP4 thymocytes give rise into either conventional $CD4^+$ αβT cells or nTreg in the medulla. In the condition of absent medulla, conventional $CD4^+$ αβT cells have normal maturation but the development of nTregs is severely defected (Cowan et al., 2013). Overall, the thymus provides microenvironment for the development of conventional αβT cells and it is also required to produce non-conventional T cells such as iNKTs and nTregs.

1.3. Development Of The Thymus

1.3.1. Thymus Organogenesis

1.3.1.1. Origin Of The Thymus

The thymus sits in the anterior mediastinum in the chest cavity, in front of the heart and behind the sternum. During mouse embryogenesis, the thymus develops from the third pharyngeal pouch and it shares a common primordium with the parathyroid. For many years, it was thought that both the ectoderm and endoderm layers of the third pharyngeal pouch and cleft contribute to the thymic epithelium. This assumption had been suggested from the observation of physical contact between pharyngeal endoderm and ectoderm during early embryonic development. Furthermore, this idea led to the proposal of 'dual-origin' model, in which mTECs are generated from the endoderm and cTECs are originated from the ectoderm (Cordier and Haumont, 1980; Cordier and Heremans, 1975). This model was tested in experiments grafting the third pharyngeal endoderm of E9.5 embryos and the third pharyngeal ectoderm of E10.5 embryos separately under the kidney capsule of athymic nude mice. Only the endoderm-grafted tissue developed into both cTECs and mTECs (Gordon et al., 2004). Moreover, the endoderm-grafted tissues contained the subsets of thymocytes, confirming their capability of T-cell production. In contrast, the ectoderm-grafted tissue failed to develop normal thymic histology and generate T cells. Overall, this validates the notion that endoderm of third pharyngeal pouch solely gives rise to the thymic epithelium. However, the endoderm-grafted tissues showed reduced cellularity compared to adult thymus, suggesting that support from ectoderm may be needed for normal thymic cellularity (Gordon and Manley, 2011; Gordon et al., 2004).

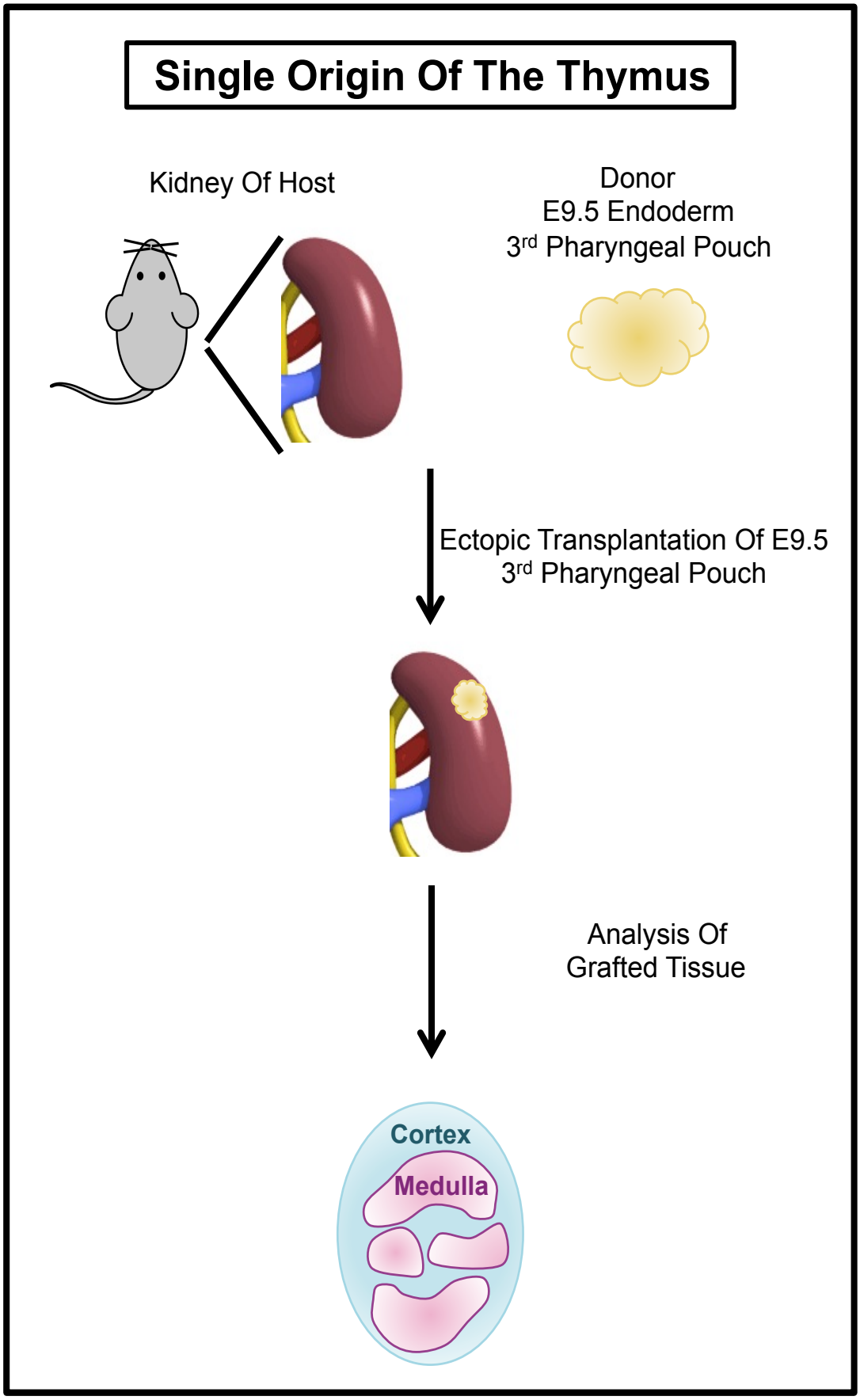

Single Origin Of The Thymus
Kidney Of Host
Donor
E9.5 Endoderm
3rd Pharyngeal Pouch
Ectopic Transplantation Of E9.5
3rd Pharyngeal Pouch
Analysis Of
Grafted Tissue
Cortex
Medulla

Figure 1.4. Origin of the thymus

Ectopic transplantation of the third pharyngeal endoderm of E9.5 embryos proves the single origin of the thymus.

1.3.1.2. Molecular Regulation In Thymus Organogenesis

Several transcription factors are involved in thymus organogenesis. A sequential process, controlled by four different groups of transcription factor, must occur to complete normal thymus development. The first group of molecules important for pharyngeal pouch formation includes paired box 1 (Pax1), Pax9, and T-box 1 (Tbx1). A mutation affecting those three genes interrupts the formation of pharyngeal pouches at E9.5. In addition to the three transcription factors, the deletion of fibroblast growth factor 5 (Fgf5) also leads to the disruption of pharyngeal pouch formation. The second group includes homeobox A3 (Hoxa3), which is needed for normal pouch development and is specific for the endoderm of third pharyngeal pouch (Blackburn and Manley, 2004; Peters et al., 1998; Rodewald, 2008). At E11, the third group of transcription factors, the network of Hoxa3, eye absent homolog 1 (Eya1), Pax1/9, and sine oculis homolog 1/4 (Six1/4), promotes the outgrowth of pouch rudiment (Peters et al., 1998).

Between E11.5 And E12.5, the further outgrowth and pattering of thymic rudiments occur. The patterning of third pharyngeal pouch region is regulated by the fourth group of transcription factors: forkhead box N1 (FoxN1) and the mouse homolog of the Drosophila transcription factor Glial Cells Missing (Gcm2). FoxN1 is a skin and a thymus specific marker required for TEC proliferation and differentiation, and its expression starts at E11 (Gordon et al., 2001; Nehls et al., 1996). Gcm2 is a parathyroid specific marker and its expression initiates around E9.5 in a discrete domain within the endoderm (Blackburn and Manley, 2004; Rodewald, 2008). The expression of FoxN1 and Gcm2 is regulated by distinctive transcription factors. Bone morphogenic protein 4 (Bmp4) expression is found prior to FoxN1 expression and Bmp signaling is known to be required for the maintenance of FoxN1 expression (Bleul and Boehm, 2005; Tsai et al., 2003). However whether Bmp4

signaling initiates FoxN1 expression during thymus organogenesis has not been defined. Moreover, the expression of wingless-int 4 (Wnt4) is also detected prior to that of FoxN1 but there is no clear evidence showing that these two transcription factors directly control and specify thymus fate (Balciunaite et al., 2002). Besides, sonic hedgehog (Shh) promotes the differentiation of pharyngeal pouch endoderm into an parathyroid fate and it acts as a negative regulator of thymus fate (Gordon and Manley, 2011).

There is a timing gap between the initial expression of FoxN1 and Gcm2. Thus, it has been assumed that there could be another transcription factor regulating thymus development prior to initial FoxN1 expression (Wei and Condie, 2011). As explained in the previous section, the ectopic transplantation of E9.5 third pharyngeal pouch endoderm results in normal thymic histology, confirming the sufficient intrinsic capability of TEC development by this stage (Gordon et al., 2004). Moreover, a recently published paper suggests possible candidates of additional transcription factors that may regulate early thymus development: forkhead box G1 (FoxG1) and islet 1 (Isl1). These two genes are expressed from E9 within the part of third pharyngeal pouch endoderm, which is negative for Gcm2. FoxG1 and Isl1 expression on TECs persist through postnatal stage. This analysis of expression pattern suggests that FoxG1 and Isl1 might have a role in TEC differentiation but this should be more thoroughly examined (Wei and Condie, 2011).

At E12.5, the network of Hoxa3-Pax-Eya-Six signaling is thought to aid the separation of the thymus and parathyroid rudiments from the pharynx because such separation does not occur in Pax9 deficient mice and it is delayed in the Pax1/Hoxa3 disrupted mice (Hetzer-Egger et al., 2002; Su et al., 2001). Instead of the direct control of Hoxa3-Pax-Eya-Six network in this separation, this defect may result from defects at earlier developmental stages that involve the outgrowth of the thymus rudiment at E11 (Peters et al., 1998). Around E13.5,

the physical separation of the thymus from parathyroid is usually complete. The separation of thymus from pharynx and parathyroid is mediated by cellular regulation that will be discussed in the next section.

1.3.1.3. Cellular Regulation In Thymus Organogenesis

Other than the transcription factors described above, the interaction of endoderm-derived epithelium with both ectoderm-derived neural crest mesenchyme and mesoderm-derived hematopoietic cells is crucial for thymus organogenesis (Gill et al., 2003; Manley, 2000). Before thymic colonization by hematopoietic cells, signals from neural crest-derived mesenchyme must be provided for early thymus organogenesis. Neural crest cells (NCCs) migrate into the third pharyngeal pouch, surround the pouch, and then form the thymic mesenchyme (Le Lievre and Le Douarin, 1975). The role of NCC-derived mesenchyme in thymus organogenesis has been investigated in studies using Splotch mutant mice (Pax3-null). NCCs express Pax3, which is responsible for the migration of NCCs to pharyngeal pouches. Thus, mutation of Pax3 causes the failure of NCC-derived mesenchyme formation (Conway et al., 1997; Epstein et al., 2000). Thus, while Pax3 mutant mice have normal organ-fate specification of the third pharyngeal pouch, they show delayed separation of thymus and parathyroid from the pharynx. Moreover, there is a shift in the boundary between two organs, collectively resulting in ectopically placed thymus (Gordon and Manley, 2011; Manley, 2000).

In addition to the role of mesenchyme in thymic positioning, the mesenchyme is also involved in the proliferation of embryonic TEC progenitors. It is known that the capability of embryonic TECs to proliferate reduces with the increasing gestational age (Anderson et al., 1998; Jenkinson et al., 2003). In order to study the role of mesenchyme in early embryonic TEC proliferation, freshly dissected E12 thymus lobes were treated with collagenase D to s

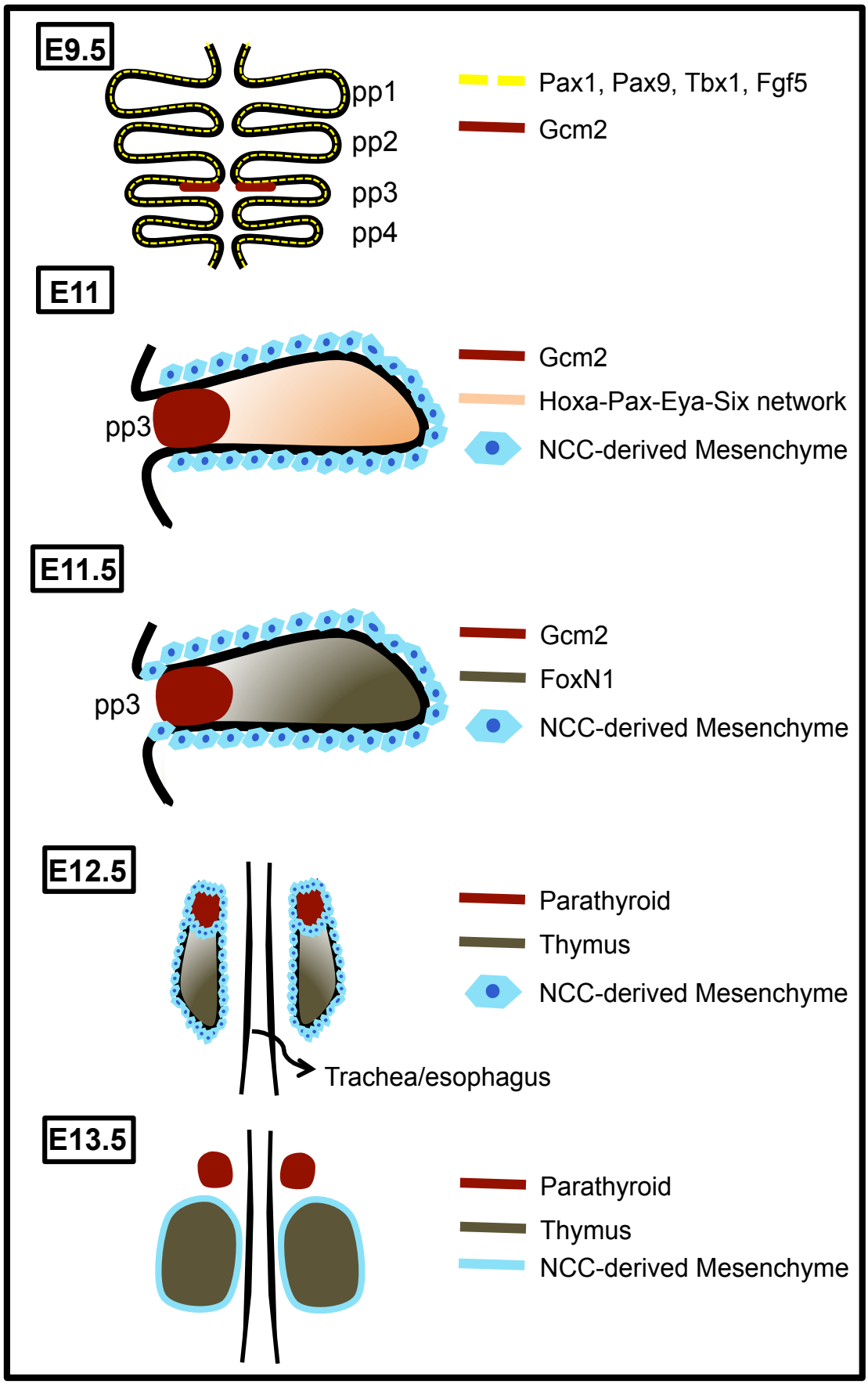

E9.5
pp1
pp2
pp3
pp4
Pax1, Pax9, Tbx1, Fgf5
Gcm2
E11
pp3
Gcm2
Hoxa-Pax-Eya-Six network
NCC-derived Mesenchyme
E11.5
pp3
Gcm2
FoxN1
NCC-derived Mesenchyme
E12.5
Parathyroid
Thymus
NCC-derived Mesenchyme
Trachea/esophagus
E13.5
Parathyroid
Thymus
NCC-derived Mesenchyme

Figure 1.5. Overview of thymus organogenesis

Molecular and cellular regulations important in thymus organogenesis at different stage are presented. At 9.5, the pharyngeal pouch formation occurs and it is controlled by Pax1, Pax9, Tbx1, and Fgf5. At E11, the network of Hoxa3, Eya1, Pax1/9, and Six1/4 promotes the outgrowth of third pharyngeal pouch rudiment. Between E11.5 And E12.5, the further outgrowth and pattering of thymic rudiments occur. The patterning of third pharyngeal pouch region is regulated by FoxN1 and Gcm2. FoxN1 expression starts at E11 and Gcm2 expression initiates around E9.5 in a discrete domain within the endoderm. NCC-derived mesenchyme provide signal required for separation of thymus and parathyroid from the pharynx at E12.5. Around E13, the separation between thymus and parathyroid occurs.

trip off the outer mesenchyme from the thymus and then the E12 thymus with/without mesenchyme was cultured for overnight. After culture, decreased proliferation was found in E12 thymus without mesenchyme compared to E12 thymus with mesenchyme (Jenkinson et al., 2003). Particularly, the contribution of FGF7/FGF10 signaling to TEC proliferation was further examined because of the hypoplastic thymus in the mice lacking FGF-R2IIIb, a receptor for FGF7 and Fgf10. Moreover, FGF7 and FGF10 are expressed by the mesenchyme and FGF-R2IIIb is expressed on TECs and mesenchyme. (Revest et al., 2001). When E14 TECs were stimulated with recombinant FGF7/FGF10, compared with control samples, proliferation was increased in FGF-treated TEC, indicating that mesenchyme directly controls embryonic TEC proliferation via Fgf7/Fgf10 signal. However, the differentiation of embryonic TECs was independent of the mesenchyme and it was even functional for T-cell development in the absence of mesenchyme (Jenkinson et al., 2003).

The mesoderm-derived hematopoietic cells colonize the thymus from E11.5. The thymus is essential for T-cell development and developing thymocytes are also crucial for thymus development. Studies with mutant mice with defects in several genes, that are intrinsically critical for T-cell development, revealed how developing thymocytes affect TEC organization and proliferation at different stages (Gill et al., 2003). For example, either CD3ε transgene expression or RAG1/2 deficiency results in the complete block of T-cell development at DN stages and consequently leads to a failure in developing normal thymic architecture due to the lack of crosstalk with thymocytes (Hollander et al., 1995; Mombaerts et al., 1992; Roberts et al., 2009; Shinkai et al., 1992). While abnormal cortex and medulla are found in such mutant mice, an arrest at DP stage of T-cell development causes the loss of medulla but unaltered cortex. In *Tcra*$^{-/-}$ mice that fail to generate αβ TCR expressing SP thymocytes, T-cell development is blocked at DP stage and only cortical epithelium is found

(Palmer et al., 1993). Despite an understanding of the requirement of normal thymocyte development for normal cTEC development, the molecules regulating this process are not clear. After positive selection, SP thymocytes migrate into the medulla and they provide signals for mTEC proliferation and differentiation. This will be more discussed in section 1.3.2.3. (mTEC development and Their Role In Central Tolerance). Collectively, the development of thymocytes and TECs is interdependent. The crosstalk between developing thymocytes and TECs is indispensible and is initiated as soon as the hematopoietic precursors colonize the embryonic thymus.

1.3.2. TEC Development

1.3.2.1. Identification Of TEC Progenitors

The presence of both cTEC and mTEC compartments is essential for normal T-cell development. However, TEC development is poorly understood because of the limited experimental models and tools. One of the reasons that make it difficult to study TEC development is the relative lack of availability of markers identifying TEC progenitors during the pathways of cTEC and mTEC development.

The phenotype of adult cTEC is $K5^{-}K8^{+}$ and the phenotype of adult mTEC is $K5^{+}K8^{-}$ but early embryonic TECs express both Keratin-5 (K5) and Keratin-8 (K8). The observation of K5 and K8 co-expression in embryonic TECs had led to the notion that two different lineages of TEC might develop from a common progenitor (Rodewald, 2008). This idea has been tested by clonal analysis. At the age of E12, the TEC population is homogeneous according to the expression of EpCAM and MTS24. A single epithelial cell gated on $EpCAM^{+}MTS24^{+}$ was sorted from E12 total TEC that is genetically labeled with enhanced yellow fluorescent protein (eYFP) (Rossi et al., 2006). The sorted single cell was microinjected into a WT E12 thymus lobe, which was grafted under the kidney capsule to

analyze further development. eYFP was used to trace the microinjected cell and eYFP positive TECs were found in both cortex and medulla, demonstrating that the injected cell had successfully proliferated and differentiated into both cTEC and mTEC (Rossi et al., 2006). This idea that the bipotent progenitor can give rise to both cTECs and mTECs was also demonstrated by a lineage tracing experiment (Bleul et al., 2006). Consequently, this supports 'single thymic origin' model that only third pharyngeal pouch endoderm gives rise to the thymus.

The studies by Bennett *et al* and Gill *et al* tested whether the MTS24 expression exclusively marks TEC progenitor. Both Bennett *et al* and Gill *et al* demonstrated that only $MTS24^+$ cells of embryonic thymus could differentiate into both cTECs and mTECs but $MTS24^-$ cells could not (Bennett et al., 2002; Gill et al., 2002). However, the progenitor capability of $MTS24^-$ cells was re-tested by Rossi *et al*. Within $EpCAM^+$ TEC population, the heterogeneity starts to appear at E14 according to the expression of MTS24 (Rossi et al., 2007a). After E16, the most of $EpCAM^+$ TECs lose the MTS24 expression. Therefore, $EpCAM^+MTS24^+$ and $EpCAM^+MTS24^-$ TECs of E14 were sorted and then used to make reaggregate thymic organ culture (RTOC). RTOCs were grafted under the kidney capsule of host mice for further development. Normal thymic architecture including cTECs and mTECs was found in the grafts of both $EpCAM^+MTS24^+$ and $EpCAM^+MTS24^-$ RTOCs. Thus, this disproves the MTS24 as a progenitor marker (Rossi et al., 2007a). The discrepancy between studies might result from different pre-gating strategy for the cells of interest. Rossi *et al* pre-gated the targeted cells with EpCAM that eliminates any contamination of non-epithelial cells. However, the analysis by Bennett *et al* missed the pre-gating step and Gill *et al* only gated out $CD45^+$ cells (hematopoietic cells), which still left the possibility of contamination

by mesenchyme. Collectively, the incapability of MTS24$^-$ cells as TEC progenitors shown by Bennett *et al* and Gill *et al* needs to be further investigated.

Despite these findings, many questions about TEC progenitors and their development remain still unanswered. First, it has not been proven whether the developmental pathway from bipotent progenitor to lineage-committed TECs, cTECs and mTECs, is bi-directional or serial. Current understanding about TEC development is based on a simple binary model that cTEC and mTEC development are separate and there is no relation between two lineage developments. However, the differential stages from progenitors to cTECs and/or mTECs require further analysis. Second, the initial appearance of cTEC and mTEC lineages during development requires examination, because it is not clear whether both lineages appear simultaneously or not. Third, there is no reliable marker that can classify TEC progenitors in the early embryo. If there were markers identifying TEC progenitors, it would be much easier to understand the process of TEC development from bipotent progenitors to mature cTEC/mTEC lineages, which may help future projects to regenerate thymic tissues.

1.3.2.2. cTEC Development And Their Role In Positive Selection

cTECs are classified by the markers K8, ERTR4, CD205, and Ly51. In addition to those markers, cTEC exclusively express β5t and prss16, which are required for positive selection of DP thymocytes (Gordon and Manley, 2011). Moreover, CD40 and MHC class II are known maturation markers and are expressed by both cTECs and mTECs. The ontogeny of cTECs was investigated by using cTEC specific markers and maturation markers (Shakib et al., 2009). The acquisition of CD205 and β5t expression occurs at E12 and it relies on the expression of FoxN1. At the age of E12, putative immature cTECs, with a CD40$^-$CD205$^+$ phenotype, start to appear, which then acquire CD40 expression around E14. At E15, there are three distinct TEC populations: subset 1 (CD40$^-$CD205$^-$), subset 2 (CD40$^-$CD205$^+$), and

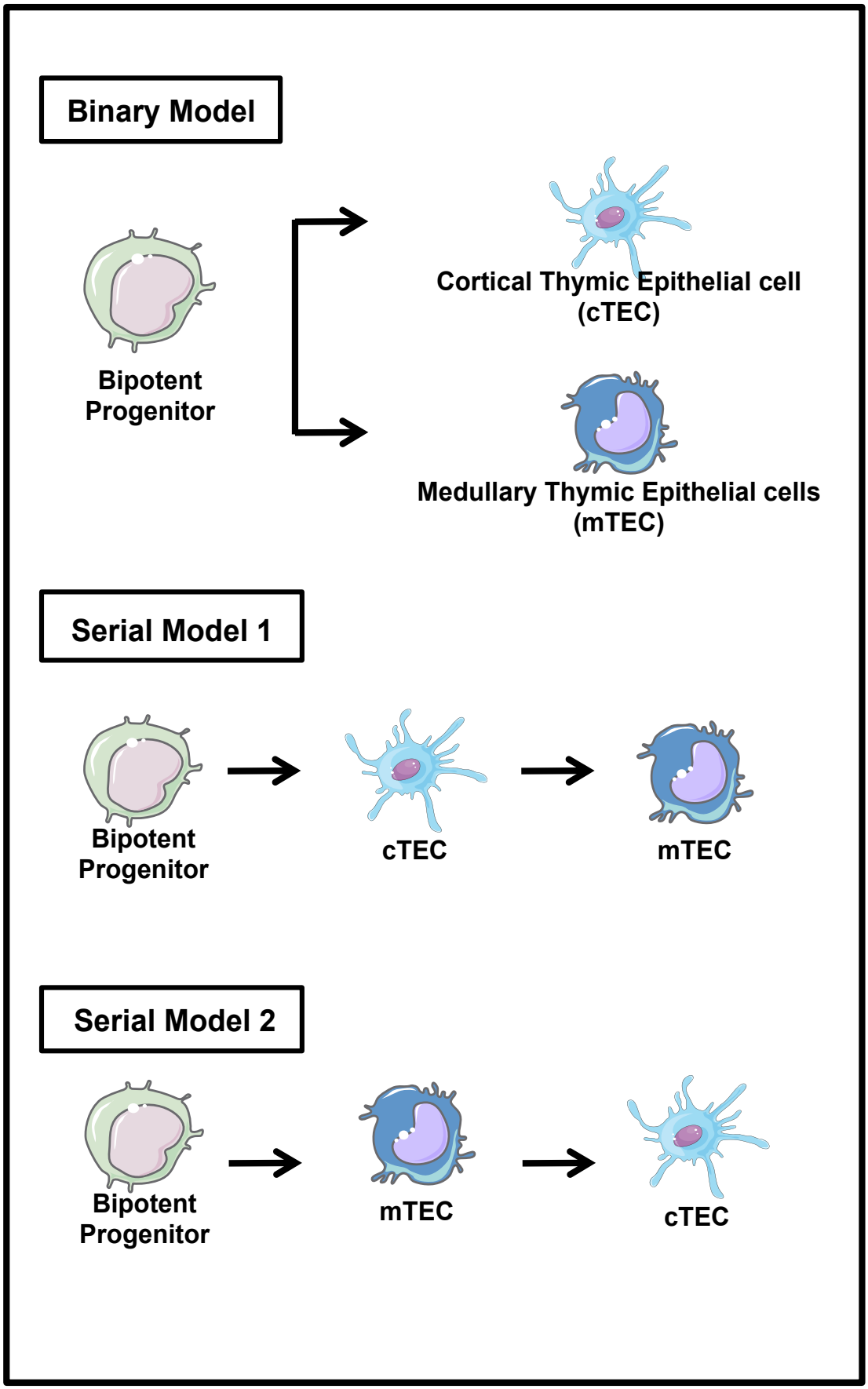

Binary Model
Bipotent Progenitor
Cortical Thymic Epithelial cell (cTEC)
Medullary Thymic Epithelial cells (mTEC)
Serial Model 1
Bipotent Progenitor
cTEC
mTEC
Serial Model 2
Bipotent Progenitor
mTEC
cTEC

Figure 1.6. Models of thymic epithelial cell development

In binary model, bipotent TEC progenitors give rise to cTEC and mTEC simultaneously via independent pathways. On the contrary, in serial model either lineage develops first from TEC progenitors and then the lineage committed-TECs give rise to another TEC lineage. For example, TEC progenitor differentiates into phenotypically defined cTECs and then the cTECs develop into mTECs.

subset 3 ($CD40^{+}CD205^{+}$). The expression of another maturation marker, MHC class II, was investigated within those three populations. MHC class II expression was found in both subset 2 and subset 3 but not in subset 1. This shows that the acquisition time of MHC class II expression lies in between that of CD40 and CD205 expression (Shakib et al., 2009).

CD205 (also known as DEC205) is an endocytic receptor and is expressed on cTECs and DCs (Jiang et al., 1995). Its functional role in positive selection was analyzed by using the mice deficient CD205 expression. As explained earlier, thymocytes are selected by recognizing self-peptide (endogenously derived-self antigen) bound on MHC class I/II during positive and negative selections. However, it has been suggested that CD205 internalizes the exogenous protein from dead thymocytes to prepare self-peptide (exogenously derived-self antigen) loading on MHC class I/II for positive selection. Normal T-cell development and no defect in thymic selection were found in the mice lacking CD205 expression (Jenkinson et al., 2012). This implies that CD205 has a redundant role with any other endocytic receptor expressed on cTECs for positive selection or the exogenously derived-self antigens are not used during positive selection (Jenkinson et al., 2012). Unlike the understanding of mTEC development, there is limited understanding about cTEC development. For example, there is no marker that can define the heterogeneity within cTEC population other than the maturation markers.

1.3.2.3. Development Of mTEC And Their Role In Central Tolerance

mTECs are identified by markers such as K5, keratin-14 (K14), Ulex Europeaus Agglutinin-1 (UEA-1), ERTR5, and MTS10 (Farr and Anderson, 1985; Godfrey et al., 1990; Van Vliet et al., 1984). Additionally, mTECs can be subdivided into three subsets based on the expression of CD40, MHC class II, CD80, and Aire. CD40 and MHC class II are also expressed on cTECs, but the expression of CD80 and Aire is unique to mTECs. Using these

markers, the three mTEC subsets are $mTEC^{Low}$ ($MHCII^{Low}CD80^{-}Aire^{-}$), $mTEC^{High}$ ($MHCII^{High}CD80^{+}Aire^{-}$), and $Aire^{+}$ mTECs ($MHCII^{High}CD80^{+}Aire^{+}$). The observation that $CD80^{+}$ mTECs first appear at E16 of gestation, and the up-regulation of *Aire* gene expression within mTECs after E16 led to the idea of linear mTEC development from $mTEC^{Low}$ to $Aire^{+}$ mTECs (Gabler et al., 2007). This was directly confirmed by precursor-product experiments; isolated $CD80^{-}Aire^{-}$ mTECs developed into $CD80^{+}Aire^{+}$ mTECs when placed in culture (Gabler et al., 2007). Nevertheless, it was not clear whether the acquisition of Aire expression by mTECs is followed by apoptosis, as a consequence of developmental termination. Recent studies have shown that $Aire^{+}$ mTECs down-regulate both Aire and CD80 expression and then start to express Involucrin, which marks the terminally differentiated epithelium including keratinocytes and Hassalls Corpuscles (Nishikawa et al., 2010; White et al., 2010). Moreover, Aire deficient mice have a lower number of $Involucrin^{+}$ mTECs, suggesting a possible role for Aire in mTEC terminal differentiation with the induction of Involucrin expression (Yano et al., 2008). The number of $Involucrin^{+}$ mTECs is low in the adult thymus of wild type and it is not easy to isolate $Involucrin^{+}$ mTECs for further analysis (White et al., 2010). This might be due to that $Involucrin^{+}$ mTECs have short lifespan resulting in the efficient clearance of a terminally differentiated cell population. A subset of post-Aire mTEC within $mTEC^{Low}$ ($MHCII^{Low}CD80^{-}Aire^{-}$) population was also identified by using Aire fate-mapping mice (Metzger et al., 2013). Furthermore, the post-Aire mTECs have lower expression of TSAs compared to $Aire^{+}$ mTECs and Tregs are absent when both $Aire^{+}$ mTECs and post-Aire mTECs are deleted in postnatal state, suggesting a direct role of post-Aire mTECs in induction of Tregs rather than in negative selection (Metzger et al., 2013).

As mentioned earlier, the interaction between developing thymocytes and TECs is reciprocal and indispensable for normal thymus development and function. The depletion of

hematopoietic cells by sub-lethal irradiation causes severe defects in the thymic medulla (Adkins et al., 1988). In later studies, Severe Combined Immunodeficiency (SCID) mice reconstituted with hematopoietic cells resulted in a rescue of the disorganized thymic medulla, demonstrating the important cellular regulation of developing thymocytes in TEC development (Shores et al., 1994). For the medulla development, SP thymocytes expressing αβTCR are crucial (Palmer et al., 1993; Shores et al., 1994). The differentiation from DP to SP thymocytes causes the up-regulation of eight Tumor Necrosis Factor Super Family (TNFSF) members: TNFα, FasL, LTα, LTβ, CD30L, OX40L, CD40L, and RANKL (Hikosaka et al., 2008). The receptors to TNFSF members belong to the Tumor Necrosis Factor Receptor Super Family (TNFRSFs). Among those, RANK (TNFRSF11a), CD40 (TNFRSF5), and Lymphotoxin β Receptor (LTβR, TNFRSF3) are expressed by mTECs and are known to be up-stream of NF-κB signaling (Hikosaka et al., 2008). It has been suggested that mTEC development relies on the regulation of NF-κB signaling because the mutations in genes involved in downstream of NF-κB signaling, such as RelB, TRAF6, and NIK, causes a severe defect in mTEC development (Akiyama et al., 2005; Burkly et al., 1995; Heino et al., 2000; Kajiura et al., 2004; Weih et al., 1995). Therefore, many studies have further investigated the different roles of RANK, CD40, and LTβR in mTEC development.

It has been reported that RANK/RANKL interaction is responsible for differentiation and homeostasis of $Aire^+$ mTECs (Rossi et al., 2007b). In the absence of RANK expression, there is a severe reduction in $CD80^+$ and $Aire^+$ mTEC population of adult thymus, subsequently resulting in autoimmunity. However, the architecture of mTECs expressing K5 is not affected by RANK deficiency (Rossi et al., 2007b). During embryogenesis, $Aire^+$ mTECs appear prior to the emergence of mature SP thymocytes that can provide RANKL signals. Additional cell populations, including $ROR\gamma t^+$ Lymphoid Tissue Inducer (LTi) cells

and invariant Vγ5^{+} Dendritic Epidermal T Cell (DETC) progenitor, also express RANKL and start to appear before mature SP thymocytes appear during embryogenesis (Roberts et al., 2012; White et al., 2008). Thus, RANKL signals provided by LTi cells and DETC progenitors induce initial Aire expression in fetal thymus (Rossi et al., 2007b; White et al., 2008). In contrast, mice lacking CD40 expression show only a mild impairment in mTEC development compared to RANK deficient mice, the double deficiency of CD40 and RANK resulting in more severe defects than either single deficient mice (Akiyama et al., 2008). Several studies have confirmed that while the induction of Aire expression is not dependent on CD40/CD40L, the maintenance of Aire^{+} mTECs requires both RANK/RANKL and CD40/CD40L interactions in adult thymus (Akiyama et al., 2008; White et al., 2008).

Unlike the higher expression of RANK on mTECs than cTECs, the level of LTβR expression on mTECs is comparable to that of cTECs (Hikosaka et al., 2008). Therefore, studies using LTβR deficient mice do not show the direct effect of LTβR deficiency in mTECs and it is not clear which phenotype properties of LTβR$^{-/-}$ mice are linked to the absence of LTβR expression in either mTECs or cTECs. However, the ligands of LTβR, LTα and LTβ, are predominantly expressed by medullary resident SP thymocytes and not cortical resident DP thymocytes, suggesting much of the thymic phenotype of LTβR$^{-/-}$ mice maps to a medullary defect (Boehm et al., 2003; Hikosaka et al., 2008). LIGHT is an additional ligand that binds LTβR and it is also expressed by SP thymocytes. The impairment in mTEC development is more severe in LTβR$^{-/-}$ mice compared to mice with double deficiency in LTα$^{-/-}$LIGHT$^{-/-}$ and LTβ$^{-/-}$LIGHT$^{-/-}$ (Boehm et al., 2003; Mouri et al., 2011). This discrepancy might be caused by additional unknown LTβR ligands. In addition, involucrin^{+} mTECs are absent in LTβR$^{-/-}$ mice, suggesting its role in induction of involucrin expression on mTECs (White et al., 2010). Recently, it has been demonstrated that CCL21 expression marks the late

stage of mTEC development like the expression of involucrin. Similar to involucrin^{+} mTECs, the lower frequency of CCL21^{+} mTECs in LTβR$^{-/-}$ and Aire$^{-/-}$ mice was found (Lkhagvasuren et al., 2013). While it is known that the signal via LTβR, possibly with Aire, plays major role in post-Aire mTEC development by regulating both involucrin and CCL21 expression, the heterogeneity in late mTEC population (Aire^{Low}CD80^{Low} mTECs) according to the expression of involucrin and CCL21 in mTECs requires further investigation.

One of the reasons linked to the onset of autoimmunity is the failure to acquire self-tolerance during T-cell development. Positively selected SP thymocytes spend about 4-5 days in the medulla where they are screened for potential auto-reactivity (McCaughtry et al., 2007). Thymocytes, which recognize TRAs expressed by mTECs, undergo negative selection by apoptosis to prevent these cells leaving the thymus and promoting the development of multi-organ autoimmune diseases. The expression of a wide range of TRAs is controlled by transcriptional regulator Aire (Liston et al., 2003). However, not all TRA expression in mTECs is regulated by Aire. There are two different categories of TRAs: Aire-dependent TRAs and Aire-independent TRAs that are expressed by mTECs. For example, Aire-dependent TRA genes are *Insulin 2*, *Salivary Protein 1* (*SAP1*), and *Casein* α, and Aire-independent TRA genes include *C-reactive Protein* (*CRP*), *Glutamate Decarboxylase 67* (*GAD67*), and *Casein* β (Derbinski et al., 2005; Yano et al., 2008). It is still uncertain how intra-thymic TRA expression is separately regulated by Aire-dependent or Aire-independent manner. Besides, it has been recently shown how Aire controls the gene expression. To efficiently regulate a large array of TSA expression, Aire utilizes non-classical transcription factor and unusual way of promoter binding (Abramson et al., 2010).

1.3.3. Thymic Atrophy

1.3.3.1. Ageing And Thymic Atrophy

The thymus is capable of producing T cells throughout life but with advancing age the amount of T-cell output starts to decrease (Gruver et al., 2007). In human, it is reported that thymic involution starts after birth and that there is significant reduction of thymic mass observed after puberty (George and Ritter, 1996). Approximately 3% of thymic tissue continues to reduce annually until middle age. Empty space is filled with adipocytes causing a dramatic drop of thymocytes in the thymus (George and Ritter, 1996). Thymic atrophy also occurs in the mice; the thymus of old mice (12 month old) holds less than 1% of T cells in newborn thymus (Taub and Longo, 2005). In contrast, the size of the peripheral T cell pool is maintained by continuously proliferating mature T cells. However, there are higher chances of succumbing to infections in the elderly because of less diverse TCR repertoire resulting from the reduction in naïve T-cell production by the thymus (Hulstaert et al., 1994; Taub and Longo, 2005).

It had been thought that the decreased production in naïve T-cells might be caused by an intrinsic problem in seeding lymphoid progenitor cell populations from bone marrow (Gruver et al., 2007; Min et al., 2006). To address this, early thymic progenitors from aged or young mice were separately seeded into fetal thymic organ culture (FTOC), less proliferation and differentiation were found in FTOC with aged early thymic progenitors compared to FTOC with young early thymic progenitors (Min et al., 2004). Moreover, higher apoptosis was observed in aged thymic progenitors (Heng et al., 2005). However, there are also evidences arguing against a possible intrinsic defect in hematopoietic cells that causes thymic atrophy. When fetal thymus was grafted into aged or young mice, a similar repopulation of grafted-thymus lobe by aged and young host cells and a similar T-cell development within

grafted-thymus were observed (Gui et al., 2007; Zhu et al., 2007). Therefore, it is still controversial whether aged-associated thymic atrophy is resulted from the intrinsic defect in hematopoietic cells. Hence, it is questioned that the thymic intrinsic change with ageing is related to thymic atrophy. In order to investigate whether thymic involution is caused by a thymic stromal problem, bone marrow cells from young mice were administered into old host mice but the donor cells failed to regenerate thymic tissues. This shows that thymic involution is resulted from stromal problem (Mackall et al., 1998). Collectively, age-associated thymic atrophy is thought to be caused at least in part by a thymic stromal defect, rather than simply intrinsic problems in the thymus seeding cell populations.

Age-associated thymic size reduction is accompanied with the phonotypical and morphological changes in the thymus; the smaller area of both $CD205^+$ cTECs and UEA-1^+ mTECs were found in old mice compared to that in young mice (Aw et al., 2009). Moreover, not only the quantity of T-cell production by thymus reduces but also the quality of peripheral T cells is affected with ageing (Aw et al., 2010). Less spontaneous or induced apoptosis of thymocytes in old mice was found, suggesting inefficient positive and negative selection during T-cell development (Aw et al., 2010). Overall, ageing results in the qualitative alteration of TECs and T cells as well as the quantitative change of thymic size and T-cell pool. However, it is not known whether the changes in TECs and thymocytes occur at the same time or one change leads to another alteration with ageing.

Since puberty leads to a massive reduction of thymic tissue, the increased level of steroid hormones is speculated as a main cause (Hince et al., 2008). Moreover, thymic rebound was observed following chemical or surgical castration resulting in sex-steroid ablation (SSA) (Min et al., 2006; Olsen et al., 2001). However, a natural decrease in sex-

steroid with ageing does not appear to recover thymic size (Gruver et al., 2007) and so it is still not clear how sex-steroids relate to the thymic atrophy.

1.3.3.2. Harnessing TEC Progenitors For Thymus Regeneration

In order to combat thymic atrophy, many efforts to regenerate thymic epithelium have been made both in vivo and vitro (Jenkinson et al., 2008; Liu et al., 2013; Zook et al., 2013). The one of most promising therapeutic strategies to regenerate damaged tissues including liver, lung, and heart is cell therapy using embryonic stem cells (ESCs) (McIntyre et al., 2013; Pfister et al., 2013; Streckfuss-Bomeke et al., 2013). Same approach has been employed to recapitulate thymic tissue in vitro.

As the anterior foregut endoderm (AFE), which is originated from definitive endoderm (DE), develops into the pharyngeal endoderm that gives rise to the thymus, many efforts to find exogenous signals that can direct sequential differentiation from ESCs to DE, AFE, and then the pharyngeal endoderm have been made, mimicking the embryonic developmental stages (Green et al., 2011; Kearns et al., 2013; Parent et al., 2013; Sun et al., 2013). Kearns *et al* used $Sox17^{GFP}$ and $Pax9^{venus}$ reporter ESC lines to generate TEC progenitors in vitro; Sox17 expression is only found in DE and Pax9 expression is specific to pharyngeal endoderm. If there are any $Sox17^{GFP+}$ and $Pax9^{Venus+}$ cells after the induced differentiation, this suggests the successful generation of DE and the pharyngeal endoderm from stem cells in vitro. $Sox17^{GFP+}$ DE and $Pax9^{Venus+}$ AFE cells were found after culture with certain regulators and then checked further for DE, AFE, and pharyngeal endoderm specific markers (Kearns et al., 2013). To ascertain the capability of the ESC-derived AFE or TEC progenitors to further develop in vivo, the cells were either injected into thymus or grafted under the kidney capsule (Kearns et al., 2013; Lai et al., 2011; Parent et al., 2013). In vitro-derived AFE, which was grafted under the kidney capsule, was differentiated into epithelial

cells of pharynx, esophagus, and salivary glands, but not the third pharyngeal pouch derivatives including $FoxN1^+$ thymus and $Gcm2^+$ parathyroid (Kearns et al., 2013). This shows that the directed differentiation of ESCs to AFE in vitro is not enough for thymic lineage specification.

Recently, Parent *et al* has succeeded in the generation of TEC progenitors from human embryonic stem cells (hESCs) in vitro, demonstrating sequential regulation of retinoic acid (RA), TGFβ, Wnt3a, BMP4, Fgf8b, and Shh signals (Parent et al., 2013). There were four serial stages of exogenous signal regulation to generate TEC progenitors from hESCs. At the final stage, the expression of Hoxa3, Eya1, FoxN1, and EpCAM in cells was checked for the efficient generation of TEC progenitors from hESCs. The TEC progenitors were grafted under the kidney capsule of athymic nude mice to test the developmental potential of hESCs-derived TEC progenitors in vivo and the capability of T cell production. The normal thymic architecture with $K8^+$ cTECs and $K5^+$ mTECs was found in the graft. However, Aire expression in the grafted was not detected which implies the defects of hESC-derived TEC progenitors in the maturation of mTECs. Moreover, T cells were found in the periphery but with lower TCR diversity and lower level of TCR activation-associated proliferation (Parent et al., 2013). One possible explanation of lacking Aire expression on mTECs and causing functional problems in T cells is xenogeneic thymic microenvironment.

Sun *et al* used a three-step protocol to generate TEC progenitors form hESCs instead of four-step protocol and in vitro-derived TEC progenitors were grafted under the kidney capsule of athymic nude mice with human embryonic fibroblasts (HEFs) to provide mesenchymal support (Sun et al., 2013). Aire expressing TECs and developing thymocyte subsets including $FoxP3^+$ Tregs were found in the grafts (Sun et al., 2013). While there are successes of generating thymic tissues from ESCs, it is still limited in the context of future

therapeutic strategies. For example, it is not clear whether the transplanted cells are capable of self-renewal with or without support from other tissues such as mesenchyme to maintain and expand its size. Moreover, the quality of T cells produced by the transplanted tissue has to be thoroughly analyzed for the responsiveness to foreign antigens with self-tolerance. Furthermore, even though ESCs allows numerous applications for future therapy, it is not the best candidate for cell therapy due to ethical issues and immune rejection. Therefore, induced pluripotent stem cells (iPSCs) were investigated to regenerate thymic tissues in this study.

CHAPTER 2. General Methods And Materials

2.1. Mice

Biomedical Services Unit (BMSU) of the University of Birmingham is in charge of breeding and housing of the mice used in this study. All mice handling follows Home Office Regulations. The day of vaginal plug detection was considered as Day 0 (D0) of gestation and the average gestation period of mice is approximately 20 days. In addition to wild type mice, a key mouse strain used in this study is the FoxN1-eGFP transgenic reporter line. This reporter mouse strain (FoxN1:eGFP) was created for better and easier identification of early embryonic thymic epithelium (Terszowski et al., 2006). Expression of the enhanced Green Fluorescent Protein eGFP transgene in FoxN1:eGFP mice is driven by FoxN1 regulatory sequences, and so fluorescence is skin and thymus specific, helping to trace thymic epithelium via EGFP expression using flow cytometry and confocal microscopy (Terszowski et al., 2006). The complete list of mice used in this study is outlined in Table 2.1.

Table 2.1. Wild Type And Genetically Modified Mice Strain Used In This Study

Strain	CD45 Isotype	Phenotype	Source
Balb/c	CD45.2	Wild type	BMSU
C57 BL/6	CD45.2	Wild type	BMSU
FoxN1 EGFP C57 BL/6 Background	CD45.2	TEC, Skin Epithelium GFP+ (Terszowski et al., 2006)	Max Planck Institute for Immunology, Germany
Nude C57 BL/6 Background	CD45.2	FoxN1 mutation leads to absent thymus	BMSU
Nude Balb/c Background	CD45.2	FoxN1 mutation leads to absent thymus	Jackson Labs
CD3 Epsilon Transgenic (CD3e26Tg)	CD45.2	Lack of T cells in periphery due to a block of T cell development at DN1 stage	Jackson Labs
$CD205^{-/-}$ C57 BL/6 background	CD45.2	Lack of CD205 expression on cTECs and DCs	Jackson Labs
$LT\beta R^{-/-}$ C57 BL/6 background	CD45.2	Lack of all lymph nodes, Peyer's patches, and colon-associated lymphoid tissues	Dr. Klaus Pfeffer, Technical University of Munich (Futterer et al., 1998)
$RANK^{-/-}$ C57 BL/6 background	CD45.2	Lack of all lymph nodes but not Peyer's patches, and colon-associated lymphoid tissues, and osteopetrosis	Josef M. Penninger Institute of Molecular Biotechnology of the Austrian Academy of Sciences, Institute of Molecular Biology
$Wnt5a^{-/-}$ C57 BL/6 background	CD45.2	Limb abnormalities, cranial defects, dwarfism, and intestinal elongation defects. Embryonic lethal-Knock out mice. (Het to Het mice breeding and embryos were harvested before birth) (Yamaguchi et al., 1999)	Jackson Labs

2.2. Medium And Additives

RF10-H is used for the short-term handling of isolated tissues and cells. Dulbecco's Modified Eagle's Medium (DMEM) is used for longer-term cultures. Both media were prepared in and stored at 4°C in advance of use. The details of RF10-H and DMEM constituents are summarized in Table 2.2 and Table 2.3.

Table 2.2. RF10-H Constituents

Medium And Additives	Volume	Final Concentration	Source
RPMI-1640 + 20mM Hepes with L-Glutamine without bicarbonate	20ml	-	Sigma, Poole,UK
200mM L- Glutamine	200µl	2mM	Sigma, Poole,UK
5000 IU/ml Penicillin and Streptomycin	400µl	100 IU/ml	Sigma, Poole,UK
Heat-inactivated FCS	2ml	10%	Sigma, Poole,UK

Table 2.3. DMEM Constituents

Medium And Additives	Volume	Final Concentration	Source
Dulbecco's Medium with 3.7g/l bicarbonate and without glutamine	20ml	-	Sigma, Poole,UK
100X non-essential amino acids (for component details see Table 2.4.)	200µl	-	Sigma, Poole,UK
1M Hepes	200µl	10mM	Sigma, Poole,UK
$5x10^3$ M2-Mercaptoethanol	200µl		Sigma, Poole,UK
200mM L-Glutamine	400µl	4mM	Sigma, Poole,UK
5000 IU/ml Penicillin and Streptomycin	400µl	100 IU/ml	Sigma, Poole,UK
Heat-inactivated FCS	2ml	10%	Sigma, Poole,UK

Table 2.4. Constituents Of 100x Non-Essential Amino Acids

Constituents	Concentration (mg/ml)
L-alanine	8.9
L-asparagine	15.0
L-aspartic Acid	13.0
Glycine	7.5
L-glutamic Acid	14.2
L-proline	11.5
L-serine	10.5

2.3. Tissue Isolation And Single Cell Suspension Isolation

2.3.1. Tissue Isolation

In accordance to Home Office regulations, cervical dislocation was used as the method of culling mice required for this study. Embryos were harvested from pregnant mice 11 to 17 days after vaginal plug detection. The womb and egg sac were removed and embryos washed in a solution of 1:1 Ca^{2+}/Mg^{2+} Phosphate Buffered Saline (PBS) to RF-10H. Thymus was dissected from embryos and the tissues were stored in RF-10H medium at 4°C prior to further manipulation. Tissues including thymus, spleen, and lymph nodes from adult mice were dissected and transferred to RF-10H. All handling of murine tissues was performed in a laminar flow hood to provide a sterile environment using sterile surgical instruments and media.

2.3.2. Isolation Of Thymocytes Or Peripheral T-Cells

Embryonic thymic lobes were gently teased with find forceps to collect single cell suspensions for flow cytometry in RF-10H. Glass slides were used for teasing adult thymus lobes or lymph nodes/spleen to obtain a cell suspension. To remove red blood cells in spleen, splenocytes were incubated with 2mls of red blood cell lysis buffer (Sigma-Aldrich) for 10 minutes at room temperature. After 10 minutes, an equal volume of RH-10H was added to neutralize the lysis buffer. The cells were spun down at the speed of 1400 rpm for 4 minutes at 4°C and then cell numbers were acquired by using haemocytometer.

2.3.3. Isolation Of Thymic Stromal Cells

2.3.3.1. Isolation Of Embryonic Thymic Stromal Cells

In order to isolate stromal cells from embryonic thymus, the tissues were disaggregated using trypsin. Since serum in RF-10H prevents the activity of trypsin, the tissues were washed twice with Ca^{2+}/Mg^{2+} free PBS before disaggregation. After two washes,

thymic lobes were suspended in 600µL of 0.25% trypsin solution in 0.2 % EDTA and then incubated at 37°C for 10 minutes. Cells were then pipetted to aid disaggregation and the suspension was neutralized with an equal volume of RF-10H and cells were spun down at the speed of 1000 rpm for 10 minutes at 4°C. Supernatant was removed and the pellet was re-suspended with 1ml of RF-10H for cell number calculation with a haemocytometer.

2.3.3.2. Isolation Of Adult Thymic Stromal Cells

To isolate stromal cells, adult thymus or thymic grafts were digested with enzymes. Tissues were cut into pieces in 1ml of RF-10H and transferred into polypropylene FACS tubes. Liberase (Roche, Final Concentration: 0.325 Wunsh U/ml) and DNase 1 (Sigma, Final Concentration: 40Kunitz U/ml) were added to samples and incubated for 30 minutes at 37°C in a water bath. After 30 minutes, supernatants were transferred to 15ml falcon tubes with an equal volume of MACs buffer (Ca^{2+}/Mg^{2+} PBS, 0.5% FCS, 2mM EDTA) on ice. Enzyme digestion was repeated for the rest of tissues in polypropylene FACs tubes. Following the second digestion, 10µL of 0.5M EDTA was added into polypropylene FACs tube and then left for 10 minutes on ice. Cell suspensions from first and second digestions were combined and spun down at the speed of 1400 rpm for 4 minutes at 4°C.

Due to the low percentage of stromal cells compared to thymocytes, $CD45^+$ thymocytes were removed using CD45 microbeads (Miltenyi). Cells were resuspended with 500µL of MACs buffer, 50µL of CD45 microbeads (Miltenyi) was added, and left on ice for 15 minutes. After 15 minutes, 3ml of MACs buffer was added to samples and the cells were run through LS Columns (Miltenyi). $CD45^+$ thymocytes were depleted and stromal cells were collected for cell counting. Cells were handled in the MACs buffer for flow cytometic analysis.

2.3.4. Bead Coating And Immunomagnetic Separation Techniques

2.3.4.1. Immunomagnetic Separation Of Embryonic Stromal Cells

For further enrichment of embryonic thymic epithelial cells, $CD45^+$ cells were depleted using anti-Rat IgG Dynabeads (Dynal, Wirral, UK). Beads were prepared the day before use by washing three times with RF-10H to get rid of sodium azide and then incubated with supernatant generated from a hybridoma producing pan-anti-cd45 antibodies for overnight at 4°C. After overnight incubation, beads were washed three times again with RF-10H to remove any excess antibody and re-suspended with 100µL of RF-10H. 10µL of beads was added into the sample in 200µL of RH-10H. Cells with beads were centrifuged at a speed of 1000 rpm for 10 minutes at 4°C in round bottomed sterile cryogenic vials (Cryovial, Quebec, Canada). The cryogenic vial provides cells a large surface area for optimal interaction with beads. The cells were spun down twice and then checked for the formation of 'rosettes', clusters of cells bound to beads. Once rosettes were detected under the light microscope, $CD45^-$ (unbound) cells were isolated using an Eppendorf (1.5ml) Dynal Magnetic Particle Concentrator (Dynal). CD45 depleted cells were used for high speed cell sorting to make reaggregate thymic organ culture or RT-PCR.

2.4. Immunolabeling And Flow Cytometry

2.4.1. Immunolabeling For Flow Cytometric Analysis

Cell suspensions were prepared as described in Section 2.3. 1.0 x 10^6 cells were aliquoted into 1.5ml Eppendorf tubes and spun down at the speed of 1400 rpm for 4 minutes at 4°C. Cell pellets were re-suspended in 50µL of antibody mix. All antibody mixes were made up in Fluorescence-activated cell sorting (FACS) medium ($Ca2^+$/$Mg2^+$ PBS, 3% FCS). Details of antibodies used in this study are outlined in Table 2.5. Cells were incubated for 30 minutes on ice and washed with 1ml of FACS medium. Then, cells were centrifuged at the

speed of 1400 rpm for 4 minutes at 4°C and supernatant was removed. After two washes, if secondary antibody is needed, staining was performed in the same manner as with primary antibodies. Cells with complete staining were washed twice, re-suspended with 200µL of FACS buffer and then transferred into 12.5ml polystyrene FACS tubes. Samples were stored in the dark on ice until flow cytometric analysis was performed.

2.4.2. Intracellular Immunolabeling For Flow Cytometric Analysis

For intracellular staining of FoxP3, cells were fixed and permeablized by using the Foxp3/Transcription Factor Staining Buffer Set (eBioscience) after cell surface staining as described in the previous section. 200µL of fixation buffer was added into each sample and incubated for 30 minutes on ice. Then, the samples were washed with 1ml of 1x permeablization buffer diluted with distilled water. After two washes, cells were stained with PE conjugated-FoxP3 antibody in 50µL of 1x permeablization buffer for 30 minutes on ice. Then the samples were washed twice with 1x permeablization buffer. Cells with complete staining were washed twice, re-suspended with 200µL of FACS buffer and then transferred into 12.5ml polystyrene FACS tubes. Samples were stored in the dark on ice until flow cytometric analysis was performed. The same method was used for intracellular staining of Aire, except using IC fixation/permeablization buffer (eBioscience) and eFluor® 488 conjugated-Aire antibody.

For intracellular staining of IFN-γ, cells were culture in anti-CD3-coated plates for 4 hours at 37°C. The plates were coated with 5µg/ml anti-CD3 in the presence of GolgiStop (BD). The plates were coated for overnight at 4°C. On the next day, the plates were washed with PBS. The same method was used for intracellular staining of IFN-γ, except using Cytofix/Cytoperm Plus (BD) and APC conjugated- IFN-γ antibody.

2.4.3. Flow Cytometric Analysis

A BD LSR Fortessa flow cytometer with BD FACS diva software was used to acquire samples. After acquisition, FlowJo Software was used for subsequent analysis. Before the acquisition of experimental samples, negative peaks were set examining negative control samples. For experiments using more than two fluorochromes, single color controls were used to compensate levels between various fluorochromes detection channels. In majority of cases a minimum of 10,000-gated events were collected. Non-viable cells were excluded from forward and side gates.

Table 2.5. Antibodies Used For Flow Cytometric Immnolabeling

Specificity	Host / Isotype	Clone	Working Dilution	Suppliers/ Cat #
CD3 PE	Hamster/IgG	eBio500A2	1:400	eBioscience/ 12-0033-83
CD4 PECy7	Rat/IgG2bκ	GK1.5	1:3000	eBioscience/ 25-0041-82
CD4 PerCP-Cy5.5	Rat/IgG2aκ	RM4-5	1:400	eBioscience/ 45-0042-82
CD8α FITC	Rat/IgG2aκ	55-6.7	1:200	eBioscience/ 11-0081-85
CD8α PB	Rat/IgG2aκ	53-6.7	1:200	eBioscience/ 48-0081-82
CD8α V500	Rat/IgG2aκ	53-6.7	1:200	BD Biosceinces/ 560776
CD25 APC	Rat/IgG1λ	PC61	1:500	Biolegend/ 102012
CD25 PECy7	Rat/IgG λ	PC61.5	1:400	eBioscience/ 25-0251-81
CD44 FITC	Rat/IgG2bκ	IM7	1:600	BD Biosceinces/ 553133
CD69 FITC	Hamster/IgG	H1.2F3	1:200	eBioscience/ 11-0691-85
TCRβ 780	Hamster/IgG	H57-597	1:100	eBioscience/ 47-5961-82
FoxP3 PE	Rat/IgG2aκ	FJK-16s	1:100	eBioscience/ 12-577-82
B220 450	Rat/IgG2aκ	RA3-6B2	1:200	eBioscience/ 48-0452-82
IFN-γ APC	Rat/IgG1κ	XMG1.2	1:100	BD Biosceinces/ 554413
CD45 780	Rat/IgG2bκ	30F-11	1:800	eBioscience/ 47-0451-82
CD40 PE	Rat/IgG2aκ	3/23	1:100	BD Biosceinces/ 553791
CD205 PECy7	Rat/IgG2aκ	205yekta	1:50	eBioscience/ 25-2051-42
EpCAM	-	G8.8	1:1000	Hybridoma
CD205 Biotin	Rat/IgG2a	NLDC-145	1:100	Abcam/a b51820
Ly51 PE	Rat/IgG2aκ	D7	1:1000	eBioscience/ 12-5981-82
Streptavidin PECy7	-	-	1:500	eBioscience/

				25-4317-82
Streptavidin PerCP-Cy5.5	-	-	1:800	eBioscience/ 45-4317-82
CD80 PB	Hamster/IgG	16-10A1	1:150	Biolegend/ 104724
IAb Biotin	-	AF6-120.1	1:300	BD Biosceinces/ 553550
IAd Biotin	-	AMS-32.1	1:300	BD Biosceinces/ 553546
Streptavidin Pacific Blue	-	-	1:400	eBioscience/ 48-4317-82
IAb Pacific Blue	-	AF6-120.1	1:400	Biolegend/ 116422
Pan IA/IE Pacific Blue	-	M5/114.15.2	1:400	Biolegend/ 107620
Aire 488	Rat/IgG2aκ	5H12	1:100	eBioscience/ 43-5934-82
Vg5 FITC	Rat/IgG1κ	536	1:100	BD Biosceinces/ 553229
CD45RB PE	Rat/IgG2aκ	C363.16A	1:500	eBioscience/ 12-0445-82

2.5. Fetal Thymic Organ Culture (FTOC) And 2-Deoxyguanosine Treated FTOC

Thymus lobes were dissected out of embryos at the gestation stage from E11 to E17. 90mm Petri dishes containing 4ml of DMEM were prepared with two 0.8μm sterile Nucleopore filters placed on the top of a sterile Anti-wrap sponge support. Up to 6 thymus lobes were placed on each filter using a mouth pipette and a finely drawn glass pipette. A maximum of three petri dishes were placed within a sterile humidified chamber and purged with 10% CO_2 air for 5-10 minutes to achieve the desired pH of the medium. The tissues were placed into a 37°C incubator for approximately 7 days. The number of thymus lobes placed on each filter was dependent upon the size of tissue. Every step of organ culture was completed in a sterile environment. In addition to DMEM, 600μl of 1.35mM 2-deoxyguanosine was added to a large dish with 4ml of DMEM to eliminate hematopoietic cells in FTOC.

2.6. Fetal Thymic Organ Culture (FTOC) For RANK Stimulation

Early embryonic (E11/E12) FoxN1:eGFP^{+} thymus/parathyroid rudiments were dissected out from embryo. Center-well organ culture dishes (Falcon 353037, Becton Dickinson, 60 x 15mm style polystyrene) containing 190μl of DMEM and 10μl of goat-anti mouse RANK antibody (R&D Systems AF692, Final Concentration: 10μg/ml) were prepared and the dissected tissues were placed on each 0.8μm sterile Nucleopore filters (Baik et al., 2013). Up to 3 dissected tissues were placed on each filter using a mouth pipette and a finely drawn glass pipette.

2.7. High Speed Sorting And Reaggregate Thymic Organ Culture (RTOC)

2.7.1. Preparation Of Cells For High Speed Sorting

Stromal cells or thymocytes were prepared as described in Section 2.4.2. and immunolabeled in a similar manner for flow cytometric analysis. Immunolabeled cells were re-suspended with 1ml of RH-10H and were filtered to get rid of any adherent cell clumps through a 30µm mesh-membrane filter (Miltenyi Biotech). Cells were collected within polypropylene FACS tube (Becton Dickinson). Sorting was performed on MoFlo high speed sorter (Dako Cytomations). Sorted cells were collected in 1.5ml Eppendorf tubes, spun down at the speed of 1400 rpm for 4 minutes at 4°C, and then re-suspended with 1ml of FACS medium. Cell number counts were calculated and the purity was checked before further use for either RTOC or RT-PCR.

2.7.2. RTOC And Ectopic Tissue Transplantation

Cells were sorted either in polypropylene FACS tubes or in 1.5ml Eppendorf tubes containing 500µl of RF10-H. The cell number was determined using a haemocytometer, and the purity of sorted populations was checked by BD LSR Fortessa flow cytometry. The sorted populations were centrifuged at the speed of 1400 rpm for 4 minutes at 4°C and then supernatant was removed as much as possible. In order to produce a slurry of cells in a volume of 2-3µl, the cell pellet was vortexed. By using a mouth pipette, the cell slurry was removed from the 1.5ml Eppendorf tube into a finely drawn glass pipette. The cell slurry was placed onto the center of 0.8µm sterile Whatman filter which was supported by Arti-Wrap sponge in the same manner to FTOC. RTOCs were left in culture for a desired period of time prior to be grafted under the kidney capsule of host mice. The ectopic transplant of RTOCs under the kidney capsule was done according to the Home Office regulation, as described

previously (Rossi et al., 2006). After 6-8 weeks, mice were sacrificed and the grafts were used for flow cytometric analysis and immunohistochemical analysis as described in Sections 2.4 and 2.7.

2.8. Immunohistology Techniques

Embryonic thymus lobes were dissected, embedded in OCT compound using a mouth pipette and a finely drawn pipette and then frozen via dry ice. Frozen tissues were stored at -80°C until ready to be cut into sections. 7µm sections were cut by cryostat and the sections were collected on multi-spot glass slides. Sections were air dried for one hour prior to fixation in acetone at 4°C for 20 minutes. After fixation, sections were air dried again for 30 minutes and then stored in -20°C until needed.

To preserve GFP expression, GFP transgenic tissues were fixed with 4% PFA for overnight instead of 20 minutes acetone fixation. The tissues were washed with 12%, 15%, 18%, and 30% sucrose. First wash was with 12% for overnight. Each of other three washes was also for overnight with increasing sucrose concentration. 7µm sections were cut by cryostat and the sections were collected on Superfrost Slides (Fisher).

75µl of primary antibody diluted in Ca^{2+}/Mg^{2+} PBS containing 1% bovine serum albumin (BSA) was placed on each spot of glass slides for section staining. Sections with antibody on were incubated in the dark at room temperature for 30 minutes and then washed with PBS under same conditions of staining. If secondary and tertiary staining were required, antibodies were applied in an identical manner to the primary. Before mounting with DABCO and a cover slip, slides were submerged in DAPI in distilled water for 30 seconds and then subsequently washed with PBS for 30 seconds. After staining, slides and cover slides were sealed with clear nail varnish. Slides were stored at -20°C before the analysis by confocal microscopy. Details of antibodies used in this study are outlined in table 2.6.

Images of stained sections were acquired using either a Zeiss LSM 510 Meta confocal microscope or a Zeiss LSM 780 Zen confocal microscope. DAPI were excited with 405nm diode laser, FITC/Alexa 488 conjugated antibodies were excited with a 488nm argon laser, TRITC/Alexa 555 and 594 conjugated antibodies were excited with a 561nm helium laser, and Alexa 647 conjugated antibodies were excited with a 633nm helium laser. ImageJ software was used for any other analysis.

Table 2.6. Antibodies Used For Immunohistology

Specificity	Host / Isotype	Clone	Working Dilution	Suppliers/ Cat #
CD4 647		RM4-5	1: 200	-
CD8 Biotin	Rat/IgG2b κ	YTS156.7.7	1: 300	Biolegend/126604
FoxP3 FITC	Rat/IgG2b κ	FJK-16s	1:100	eBioscience/ 11-5773-82
MTS10	Rat/ IgM		1: 10	Gift from Richard Boyd's lab (Godfrey et al., 1990)
DEC 205 FITC	Rat/ IgG2a	NLDC-145	1:100	Abcam/ab51817
Anti Rat IgM 594	Goat/ IgM	-	1: 400	Invitrogen/A21213
Streptavidin 555	Goat/IgG	-	1:1000	Invitrogen/S21381
Anti Fluorescein/Oregon Green®, eFluor®488	Rabbit/ IgG	-	1:100	Invitrogen/A11090
Anti Rabbit eFluor®488	Donkey/IgG	-	1:100	Invitrogen/A21206
ER-TR5	Rat/ IgM		1: 1000	Gift from W. van Ewijk, Leiden University, Netherlands
CD25 FITC		7D4	1: 100	BD/553071
β5t	Rabbit/IgG	-	1: 100	MBL/PD021
ER-TR7	Rat/IgG		Neat	Antibodies made from hybridoma cell line. (Gift from W. van Ewijk, Leiden University, Netherlands)
Anti Rat IgG 596	Goat/IgG	-	1:400	Molecular Probes/ 38482A
Aire 488	Rat/IgG2aκ	5H12	1:100	eBioscience/ 43-5934-82
Vγ5 FITC	Rat/IgG1κ	536	1:100	BD/553229

2.9. Preparation Of Samples For Gene Expression Analysis

All gene expression analysis was carried in collaboration with S. Parnell, University of Birmingham.

2.9.1. Snap Freezing Of Cell Populations

Cell populations acquired via high speed sorting or immunomagenetic bead separation were transferred into 1.5ml RNase-free eppendorf tubes (Camlab) and spun down at the speed of 1400 rpm for 4 minutes at 4°C. The supernatants were removed to leave dry cell pellets and then the tubes were immersed in liquid nitrogen before storage at -80°C until needed.

2.9.2. mRNA Extraction

mMACSTM one-step mRNA Isolation and reverse transcription kit (Miltenyi Biotec) were used to extract mRNA from snap frozen cells. The snap frozen cells from Section 2.8.1. were re-suspended with 1ml of lysis/binding buffer. To ensure their complete lysis, the cells were either vortexed or passed through a 21 gauge needle. Then, the cells were spun down at the speed of 13,000 g for 3 minutes at 4°C in LysateClear columns. To allow the polyA tails of any present mRNA to hybridize to the oligo microbeads, 50ml of mMACS oligo deoxy-thymidine (dT) microbeads was added to the lysate sample and gently mixed. After priming of mMACS columns with 100ml of lysis/binding buffer, the lysates were loaded on the mMACS columns. While the samples passed through the mMACS columns, the magnetically labeled mRNA remained bound to the column. To remove proteins and DNA, the column was washed twice with 200ml of lysis/binding buffer and then to remove ribosomal RNA and DNA, the column was washed four times with 100ml of wash buffer. The column bound mRNA was directly used for cDNA synthesis. 100ml of equilibration/wash buffer was added to the column twice and allowed to run through. 20ml of resuspension buffer was used to dissolve lyophilized enzyme mix and it was added to the column followed by 1ml of sealing

solution to prevent sample evaporation. For reverse transcription to take place, the column was incubated in the thermoMACS^{TM} at 42°C for 1 hour. Following the incubation, two washes of the column with 100ml of equilibration/wash buffer took place. 20ml of releasing solution was added to the column and then left for 30 minutes at 42°C. After the incubation, 50ml of elution buffer was added to column and the eluted cDNA was collected in an eppendorf. The collected cDNA was stored at -20°C until ready for use.

2.9.3. Quantitative RT-PCR

Quantitative RT-PCR was performed on the RotorGene RG-3000 (Corbett Research) using SYBR green with primers specific for several genes of interest. The details of primers used in this study are outlined in table 2.7. To normalize samples before amplifying target genes of interest, β-actin was used as a housekeeping gene. β-actin primers were designed and synthesized as a 10x Quantitect Primer Assay (QIAGEN). To avoid possible non-specific PCR amplification, primers for the target genes were designed, where possible using PrimerBank software (http://pga.mgh.harvard.edu/primerbank/index.html) and synthesized by Sigma Genosys. PCR reactions were carried out either as triplicates or duplicates within 15ml of reaction buffer, which is consisted of 7.5ml qPCR mastermix at a 2x concentration (Bioline Sensimix NoRox SybrGreen), 0.15ml (20mM stock concentration) forward and reverse target primer pairs (final concentration of 0.2mM), 6.2ml DNAse-free/RNAse-free PCR grade water (Sigma) and 1ml cDNA template. The amplification program was composed of several steps. The initial step, known as the 'hot start', lasted for 15 minutes at 95°C. The second step, known as the cycle step, had three different stages: 15 seconds denaturation at 95°C, 20 seconds primer annealing at 58°C to 62°C (depending on primer pairs), and 15 seconds amplification at 72°C. At the end of each cycle, the fluorescent signal produced from the amplicon was acquired. 39 repeats of the cycling parameters was performed. The final step

involved the acquisition of a melt curve (dissociation) profile (72-99°C, hold 30 seconds on 1st step and then 5 seconds on following steps) in order to check the specificity of amplicon. The Ct values and the reaction amplification efficiency were obtained from Rotor Gene 6.0 software (Corbett Research, Qiagen UK) utilizing standard curve produced from mouse universal cDNA (Biochain) or from FTOCs. The Pfaffl method (Pfaffl, 2001) was used to analyze the relative expression values of each sample normalized to β-actin, because it takes into account gene dependent efficiencies in the amplification process. Fold levels of the indicated genes represent the mean (±SEM) of replicate reactions and data shown are representative of at least two independent experiments

Table 2.7. Details Of Primer

Primer	Forward 5’ end primer sequence	Reverse 3’ end primer sequence	Size
FoxN1 NM_008238.1	CAAATTCTGCAGGGGTCAGA	TGGGGTGCAATCCTCTGATA	129
Gcm2 NM_008104.2	AGGAACCAACCCACTTTGACC	GCAGGACTTCTTGAGGATGTG	155
IL-7 NM_008371.4	TTCCTCCACTGATCCTTGTTCT	AGCAGCTTCCTTTGTATCATCAC	200
CCL21 NM_011124.4	ATCCCGGCAATCCTGTTCTC	GGGGCTTTGTTTCCCTGGG	129
CCL25 NM_009138.3	TTACCAGCACAGGATCAAATGG	CGGAAGTAGAATCTCACAGCA	105
RANK NM_009399.3	GCTGGCTACCACTGGAACTC	GTGCAGTTGGTCCAAGGTTT	185
Wnt5a NM_009524.3	CAAATAGGCAGCCGAGAGAC	CTCTAGCGTCCACGAACTCC	217
Wnt4 NM_009523.2	AGACGTGCGAGAAACTCAAAG	GGAACTGGTATTGGCACTCCT	126
Ror2 NM_013846.3	CCCAACTTCTACCCAGTCCA	TGTCCGCCACAGATGTATTG	154
Ryk NM_013649.3	GGTCTTGATGCAGAGCTTTACT	CCCATAGCCACAAAGTTGTCTAC	170
Fz2 NM_020510.2	CTTCACGGTCACCACCTATTTAG	CGCAATGTAGGCCACTGACA	109
Fz3 NM_021458.2	GCAGATAGGTGGGCACAGTT	ATAGGGTGGAAGGGCTCCAT	150
Fz7 NM_008057.3	GCCACACGAACCAAGAGGAC	CGGGTGCGTACATAGAGCATAA	111
Fz8 NM_008058.2	CCAGAGCCTTGACAACCTAC	AGAAAAGGCAGGCGACAAC	233

2.10. Analysis of Vγ5$^+$ DETCs in ear

2.10.1. Immunolabeling And Flow Cytometry

Skin of ear was incubated in 20mM EDTA (Sigma) for 2 hours at 37°C. Epidermal sheet were peeled from the dermis and then washed with PBS. Collagenase D (Roche, Final Concentration: 1mg/ml) and DNase 1 (Sigma, Final Concentration: 40Kunitz U/ml) were added to samples and incubated for 2 hours at 37°C in a water bath. Cells were then pipetted to aid disaggregation and the suspension was neutralized with an equal volume of RF-10H and cells were spun down at the speed of 1000 rpm for 10 minutes at 4°C. Supernatant was removed and the pellet was re-suspended with 1ml of RF-10H. Cells were filtered and stained with Vγ5, CD3, and CD45RB antibodies.

2.10.2. Immunohistology Techniques

Skin of ear was incubated in 20mM EDTA (Sigma) for 2 hours at 37°C. Epidermal sheet were peeled from the dermis and then washed with PBS. After washes, cold acetone was added into sample and the sample was incubated at -20°C for 20 minutes. The tissues were washed with PBS for twice. After washes, the epidermal sheet was culture in 2% BSA for 1 hour at 37°C. Then Vγ5 FITC antibody was added into sample and left for overnight at 4°C. On the next day, the sheets were washed with PBS, placed onto Superfrost Slides (Fisher) and embedded with VectorSheild (Vector).

2.11. Statistical Analysis

The statistical analysis used in this study was the unpaired student t test. P values below 0.05 were considered as significant.

2.12. Generation of iPS chimera

Experiments involving iPS cells were performed in collaboration with Professor Jon Frampton. iPS cells were made from C56BL6 mouse embryonic (E13.5) fibroblasts in the Frampton laboratory using published method (Sommer et al., 2009). To make iPS/nude embryo chimeras, 10 to 15 iPS cells were injected into 3.5 days post coitum (DPC) nude blastocyst. The injected nude blastocyst was incubated at 37°C for an hour in M16 media (Sigma, M7292) until it was transplanted into 2.5 DPC pseudo-pregnant recipient CD1 mice (Jenkinson et al., 2008). Resultant litters born were analyzed for the presence of coat and then the presence of functional thymic tissue at the age of 8 to 12 weeks.

CHAPTER 3. Defining TEC Progenitors And Towards Restoring Thymic Function

3.1. Introduction

The thymus is responsible for the production of self-tolerant T cells. Histologically, the thymus is compartmentalized into two distinct regions, which are cortex and medulla. Both cortex and medulla are composed of epithelial cells. Each region has its own role in T-cell development; thymocytes with functional TCRs are selected within the cortex and the deletion of potentially auto-reactive T cells occurs in the medulla (Anderson et al., 2006). With advancing age, naïve T-cell output from the thymus dramatically decreases owing to a loss of thymic epithelium. Consequently, this results in an increased propensity for infections and higher incidence of autoimmune diseases in the elderly (George and Ritter, 1996). Moreover, the thymus is sensitive to insults such as chemotherapy, radiation, and infections. Following those insults, thymic deterioration has been observed, consequently reducing the efficacy of immune system which links to an increased chance of infection and autoimmunity (Dudakov et al., 2012; van den Brink et al., 2004).

To overcome thymic regression caused from ageing and other external factors, several studies have sought to reconstitute thymus function by regenerating epithelial tissues. However, these approaches have had limited success, due to lack of understanding of stages in TEC development in vivo and a lack of available TEC progenitor markers. In relation to combatting thymic regression, the aims of this chapter are to:

-Identify the ontogeny of early embryonic TEC.

-Discriminate TECs from other type of epithelial cells in embryo.

-Classify thymic epithelial progenitor cells.

-Identify accessible cell lines that generate functional thymic tissue in vivo.

3.2. Results

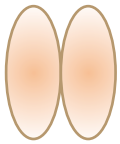
3.2.1. Defining TEC Progenitors

3.2.1.1. Analysis Of Embryonic TEC Development In Wild Type Mice

To classify TECs at different embryonic stages, thymus was dissected out from embryo at different stages of development. E12 to E17 embryonic thymus lobes of wild type were digested with trypsin, and single cell suspensions were stained with several surface markers for flow cytometry analysis. All samples were stained with CD45 (marker of bone marrow-derived hematopoietic cells) and EpCAM (pan-epithelial cell marker). We specifically investigated the cell population gated on $CD45^{-}EpCAM^{+}$. This gating strategy helps to discriminate embryonic TECs from other cell types within the thymus (Figure 3.1.).

Firstly, we analyzed the phenotype of embryonic TEC from E12 to E17 in wild type mice. Surface markers including CD40, CD205, PD-L1, and PD-L2 were used to identify the ontogeny of TEC. CD40 was used to discriminate mature TECs from immature TECs (Gray et al., 2006) and CD205 was utilized to identify cTECs (Jiang et al., 1995). Previous studies showed PD-L1 expression is dependent on FoxN1 expression (Bleul and Boehm, 2001). Moreover, Liang *et el* demonstrated PD-L1 and PD-L2 expression on TECs but the expression patterns of those two markers in embryo are still not clear (Liang et al., 2003). In this study, the expression pattern of PD-L1 and PD-L2 on embryonic TECs was explored to check their possible status as TEC progenitor markers. $CD45^{-}EpCAM^{+}$ TECs were plotted CD40 against CD205/PD-L1 to identify the induction time of each marker and to find the possible relation in between those markers (Figure 3.2. A and B). The anatomical separation of parathyroid from thymus occurs at E13 (Gordon et al., 2001). Therefore, the analysis of the $CD45^{-}EpCAM^{+}$ population prior to E14 includes the epithelial cells of parathyroid as well as thymus.

Dissected Fetal Thymus



Trypsin-Digestion for 10 min

Single Cell Suspension



Stain With Antibodies For 20 min

Flow Cytometry Analysis



Gating Strategy

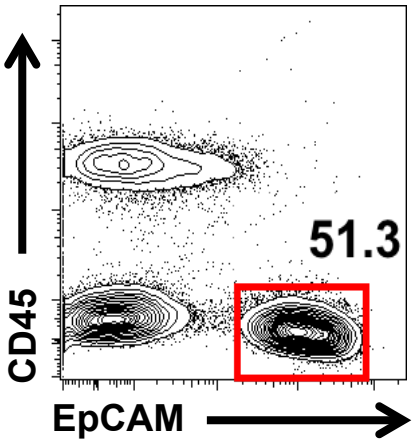


Figure 3.1. Isolation of embryonic thymic stromal cells and gating strategy

Thymus was dissected out from embryo and the embryonic thymus was disaggregated using trypsin. Before disaggregation, the tissue was washed twice with Ca^{2+}/Mg^{2+} free PBS because FCS in RF-10H media prevents the activity of trypsin. After two washes, the tissue in 1x trypsin solution diluted with 0.2% of EDTA was incubated at 37°C for 10 minutes. After disaggregation, cells were neutralized with RF-10H. Single cell suspensions were then stained with antibodies for 20 minutes. A BD LSR Fortessa flow cytometer with BD FACS diva software was used to acquire samples. To analyze epithelial cells, cells were pre-gated on $CD45^{-}EpCAM^{+}$, unless otherwise stated.

Low CD40 expression within $CD205^-$ and $PD\text{-}L1^-$ populations was found at E12 and both CD205 and PD-L1 expression were visible from E12. The $CD40^{Low}$ population within $CD205^-$ and $PD\text{-}L1^-$ was present until E13. At E14, three populations were found in terms of CD40 and CD205 expression: $CD40^-CD205^-$, $CD40^-CD205^+$, and $CD40^{Int}CD205^+$ (Figure 3.2 A). Similar heterogeneity was detected according to the expression of CD40 and PD-L1 at E14: $CD40^-PD\text{-}L1^-$, $CD40^-PD\text{-}L1^+$, and $CD40^{Int}PD\text{-}L1^+$ (Figure 3.2 B). Then, both $CD40^-CD205^-$ and $CD40^-PD\text{-}L1^-$ started to disappear at E15 and these two populations were not found from E16 onward (Figure 3.2. A and B). From E14, $CD40^{High}CD205^-$ and $CD40^{High}PD\text{-}L1^-$ populations branch out from $CD40^{Int}CD205^+$ and $CD40^{Int}PD\text{-}L1^+$ populations. The percentage of $CD40^{High}CD205^-$ TECs doubles from 6.83% at E15 to 12% at E16 and the percentage of $CD40^{High}PD\text{-}L1^-$ TECs also rises from 7.74% at E15 to 14.4% at E16. The percentage of $CD40^-CD205^+$ TECs increases until E14 and after E14 it gradually decreases (Figure 3.2. A). Similarly, $CD40^-PD\text{-}L1^+$ TECs expands until E14 and after E14 the population gradually declines (Figure 3.2. B).

To analyze whether PD-L1 and PD-L2 expression is skewed toward one of TEC lineages, namely cortex and/or medulla, $CD45^-EpCAM^+$ cells were plotted with PD-L1/PD-L2 expression against CD205 (Figure 3.2. C and D). If a marker is cTEC-specific, its expression should be found within $CD205^+$ subset. On the other hand, if a marker is mTEC-specific, its expression must be detected within $CD205^-$ population. The appearance of PD-L1 expression occurs at E12 and $PD\text{-}L1^+$ population was only found within $CD205^+$ TECs. After E13, PD-L1 and CD205 expression seems to be linear; either $CD205^-PD\text{-}L1^-$ or $CD205^+PD\text{-}L1^+$ population was observed (Figure 3.2. C). PD-L1 expression was only found in $CD205^+$ embryonic TEC population, which suggests PD-L1 as cTEC-specific marker in embryo. Moreover, the percentage of $CD205^+PD\text{-}L1^+$ TECs doubles from 31.7% at E12 to 69.2% at

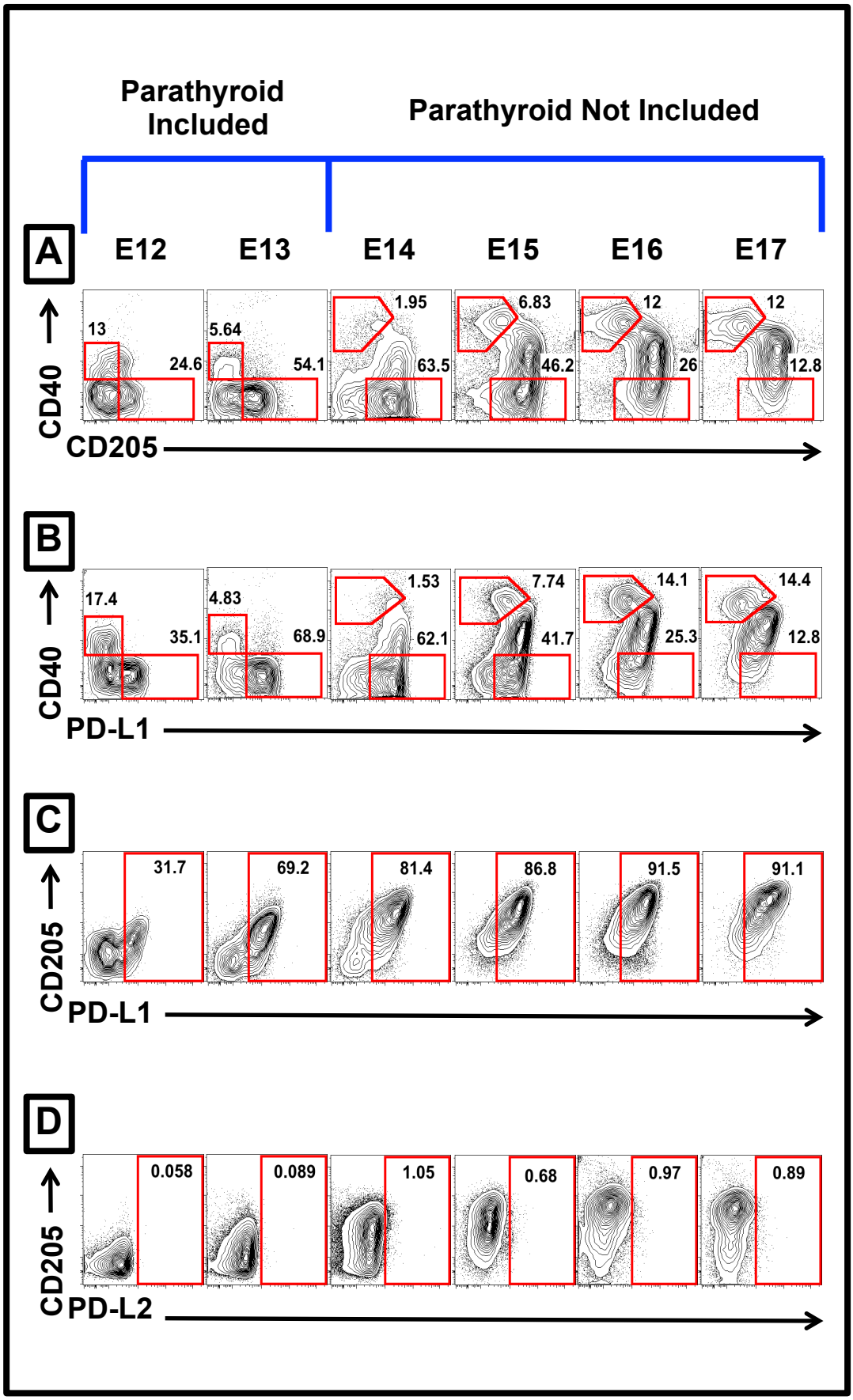

Parathyroid Included
Parathyroid Not Included
A
E12
E13
E14
E15
E16
E17
CD40
CD205
13
24.6
5.64
54.1
1.95
63.5
6.83
46.2
12
26
12
12.8
B
CD40
PD-L1
17.4
35.1
4.83
68.9
1.53
62.1
7.74
41.7
14.1
25.3
14.4
12.8
C
CD205
PD-L1
31.7
69.2
81.4
86.8
91.5
91.1
D
CD205
PD-L2
0.058
0.089
1.05
0.68
0.97
0.89

Figure 3.2. TEC ontogeny in wild type embryo

Single cell suspensions were prepared and were pre-gated on $CD45^{-}EpCAM^{+}$ as descried in Figure 3.1. Cells from embryonic thymus of wild type were stained for CD40, CD205, PD-L1, and PD-L2 in addition to CD45 and EpCAM. $CD45^{-}EpCAM^{+}$ cells were plotted CD40 versus CD205 (A), CD40 versus PD-L1 (B), CD205 versus PD-L1 (C), and CD205 versus PD-L2 (B). Percentage of cells within the gated area is shown. The contour plots illustrate the profile of CD40, CD205, PD-L1, and PD-L2 expression on $CD45^{-}EpCAM^{+}$ gated cells at different embryonic age from E12 to E17. The analysis of E12 and E13 includes parathyroid but the analysis after E13 does not include parathyroid.

E13 (Figure 3.2. C). After E15, the percentage of $CD205^{+}PD\text{-}L1^{+}$ TECs retains around 90% (Figure 3.2. C). However, PD-L2 expression on $CD45^{-}EpCAM^{+}$ was not detected at all throughout embryonic development (Figure 3.2. D). E15 FTOC cultured for 7 days was used as a positive control for PD-L2 expression. PD-L2 expression was found only in E15 FTOC but not in fresh embryonic thymus lobes, which suggests PD-L2 as a postnatal TEC marker (data not shown).

There are five subsets of cells within the $CD45^{-}EpCAM^{+}$ population according to the expression of CD40 and CD205: $CD40^{-}CD205^{-}$, $CD40^{Low}CD205^{-}$, $CD40^{-}CD205^{+}$, $CD40^{Int}CD205^{+}$, and $CD40^{High}CD205^{-}$. To see how distinct TEC subsets change in proportion through embryonic stage, the quantitative analysis of $CD40^{Low}CD205^{-}$, $CD40^{-}CD205^{+}$, and $CD40^{High}CD205^{-}$ populations among those five subsets is presented in Figure 3.3 A, B, and C. Figure 3.3. A displays a proportion change of $CD40^{Low}CD205^{-}$ cells from E12 to E17 in wild type mice, while the $CD40^{Low}CD205^{-}$ population was only observed at E12 and E13. Approximately 13% of $CD45^{-}EpCAM^{+}$ is $CD40^{Low}CD205^{-}$ at E12 and around 6% of $CD45^{-}EpCAM^{+}$ is $CD40^{Low}CD205^{-}$ at E13 but $CD40^{Low}CD205^{-}$ cells were not found after E13 (Figure 3.3. A). On the other hand, $CD40^{-}CD205^{+}$ cells are present throughout embryonic stages. At E12, $CD40^{-}CD205^{+}$ cells comprise about 18% of $CD45^{-}EpCAM^{+}$ population. It gradually expands to 65% until E14, and then after E14 progressively declines to 15% at E17 (Figure 3.3. B). The percentage change of $CD40^{High}CD205^{-}$ subset is opposite to that of the $CD40^{Low}CD205^{-}$ population: $CD40^{High}CD205^{-}$ cells starts to appear at E14 and increases until E17. There are two big rises between E14 and E16: from 3% at E14 to 7% at E15 and then to 12% at E16 (Figure 3.3. C).

Similarly, there are also five subsets within $CD45^{-}EpCAM^{+}$ cells in terms of CD40 and PD-L1 expression: $CD40^{-}PD\text{-}L1^{-}$, $CD40^{Low}PD\text{-}L1^{-}$, $CD40^{-}PD\text{-}L1^{+}$, $CD40^{Int}PD\text{-}L1^{+}$, and

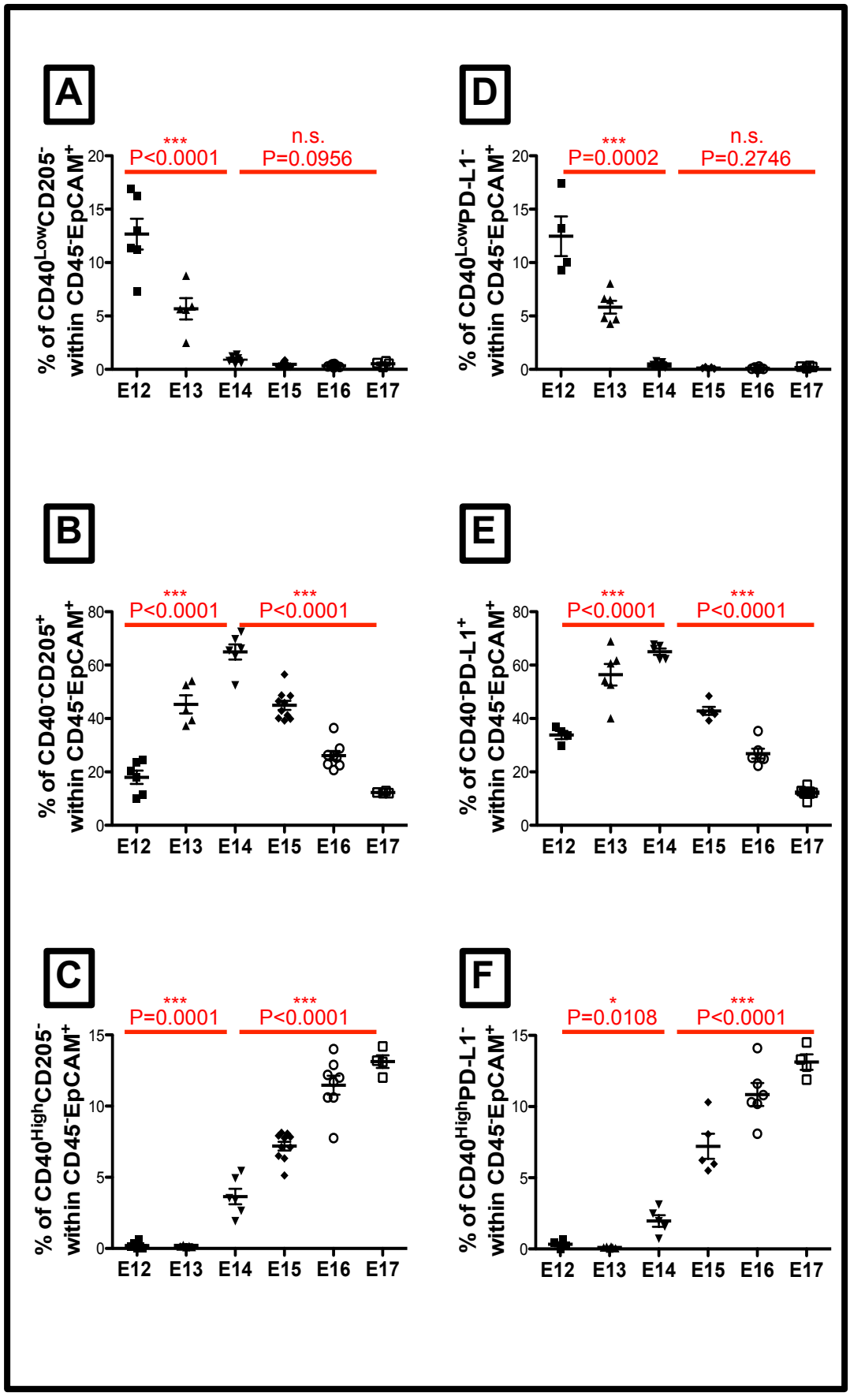

A
% of CD40LowCD205- within CD45-EpCAM+
***
P<0.0001
n.s.
P=0.0956
E12 E13 E14 E15 E16 E17
D
% of CD40LowPD-L1- within CD45-EpCAM+
***
P=0.0002
n.s.
P=0.2746
E12 E13 E14 E15 E16 E17
B
% of CD40-CD205+ within CD45-EpCAM+
***
P<0.0001
***
P<0.0001
E12 E13 E14 E15 E16 E17
E
% of CD40-PD-L1+ within CD45-EpCAM+
***
P<0.0001
***
P<0.0001
E12 E13 E14 E15 E16 E17
C
% of CD40HighCD205- within CD45-EpCAM+
***
P=0.0001
***
P<0.0001
E12 E13 E14 E15 E16 E17
F
% of CD40HighPD-L1- within CD45-EpCAM+
*
P=0.0108
***
P<0.0001
E12 E13 E14 E15 E16 E17

Figure 3.3. Quantification of subsets within CD45^{-}EpCAM^{+} at different embryonic age in wild type

Graphs show the proportions of CD40^{Low}CD205^{-} (A), CD40^{-}CD205^{+} (B), and CD40^{High}CD205^{-} (C) cells within CD45^{-}EpCAM^{+} at different embryonic age from E12 to E17 in wild type. Graphs demonstrates the proportions of CD40^{Low}PD-L1^{-} (D), CD40^{-}PD-L1^{+} (E), and CD40^{High}PD-L1^{-} (F) cells within CD45^{-}EpCAM^{+} at different embryonic age from E12 to E17 in wild type. The analysis of E12 and E13 includes parathyroid but the analysis after E13 does not include parathyroid. Each point represents one experiment. The bar indicates the calculated mean value and the error bar represents the standard error of the mean.

$CD40^{High}PD\text{-}L1^{-}$. Overall, the percentage changes of $CD40^{Low}PD\text{-}L1^{-}$ (Figure 3.3. D), $CD40^{-}PD\text{-}L1^{+}$ (Figure 3.3. E), and $CD40^{High}PD\text{-}L1^{-}$ (Figure 3.3. F) subsets from E12 to E17 are comparable to those of $CD40^{Low}CD205^{-}$, $CD40^{-}CD205^{+}$, and $CD40^{High}CD205^{-}$ populations. One difference important to note is that there are more cells expressing PD-L1 at E12 (35%, Figure 3.3. E) than cells expressing CD205 at E12 (18%. Figure 3.3. B). All $CD205^{+}$ cells are within $PD\text{-}L1^{+}$ cells at E12 and onwards (Figure 3.2. C). This demonstrates heterogeneity within the $PD\text{-}L1^{+}$ population according to CD205 expression at E12 and cells acquire PD-L1 expression prior to CD205 expression (Figure 3.2. C). However, the acquisition time gap between the two markers is shorter than 1 day and this time difference is only found in early stages such as E12 and E13. After E13, the $PD\text{-}L1^{+}$ population is homogeneous in terms of CD205 expression; $CD45^{-}EpCAM^{+}$ cells have phenotype either double negative ($CD205^{-}PD\text{-}L1^{-}$) or double positive ($CD205^{+}PD\text{-}L1^{+}$) (Figure 3.2. C).

3.2.1.2. Mechanical Separation Of Thymus And Parathyroid (Wild Type)

Anatomical separation between parathyroid and thymus is visible under the microscope at E13 and it is possible to mechanically separate these two organs without disturbing tissues. In order to find whether there is any contamination in the early embryonic TEC analysis from parathyroid epithelial cells before its separation at E13, we separated parathyroid from the thymus of E13. We stained separately E13 parathyroid and E13 thymus with markers used in Figure 3.2. A, B, and C. Cells were pre-gated as shown in Figure 3.1 and then $CD45^{-}EpCAM^{+}$ cells were plotted in the same manner as in Figure 3.2. A, B, and C. Figure 3.4. A shows before and after mechanical separation of parathyroid and thymus. CD40 expression was not found in E13 TECs but was detectable in the epithelial cells of E13 parathyroid. About half of parathyroid epithelial cells were positive for CD40 expression and its expression level is as low as seen in parathyroid included TEC analysis (Figure 3.2. A and

B). In contrast, the expression of CD205 and PD-L1 was only detected in E13 thymus but not in E13 parathyroid (Figure 3.4. B). Therefore, epithelial cells expressing low levels of CD40 within $CD205^-$ and $PD\text{-}L1^-$ populations before E14 in Figure 3.2. are from the parathyroid.

To enrich epithelial cells from E13 parathyroid, E13 thymus and E13 combined parathyroid/thymus, $CD45^+$ bone marrow-derived hematopoietic cells were depleted by an immunomagnetic bead separation technique as described in section 2.3.4. Bead Coating And Immunomagnetic Separation Techniques. Then, the CD45 depleted cells were processed for mRNA and quantitative RT-PCR was carried out for parathyroid-specific Gcm2 and thymus-specific FoxN1 expression to check the efficiency of mechanical separation (Figure 3.4. A and B). The parathyroid-specific Gcm2 is highly expressed in E13 parathyroid and the low expression of Gcm2 was detected in E13 parathyroid attached thymus sample but Gcm2 expression was not found in E13 thymus (Figure 3.5 A). In contrast, the thymus-specific FoxN1 is highly expressed in E13 thymus and the relatively low expression of FoxN1 was observed in E13 parathyroid attached thymus sample but FoxN1 expression was not found in E13 parathyroid (Figure 3.5. B). Furthermore, TEC-specific IL-7 (Mazzucchelli et al., 2009) and CCL25 expression (Vicari et al., 1997) was further investigated. The expression pattern of IL-7 and CCL25 is similar to that of FoxN1 in Figure 3.4. B (Figure 3.5. C and D). E13 TECs highly express both IL-7 and CCL25, and E13 parathyroid epithelial cells do not express those two genes. Relatively lower expression of IL-7 and CCL25 was found in the epithelial cells of E13 parathyroid attached thymus compared to that of E13 TECs only sample (Figure 3.5. C and D). It is known that CCL21 is expressed by parathyroid but not by thymus at the age of E13 (Liu et al., 2007). Therefore, CCL21 expression was used as another marker for parathyroid. The expression pattern of CCL21 is similar to that of Gcm2 in Figure 3.4. A: high expression in E13 parathyroid epithelial cells, no expression in E13 TECs, and

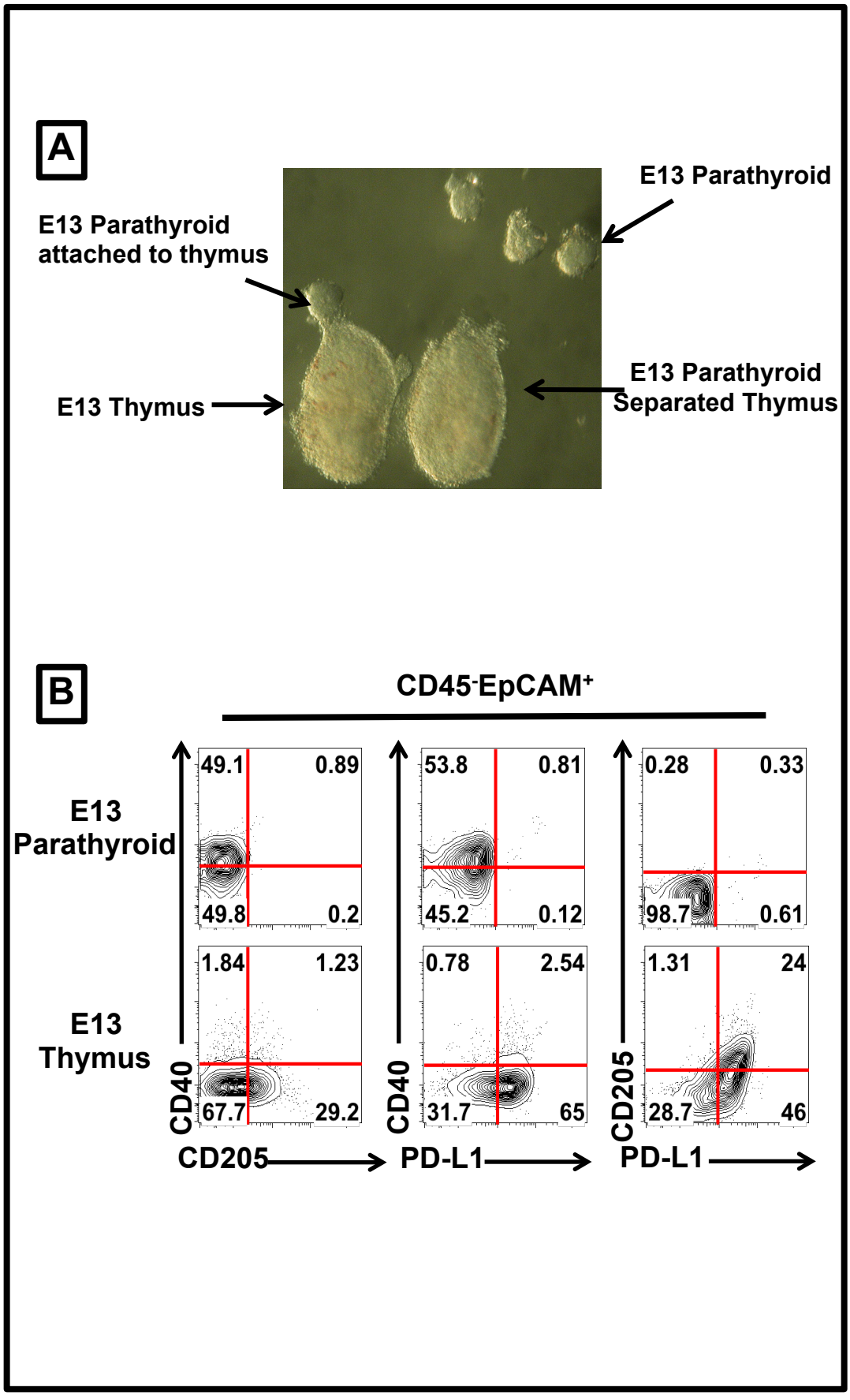

A
E13 Parathyroid
E13 Parathyroid attached to thymus
E13 Thymus
E13 Parathyroid Separated Thymus
B
CD45-EpCAM+
E13 Parathyroid
E13 Thymus
49.1
0.89
49.8
0.2
53.8
0.81
45.2
0.12
0.28
0.33
98.7
0.61
1.84
1.23
67.7
29.2
0.78
2.54
31.7
65
1.31
24
28.7
46
CD40
CD205
CD40
PD-L1
CD205
PD-L1

Figure 3.4. Mechanical separation of thymus from parathyroid (Wild Type)

The picture shows E13 thymus with parathyroid attached on the top (left lobe A). Right lobe in the picture is E13 thymus after the mechanical separation from E13 parathyroid. The three separated parathyroid lobes are on the right corner (A).

Single cell suspensions from E13 thymus and E13 parathyroid were separately prepared and were pre-gated on $CD45^{-}EpCAM^{+}$ as described in Figure 3.1. Cells were stained for CD40, CD205, and PD-L1 in addition to CD45 and EpCAM. $CD45^{-}EpCAM^{+}$ cells were plotted CD40 versus CD205, CD40 versus PD-L1, and CD205 versus PD-L1 (B). Percentage of cells within the gated area is shown. The contour plots illustrate the different expression pattern of CD40, CD205, and PD-L1 between thymus and parathyroid at E13.

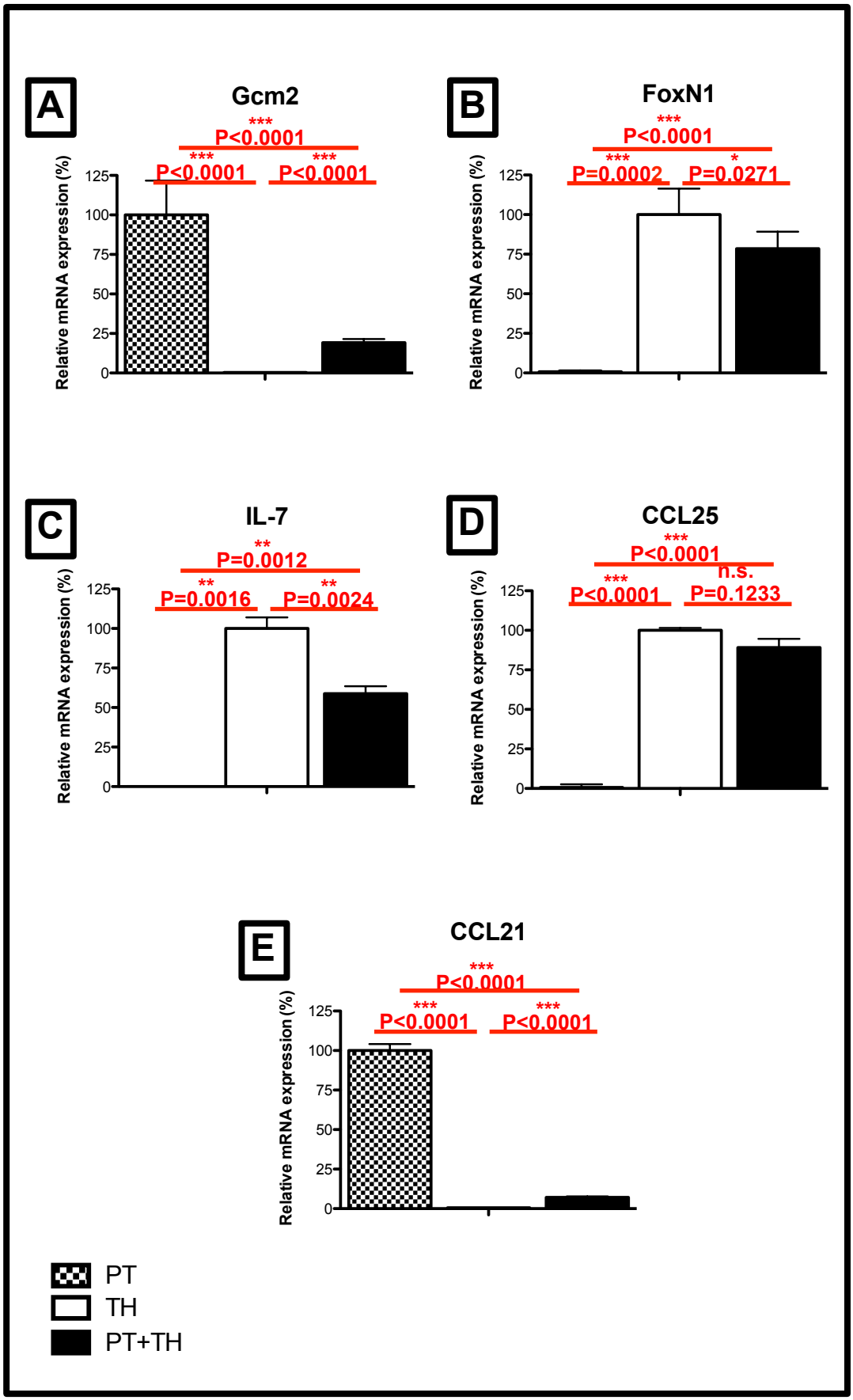

A
Gcm2
***
P<0.0001
***
P<0.0001
***
P<0.0001
Relative mRNA expression (%)
125
100
75
50
25
0
B
FoxN1
***
P<0.0001
***
P=0.0002
*
P=0.0271
Relative mRNA expression (%)
125
100
75
50
25
0
C
IL-7
**
P=0.0012
**
P=0.0016
**
P=0.0024
Relative mRNA expression (%)
125
100
75
50
25
0
D
CCL25
***
P<0.0001
***
P<0.0001
n.s.
P=0.1233
Relative mRNA expression (%)
125
100
75
50
25
0
E
CCL21
***
P<0.0001
***
P<0.0001
***
P<0.0001
Relative mRNA expression (%)
125
100
75
50
25
0
PT
TH
PT+TH

Figure 3.5. Different gene expression in E13 parathyroid and E13 thymus (Wild Type)

Cell suspensions from E13 parathyroid (PT), E13 thymus (TH), and E13 parathyroid + thymus (PT+TH) were prepared as described in Figure 3.1. $CD45^+$ cells were depleted by using Dynabeads. $CD45^-$ cells from each sample were used to compare relative mRNA expression. Relative expression of Gcm2 (A), FoxN1 (B), IL-7 (C), CCL25 (D), and CCL21 (E) was normalized to the housekeeping gene, β-actin. The bar indicates the mean of triplicate and the error bar represents the standard error of the mean. The data shown is the representative of two independent experiments.

very low expression in epithelial cells of E13 thymus and parathyroid combined (Figure 3.5. E). Collectively, the efficacy of mechanical separation was proved by RT-PCR analysis and this supports the finding that low CD40 expression on epithelial cells in early embryo is from parathyroid.

3.2.1.3. Phenotypical Analysis Of Parathyroid Epithelial Cells In FoxN1 Deficient Mice

The FoxN1 gene is crucial for TEC development, and mutations within FoxN1 gene lead to a deteriorated or absent thymus (Nehls et al., 1994). TEC development in nude mice, which has FoxN1 genetic mutation, is severely compromised by E11. Therefore, the embryonic thymus of nude mice is beneficial to study TEC progenitors. In addition, the development of parathyroid is independent of the FoxN1 gene and there is no disturbance to parathyroid development in nude mice. However, the mechanical separation of nude thymus from parathyroid at E13 was difficult due to the deterioration in TEC development of nude embryos. The clear mechanical separation of nude thymus from parathyroid is possible at E14. Figure 3.6. A shows before (right pair) and after (left pair) mechanical separation of E14 nude thymus from parathyroid. Using embryonic thymus from nude mice is another way to identify differential expression of surface markers between early embryonic TECs and parathyroid epithelial cells. The analysis of E13 nude thymus includes the epithelial cells of parathyroid but the analysis of E14 nude thymus excludes the parathyroid epithelial cells (Figure 3.6. B). Cells were prepared as shown in Figure 3.1. and then $CD45^{-}EpCAM^{+}$ cells were plotted with similar manner as in Figure 3.4. B. The different expression of CD40, CD205, and PD-L1 between E13 and E14 samples is from the parathyroid epithelial cells. CD205 and PD-L1 expression was not detected in both E13 and E14 samples. However, approximately 17% of $CD40^{Low}$ population was observed only in E13 sample with

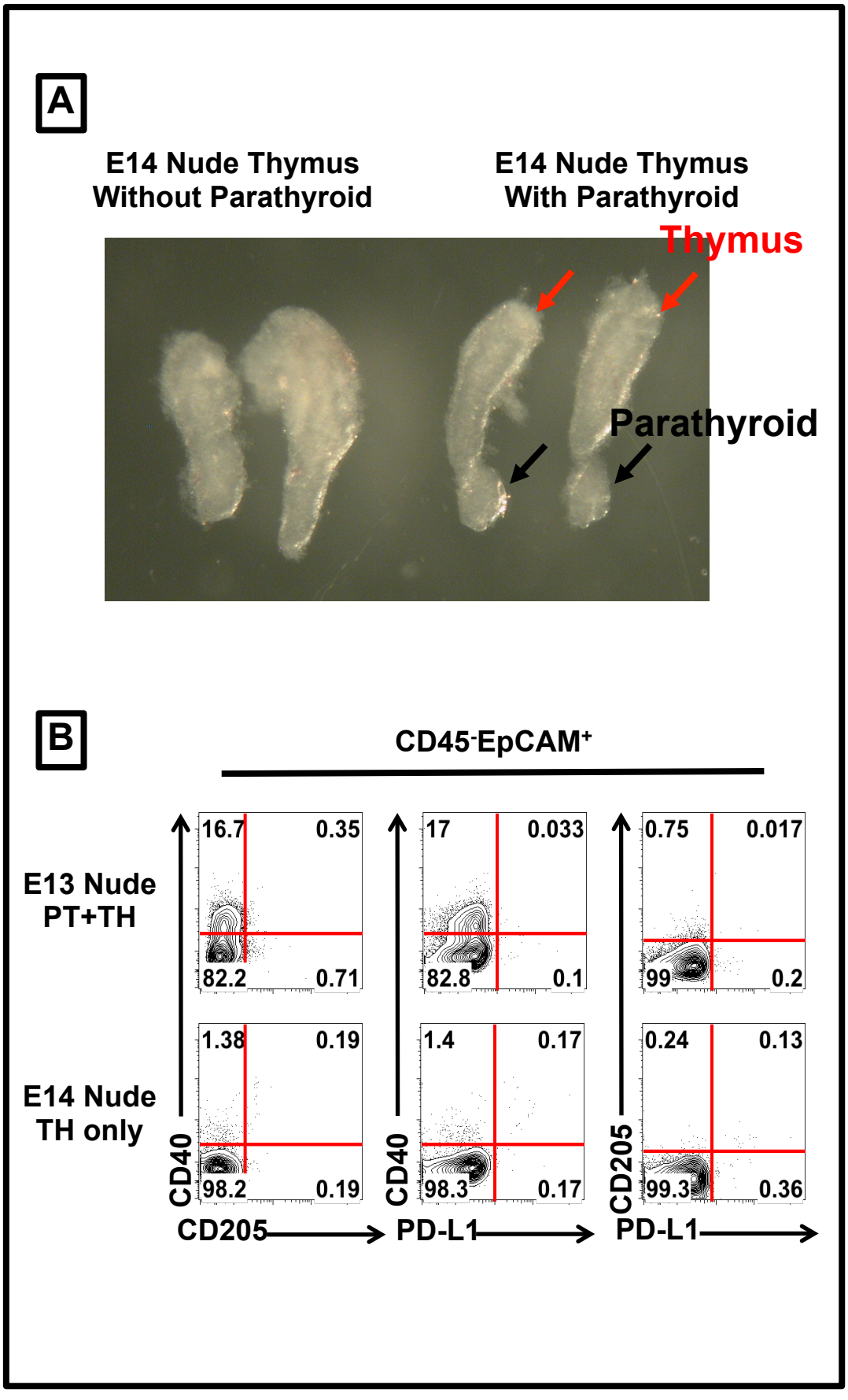

A
E14 Nude Thymus
Without Parathyroid
E14 Nude Thymus
With Parathyroid
Thymus
Parathyroid
B
CD45-EpCAM+
E13 Nude
PT+TH
E14 Nude
TH only
16.7
0.35
82.2
0.71
17
0.033
82.8
0.1
0.75
0.017
99
0.2
1.38
0.19
98.2
0.19
1.4
0.17
98.3
0.17
0.24
0.13
99.3
0.36
CD40
CD205
CD40
PD-L1
CD205
PD-L1

Figure 3.6. Phenotypical analysis of TECs and parathyroid epithelial cells in FoxN1 deficient mice (nude mice)

The left pair in the picture is E14 thymus of nude mice without parathyroid and the right pair is E14 thymus of nude mice with parathyroid (A).

Single cell suspensions from E13 thymus with parathyroid (Nude Mice) and E14 thymus without parathyroid (Nude Mice) were separately prepared and were pre-gated on $CD45^{-}EpCAM^{+}$ as described in Figure 3.1. Cells were stained for CD40, CD205, and PD-L1 in addition to CD45 and EpCAM. $CD45^{-}EpCAM^{+}$ cells were plotted CD40 versus CD205, CD40 versus PD-L1, and CD205 versus PD-L1 (B). Percentage of cells within the gated area is shown. The contour plots illustrate the different expression pattern of CD40, CD205, and PD-L1 between E13 thymus with parathyroid (Nude Mice) and E14 thymus without parathyroid (Nude Mice).

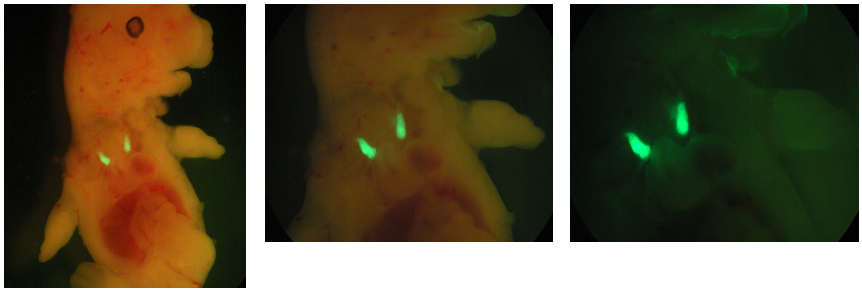
parathyroid (Figure 3.6. B). This confirms low CD40 expression by parathyroid epithelial cells at E13, which is consistent with the data from wild type mice (Figure 3.2. A/B and Figure 3.4. B)

3.2.1.4. Use Of FoxN1:eGFP Transgenic Mice To Analyze TEC Development In Early Embryo

The findings above show that early embryonic TECs are difficult to analyze due to the contamination from the epithelial cells of parathyroid. Surface markers such as CD45 and EpCAM that we used to distinguish epithelium from other types of cells are not sufficient to discriminate between TECs and parathyroid epithelial cells. To overcome this problem, we used FoxN1:eGFP transgenic mice in this study. Since the expression of enhanced green fluorescent protein (eGFP) transgene is driven by FoxN1 regulatory sequences, FoxN1:eGFP transgenic mice is useful for better identification of thymic epithelium in early embryo (Terszowski et al., 2006). FoxN1 is a skin and a thymus specific marker required for TEC proliferation and differentiation and its expression in thymus starts at E11 (Nehls et al., 1996). Hence, the green fluorescence is specific to skin and thymic epithelium. The pictures shown in Figure 3.7. were taken using a fluorescence dissecting microscope. Embryonic thymus lobes of FoxN1:eGFP transgenic mice can be easily detected from E11 under the green fluorescence microscope. Whole embryos of E13 FoxN1:eGFP mice were checked for green fluorescence and the fluorescence was only observed in thymic tissues at E13 (Figure 3.7. A). At E13 the two GFP^+ thymus lobes were located above the heart. The far right picture of Figure 3.7. A was taken without help of extra light to give an indication of the high levels of green fluorescence. The green fluorescence on skin was detectable after E15 (Figure 3.7. B). To check whether the green fluorescence is TEC-specific in thymus, E12 (with mesenchyme, Figure 3.7. C) and E13 (with parathyroid, Figure 3.7. D) FoxN1:eGFP thymus were cleanly

A

E13 FoxN1:eGFP+ Embryo



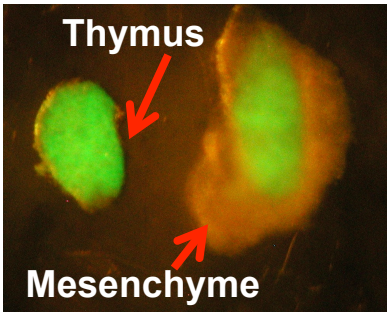
B

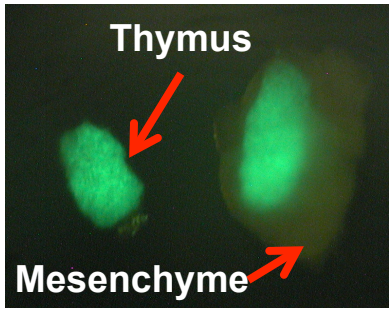
E15 FoxN1:eGFP+ Embryo



C

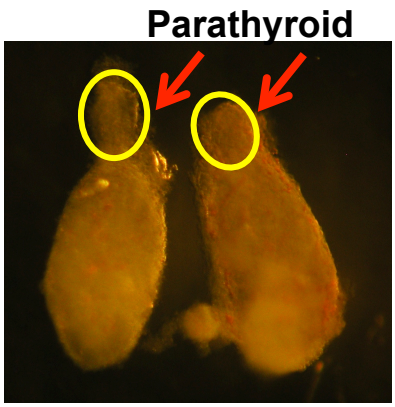
E12 FoxN1:eGFP+ Thymus





D

E13 FoxN1:eGFP+ Thymus



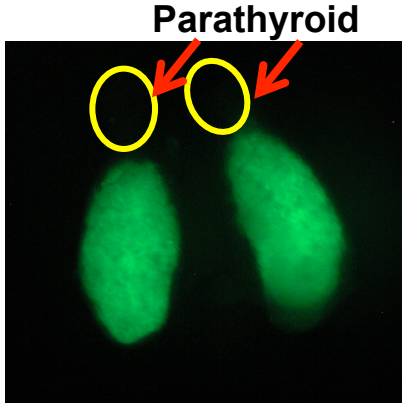


Figure 3.7. FoxN1:eGFP transgenic mice

Whole embryo of E13 (A) and E15 (B) FoxN1:eGFP transgenic mice was checked for green fluorescence under the fluorescent microscope. Two lobes of E13 thymus were only positive for GFP (A). Green fluorescence on skin was detected after E15 (B). Picture of far left and middle was taken with light on and picture of far right was taken without light (A). Cleanly dissected E12 thymus of FoxN1:eGFP transgenic mice with/without mesenchyme was checked for green fluorescence (C). Cleanly dissected E13 thymus of FoxN1:eGFP transgenic mice with parathyroid was also checked for green florescence (D). Green fluorescence was thymus/skin-specific and it was not detected on mesenchyme and parathyroid.

dissected. The picture of Figure 3.7. C shows E12 FoxN1:eGFP thymus lobes with mesenchyme. Mesenchyme, phenotypically defined as $CD45^{-}EpCAM^{-}$, was GFP^{-}. The picture of Figure 3.7. D displays E13 FoxN1:eGFP thymus lobes with parathyroid attached on the top. GFP was only expressed by thymus but not by parathyroid. Therefore, examining GFP^{+} cells within $CD45^{-}EpCAM^{+}$ guarantees the analysis of a pure TEC population in early embryos.

The green fluorescence on thymus was checked by confocal microscopy and flow cytometry (Figure 3.8.). E11 FoxN1:eGFP thymus lobe was dissected and prepared for confocal microscopy and stained with DAPI as described in 2.8. Immunohistology Techniques. Bright fluorescence within thymic lobes of E11 FoxN1:eGFP was observed without any help of FITC amplification (Figure 3.8. A). FoxN1:eGFP embryonic thymus of E11, E12, and E13 were dissected and prepared for flow cytometry analysis, confirming that GFP is detected only within $CD45^{-}$ (Figure 3.8. B) and $EpCAM^{+}$ population (Figure 3.8. C). Collectively, the analysis of the GFP^{+} population within $CD45^{-}EpCAM^{+}$ cells of FoxN1:eGFP mice excludes any contamination from other type of cells and other type of epithelium including parathyroid epithelium.

3.2.1.5. Phenotypical Analysis Of TECs And Parathyroid Epithelial Cells Using FoxN1:eGFP Transgenic Mice

The expression of parathyroid-specific Gcm2 initiates at E9.5 and the expression of thymus-specific FoxN1 starts at E11 (Gordon et al., 2001; Nehls et al., 1996). Even though the anatomical separation between thymus and parathyroid at E12 is not visible, if we investigate GFP^{+} epithelial cells of E12 FoxN1:eGFP thymus, we can investigate a pure TEC population. Moreover, GFP^{-} cells within $CD45^{-}EpCAM^{+}$ represent the epithelial cells of parathyroid. Therefore, we cleanly dissected E12 FoxN1:eGFP thymic lobe and then we

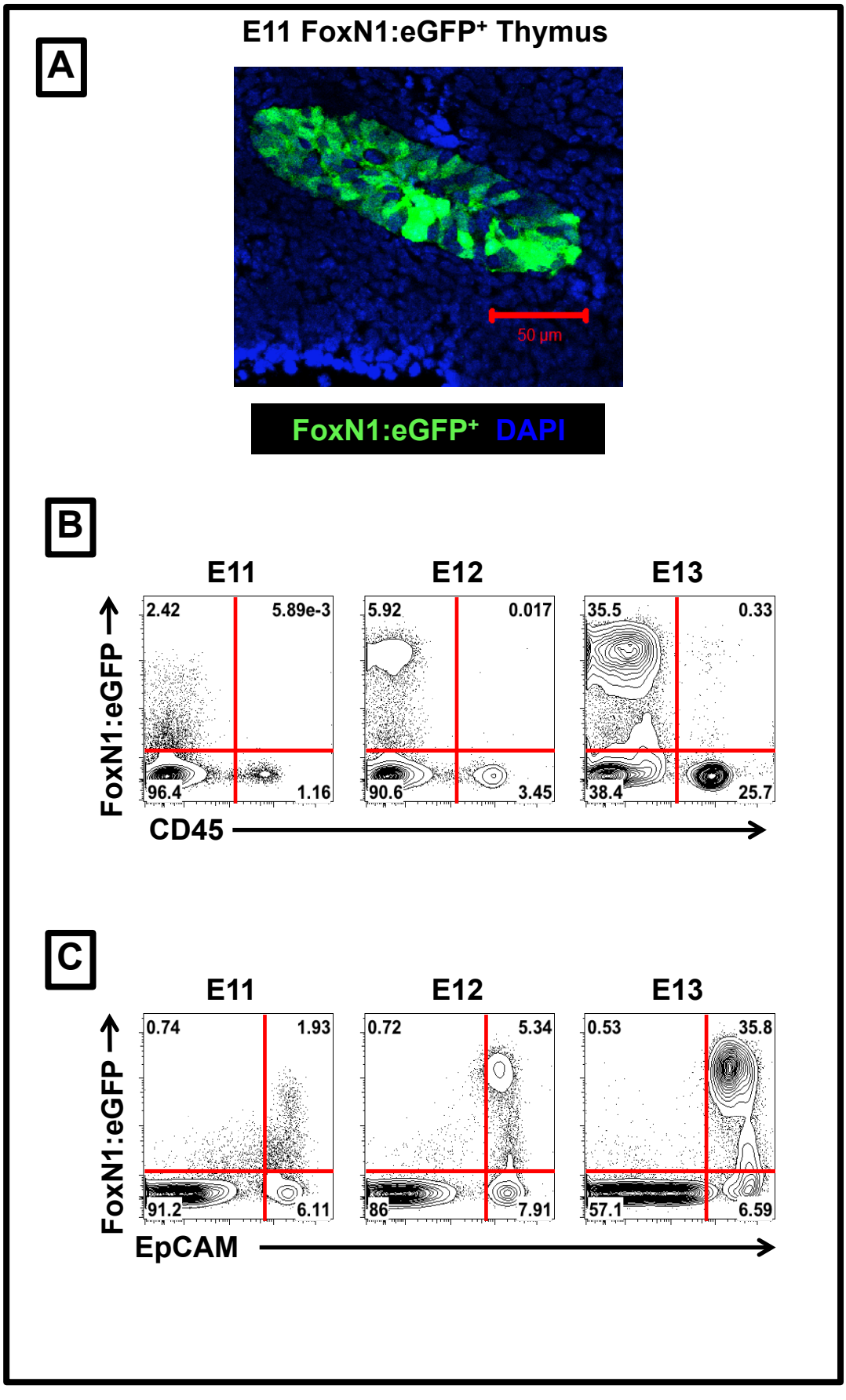

A
E11 FoxN1:eGFP+ Thymus
50 µm
FoxN1:eGFP+ DAPI
B
E11
E12
E13
2.42
5.89e-3
96.4
1.16
5.92
0.017
90.6
3.45
35.5
0.33
38.4
25.7
FoxN1:eGFP
CD45
C
E11
E12
E13
0.74
1.93
91.2
6.11
0.72
5.34
86
7.91
0.53
35.8
57.1
6.59
FoxN1:eGFP
EpCAM

Figure 3.8. GFP expression on thymus of FoxN1:eGFP transgenic mice

Frozen thymic tissue section of E11 FoxN1:eGFP transgenic mice was stained with DAPI for confocal microscopy (A). Bar indicates a scale of 50μm.

Single cell suspensions from E11, E12, and E13 thymus of FoxN1:eGFP transgenic mice were prepared as described in figure 3.1. Cells were stained for CD45 and EpCAM. Cells were plotted FoxN1:eGFP versus CD45 (B) and FoxN1:eGFP versus EpCAM (C) to check which population expresses GFP. GFP was detected within $CD45^-$ (B) and $EpCAM^+$ (C) populations from E11 and onward.

compared GFP^- and GFP^+ populations within $CD45^-EpCAM^+$ for CD40, CD205, and PD-L1 expression (Figure 3.9.). There are three populations in terms of GFP and CD205 expression within $CD45^-EpCAM^+$ population: GFP^-CD205^- (18.6%), GFP^+CD205^- (49.1%), and GFP^+CD205^+ (31.9%). CD205 expression was only observed within GFP^+ population, which confirms TEC-specific CD205 expression. Like CD205, all of PD-$L1^+$ cells are within $CD45^-EpCAM^+GFP^+$ population but not all of GFP^+ TECs were positive for PD-L1 expression. Approximately 60% of $CD45^-EpCAM^+$ is positive for both PD-L1 and GFP and about 20% of $CD45^-EpCAM^+$ is positive only for GFP. This also demonstrates TEC-specific PD-L1 expression. On the contrary, CD40 was detected within the $CD45^-EpCAM^+GFP^-$ population, which is parathyroid epithelium. About 6% of $CD45^-EpCAM^+$ cells express low levels of CD40. This illustrates that the expression of the maturation marker CD40 in early embryos at E12 and E13 is not by thymic epithelium but by the parathyroid epithelium.

One possible TEC progenitor marker is MTS 24. Early embryonic TECs express MTS 24, and Bennett *et al* and Gill *et al* demonstrated that $MTS24^+$ TECs can give rise to both cTECs and mTECs (Bennett et al., 2002; Gill et al., 2002). To find whether MTS24 expression is thymus-specific, cells from E12 FoxN1:eGFP thymus with parathyroid (Figure 3.10. A), E13 FoxN1:eGFP thymus with and without parathyroid (Figure 3.10. B and C), mechanically separated E13 FoxN1:eGFP parathyroid (Figure 3.10. D) were prepared and stained for flow cytometry analysis as described in Figure 3.1. $CD45^-EpCAM^+$ cells were then plotted FoxN1:eGFP versus MTS24. GFP^+ epithelial cells of E12 FoxN1:eGFP thymus express high level of MTS24. At E12, GFP^+ TECs are homogeneous in terms of MTS24 expression. GFP^- epithelial cells of E12 FoxN1:eGFP also express comparable levels of MTS24 to GFP^+ TECs (Figure 3.10. A). At E13, some GFP^+ TECs start to down-regulate MTS24 expression and GFP^- epithelial cells show lower MTS24 expression than both E13

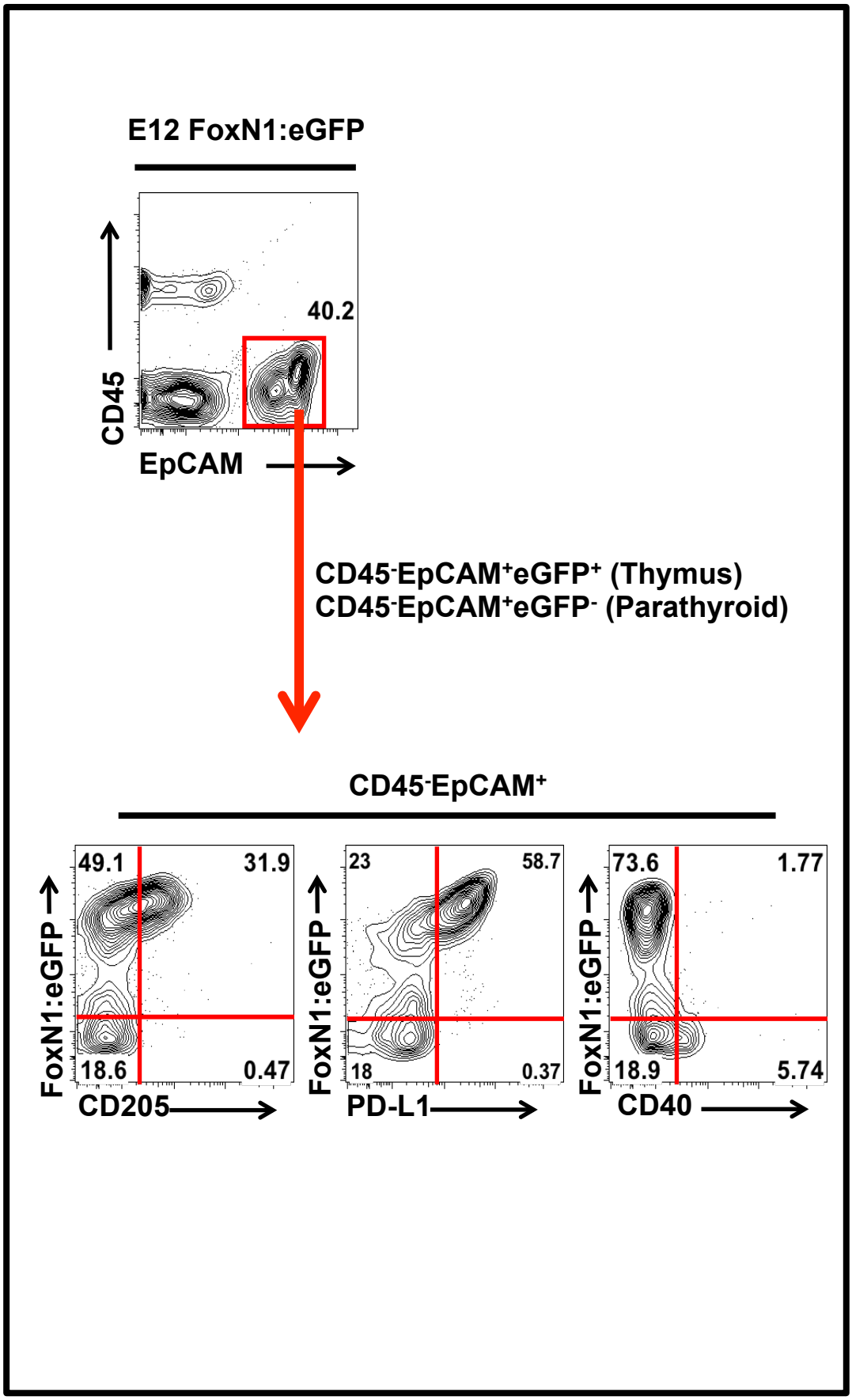

E12 FoxN1:eGFP
CD45
EpCAM
40.2
CD45-EpCAM+eGFP+ (Thymus)
CD45-EpCAM+eGFP- (Parathyroid)
CD45-EpCAM+
FoxN1:eGFP
CD205
49.1
31.9
18.6
0.47
PD-L1
23
58.7
18
0.37
CD40
73.6
1.77
18.9
5.74

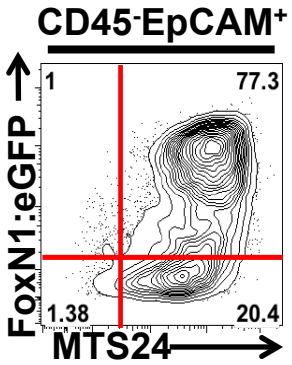
Figure 3.9. Phenotypical analysis of TECs and parathyroid epithelial cells in FoxN1:eGFP transgenic mice

Single cell suspensions from cleanly dissected E12 thymus of FoxN1:eGFP transgenic mice were prepared and were pre-gated on $CD45^{-}EpCAM^{+}$ as described in Figure 3.1. Cells were stained for CD40, CD205, and PD-L1 in addition to CD45 and EpCAM. $CD45^{-}EpCAM^{+}$ cells were plotted FoxN1:eGFP versus CD205/PD-L1/CD40. $CD45^{-}EpCAM^{+}FoxN1:eGFP^{+}$ cells are TECs and $CD45^{-}EpCAM^{+}FoxN1:eGFP^{-}$ cells are parathyroid epithelial cells. Percentage of cells within the gated area is shown. The contour plots show which surface markers express on parathyroid epithelial cells or TECs at age of E12 in FoxN1:eGFP transgenic mice.

A

E12 FoxN1:eGFP

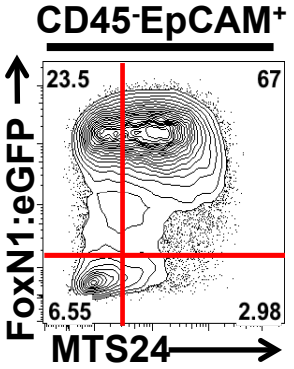
CD45$^-$EpCAM$^+$eGFP$^+$ (Thymus)
CD45$^-$EpCAM$^+$eGFP$^-$ (Parathyroid)



B

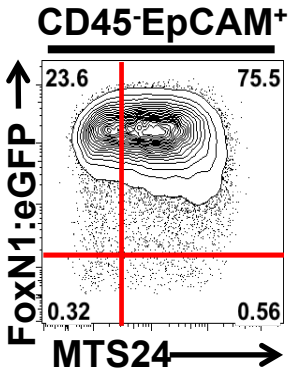
E13 FoxN1:eGFP

CD45$^-$EpCAM$^+$eGFP$^+$ (Thymus)
CD45$^-$EpCAM$^+$eGFP$^-$ (Parathyroid)



C

E13 FoxN1:eGFP
Mechanically separated Thymus



D

E13 FoxN1:eGFP
Mechanically separated Parathyroid

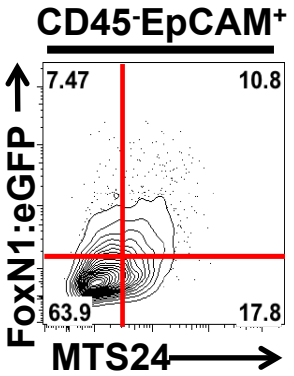


Figure 3.10. MTS24 expression on thymus and parathyroid at E12 and E13 in FoxN1:eGFP transgenic mice

Single cell suspensions from cleanly dissected E12 thymus (A), E13 thymus with parathyroid (B), mechanically separated E13 thymus (C) and E13 parathyroid (D) of FoxN1:eGFP transgenic mice were prepared and were pre-gated on $CD45^{-}EpCAM^{+}$ as described in Figure 3.1. Cells were stained for MTS24 in addition to CD45 and EpCAM. $CD45^{-}EpCAM^{+}$ cells were plotted FoxN1:eGFP versus MTS24. $CD45^{-}EpCAM^{+}FoxN1{:}eGFP^{+}$ cells represent TECs and $CD45^{-}EpCAM^{+}FoxN1{:}eGFP^{-}$ cells are parathyroid epithelial cells. The contour plots show which type of epithelial cells expresses MTS24.

GFP^+ TECs and E12 GFP^- epithelial cells (Figure 3.10. B). About 25% of GFP^+ TECs at the age of E13 lack MTS24 expression (Figure 3.10. C) and approximately 20% of GFP^- parathyroid epithelial cells express low level of MTS24 (Figure 3.10. D). Collectively, epithelial cells of early embryonic thymus and parathyroid express MTS24, indicating that MTS24 is not uniquely expressed by TEC progenitors.

3.2.1.6. Phenotypical Analysis Of TEC Progenitors Using FoxN1:eGFP Transgenic Mice

GFP expression level of TECs at different embryonic age from E11 to E17 was explored to find whether early embryonic TECs show different profiles of GFP expression from late embryonic TECs. At 11, TECs are composed of cells expressing low and intermediate levels of GFP, and the TEC population with intermediate levels of GFP expression expands at E12. Then, TECs highly expressing GFP start to appear at E13. From E14, approximately 95% of embryonic TECs express high levels of GFP and around 5% of $CD45^-EPCAM^+$ cells are negative for GFP (Figure 3.11). Since spontaneous parathyroid separation occurs at E13, $CD45^-EpCAM^+GFP^-$ cells after E13 are not contaminated by any other type of epithelium while $CD45^-EpCAM^+GFP^-$ cells before E14 likely represent the epithelial cells of the parathyroid. Absolute cell numbers of total $CD45^-EpCAM^+$ (Figure 3.12. A), $CD45^-EpCAM^+FoxN1{:}eGFP^+$ (Figure 3.12. B), and $CD45^-EpCAM^+FoxN1{:}eGFP^-$ (Figure 3.12. C) populations per thymus lobe were calculated to show how TEC numbers changed through embryonic stages from E11 to E17. Epithelial cell ($CD45^-EpCAM^+$) numbers of thymic rudiments is around 12,000 at E11 and the number reduces to roughly half of the initial number until E13. Then, the total $CD45^-EpCAM^+$ population shows two big expansions between E13 and E15: a 4-fold increase from E13 to E14 and a 1.5-fold increase between E14 and E15. After E15, cell numbers of the total $CD45^-EpCAM^+$ population slightly

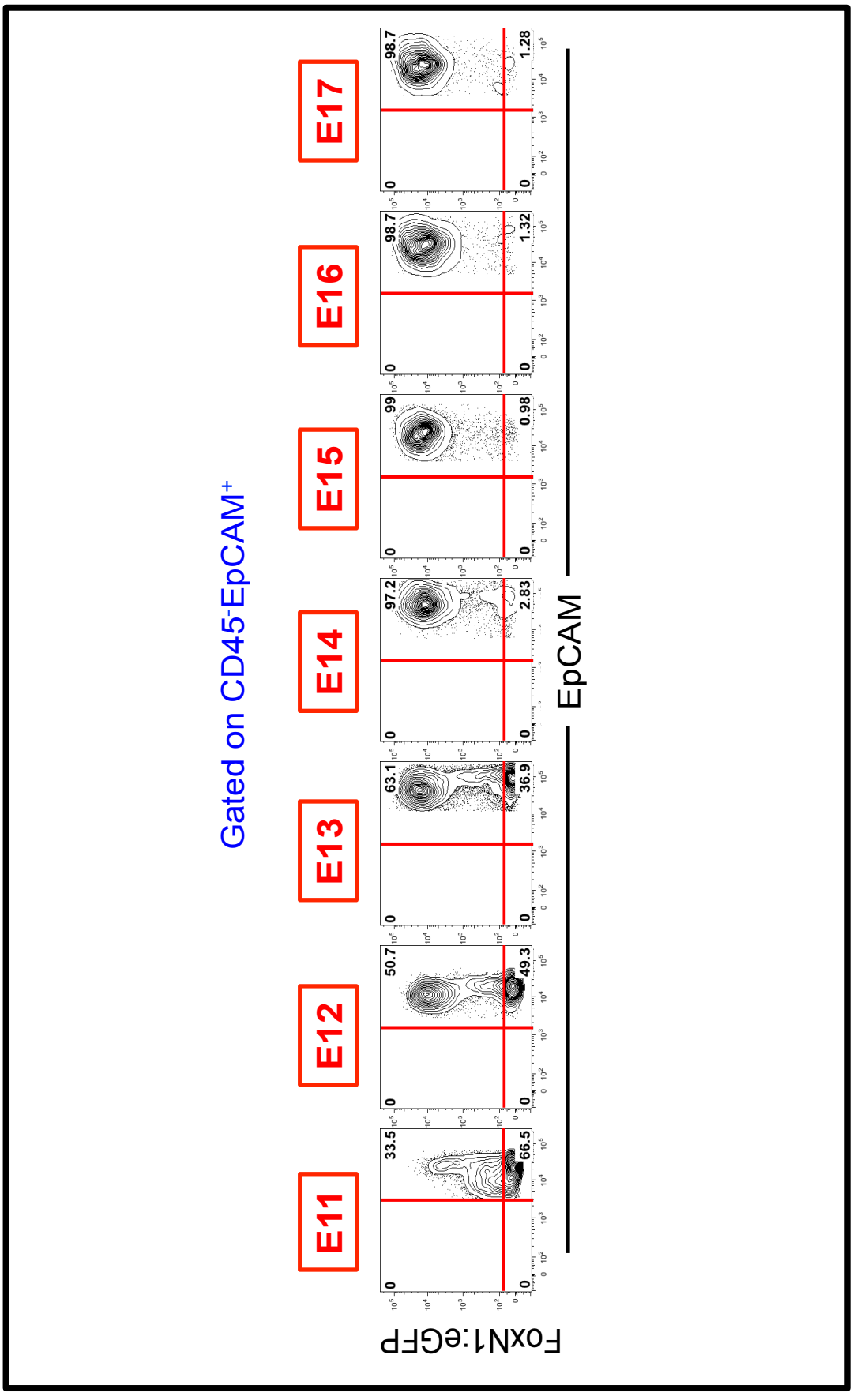

Gated on CD45-EpCAM+
E11
E12
E13
E14
E15
E16
E17
33.5
66.5
50.7
49.3
63.1
36.9
97.2
2.83
99
0.98
98.7
1.32
98.7
1.28
FoxN1:eGFP
EpCAM

Figure 3.11. Ontogeny of GFP$^+$ TEC in FoxN1:eGFP transgenic mice

Single cell suspensions from embryonic thymus of FoxN1:eGFP transgenic mice were prepared and were pre-gated on CD45$^-$EpCAM$^+$ as described in Figure 3.1. CD45$^-$EpCAM$^+$ cells were plotted FoxN1:eGFP versus EpCAM. The analysis of E11, E12, and E13 includes parathyroid but the analysis after E13 does not include parathyroid. Percentage of cells within the gated area is shown. The contour plots show the percentage change of CD45$^-$EpCAM$^+$FoxN1:eGFP$^+$ and CD45$^-$EpCAM$^+$FoxN1:eGFP$^-$ from E11 to E17 in FoxN1:eGFP transgenic mice.

decline until E17 (Figure 3.12. A). Contrastingly to that the cell number decrease in total $CD45^{-}EpCAM^{+}$ population from E15 to E17 (p value=0.1628) is statistically not significant, both the decrease from E11 to E13 (p value=0.0083) and the increase from E13 to E15 (p value=0.0002) are statistically significant (Figure 3.12. A).

The cell number of the $CD45^{-}EpCAM^{+}FoxN1{:}eGFP^{+}$ population at E11 is approximately 4,000 which is one third of total $CD45^{-}EpCAM^{+}$ population at E11. The $CD45^{-}EpCAM^{+}FoxN1{:}eGFP^{+}$ population maintains its cellularity until E13. Like the total $CD45^{-}EpCAM^{+}$ population, a 5-fold increase from E13 to E14 and 1.5-fold increase from E14 to E15 were observed (Figure 3.12. B). Changes from E11 to E13 (p value=0.6487) and from E15 to E17 (p value=0.1607) are not statistically significant but the increase between E13 and E15 has statistical significance (p value=0.0001) (Figure 3.12. B). Two-thirds of total $CD45^{-}EpCAM^{+}$ cells are epithelial cells which is negative for FoxN1:eGFP within thymic rudiments at E11. A statistically significant reduction (p value<0.0001) in its cellularity occurs between E11 and E13. After E13, around 400 $CD45^{-}EpCAM^{+}FoxN1{:}eGFP^{-}$ cells are present within thymic tissue; change in its cellularity from E13 to E17 has no statistical significance (from E13 to E15, p value=0.1025 and from E15 to E17, p value=0.9177) (Figure 3.12. C).

To further identify possible TEC progenitor markers, the expression of several surface markers including Integrin-α6, LTβR, Claudin-3,4, ICAM-1, VCAM-1, and Ly51 was analyzed using FoxN1:eGFP embryos from E11 to E17 (Figure 3.13. to Figure 3.16.). Adhesion molecules such as Integrin-α6, ICAM-1, and VCAM-1, which are expressed on TECs, promote interaction between thymocytes and TECs during T-cell development (Emre et al., 2013; Paessens et al., 2008). LTβR belongs to the TNFR Super Family and it is known to be up-stream of NF-κB signaling which is important for mTEC development (Hikosaka et al., 2008). Moreover, it is demonstrated that tight-junction component Claudin-3,4 expression

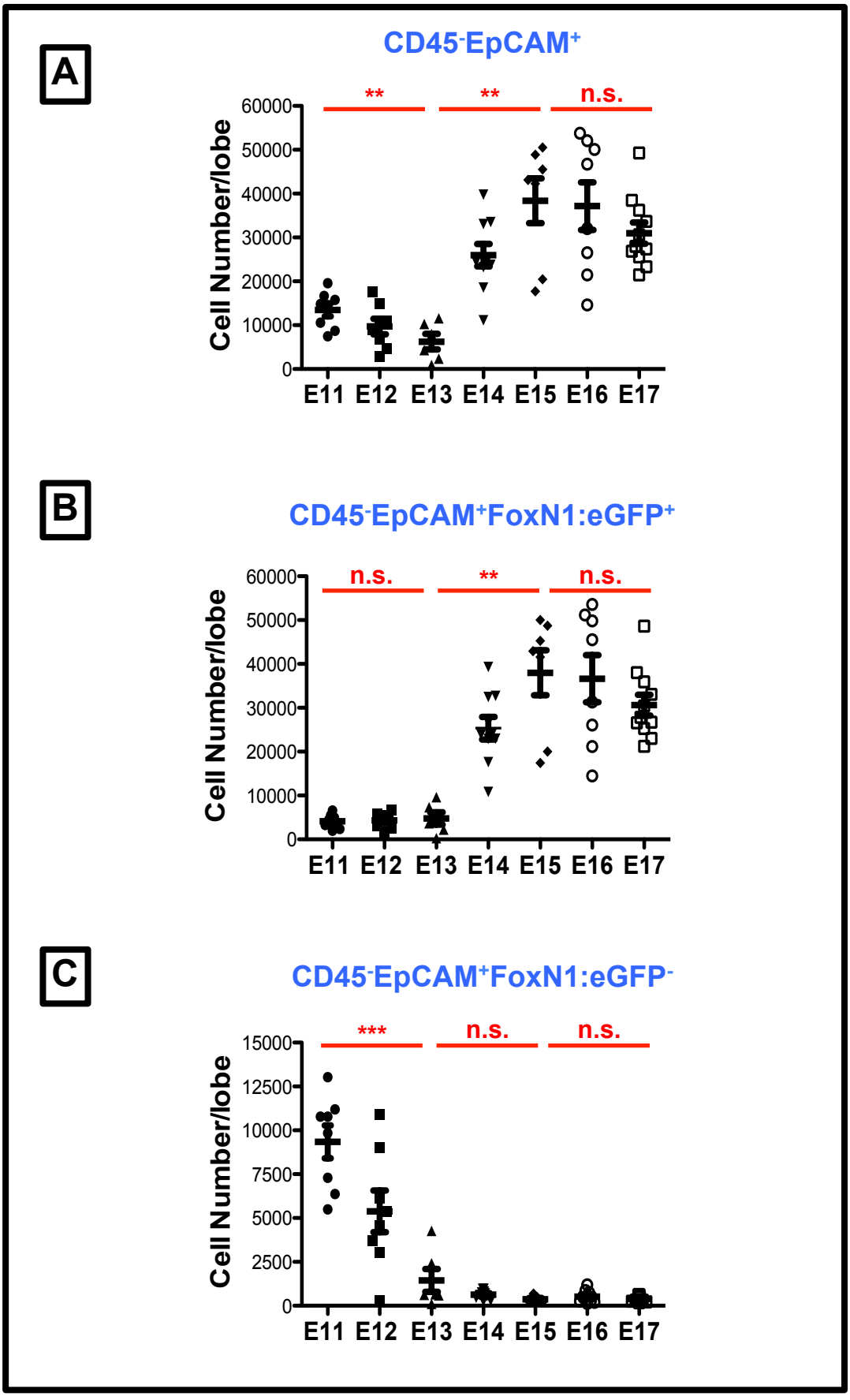

A
CD45-EpCAM+
**
**
n.s.
Cell Number/lobe
60000
50000
40000
30000
20000
10000
0
E11 E12 E13 E14 E15 E16 E17
B
CD45-EpCAM+FoxN1:eGFP+
n.s.
**
n.s.
Cell Number/lobe
60000
50000
40000
30000
20000
10000
0
E11 E12 E13 E14 E15 E16 E17
C
CD45-EpCAM+FoxN1:eGFP-
***
n.s.
n.s.
Cell Number/lobe
15000
12500
10000
7500
5000
2500
0
E11 E12 E13 E14 E15 E16 E17

Figure 3.12. Quantification of subsets within CD45$^-$EpCAM$^+$ at different embryonic age in FoxN1:eGFP transgenic mice

Graphs show the absolute cell number of total CD45$^-$EpCAM$^+$ (A), CD45$^-$EpCAM $^+$FoxN1:eGFP$^+$ (B) and CD45$^-$EpCAM$^+$FoxN1:eGFP$^-$ (C) per lobe at different embryonic age from E11 to E17 in FoxN1:eGFP transgenic mice. The analysis of E11, E12, and E13 includes parathyroid but the analysis after E13 does not include parathyroid. Each point represents one experiment. The bar indicates the calculated mean value and the error bar represents the standard error of the mean. Level of significance, which was calculated using an unpaired T test, was shown (* = $P < 0.05$, ** = $P < 0.01$, *** = $P < 0.001$). P value greater than 0.05 considered as non-significant (n.s.).

marks mTEC progenitor (Hamazaki et al., 2007). Ly51 is one of the known markers that identify cTECs (Gray et al., 2006). Despite the importance of those markers in both TEC and T-cell development, the expression pattern in early embryos has not been thoroughly studied. Therefore, the expression pattern of those markers in early embryo was investigated and it was also examined whether those surface markers can be used as a TEC progenitor marker in this study.

If a marker is TEC progenitor marker, it would be ideal to satisfy two conditions. First, the marker must be thymus-specific, which means it should be expressed by GFP^+ TECs. Second, TEC development begins at E11 following the initiation of FoxN1 expression (Gordon et al., 2001). Therefore, the expression of TEC progenitor markers must be found as early as E11. FoxN1:eGFP embryos from E11 to E17 were prepared and pre-gated as described in Figure 3.1. To see whether the expression of each marker is thymus-specific, $CD45^-EpCAM^+$ cells were plotted FoxN1:eGFP versus a marker (Figure 3.13. and 3.14.). Samples before E14 include the epithelial cells of parathyroid. Hence, $CD45^-EpCAM^+GFP^-$ cells before E14 represent parathyroid epithelial cells. Integrin-α6, LTβR, and Claudin-3,4, start to be expressed at E11 and the expression of those markers is found both within $CD45^-EpCAM^+FoxN1{:}eGFP^-$ and $CD45^-EpCAM^+FoxN1{:}eGFP^+$ populations from E11 to onward. In other words, Integrin-α6, LTβR, and Claudin-3,4 are expressed on not only embryonic TECs but also parathyroid epithelial cells (Figure 3.13.). Integrin-α6 and LTβR expression on GFP^+ TECs sustains through embryonic development but some of GFP^+ TECs lower Claudin-3,4 expression after E14 showing a heterogeneity (Figure 3.13.). Collectively, this expression argues against these markers being specific to TEC progenitors.

At E11, there are four subsets within $CD45^-EpCAM^+$ population according to FoxN1:eGFP and ICAM-1 expression: $GFP^-ICAM\text{-}1^-$, $GFP^+ICAM\text{-}1^-$, $GFP^+ICAM\text{-}1^+$, and

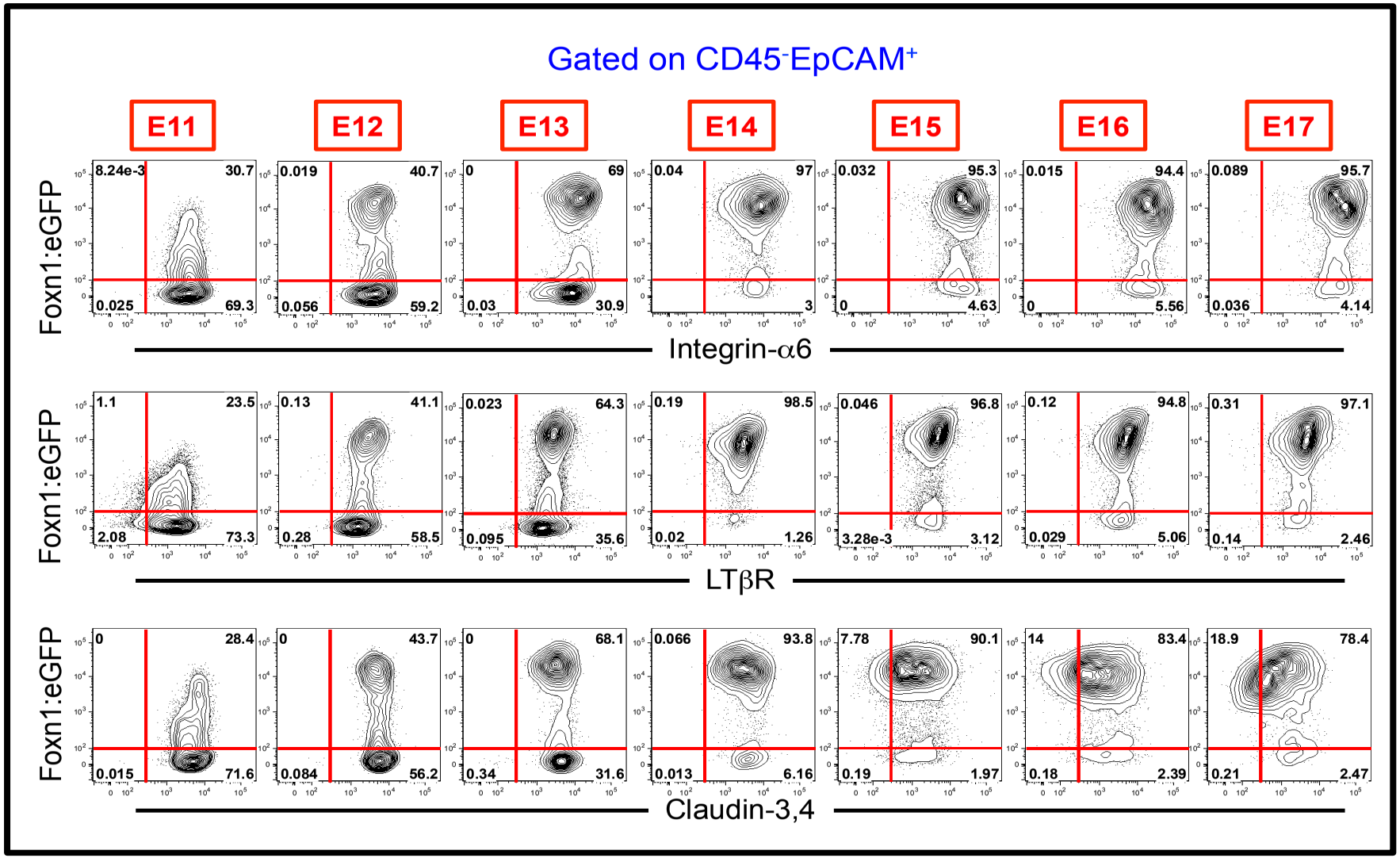

Gated on CD45-EpCAM+
E11
E12
E13
E14
E15
E16
E17
Foxn1:eGFP
8.24e-3
30.7
0.025
69.3
0.019
40.7
0.056
59.2
0
69
0.03
30.9
0.04
97
3
0.032
95.3
0
4.63
0.015
94.4
0
5.56
0.089
95.7
0.036
4.14
Integrin-α6
1.1
23.5
2.08
73.3
0.13
41.1
0.28
58.5
0.023
64.3
0.095
35.6
0.19
98.5
0.02
1.26
0.046
96.8
3.28e-3
3.12
0.12
94.8
0.029
5.06
0.31
97.1
0.14
2.46
LTβR
0
28.4
0.015
71.6
0
43.7
0.084
56.2
0
68.1
0.34
31.6
0.066
93.8
0.013
6.16
7.78
90.1
0.19
1.97
14
83.4
0.18
2.39
18.9
78.4
0.21
2.47
Claudin-3,4

Figure 3.13. Expression pattern of Integrin-α6, LTβR, and Claudin-3,4 on thymus of FoxN1:eGFP transgenic mice at different embryonic age from E11 to E17

Single cell suspensions from embryonic thymus of FoxN1:eGFP transgenic mice were prepared and were pre-gated on $CD45^{-}EpCAM^{+}$ as described in Figure 3.1. Cells were stained for Integrin-α6, LTβR, and Claudin3,4 in addition to CD45 and EpCAM. $CD45^{-}EpCAM^{+}$ cells were plotted FoxN1:eGFP versus Integrin-α6/LTβR/Claudin-3,4. The analysis of E11, E12, and E13 includes parathyroid but the analysis after E13 does not include parathyroid. Percentage of cells within the gated area is shown. The contour plots show the expression pattern of Integrin-α6, LTβR, and Claudin-3,4 on embryonic thymus at different age from E11 to E17 in FoxN1:eGFP transgenic mice.

GFP$^-$ICAM-1$^+$. Both GFP$^-$ICAM-1$^-$ and GFP$^+$ICAM-1$^-$ subsets up-regulate ICAM-1 expression at E12, expanding GFP$^+$ICAM-1$^+$ and GFP$^-$ICAM-1$^+$ populations. While GFP$^+$ TEC population is homogeneous in terms of ICAM-1 expression, ICAM-1$^-$ and ICAM-1$^+$ subsets are present within GFP$^-$ epithelial cells at E13. After E14, both GFP$^+$ and GFP$^+$ TECs highly express ICAM-1 but GFP$^-$ TECs show lower ICAM-1 expression than GFP$^+$ TECs at E14 (Figure 3.14.). Even though ICAM-1 expression was found as early as E11, its expression was not specific for TECs.

The acquisition of VCAM-1 expression on epithelial cells occurs at E13 and its expression was found on both GFP$^-$ and GFP$^+$ epithelial cells. At E14, only GFP$^+$ TECs express VCAM-1 but after E14 both GFP$^-$ and GFP$^+$ TECs are positive for VCAM-1 (Figure 3.14.). Ly51 expression pattern in embryo is similar to VCAM-1 expression except one noticeable difference. GFP$^+$ TECs acquire Ly51 expression 1-day earlier than VCAM-1 expression and GFP$^-$ epithelial cells at E12 and E13 express low level of Ly51 (Figure 3.14.). Since VCAM-1 and Ly51 start to be expressed later than E11 and the expression of both markers was also found in GFP$^-$ epithelial cells before spontaneous parathyroid separation, it fails to satisfy the first and second conditions of TEC progenitor category. Overall, VCAM-1 and Ly51 expression does not mark TEC progenitor populations in early embryo.

To find whether early embryonic TECs, with possible TEC progenitor phenotype, can be distinguished from mature TECs at late embryonic stages according to six surface markers, GFP$^+$ TECs were plotted a marker versus CD205 (Figure 3.15. and 3.16.). CD205 was used to see whether the expression of a marker is cTEC-specific or mTEC-specific (Jiang et al., 1995). Both CD205$^-$ and CD205$^+$ TECs express Integrin-α6 and LTβR through embryonic development from E11 to E17 (Figure 3.15.). Embryonic TECs express Claudin-3,4 from E11 and some CD205$^+$ TECs start to lower Claudin-3,4 expression after E13. Claudin-3,4$^-$ subset

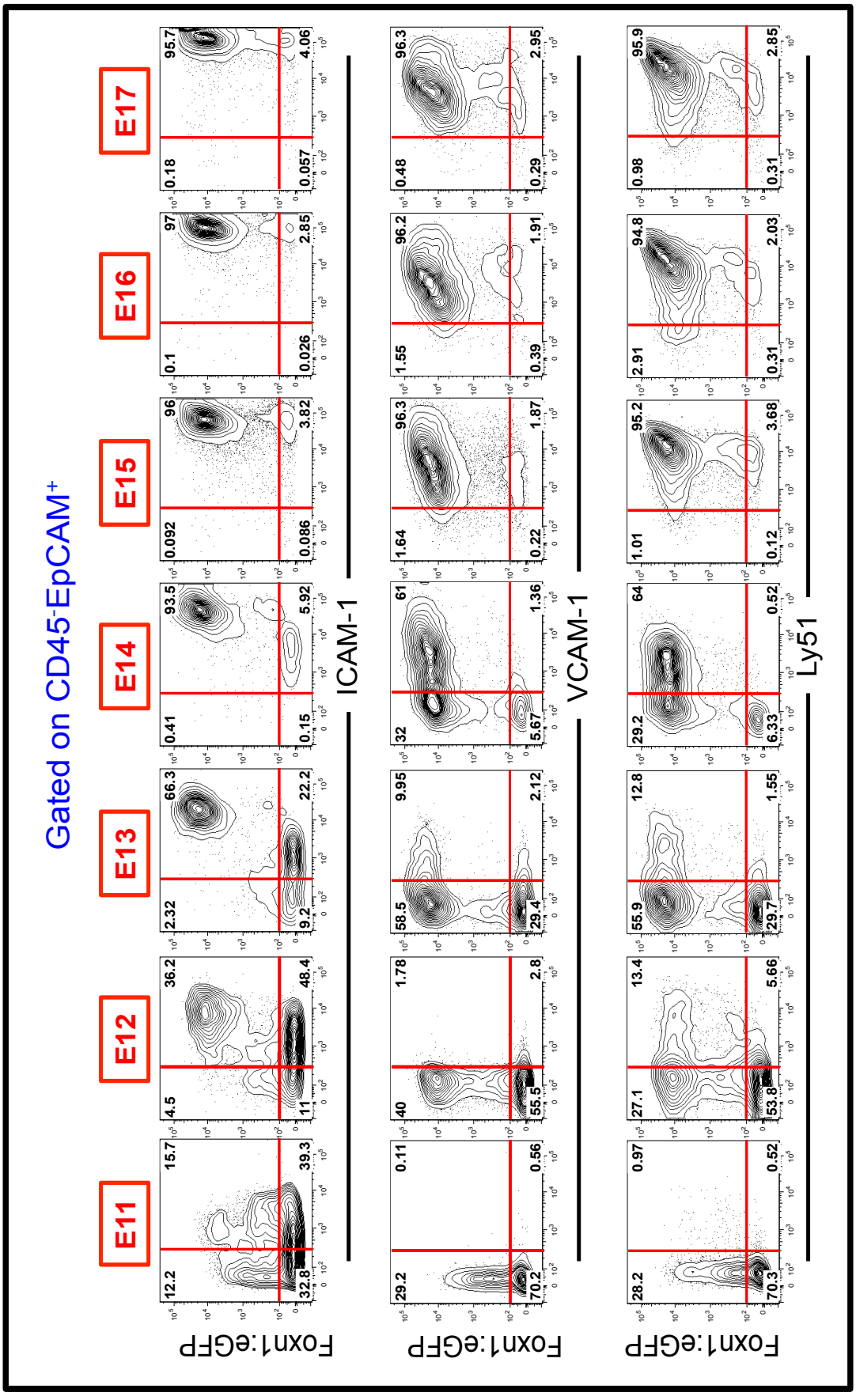

Gated on CD45-EpCAM+
E11
E12
E13
E14
E15
E16
E17
ICAM-1
VCAM-1
Ly51
Foxn1:eGFP
Foxn1:eGFP
Foxn1:eGFP

Figure 3.14. Expression pattern of ICAM-1, VCAM-1, and Ly51 on thymus of FoxN1:eGFP transgenic mice at different embryonic age from E11 to E17

Single cell suspensions from embryonic thymus of FoxN1:eGFP transgenic mice were prepared and were pre-gated on $CD45^{-}EpCAM^{+}$ as described in Figure 3.1. Cells were stained for ICAM-1, VCAM-1, and Ly51 in addition to CD45 and EpCAM. $CD45^{-}EpCAM^{+}$ cells were plotted FoxN1:eGFP versus ICAM-1/VCAM-1/Ly51. The analysis of E11, E12, and E13 includes parathyroid but the analysis after E13 does not include parathyroid. Percentage of cells within the gated area is shown. The contour plots show the expression pattern of ICAM-1, VCAM-1, and Ly51 on embryonic thymus at different age from E11 to E17 in FoxN1:eGFP transgenic mice.

within $CD205^+$ TEC population was found from E15 and onward. At E17, there are three TEC populations: $CD205^-$Claudin-$3,4^+$, $CD205^+$Claudin-$3,4^+$ and $CD205^+$Claudin-$3,4^-$ (Figure 3.15.). Among those three markers (Integrin-α6, LTβR, and Claudin-3,4,), only Claudin-3,4 expression allows to distinguish early embryonic TECs ($CD205^-$Claudin-$3,4^+$ and $CD205^+$Claudin-$3,4^+$) from mature TECs at late embryonic stage ($CD205^+$Claudin-$3,4^-$).

Embryonic TECs are heterogeneous according to CD205 and ICAM-1 expression at E11. There are four subsets at E11, which are $CD205^-$ICAM-1^-, $CD205^-$ICAM-1^+, $CD205^+$ICAM-1^+, and $CD205^+$ICAM-1^-. $CD205^-$ICAM-1^- and $CD205^+$ICAM-1^- TECs up-regulate ICAM-1 expression at E12. Approximately 97% of TECs express intermediate level of ICAM-1 at E13. High ICAM-1 expression within $CD205^-$ and $CD205^+$ TECs was found after E13 and its high expression is maintained until E17 (Figure 3.16.) In early embryos, TECs are divided into two populations according to ICAM-1 expression: ICAM-1^- and $ICAM^{Int}$ TECs. At later embryonic stages, all TECs express high level of ICAM-1. Thus it is not possible to distinguish TEC progenitors at late embryonic age in terms of ICAM-1 expression.

TECs start to express VCAM-1 at E13 and its expression is found within the $CD205^+$ TEC population. At E14, some of $CD205^+$VCAM-1^+ TECs turn off CD205 expression becoming $CD205^-$VCAM-1^+ TECs. After E14, all TECs express VCAM-1 and only two subsets, which are $CD205^-$VCAM-1^{High} and $CD205^+$VCAM-$1^{High/Low}$, were found (Figure 3.16.). TECs expressing Ly51 were found after E12 and its expression was restricted to $CD205^+$ TECs until E14. After E14, TECs express either low or high level of Ly51 and mainly two subsets are observed, $CD205^-Ly51^{Low}$ and $CD205^+Ly51^{High}$ populations (Figure 3.16.). Although TECs show different level of VCAM-1 and Ly51expression, all TECs are positive for both VCAM-1 and Ly51 from E14. In addition to late acquisition time of VCAM-

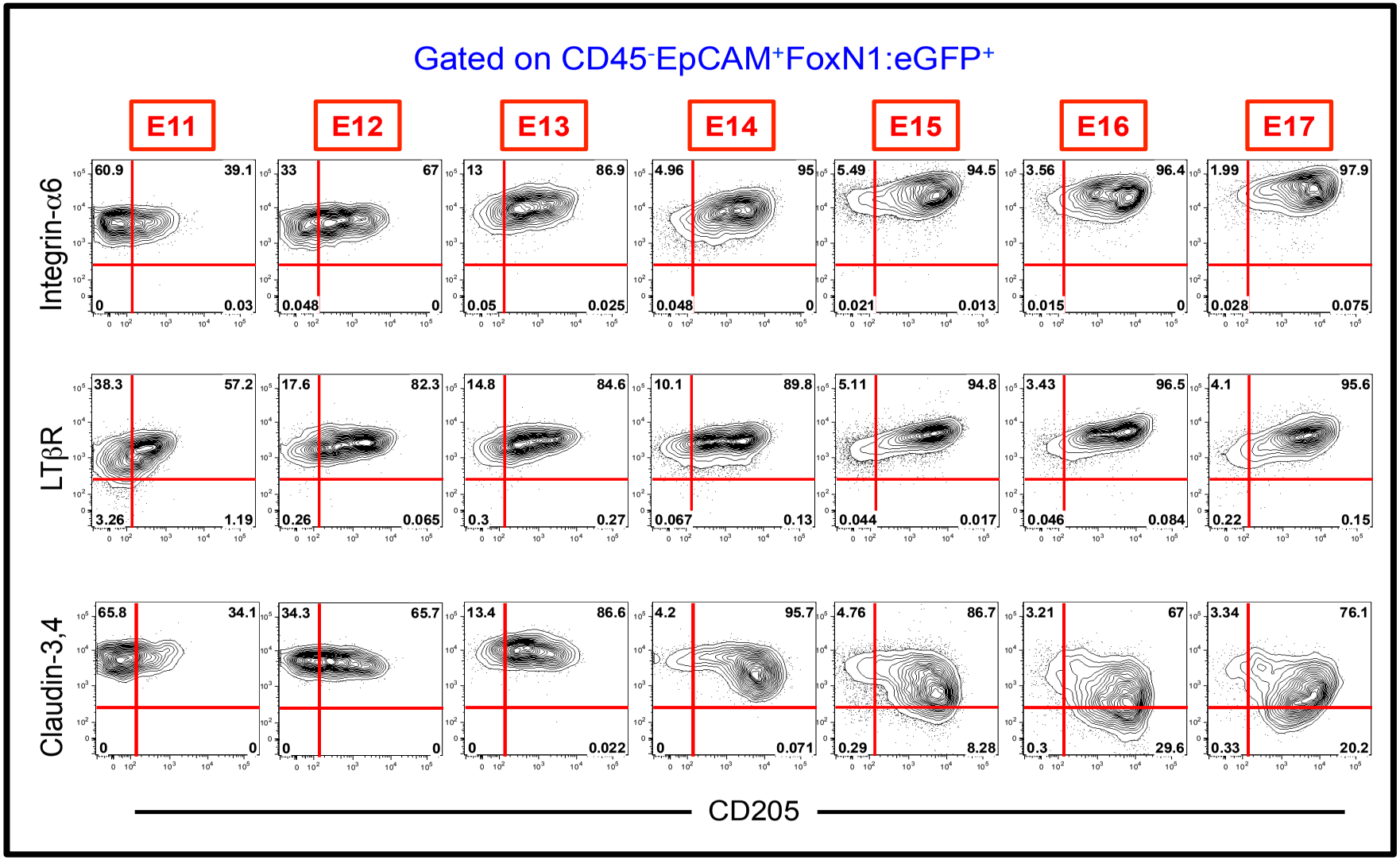

Gated on CD45-EpCAM+FoxN1:eGFP+
E11
E12
E13
E14
E15
E16
E17
Integrin-α6
LTβR
Claudin-3,4
60.9
39.1
0
0.03
33
67
0.048
0
13
86.9
0.05
0.025
4.96
95
0.048
0
5.49
94.5
0.021
0.013
3.56
96.4
0.015
0
1.99
97.9
0.028
0.075
38.3
57.2
3.26
1.19
17.6
82.3
0.26
0.065
14.8
84.6
0.3
0.27
10.1
89.8
0.067
0.13
5.11
94.8
0.044
0.017
3.43
96.5
0.046
0.084
4.1
95.6
0.22
0.15
65.8
34.1
0
0
34.3
65.7
0
0
13.4
86.6
0
0.022
4.2
95.7
0
0.071
4.76
86.7
0.29
8.28
3.21
67
0.3
29.6
3.34
76.1
0.33
20.2
CD205

Figure 3.15. Expression pattern of Integrin-α6, LTβR, and Claudin-3,4 on CD45$^-$ EpCAM$^+$FoxN1:eGFP$^+$ cells at different embryonic age from E11 to E17 in FoxN1:eGFP transgenic mice

Single cell suspensions from embryonic thymus of FoxN1:eGFP transgenic mice were prepared as described in Figure 3.1. Cells were stained for Integrin-α6, LTβR, and Claudin3,4 in addition to CD45, EpCAM, and CD205. CD45$^-$EpCAM$^+$FoxN1:eGFP$^+$ cells were plotted CD205 versus Integrin-α6/LTβR/Claudin-3,4. The analysis of E11, E12, and E13 includes parathyroid but the analysis after E13 does not include parathyroid. Percentage of cells within the gated area is shown. The contour plots show the profile of Integrin-α6, LTβR, and Claudin-3,4 expression in relation to CD205 expression on CD45$^-$ EpCAM$^+$FoxN1:eGFP$^+$ cells at different embryonic age from E11 to E17 in FoxN1:eGFP transgenic mice.

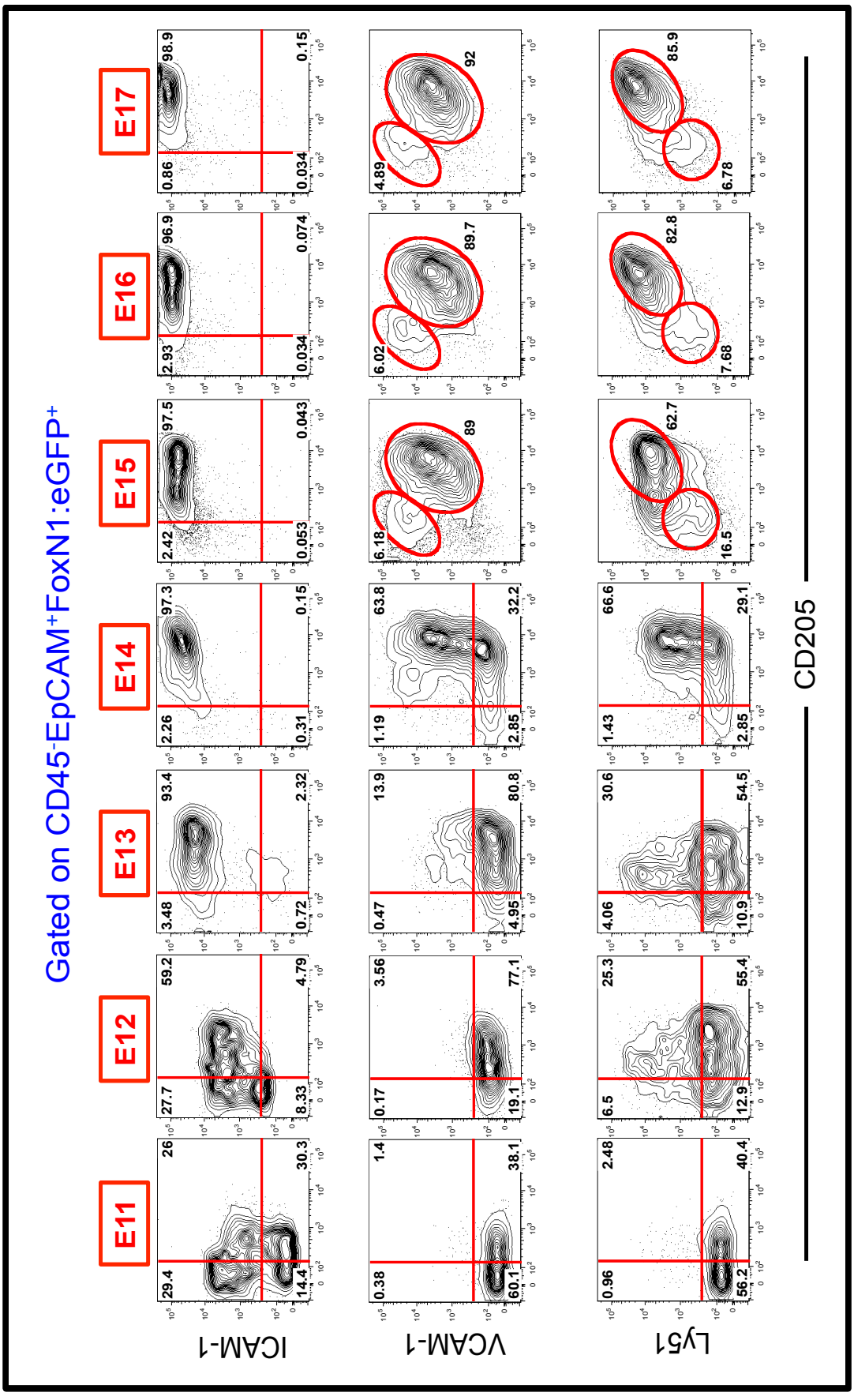

Gated on CD45-EpCAM+FoxN1:eGFP+
E11
E12
E13
E14
E15
E16
E17
ICAM-1
VCAM-1
Ly51
CD205

Figure 3.16. Expression pattern of ICAM-1, VCAM-1, and Ly51 on CD45$^-$EpCAM$^+$FoxN1:eGFP$^+$ cells at different embryonic age from E11 to E17 in FoxN1:eGFP transgenic mice

Single cell suspensions from embryonic thymus of FoxN1:eGFP transgenic mice were prepared as described in Figure 3.1. Cells were stained for ICAM-1, VCAM-1, and Ly51 in addition to CD45, EpCAM, and CD205. CD45$^-$EpCAM$^+$FoxN1:eGFP$^+$ cells were plotted CD205 versus ICAM-1/VCAM-1/Ly51. The analysis of E11, E12, and E13 includes parathyroid but the analysis after E13 does not include parathyroid. Percentage of cells within the gated area is shown. The contour plots show the profile of ICAM-1, VCAM-1, and Ly51 expression in relation to CD205 expression on CD45$^-$EpCAM$^+$FoxN1:eGFP$^+$ cells at different embryonic age from E11 to E17 in FoxN1:eGFP transgenic mice.

1 and Ly51 expression, homogeneity at late embryonic developmental stage does not allow those two markers to discriminate TEC progenitors.

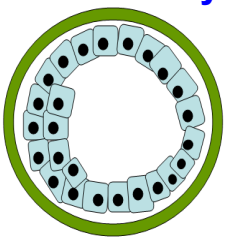
3.2.2. Restoring Thymic Function

3.2.2.1. Capability Of iPS Cells To Generate Thymic Epithelium In Vivo

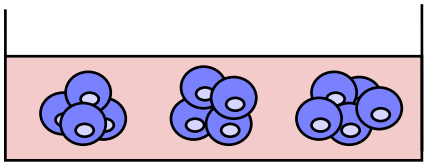
As explained earlier in the General Introduction, thymic atrophy causes problems in the immune system and many efforts to restore thymic function have been made. Reconstituting thymic epithelium is suggested as one of most promising future therapeutic strategies. In our study, we have tried to generate thymic tissue in vivo by modifying previously published methods (Muller et al., 2005). Muller *et al* injected 10 to 15 mouse embryonic stem cells (mESCs) into nude blastocysts from time-mated nude mice. Since the recipient nude blastocyst is genetically athymic, the thymus generated in mESCs/nude chimera mice can only develop from injected mESCs (Figure 3.17.). The use of ESCs has two major limitations for future therapy: ethical issues and immune rejection. In order to generate ES cells, the embryo has to be destroyed and this causes ethical issues. Moreover, the immune rejection would be another problem because ESCs would not be from patient-self. Another candidate cell line is induced pluripotent stem (iPS) cell line, which is derived from somatic cells and has pluripotency like ESCs. Thus, it resolves both ethical issues and immune rejection problem. Because it is beneficial for future therapeutic strategy, we have tested the capability of iPS cells to generate thymic tissues in vivo. iPS cells were provided by Prof. Jon Frampton. Mouse iPS cells were generated from C56BL6 mouse embryonic (E13.5) fibroblasts in the Frampton laboratory using published methods (Sommer et al., 2009).

31 mice were born from transplanted nude blastocysts, which had been injected with iPS cells. Initially, as an indication of chimerism, mice were checked for the presence of hair. Of the 31, 4 mice had patches of hair on the face, shoulder, and abdomen, indicative of

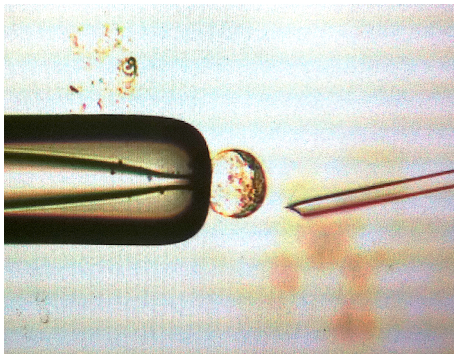
Nude blastocyst

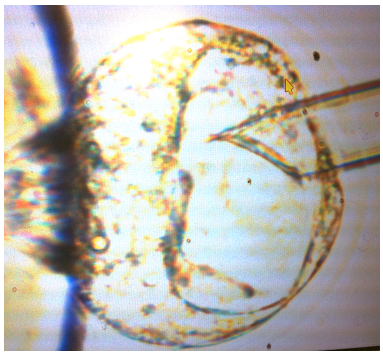


iPS cells

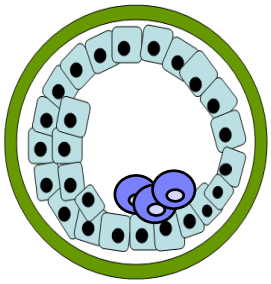


iPS cells injected into nude blastocyst





Injected iPS cells become incorporated in nude blastocyst



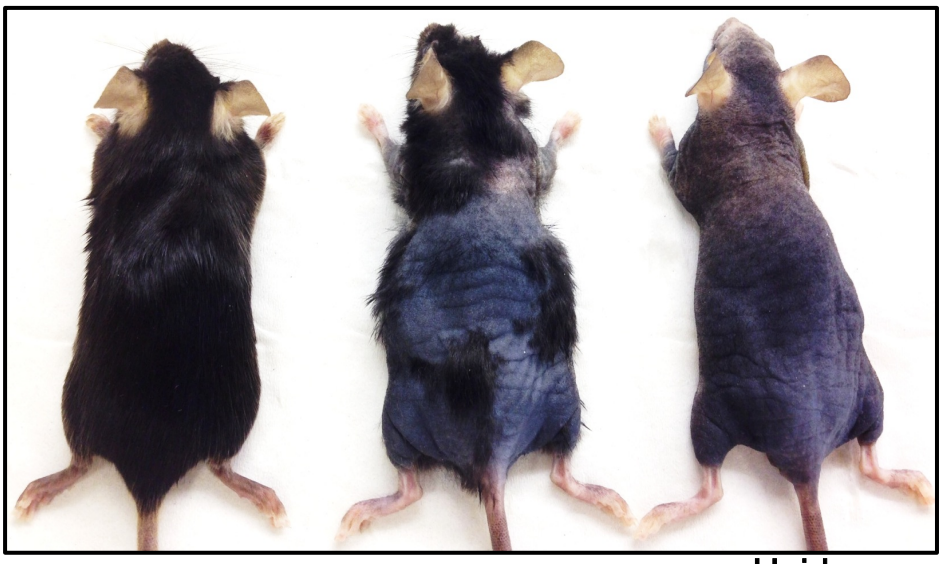
Chimera born with thymus of iPS cell origin



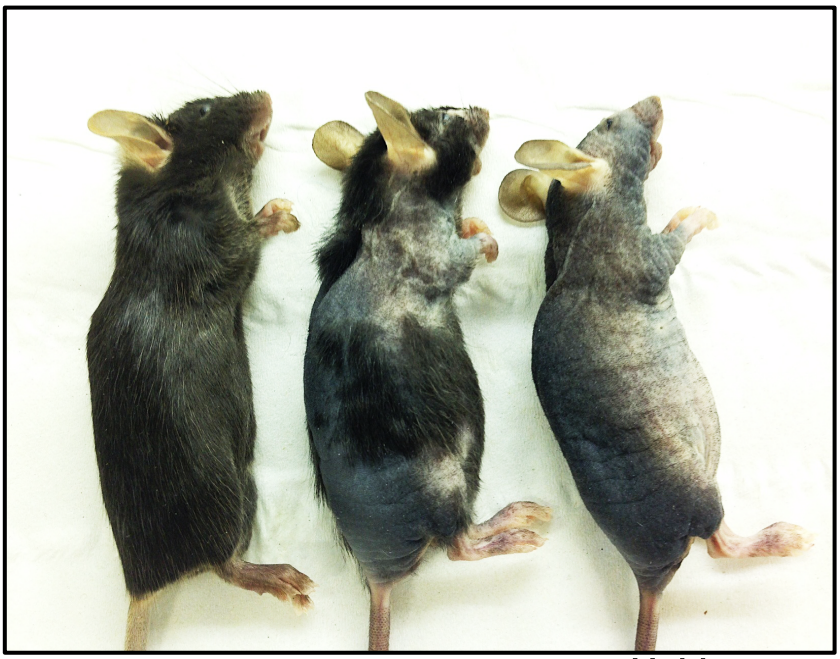
Figure 3.17. Generation of iPS chimera

iPS cells were generated from embryonic fibroblasts (E13.5) in collaboration with Professor Jon Frampton. 10 to 15 iPS cells were injected into 3.5 days post coitum (DPC) nude blastocyst. iPS-cell injected nude blastocysts were transplanted into 2.5 DPC pseudo-pregnant recipient CD1 mice. Resultant litters born were analyzed for the presence of coat and the presence of functional thymic tissue at the age of 8 to 12 weeks.

chimerism. Figure 3.18. shows wild type mice with full hair (left), iPS chimera with patches of hair (middle), and hairless nude mice (right). At the age of 4 weeks, the mice were tail-bled to check the presence of T cells in the blood would suggest the presence of thymus in chimeric animals. Lymphocytes in the blood were stained for CD4 and CD8. All 4 chimera mice with hair had both $CD4^+$ T cells and $CD8^+$ T cells in the blood. The proportion of $CD4^+$ T cells (12.5%) and $CD8^+$ T cells (7.42%) in chimera blood (Figure 3.19. C) was comparable to that of $CD4^+$ T cells (13.2%) and $CD8^+$ T cells (7.92%) in wild type mice (Figure 3.19. A). iPS chimera mice were sacrificed at the age of 6-8 weeks. Within their chest cavity we identified two lobes of thymus sitting on the top of heart (Figure 3.20. B). The location of iPS chimera thymus was similar to that of wild type (Figure 3.20. A and B). The lack of thymus in the chest cavity of nude mice is also shown in Figure 3.20. C. The size of the iPS chimera thymus was comparable to that of wild type thymus (Figure 3.20. D). Firstly, we examined the histology of iPS chimera thymus. CD205 was used to identify cortex and MTS10 was stained to identify medulla. The distinctive $CD205^+$ cortex and $MTS10^+$ medulla areas were found in iPS chimera thymus similar to that seen in wild type thymus (Figure 3.21. A). Furthermore, frozen tissue sections of iPS chimera thymus was stained with β5t (cTEC marker), MTS10 and Aire (mTEC-specific autoimmune regulator gene) (Figure 3.21. B). The presence of Aire expressing mTECs is vital for the acquisition of self-tolerance (Klein et al., 2009; Petrie and Zuniga-Pflucker, 2007). and Aire expression by mTECs verifies the normal maturation of mTECs. All three populations ($Aire^+MTS10^+$ mTECs, $Aire^-MTS10^+$ mTECs, and $\beta5t^+$ cTECs) were observed in the thymus of both iPS chimera and wild type mice (Figure 3.21. B). The picture of higher magnification displays a better view of Aire expressing mTECs, which were stained with ERTR5 (red, mTEC marker) (Figure 3.21. C). This



Wild Type　　iPS Chimera　　Hairless Nude Mice



Wild Type　　iPS Chimera　　Hairless Nude Mice

Figure 3.18. Coat chimerism

31 mice were born from transplanted nude blastocysts which iPS cell injected into. 4 (3 females, 1 male) out of 31 mice had patches of hair. The picture of iPS chimera is the representative of 4 iPS chimera. The pictures show wild type mice with hair (left), iPS chimera with patches of hair (middle), and hairless nude mice (right).

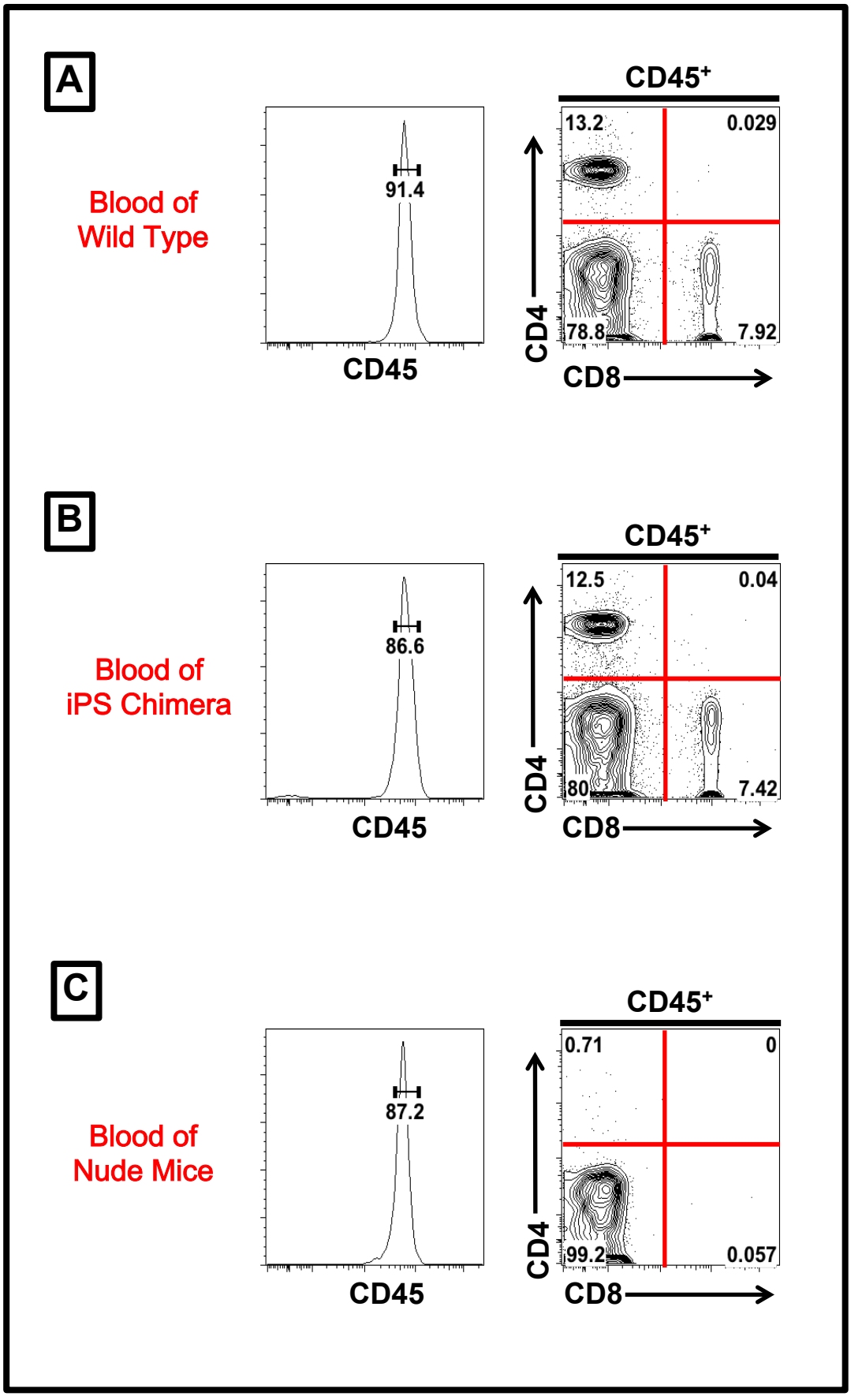
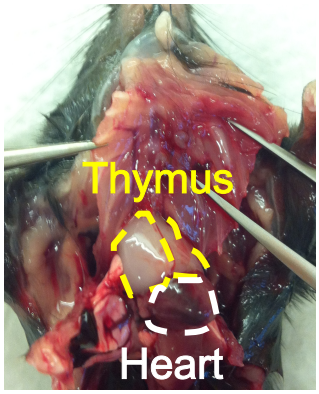

A
Blood of
Wild Type
91.4
CD45
CD45+
13.2
0.029
78.8
7.92
CD4
CD8
B
Blood of
iPS Chimera
86.6
CD45
CD45+
12.5
0.04
80
7.42
CD4
CD8
C
Blood of
Nude Mice
87.2
CD45
CD45+
0.71
0
99.2
0.057
CD4
CD8

Figure 3.19. Peripheral T cells in iPS chimera

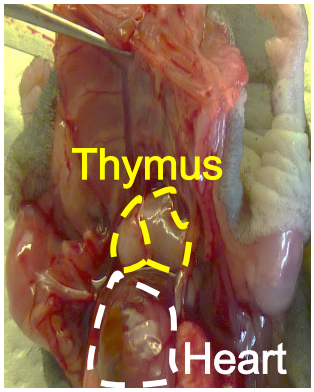
To indirectly check the presence of thymic tissue in iPS chimera, wild type (A), iPS chimera (B), and nude mice (C) were tail-bled at the age of 4 weeks. Lymphocytes in the blood were isolated and stained with CD45, CD4, and CD8 antibodies for FACS analysis. Cells were pre-gated on $CD45^+$. $CD45^+$ cells were further plotted CD4 versus CD8.

A



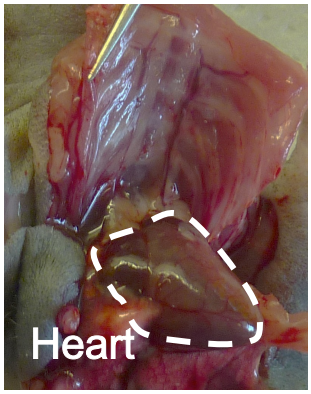
Wild Type

B



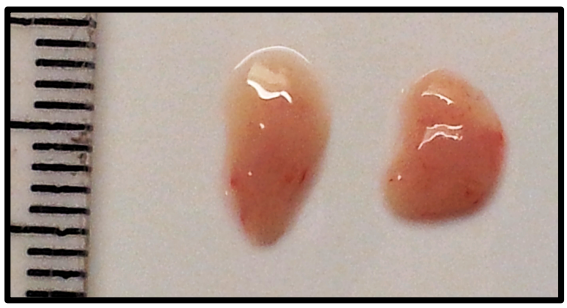
iPS Chimera

C



Nude Mouse With Absent Thymus

D



Thymus of Wild Type

Thymus of iPS Chimera

Figure 3.20. iPS cells-derived thymus in chimera

The pictures of chest cavity show the presence or absence of thymus in wild type (A), iPS chimera (B), and nude mice (C). The picture of iPS chimera is the representative of 4. 31 mice were born from transplanted nude blastocysts that iPS cell injected into. 4 mice were born with thymus (3 females, 1 male). iPS chimera were harvested at the age of 8 to 12 weeks for further analysis. The thymus size of iPS chimera was measured and compared with that of age and sex matched wild type mice (D).

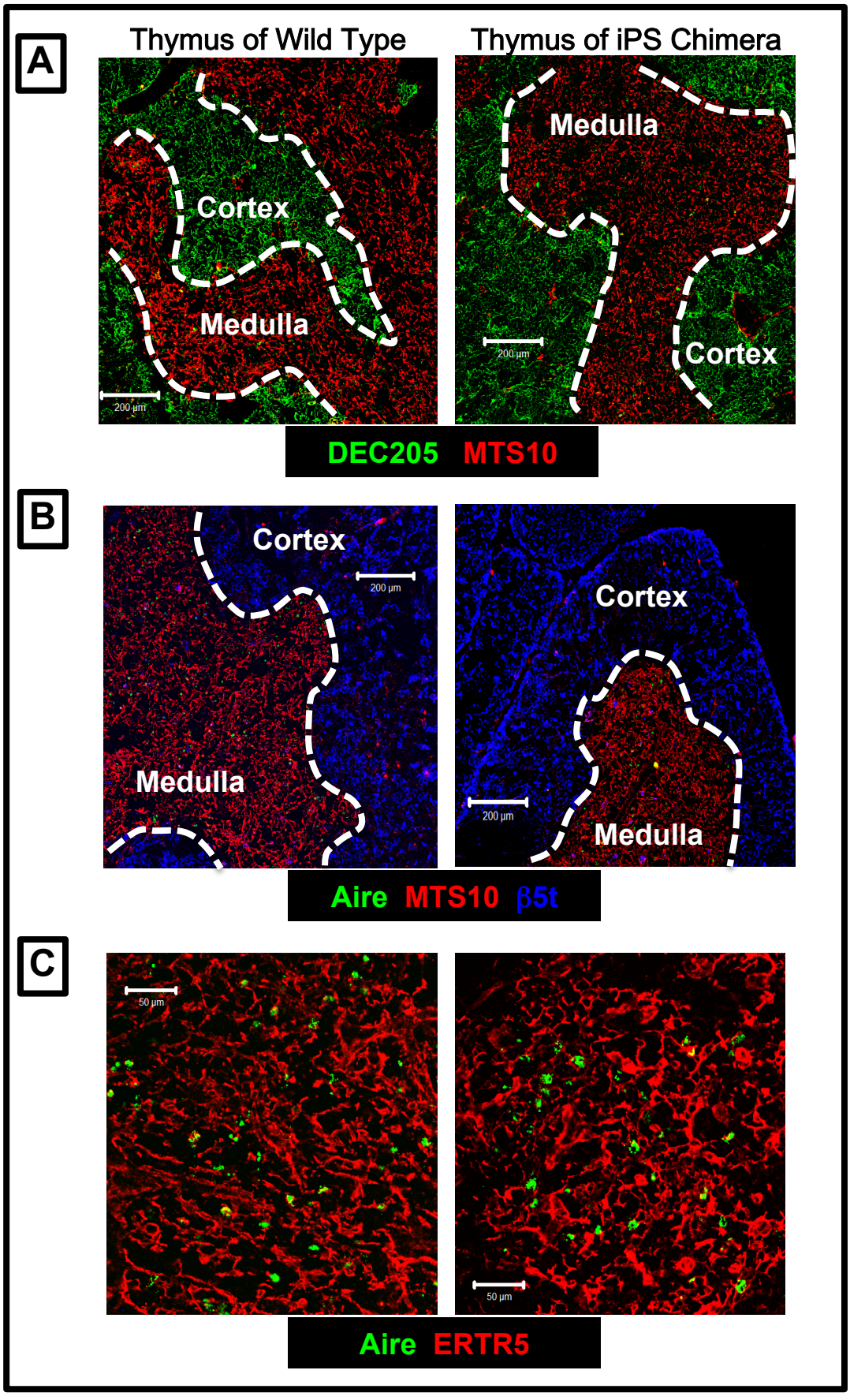

A
Thymus of Wild Type
Thymus of iPS Chimera
Cortex
Medulla
Medulla
Cortex
200 μm
200 μm
DEC205 MTS10
B
Cortex
Medulla
Cortex
Medulla
200 μm
200 μm
Aire MTS10 β5t
C
50 μm
50 μm
Aire ERTR5

Figure 3.21. Histology of iPS cells-derived thymus

(A) Frozen thymic sections of 8-12 week old iPS chimera (right) and age/sex matched wild type mice (left) were stained for DEC205 and MTS10. Bar indicates a scale of 200μm and white dashed line represents corticomedullary junction.

(B) Frozen thymic sections of 8-12 week old iPS chimera (right) and age/sex matched wild type mice (left) were stained for Aire, MTS10, and β5t. Bar indicates a scale of 200μm and white dashed line represents corticomedullary junction.

(C) Frozen thymic sections of 8-12 week old iPS chimera (right) and age/sex matched wild type mice (left) were stained for Aire and ERTR5. Higher resolution images of smaller medullary area were shown. Bar indicates a scale of 50μm and white dashed line represents corticomedullary junction.

demonstrates the normal architecture of thymic epithelium in iPS chimera, consequently confirming the capability of iPS cells to generate thymic tissues in vivo.

3.2.2.2. T-Cell Development In Thymus Of iPS Chimera Mice

Next, we examined whether thymic tissue generated from iPS cells is able to provide microenvironments for T-cell production (Figure 3.22.). The stages of T cell development can be traced by evaluating the expression pattern of co-receptors CD4 and CD8 on developing thymocytes. The most immature thymocytes are $CD4^-CD8^-$ double negative (DN) and DN thymocytes up-regulate the expression of CD4 and CD8 co-receptors, becoming DP thymocytes. After positive selection, DP thymocytes develop into either SP4 or SP8 (Klein et al., 2009). The presence of four thymocytes subsets (DN, DP, SP4, and SP8) reveals the normal T-cell development. Thymocytes were analyzed by flow cytometry. Thymus of iPS chimeras had the normal profile of developing thymocytes: DN (3.39%), DP (85.1%), SP4 (8.39%), and SP8 (3.07%) (Figure 3.22. B). We further investigated DN thymocytes because DN thymocytes are heterogeneous. The phenotype of earliest DN is $CD44^+CD25^-$ (DN1), DN1 develops into $CD44^+CD25^+$ (DN2) and then $CD44^-CD25^+$ (DN3). The most mature subset of DN is $CD4^-CD25^-$ (DN4) (Godfrey et al., 1993). All four DN subsets were present in the thymus of iPS chimera: DN1 (6.68%), DN2 (7.79%), DN3 (20.6%), and DN4 (64.9%) (Figure 3.18. B). Moreover, the proportion of four DN subsets in chimeric thymus was similar to that of wild type: DN1 (9.55%), DN2 (7.06%), DN3 (38.5%), and DN4 (44.9%) (Figure 3.22. A).

SP4 thymocytes were checked for the expression level of TCRβ and maturation markers including CD69, Qa2, CD62L, and HSA. Up-regulation of CD69 expression occurs post-positive selection. Newly generated SP thymocytes (pre-negative selection) can be distinguished from mature SP thymocytes (post-negative selection) by those four markers.

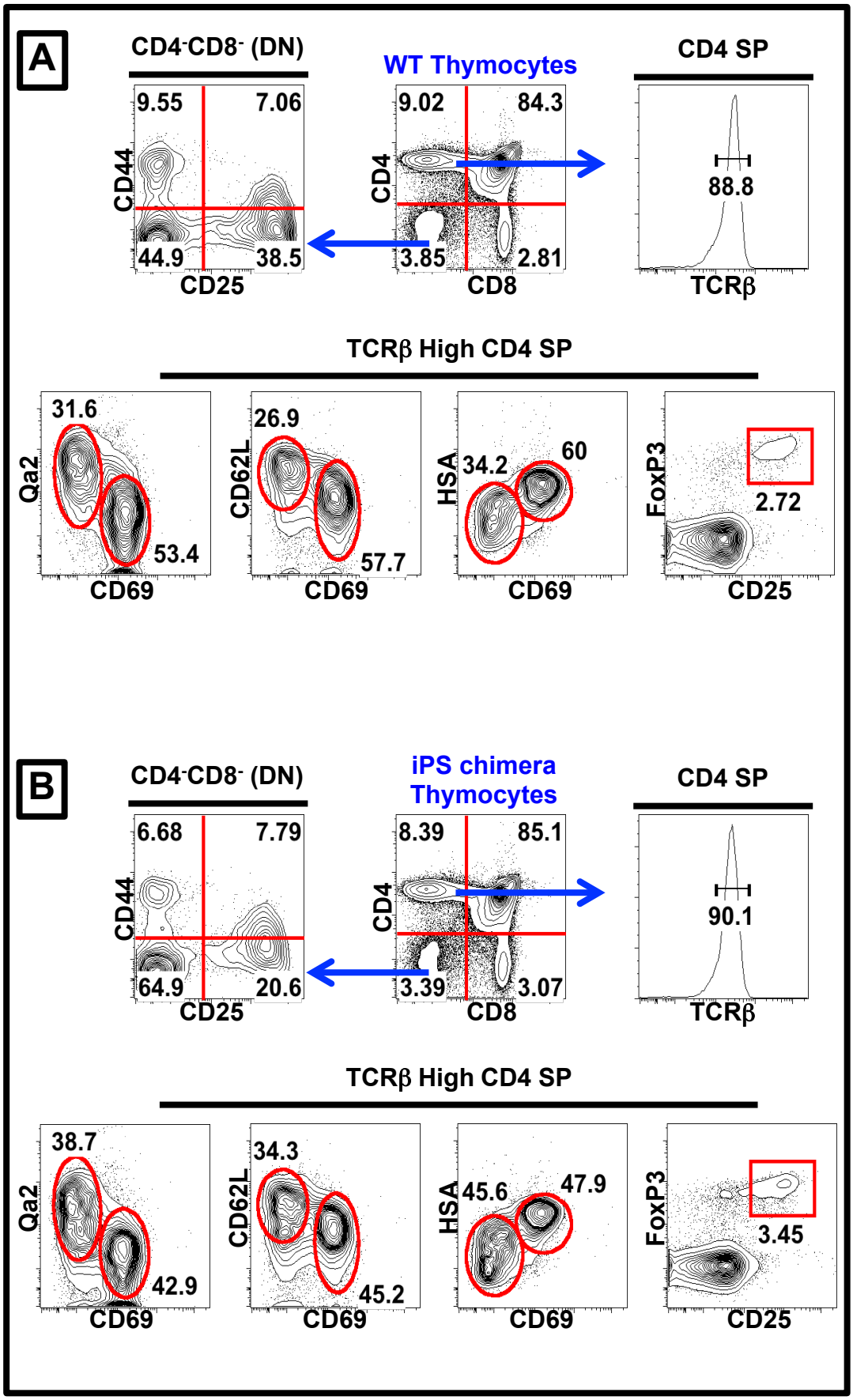

A
CD4-CD8- (DN)
WT Thymocytes
CD4 SP
9.55
7.06
44.9
38.5
CD44
CD25
9.02
84.3
3.85
2.81
CD4
CD8
88.8
TCRβ
TCRβ High CD4 SP
31.6
53.4
Qa2
CD69
26.9
57.7
CD62L
CD69
34.2
60
HSA
CD69
2.72
FoxP3
CD25
B
CD4-CD8- (DN)
iPS chimera Thymocytes
CD4 SP
6.68
7.79
64.9
20.6
CD44
CD25
8.39
85.1
3.39
3.07
CD4
CD8
90.1
TCRβ
TCRβ High CD4 SP
38.7
42.9
Qa2
CD69
34.3
45.2
CD62L
CD69
45.6
47.9
HSA
CD69
3.45
FoxP3
CD25

Figure 3.22. Analysis of T-cell development within iPS cells-derived thymus

Cells were isolated from the thymus of wild type and iPS chimera. Thymocytes were stained with antibodies of cell surface marker including CD4, CD8, CD25, CD44, CD62L, CD69, Qa2, HAS, and TCRβ for FACS analysis. Thymocytes were also analysed for intracellular FoxP3 expression within TCRβ high CD4 SP population. The contour plot of thymocytes illustrates the profile of CD4 and CD8. $CD4^{-}CD8^{-}$ double negative (DN) thymocytes were further gated to explore the profile of CD44 and CD25 expression. CD4 SP cells were checked for TCRβ expression level and then TCRβ high CD4 SP cells were further gated to analyze the profile of CD62L, CD69, Qa2, HAS, CD25, and FoxP3 expression.

The phenotype of newly generated SP4 thymocytes is $CD69^{+}Qa2^{-}CD62L^{-}HSA^{+}$ and that of mature SP4 thymocytes is $CD69^{-}Qa2^{+}CD62L^{+}HSA^{-}$ (Kishimoto and Sprent, 1997). Those two SP4 subsets were found within iPS chimera thymus in similar proportions to that in wild type thymus (Figure 3.22. A and B). Thymus of iPS chimera was also found to be capable of producing non-conventional T cells such as FoxP3 expressing Tregs, which are important for immune homeostasis and preventing autoimmune diseases (Figure 3.22. B) (Zhu and Paul, 2008). The absolute numbers of total thymocytes, TCRβ high SP4, $FoxP3^{+}$ Tregs, and TCRβ high SP8 in iPS chimera thymus were analyzed (Figure 3.23.). The cell numbers of iPS chimera were comparable with those of wild type. The difference in cell numbers between iPS chimera and wild type was not statistically significant (total thymocytes: p value=0.2601, SP4: p value=0.4874, Treg: p value=0.0811, SP8: p value=0.6061) (Figure 3.23.).

The localization of thymocytes subsets was investigated, and DP thymocytes (pink) were found in the cortex while SP4 thymocytes (blue), SP8 thymocytes (red), and FoxP3 expressing Tregs were observed within the medulla (blue: surface staining for CD4, green: intracellular staining for FoxP3), confirming the normal localization of thymocytes (Figure 3.24. A). Thymic sections of iPS chimera were also stained with CD4, CD8, and CD25 to see $CD25^{+}$ DN thymocytes (green) scattered within the cortex (Figure 3.24. B). Figure 3. 24. demonstrates the correct localization of developing thymocytes including DN, DP, SP4, SP8, and Tregs within the thymus of iPS chimera. DCs play major role in negative selection with mTECs (Spence and Green, 2008). Therefore, we next examined for the location of $CD11c^{+}$ DCs and the sections were stained with ERTR5 (Figure 3.25. A) or ERTR7 (Figure 3.25. B). $CD11c^{+}$ DCs (green) were found within $ERTR5^{+}$ medullary area (red). ERTR7 is expressed by non-epithelial cells in capsule and around blood vessels (Van Vliet et al., 1986). The

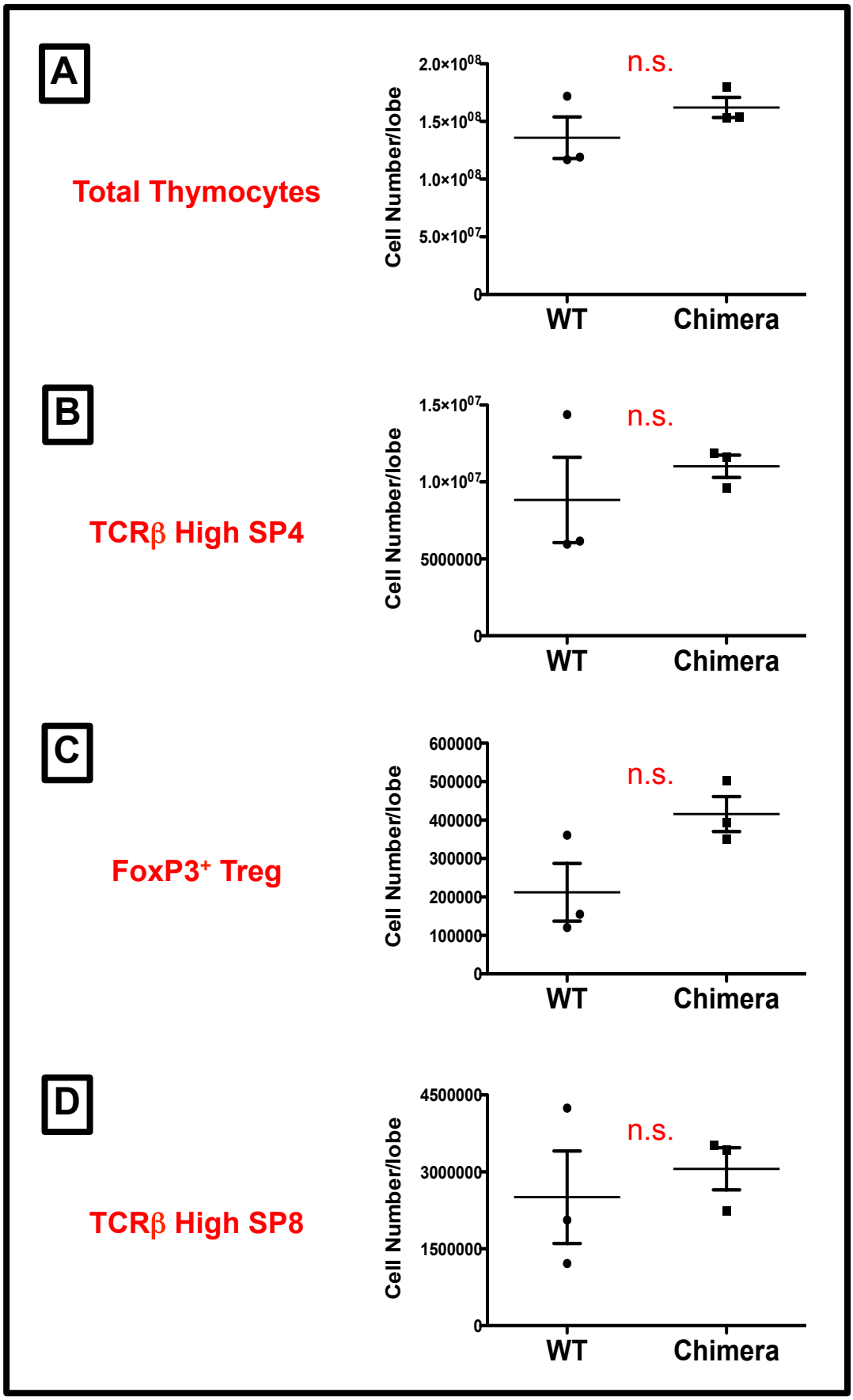

A
Total Thymocytes
Cell Number/lobe
2.0×10^08
1.5×10^08
1.0×10^08
5.0×10^07
0
n.s.
WT
Chimera
B
TCRβ High SP4
Cell Number/lobe
1.5×10^07
1.0×10^07
5000000
0
n.s.
WT
Chimera
C
FoxP3+ Treg
Cell Number/lobe
600000
500000
400000
300000
200000
100000
0
n.s.
WT
Chimera
D
TCRβ High SP8
Cell Number/lobe
4500000
3000000
1500000
0
n.s.
WT
Chimera

Figure 3.23. Quantification of thymocyte subset in iPS chimera thymus

Graph shows the absolute cell number of total thymocytes (A), TCRβ high SP4 (B), FoxP3^{+} Treg (C), and TCRβ high SP8 (D) per lobe in wild type (WT) and iPS chimera. Each point represents one mouse. The bar indicates the calculated mean value and the error bar represents the standard error of the mean. Level of significance, which was calculated using an unpaired T test, was shown (* = $P < 0.05$, ** = $P < 0.01$, *** = $P < 0.001$). P value greater than 0.05 considered as non-significant (n.s.).

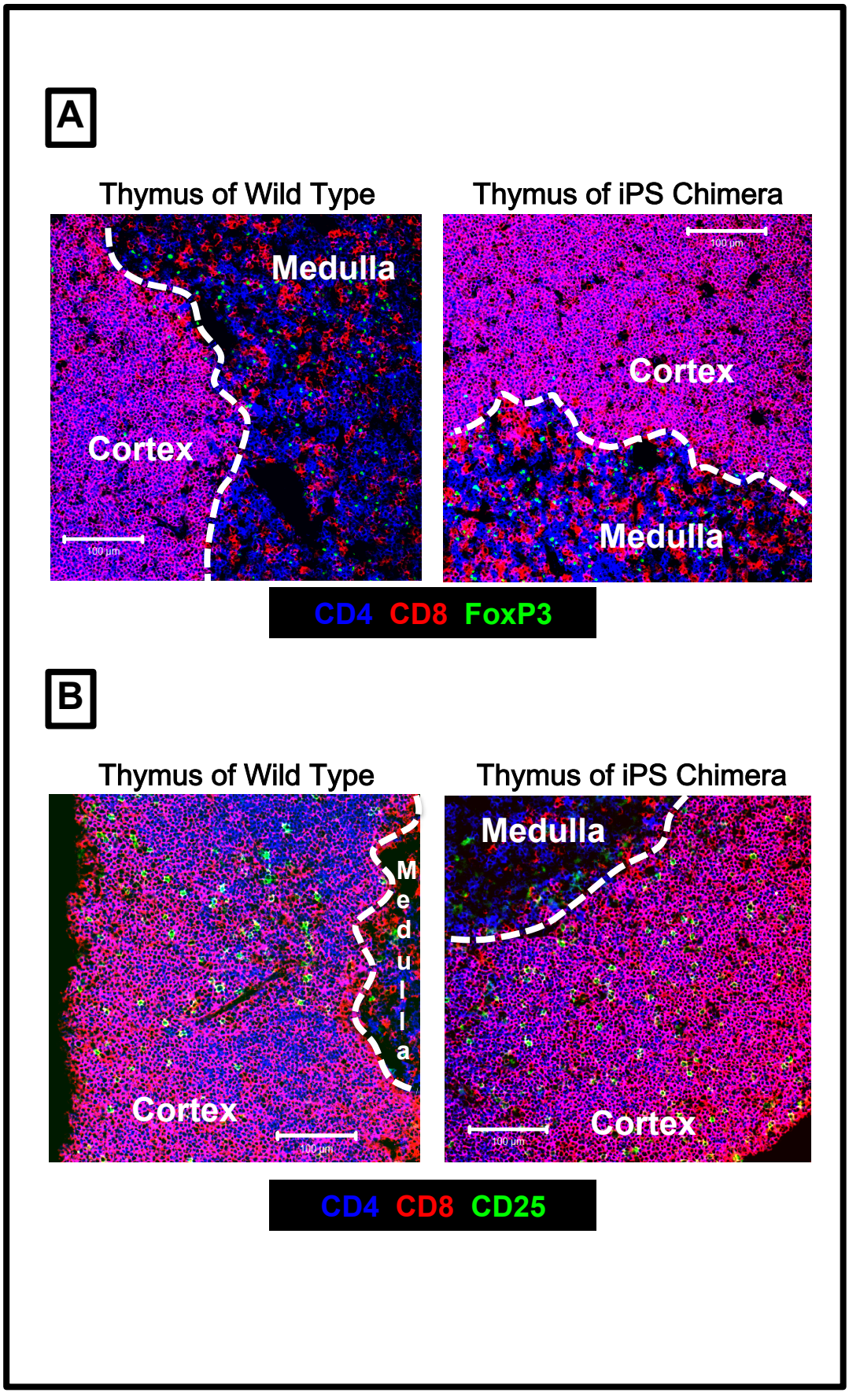

A
Thymus of Wild Type
Thymus of iPS Chimera
Medulla
Cortex
Cortex
Medulla
CD4 CD8 FoxP3
B
Thymus of Wild Type
Thymus of iPS Chimera
Medulla
Cortex
Medulla
Cortex
CD4 CD8 CD25

Figure 3.24. Localization of developing thymocytes within iPS cells-derived thymus

(A) Frozen thymic sections of 8-12 week old iPS chimera (right) and age/sex matched wild type mice (left) were stained for CD4, CD8 and FoxP3. Bar indicates a scale of 100μm and white dashed line represents corticomedullary junction.

(B) Frozen thymic sections of 8-12 week old iPS chimera (right) and age/sex matched wild type mice (left) were stained for CD4, CD8 and CD25. Bar indicates a scale of 100μm and white dashed line represents corticomedullary junction.

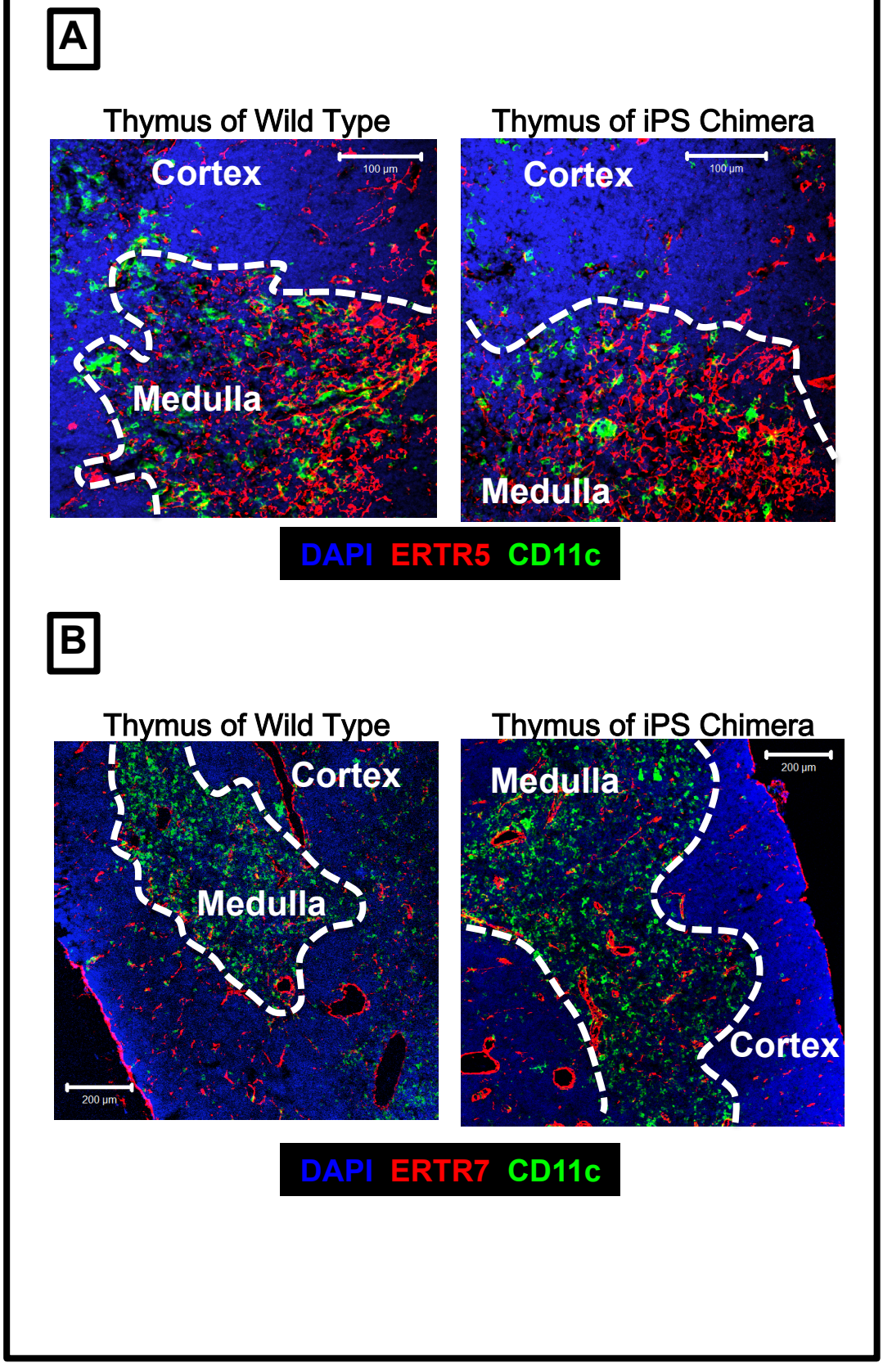

A
Thymus of Wild Type
Thymus of iPS Chimera
Cortex
Medulla
100 μm
DAPI ERTR5 CD11c
B
Thymus of Wild Type
Thymus of iPS Chimera
Cortex
Medulla
200 μm
DAPI ERTR7 CD11c

Figure 3.25. Localization of CD11c$^+$ dendritic cell within iPS cells-derived thymus

(A) Frozen thymic sections of 8-12 week old iPS chimera (right) and age/sex matched wild type mice (left) were stained for DAPI, ERTR5, and CD11c. Bar indicates a scale of 100μm and white dashed line represents corticomedullary junction.

(B) Frozen thymic sections of 8-12 week old iPS chimera (right) and age/sex matched wild type mice (left) were stained for DAPI, ERTR7, and CD11c. Bar indicates a scale of 200μm and white dashed line represents corticomedullary junction.

staining of ERTR7 (red) in iPS chimera thymic sections suggested normal vascularization of the iPS chimera thymus.

3.2.2.3. Functionality Of T cells Produced By iPS Chimeric Thymus

T cells produced by thymus have to migrate into secondary lymphoid tissues such as spleen and lymph nodes for adaptive immune response (Banchereau and Steinman, 1998). The presence of CD4 and CD8 T cells in spleen suggests the capability of iPS chimeric thymus to generate functional T cells (Figure 3.26. A). To carefully test the functionality of peripheral T cells, we investigated the activation of periphery T cells in vitro. Splenic lymphocytes were cultured in anti-CD3 coated plates and were analyzed for IFN-γ expression within T cells after 3-hour stimulation. The response to in vitro-activation was shown by the up-regulation of IFN-γ expression in CD4 and CD8 T cells (Figure 3. 26. B), indicating that T cells produced by iPS-derived thymic tissues can secrete cytokines upon stimulation.

$V\gamma5^+$ dendritic epidermal T cells (DETC) represent an example of non-conventional T cells produced by thymus, and DETCs play major role in skin immune surveillance (Macleod and Havran, 2011). To confirm whether iPS chimera thymus is able to support $V\gamma5^+$ DETC production in fetal thymus and whether $V\gamma5^+$ DETCs produced by iPS chimera thymus are able to migrate into skin, $V\gamma5^+$ DETCs in the ear of iPS chimera and wild type was checked by flow cytometry (Figure 3.27. A) and confocal (Figure 3.27. B). $V\gamma5^+$ DETC population in the ear was found by flow cytometry (Figure 3.17. A). $V\gamma5^+$ DETCs express high levels of the maturation marker CD45RB (Lewis et al., 2006). Data shown in Figure 3.27. A. indicates a normal program of $V\gamma5^+$ DETCs in iPS chimera thymic tissue, and confocal analysis of adult iPS chimera ear skin indicates normal migration of $V\gamma5^+$ DETCs from thymus into skin (Figure 3.27. B). Collectively, our data proves the capability of iPS chimera thymus to generate non-conventional T cells such as $V\gamma5^+$ DETCs.

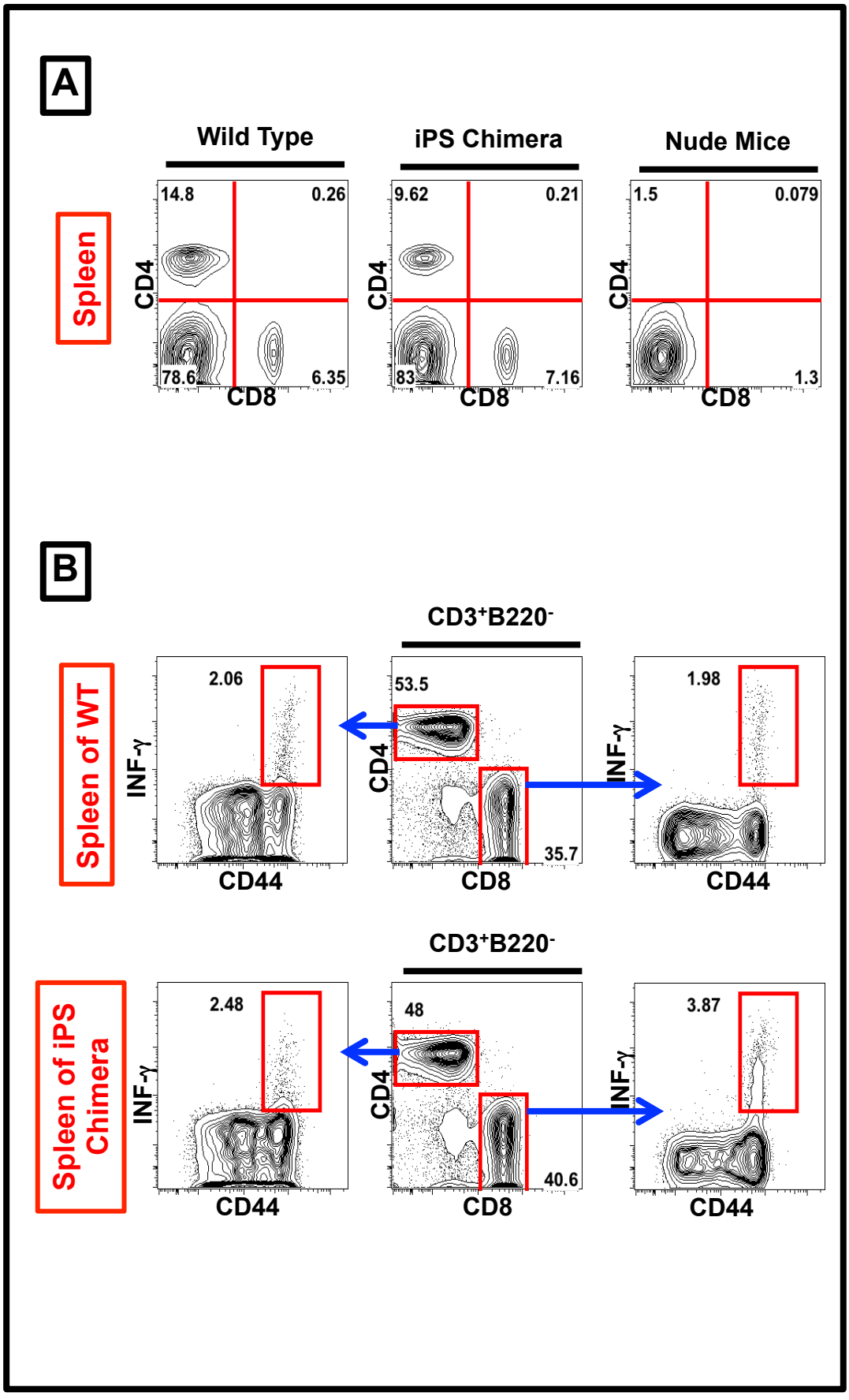

A
Wild Type
iPS Chimera
Nude Mice
Spleen
14.8
0.26
78.6
6.35
9.62
0.21
83
7.16
1.5
0.079
1.3
CD4
CD8
B
CD3+B220-
Spleen of WT
2.06
53.5
35.7
1.98
INF-γ
CD44
CD3+B220-
Spleen of iPS Chimera
2.48
48
40.6
3.87

Figure 3.26. Presence of splenic T cells in iPS chimera and functionality of peripheral T cells produced by iPS cells- derived thymus

(A) Lymphocytes were isolated from spleen of wild type (left), iPS chimera (middle), and nude mice (right). Cells were stained with CD4 and CD8 antibodies for FACS analysis to check the presence of T cells in spleen.

(B) Lymphocytes isolated from the spleen of wild type and iPS chimera were cultured in anti-CD3 coated plate for 3 hours. Cells were stained for B220, CD3, CD4, CD8, CD44 and IFN-γ. Cells were analyzed for IFN-γ expression within T cells after 3-hour incubation.

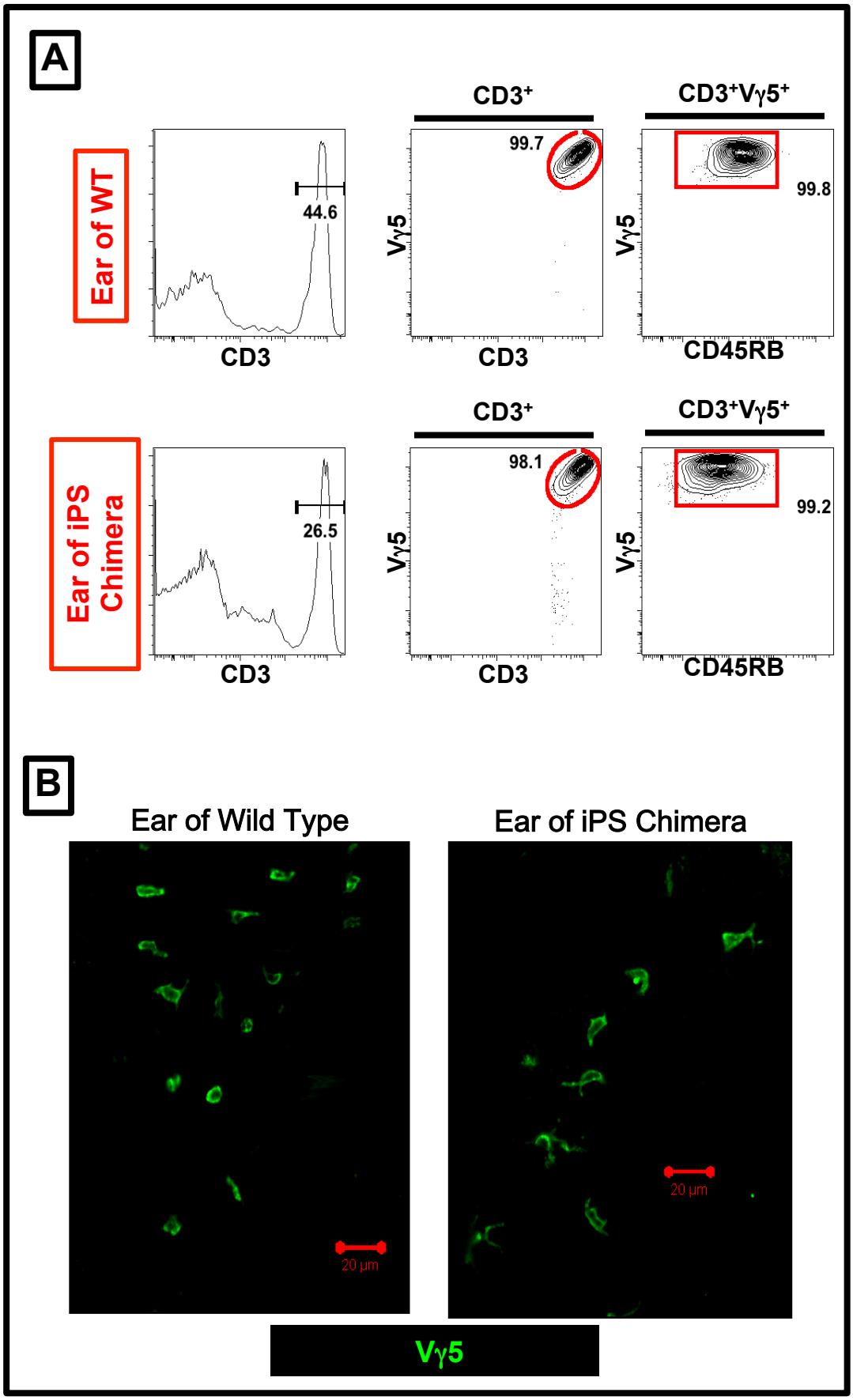

A
Ear of WT
CD3+
CD3+Vγ5+
44.6
99.7
99.8
Vγ5
CD3
CD45RB
Ear of iPS Chimera
26.5
98.1
99.2
B
Ear of Wild Type
Ear of iPS Chimera
20 μm
Vγ5

Figure 3.27. Presence of Vγ5$^+$ DETCs in ear of iPS chimera

(A) Lymphocytes were isolated from ear of wild type (top), and iPS chimera (bottom). Cells were stained with CD3, CD45RB, and Vγ5 antibodies for FACS analysis to check the presence of Vγ5$^+$ DETC in ear.

(B) Section of ear was prepared and stained with antibody for confocal as descried in chapter 2. General Method and Materials. Ear section was stained for Vγ5 to check the presence of Vγ5$^+$ DETC. Bar indicates a scale of 20μm

3.3. Discussion

3.3.1. Phenotype Of TEC Progenitors

Recently Parent *et al* and Sun *et al* have employed efforts to experimentally generate thymic tissue; using a combination of a directed TEC progenitor differentiation from ES cells in vitro and a TEC differentiation and maturation in vivo following an transplantation of in-vitro derived TEC progenitors into athymic nude mice (Parent et al., 2013; Sun et al., 2013). Before transplantation, in-vitro derived TEC progenitors were checked for FoxN1 expression because its expression is important for TEC proliferation and differentiation. Even though this approach has succeeded in generating thymic tissues from ESCs, it is still limited in the context of future therapeutic strategies. For example, the transplanted cells were not capable of self-renewal to maintain and expand its size. Moreover, T cells produced by the transplanted tissue T cells were found in the periphery but with lower TCR diversity and lower level of TCR activation-associated proliferation (Parent et al., 2013; Sun et al., 2013). If there is any other TEC progenitor marker in addition to FoxN1 to screen TEC progenitor before transplantation, it will promote the efficacy of generating functional thymic tissue. However, there are not many known progenitor markers. Therefore, we have investigated embryonic TEC development and tried to identify the phenotype of TEC progenitors in this study.

Firstly, we analyzed CD40, CD205, and PDL1 expression on early embryonic TECs using wild type, FoxN1 deficient athymic and FoxN1:eGFP mice. Consistently, data showed that embryonic TECs express both CD205 and PDL1 from E12 of gestation. Moreover, the expression of those two markers is thymus-specific and FoxN1 dependent (Figure 3.4., 3.6., and 3.9.). On the contrary, the low level of CD40 expression was found within parathyroid epithelial cells but not early embryonic TECs before E14. TEC maturation by acquiring CD40

expression within $CD205^+$ and $PDL1^+$ population initiates at E14 (Figure 3.2.). At E12, parathyroid epithelial cells, whose phenotype is $CD40^{Low}CD205^-$, comprise around 13% of total epithelial cells in thymic rudiment of wild type mouse embryos. The proportion of the subset within the $CD45^-EpCAM^+$ population declines from 13% at E12 to approximately 6% at E13 (Figure 3.3. A). A decrease in percentage of CD40 expressing parathyroid epithelial cells from E12 to E13 can be caused from two possible reasons. Firstly, it might be due to expansion of TEC; the percentage of $CD40^-CD205^+$ TECs increases from 18% at E12 to 45% at E13. Thus, parathyroid epithelial cells relatively comprise lower percentage of total $CD45^-EpCAM^+$ population. Secondly, CD40 expression by parathyroid epithelial cells might be turned off, becoming $CD40^-CD205^-$ epithelial cells. In addition to CD40, parathyroid epithelial cells also express MTS24, which is a possible TEC progenitor marker (Figure 3. 10. A and D) (Bennett et al., 2002; Gill et al., 2002). As TECs lower MTS24 expression, the epithelial cells of the parathyroid also lower its expression at E13. Overall, our data suggests that MTS24 is not TEC specific progenitor marker, and rather suggests that MTS24 might be expressed by the third pharyngeal pouch.

TECs expressing CD205 were observed from E12 in wild type mice. This population acquires CD40 expression, becoming mature cTEC $CD40^{Int}CD205^+$ at E14. The mTEC population, whose phenotype is $CD40^{High}CD205^-$, starts to appear at E14 when the percentage of $CD40^{Int}CD205^+$ cells is highest. $CD40^{High}CD205^-$ cells seem to branch out from the $CD40^{Int}CD205^+$ subset (Figure 3.2. A). The bigger the $CD40^{High}CD205^-$ subset, the smaller the $CD40^{Int}CD205^+$ population gets (Figure 3.3. A). Current understanding of TEC development is based on binary model. The binary model of cTEC and mTEC commitment suggests that cTEC and mTEC development are separate and there is no relation between two lineage developments but share a common precursor. However, our phonotypical analysis

proposes a possible developmental relationship between cTEC and mTEC lineages. Our data suggest either that CD205 expression marks TEC progenitors, which can give rise to both cTEC and mTEC, or that mTEC development has to go via the cTEC stage acquiring CD205 expression. To support the idea, the developmental stages from progenitors to lineage committed TECs needs to be thoroughly confirmed. Moreover, the initial acquisition time of cTEC and mTEC lineage should be also examined. This new model of TEC development, suggested from our data, is that one of two epithelia would be derived from the other. If the cTEC population gives rise to an mTEC population, cTEC would be the progenitors of mTEC and the emerging time of cTEC and mTEC would not be concurrent.

PD-L1 is a member of B7 family and it binds to PD-1 expressed on T cells. PD-1:PD-L1 co-stimulatory signal exerts inhibitory effects on T-cell activation and it plays a major role in balancing between activation and tolerance (Guermonprez et al., 2002; Keir et al., 2008). PD-L1 expression pattern is very similar to CD205 expression in embryo (Figure 3.2. B and C). It starts to be expressed at E12 and its expression was found within $CD205^{+}$ TECs. As explained earlier, CD205 expression might mark TEC progenitors in the embryo instead of cTECs. Therefore, to confirm whether it is cTEC-specific, PD-L1 expression should be checked with other markers like Ly51. In addition to CD40, CD205, and PD-L1, PD-L2 expression on embryonic TECs was also explored but its expression was not found, suggesting PD-L2 as a postnatal marker (Figure 3.2. D). Collectively, the phenotype of embryonic TEC at E12 is $CD40^{-}CD205^{+}PD\text{-}L1^{+}PD\text{-}L2^{-}MTS24^{+}$ and that of parathyroid epithelial cells is $CD40^{Low}CD205^{-}PD\text{-}L1^{-}PD\text{-}L2^{-}MTS24^{+}$.

Surface markers such as CD40, CD205, PD-L1, PD-L2, and MTS24 are not sufficient to identify the phenotype of TEC progenitors. Hence, we analyzed the expression pattern of surface markers that are important in TEC and T-cell development using FoxN1:eGFP

embryo. The markers including Integrin-α6, LTβR, Claudin-3,4, ICAM-1, VCAM-1, and Ly51 were analyzed in this study (Figure 3.13. to Figure 3.16.). In order to be used as a progenitor marker, it would be ideal to meet two conditions. The two conditions could be thymus-specific expression and early acquisition time of its expression like E11 when FoxN1 expression begins. However, each of those six markers fails either condition. The expression of Integrin-α6, LTβR, Claudin-3,4, and ICAM-1 is not thymus specific, though the acquisition time of those expression is at E11 and TECs sustains the expression until late embryonic stage (Figure 3.13. and 3.14.). Moreover, VCAM-1 and Ly51 are not expressed as early as E11 (Figure 3.14.). Even though none of those six markers can be used as a definitive TEC progenitor marker, we propose the putative phenotype of TEC progenitor, which is $CD205^{-/+}$Claudin-$3,4^{+}Ly51^{-}VCAM\text{-}1^{-}$Integrin-$\alpha6^{+}LT\beta R^{+}ICAM\text{-}1^{-/+}$. At E17, there are two subsets within FoxN1:$eGFP^{+}$ cells: $CD205^{-}$Claudin-$3,4^{+}Ly51^{Low}VCAM\text{-}1^{High}$ and $CD205^{+}$Claudin-$3,4^{-/+}Ly51^{High}VCAM\text{-}1^{Low/High}$. All of FoxN1:$eGFP^{+}$ TECs express Integrin-α6, LTβR, and ICAM-1 at late embryonic stage (Figure 3.15. and 3.16.). Our data emphasizes the potential of CD205 as a TEC progenitor marker rather than the six surface markers. As discussed earlier, CD205 expression specific to thymus and not expressed by parathyroid (Figure 3.4., 3.6., and 3.9.) and its expression starts at E11 (Figure 3.15. and 3.16.). Furthermore, CD205 expression is maintained until late embryonic stages, providing heterogeneity in terms of CD205 expression. Overall, our phenotypical analysis suggests CD205 as a TEC progenitor marker but molecular and functional features of $CD205^{+}$ TECs have to be investigated.

At early embryonic stages from E11 to E13, data here suggests that the embryonic TECs differentiate from progenitors rather than proliferate; absolute cell numbers are maintained until E13 and then dramatically increase from E13 to E15 (Figure 3.12.). Between

E13 and E15, TEC cellularity expands and also TECs show a dramatic change in phenotype (Figure 3.12. and 3.16.). From E15, both cellularity and phenotype of embryonic TECs are maintained according to the markers we have looked for this study (Figure 3.2. and Figure 3.12. to Figure 3.16.). However, it is known that mTEC maturation occurs at late embryonic stage, acquiring Aire expression (White et al., 2008). To summarize, it is assumed that there are three stages in embryonic TEC development: early differentiation from E11 to E13, dynamic change in both cellularity and phenotype from E13 to E15, and late mTEC maturation from E15 to E17.

Approximately 5% of TECs not expressing FoxN1:eGFP after parathyroid separation at E13 are present through late embryonic stages (Figure 3.11., 3.13., and 3.14.). The phenotype of GFP^- TECs at late embryonic age is identical with that of GFP^+ TECs except for GFP expression. Possible explanations for this might be that the GFP^- cells are a TEC lineage, which is independent of FoxN1 expression. The finding by Nowell *et el* supports this idea. Nowell *et al* identified $K5^{high}$Claudin-$3,4^{high}$ and $K5^-$Claudin-$3,4^-$ TECs in E13 nude embryo (Nowell et al., 2011) suggesting that the mTEC lineage, or at least initial commitment, might not need FoxN1 gene expression. The GFP^- TECs at late embryonic age observed in this study might be developed from the $K5^{high}$Claudin-$3,4^{high}$ TECs that Nowell *et al* found in nude embryo.

3.3.2. Capability Of iPS Cells To Generate Thymic Epithelium

With advancing age, the production of naïve T cells by thymus decreases resulting in increased incidences of viral and bacterial infections. In order to overcome thymic senescence, efforts of generating thymic epithelium have been made by several studies. Pluripotent embryonic stem cells have been studied for the purpose of recovering damaged tissues such heart, liver, pancreas. However, the method of obtaining ES cells causes practical

and ethical issues. Alternative cell lines that can regenerate damaged tissues include induced pluripotent stem cells. In 2006, Takahashi and Yamanaka had success in reprograming mouse fibroblasts into a pluripotent state by the ectopic gene expression of four transcription factors that are Oct4, Sox2, Klf4, and c-Myc (Yamanaka and Takahashi, 2006). For future therapeutic purpose, it is examined in this study whether the generation of thymic epithelium using iPS cells is feasible to combat thymic atrophy. To check the capability of iPS cells to generate functional thymic tissues in vivo, we employed the published technique. Muller *et al* showed that the generation of thymus in vivo is possible by using ES cells and nude blastocysts; thymus in chimera mice had to be differentiated from ES cells (Muller et al., 2005). Instead of using ES cells, iPS cells were used for this study.

We had a success in generating thymus from iPS cells in vivo (Figure 3.18., 3.19., and 3.20.). The thymus of iPS chimera was examined for histology, cellularity, T-cell development within the tissue, production of non-conventional T cells including Tregs and $V\gamma5^+$ DETCs (present in ear), and functionality of peripheral T cells to ascertain that iPS thymus is functional.

The iPS thymus had normal histology including distinct cortex ($CD205^+$ and $\beta5t^+$ cTECs) and medullary area ($MTS10^+$ and $ERTR5^+$ mTECs) (Figure 3.21. and 3.25.). Furthermore, one of most mature mTECs, whose phenotype is $Aire^+$ mTEC, was found, demonstrating normal TEC development (3.21. C). It also had comparable thymocyte cellularity to wild type (Figure 3.23.). We observed not only the normal cellularity of thymocyte subsets (Figure 3.23.) but also normal T-cell development having DN1-4, DP, SP4 (immature SP4 $CD69^+Qa2^-CD62L^-HAS^+$ and mature SP4 $CD69^-Qa2^+CD62L^+HAS^-$), and SP8 developing thymocytes subset within iPS thymus (3.22. B). Then, we tested whether T cells produced by the iPS-derived thymus can migrate into secondary lymphoid tissues to induce

adaptive immune response. We found $CD4^+$ helper T cells and $CD8^+$ cytotoxic T cells in both spleen (Figure 3.26. A) and lymph node (data not shown). Furthermore, peripheral T cells in iPS can be activated upon in-vitro stimulation that leads to cytokine IFN-γ production (Figure 3.26.). This confirms that T cells produced by iPS chimeric thymus are functional. Collectively, our data proves the capability of iPS cells to generate functional thymic tissue, which provides specialized microenvironment for T-cell development.

CHAPTER 4. Lineage Development of cTEC and mTEC

4.1. Introduction

Based on ontogenetic analysis shown in the previous chapter, we investigated the potential developmental relationships between cTEC and mTEC. In this study, CD205 was used to identify the cTEC lineage. We showed that the appearance of the $CD205^+$ cTEC lineage occurs prior to the emergence of the $CD205^-$ mTEC lineage. After cTEC lineage commitment, $CD205^+$ TECs up-regulate CD40 expression becoming mature cTEC, whose phenotype is $CD40^{Int}CD205^+$. Then, the $CD40^{High}CD205^-$ mTEC population branches out from the mature cTEC population. Hence, we propose a serial developmental pathway based on this phenotype analysis; with TEC progenitors developing into phenotypically defined cTECs, which then give rise to mTECs. In this chapter, we will more focus on testing the developmental potential of CD205 expressing TECs such as the functional responses to mTEC lineage-specific stimulation and the competence to differentiate into the most mature mTEC subset, $Aire^+$ mTECs. Thus, the aims of this chapter are to:

- Investigate the competence of early embryonic TECs expressing the cTEC marker CD205 to undergo maturation upon RANK stimulation, one of TNF-Receptor superfamily members essential for mTEC differentiation.
- Examine the capacity of $CD205^+$ TECs to generate functional mTECs via precursor-product analysis.
-Investigate the role of Wtn5a in TEC development, specifically in inducing RANK expression on TECs.

4.2. Results

4.2.1. Investigating The Capability Of CD205$^+$ TECs To Develop Into cTECs and mTECs

4.2.1.1. Ontogenetic Analysis of cTEC and mTEC Using FoxN1:eGFP Transgenic Mice

In the previous chapter, analysis of TEC ontogeny in wild type mice was performed. In this chapter, we explored the cTEC/mTEC ontogeny in FoxN1:eGFP embryos. In addition, the cells from CD205$^{-/-}$ embryos were stained with all the surface markers that were used for the analysis of TEC ontogeny in FoxN1:eGFP embryos, confirming the specificity of CD205 staining at early embryonic stages. Pre-gated CD45$^-$EpCAM$^+$ cells from E11 and E12 CD205$^{-/-}$ embryo were plotted to reveal expression of CD40 and C205 (Figure 4.1. A). CD45$^-$EpCAM$^+$ cells at different embryonic age from E11 to E17 were further gated on GFP$^+$ population and then CD45$^-$EpCAM$^+$GFP$^+$ TECs were plotted in the same way with CD205$^{-/-}$ embryo. CD205$^+$ TECs were found from E11 (36.9%) and the percentage of CD205$^+$ TECs within total TECs doubled in the transition between E11 and E12 (63.5%). As seen in wild type mice, TECs acquire CD205 expression prior to CD40. From E13, CD40 expression was found within CD205$^+$ TEC population. After E14, CD40^{High}CD205$^-$ TEC population (4.14%) began to appear, branching out from the CD40^{Int}CD205$^+$ population After E15, the proportion of CD40^{Int}CD205$^+$ cTECs decreased until E17, subsequently leading to the increase in the percentage of CD40^{High}CD205$^-$ mTECs (Figure 4.1. B). The phenotypical analysis of embryonic TECs in FoxN1:eGFP mice showed similar TEC development in terms of CD40 and CD205 expression with that in wild type mice, suggesting again a serial pathway in cTEC/mTEC development.

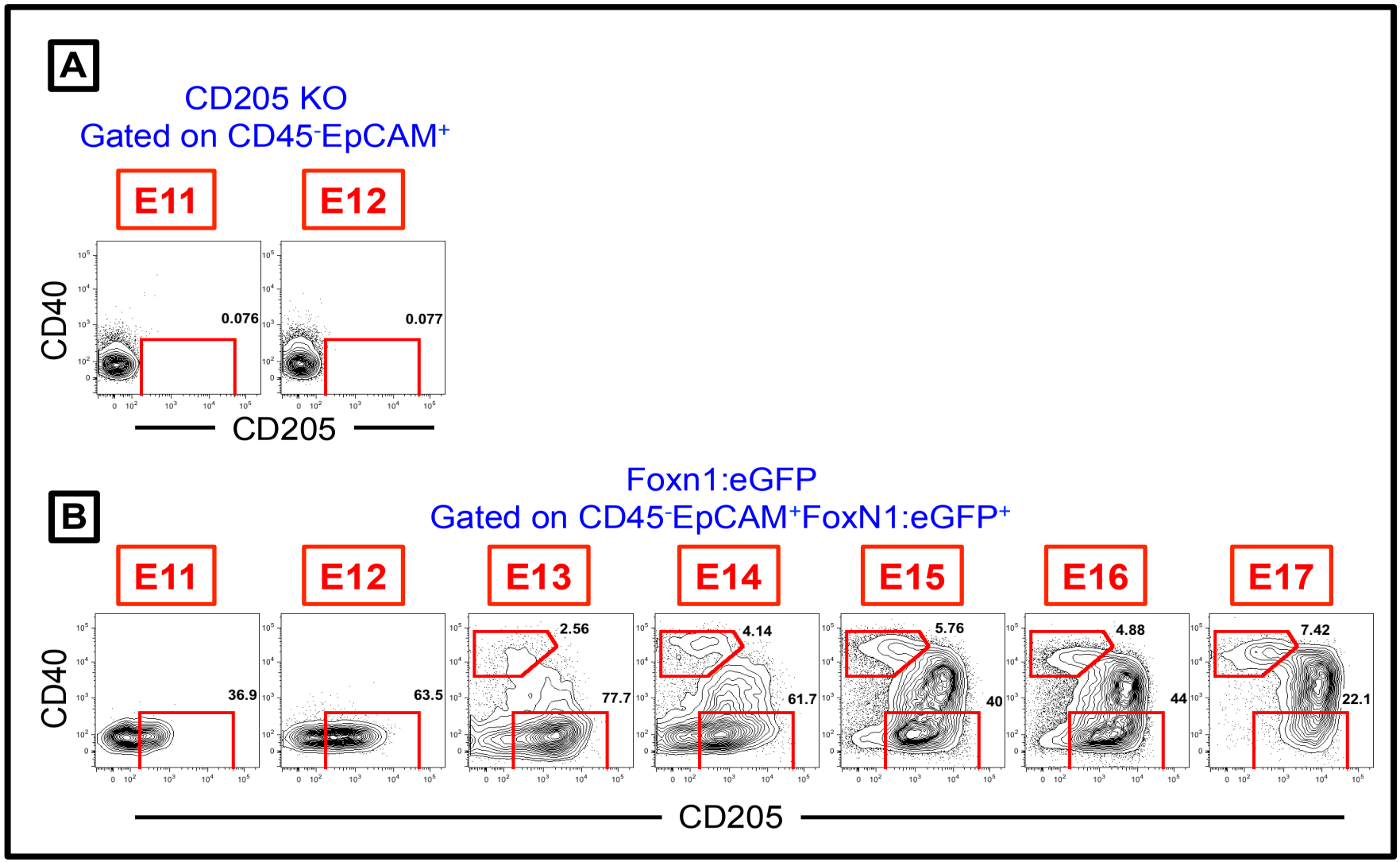

A
CD205 KO
Gated on CD45-EpCAM+
E11
E12
CD40
0.076
0.077
CD205
B
Foxn1:eGFP
Gated on CD45-EpCAM+FoxN1:eGFP+
E11
E12
E13
E14
E15
E16
E17
CD40
36.9
63.5
2.56
77.7
4.14
61.7
5.76
40
4.88
44
7.42
22.1
CD205

Figure 4.1. TEC ontogeny in FoxN1:eGFP transgenic mice

Thymic cells from embryonic FoxN1:eGFP transgenic mice and CD205 KO mice were stained for CD40 and CD205 in addition to CD45 and EpCAM. Pre-gated $CD45^{-}EpCAM^{+}$ cells of CD205 KO embryos were plotted for expression of CD40 versus CD205. $CD45^{-}EpCAM^{+}$ cells of FoxN1:eGFP transgenic mice were further gated on GFP^{+} cells, and then were plotted CD40 versus CD205. Percentage of cells within the gated area is shown. The contour plots illustrate the profile of CD40 and CD205 expression on GFP^{+} TECs at different embryonic ages, from E11 to E17.

4.2.1.2. Induction Of Maturation Within CD205$^+$ TEC By The mTEC Regulator RANK

RANK is a member of the TNF-Receptor superfamily, which is essential for mTEC maturation in embryo (Hikosaka et al., 2008). White *et al* demonstrated that the RANK signal induces Aire expression within mTEC population in late embryonic stage (White et al., 2008). However, neither the acquisition time of RANK expression in embryonic TEC nor the role of RANK signal in early embryonic TEC development were investigated previously. This is due to the lack of either antibodies to detect RANK-expressing cells by flow cytometry, or RANK-reporter mice. Therefore, we examined the competence of defined populations of early embryonic TECs to undergo maturation upon RANK stimulation. Responsiveness to RANK stimulation indirectly demonstrates its expression.

Thymus rudiments of E11 and E12 FoxN1:eGFP embryos were cultured in the absence or presence of agonistic RANK antibodies. Maturation induced by RANK stimulation was indicated by the up-regulation of MHC class II and CD40 because both markers are expressed only in mature TECs (Shakib et al., 2009). Moreover, the expression of MHC class II and CD40 is absent before E13 (Figure 4.1. B). Upon 1-day RANK stimulation, the up-regulation of MHC class II and CD40 expression was not found in E11 FoxN1:eGFP$^+$ TEC population but the percentage of MHCII$^+$CD40$^+$ cells within E12 FoxN1:eGFP$^+$ TECs increased from 18.5% to 55.9% (Figure 4.2. A and B). Moreover, the maturation induced by RANK stimulation was only observed in FoxN1:eGFP$^+$ TECs but not in FoxN1:eGFP$^-$ epithelial cells of E12 thymus rudiments (Figure 4.2. B). One could raise a question that lack of response of E11 FoxN1:eGFP$^+$ TECs to stimulation might be due to suboptimal culture conditions. However, responses of E11 FoxN1:eGFP$^+$ TECs to 2-day RANK stimulation, by up-regulating MHC class II and CD40 expression was observed (data not shown), arguing against this possibility. Collectively, the induction of TEC development upon RANK

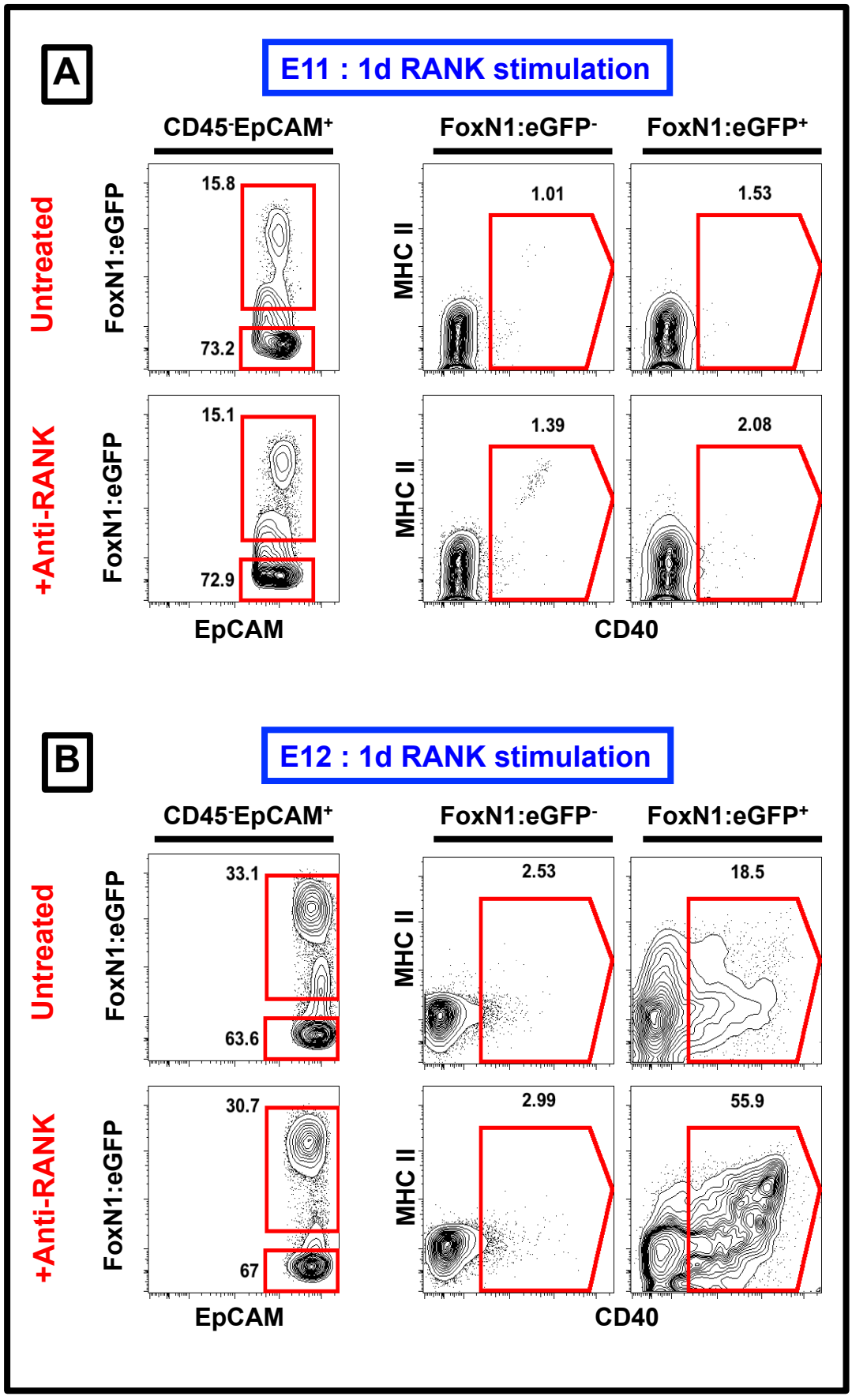

A
E11 : 1d RANK stimulation
CD45-EpCAM+
FoxN1:eGFP-
FoxN1:eGFP+
Untreated
+Anti-RANK
FoxN1:eGFP
MHC II
15.8
73.2
1.01
1.53
15.1
72.9
1.39
2.08
EpCAM
CD40
B
E12 : 1d RANK stimulation
CD45-EpCAM+
FoxN1:eGFP-
FoxN1:eGFP+
Untreated
+Anti-RANK
FoxN1:eGFP
MHC II
33.1
63.6
2.53
18.5
30.7
67
2.99
55.9
EpCAM
CD40

Figure 4.2. 1-day RANK stimulation of E11 and E12 TECs

Thymus/Parathyroid rudiments of E11 and E12 Foxn1 FoxN1:eGFP transgenic mice were dissected out and then cultured without/with agonistic RANK antibody for 1 day. After 1-day culture, tissues were harvested for FACS analysis. Cells were isolated and stained with CD45, EpCAM, CD205, CD40, and MHC class II antibodies. Percentage of cells within the gated area is shown. The contour plots illustrate the profile of CD40 and MHC class II expression on GFP^- and GFP^+ epithelial cells.

stimulation is specific for cells within the FoxN1:eGFP^{+} TEC population in embryonic thymus and the acquisition of this property occurs between E11 and E12 of gestation, demonstrating that RANK-expressing TECs emerge in a transition from E11 to E12.

To find which TEC subset expresses RANK in early embryo, we further examined the response to RANK stimulation in the context of CD205 expression within TEC. Since the CD205 expression pattern of FoxN1:eGFP TECs is continuous, we divided TEC into three populations: CD205^{-}, CD205^{Low}, and CD205^{High}. All three populations within E11 TEC failed to undergo maturation upon 1-day RANK stimulation (Figure 4.3. A). However, surprisingly not only CD205^{-} but also CD205^{Low} and CD205^{High} TECs of E12 FoxN1:eGFP successfully responded to RANK stimulation by up-regulating MHC class II and CD40: CD205^{-} (13.7% to 37%), CD205^{Low} (17.7% to 53.1%), and CD205^{High} (23.3% to 83%) (Figure 4.3. B). This indicates that a TEC subset expressing the cTEC marker CD205 in embryonic thymus co-expresses a key regulator of mTEC development, RANK.

The quantitative analysis demonstrating an increase in the percentage of the MHCII^{+}CD40^{+} TEC population upon 1-day RANK stimulation is presented in Figure 4.4. None of the E11 GFP^{+} TEC subsets had a statistically significant increase in MHCII^{+}CD40^{+} cells upon 1-day RANK stimulation (CD205^{-}: p value=0.4735, CD205^{Low}: p value=0.7116, CD205^{High}: p value=0.5369) (Figure 4.4. A). Contrastingly to E11 GFP^{+} TECs, all three subsets within E12 GFP^{+} TECs showed a statistically significant increase in MHCII^{+}CD40^{+} population after 1-day culture with RANK antibodies (CD205^{-}: p value=0.0004, CD205^{Low}: p value=0.0024, CD205^{High}: p value=0.0007) (Figure 4.4. B). Overall, our data reveals the RANK expression on E12 TECs within CD205^{+} subset and the RANK-expressing TECs are able to induce statistically significant maturation upon 1-day stimulation.

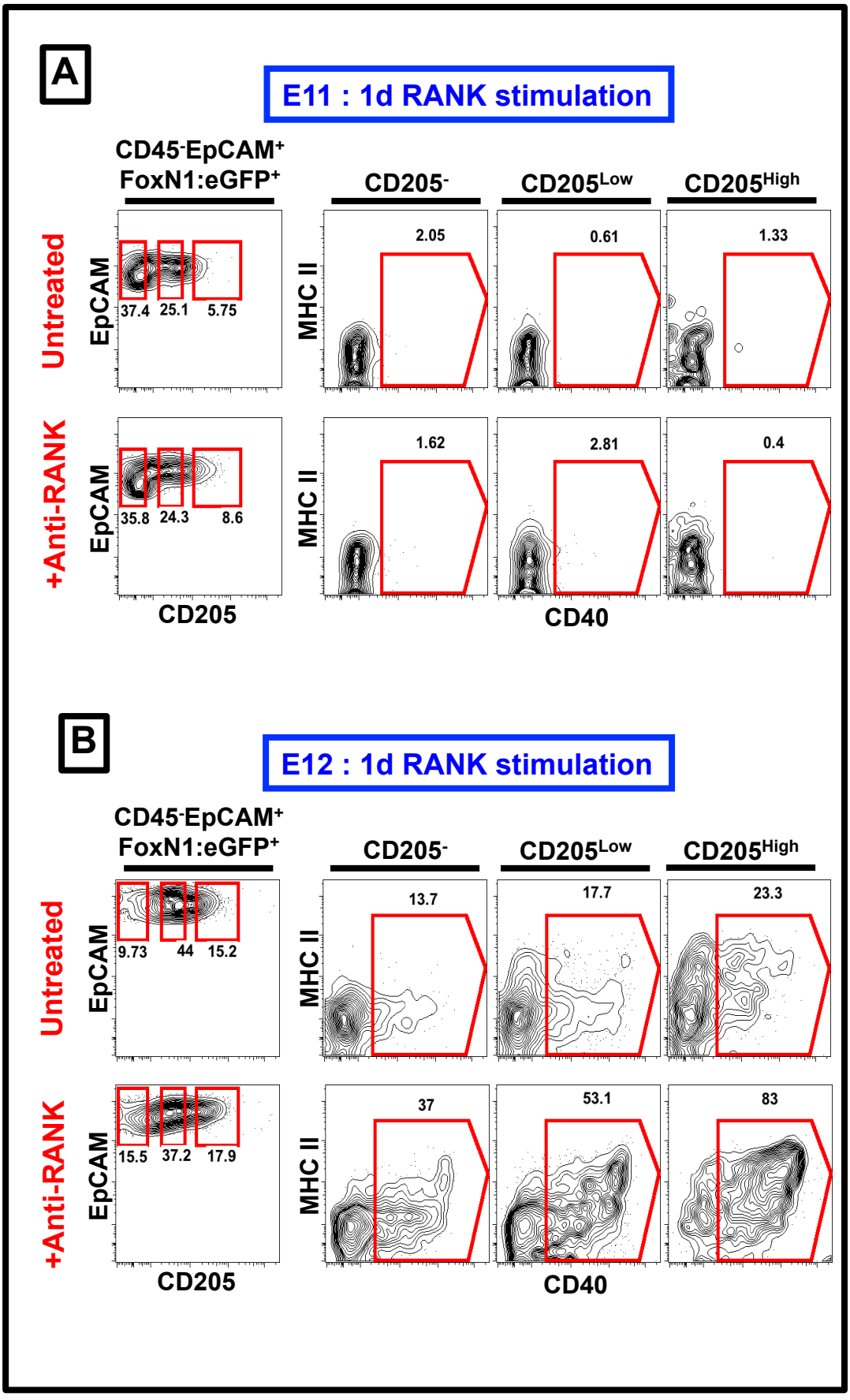

A
E11 : 1d RANK stimulation
CD45-EpCAM+
FoxN1:eGFP+
CD205-
CD205Low
CD205High
Untreated
+Anti-RANK
EpCAM
MHC II
37.4 25.1 5.75
2.05
0.61
1.33
35.8 24.3 8.6
1.62
2.81
0.4
CD205
CD40
B
E12 : 1d RANK stimulation
CD45-EpCAM+
FoxN1:eGFP+
CD205-
CD205Low
CD205High
Untreated
+Anti-RANK
EpCAM
MHC II
9.73 44 15.2
13.7
17.7
23.3
15.5 37.2 17.9
37
53.1
83
CD205
CD40

Figure 4.3. 1-day RANK stimulation of E11 and E12 TECs

Thymus/Parathyroid rudiments of E11 and E12 Foxn1 FoxN1:eGFP transgenic mice were dissected out and then cultured without/with agonistic RANK antibody for 1 day. After 1-day culture, tissues were harvested for FACS analysis. Cells were isolated and stained with CD45, EpCAM, CD205, CD40, and MHC class II antibodies. Percentage of cells within the gated area is shown. GFP^{+} epithelial cells were further divided into three populations in the context of CD205 expression. CD40 and MHC class II expression within $CD205^{-}$, $CD205^{low}$, and $CD205^{high}$ TECs was illustrated by the contour plot.

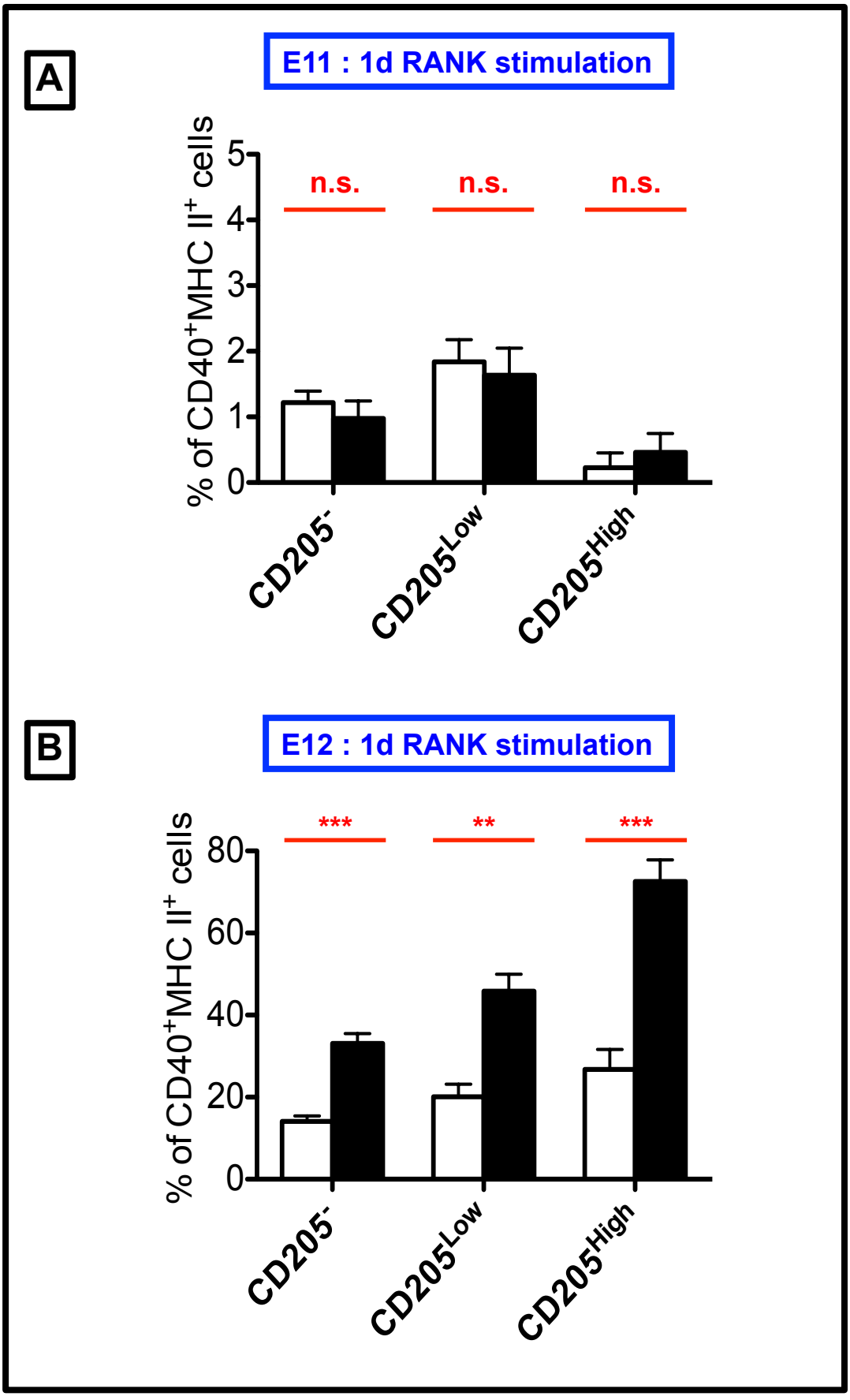

A
E11 : 1d RANK stimulation
% of CD40+MHC II+ cells
0
1
2
3
4
5
n.s.
n.s.
n.s.
CD205-
CD205Low
CD205High
B
E12 : 1d RANK stimulation
% of CD40+MHC II+ cells
0
20
40
60
80
***
**
***
CD205-
CD205Low
CD205High

Figure 4.4. Quantitative analysis of $CD40^{+}MHCII^{+}$ TEC induction upon 1-day RANK stimulation

Graphs show the percentage of $CD40^{+}$MHC II^{+} cells within $CD205^{-}$, $CD205^{Low}$, and $CD205^{High}$ TEC populations after 1-day culture without (white bar) or without (black bar) agonistic RANK antibodies. Graph A shows the mean of n=5, RANK stimulated E11 FoxN1:$eGFP^{+}$ TECs. Graph B shows the mean of n=4, RANK stimulated E12 FoxN1:$eGFP^{+}$ TECs. The bar indicates the calculated mean value and the error bar represents the standard error of the mean. Level of significance, which was calculated using an unpaired T test, was shown (* = $P < 0.05$, ** = $P < 0.01$, *** = $P < 0.001$). P value greater than 0.05 considered as non-significant (n.s.).

4.2.1.3. Potential Of CD205$^+$ TEC Progenitors To Differentiate Into mTEC Including Aire$^+$ Subset

One of the most effective ways to test the developmental potential of CD205$^+$ TEC is the ectopic transplant of the isolated CD205$^+$ TEC population under the kidney capsule. We sorted CD40$^-$CD205$^+$ TECs from the total CD45$^-$EpCAM$^+$ population at E15 thymus lobes (Figure 4.5. A). Then, the sorted cells were used to form reaggregate thymus organ cultures (RTOC) in vitro. To allow the sorted cells to develop further in vivo, RTOCs were grafted under the kidney capsule of syngeneic wild type or nude mice (Figure 4.5. B). As a control, 5-day dGuo treated FTOC of E15 was grafted alongside. After 8 weeks, grafted tissues were analyzed for either cellularity or histology (Figure 4.5. C). All analysis was done in an identical manner for both RTOC and dGuo treated FTOC grafts.

Firstly, we examined whether CD40$^-$CD205$^+$ RTOC grafts developed into mTEC. Figure 4.6. A shows that both Ly51$^-$ mTECs and Ly51$^+$ cTECs were present in the RTOC graft (bottom), as seen in dGuo graft (top). Moreover, we found 6.27% of CD80$^+$Aire$^+$ cells within Ly51$^-$ mTECs, confirming the capability of CD40$^-$CD205$^+$ TECs to give rise to CD80$^+$Aire$^+$ mTEC population (Figure 4.6. A). The proportion of CD80$^+$Aire$^+$ cells in total RTOC-derived mTECs was similar to that of mature mTECs in control (7.08%). Next, we explored the histology of CD40$^-$CD205$^+$ RTOC grafts. Anatomically distinct cortex (β5t$^+$ and CD205$^+$) and medulla (ERTR5$^+$ and MTS10$^+$) were found in CD40$^-$CD205$^+$ RTOC grafts (Figure 4.6. B). Furthermore, the picture of higher magnification displays a better view of medullary area with Aire$^+$ mTEC subset (red: surface staining for ERTR5, green: intracellular staining for Aire), (Figure 4.6. C). The analysis of thymic epithelium within CD40$^-$CD205$^+$ RTOC grafts via flow cytometry and confocal microscopy demonstrated the capability of embryonic CD205$^+$ TECs to develop into mTEC including Aire$^+$ mTEC subset in vivo.

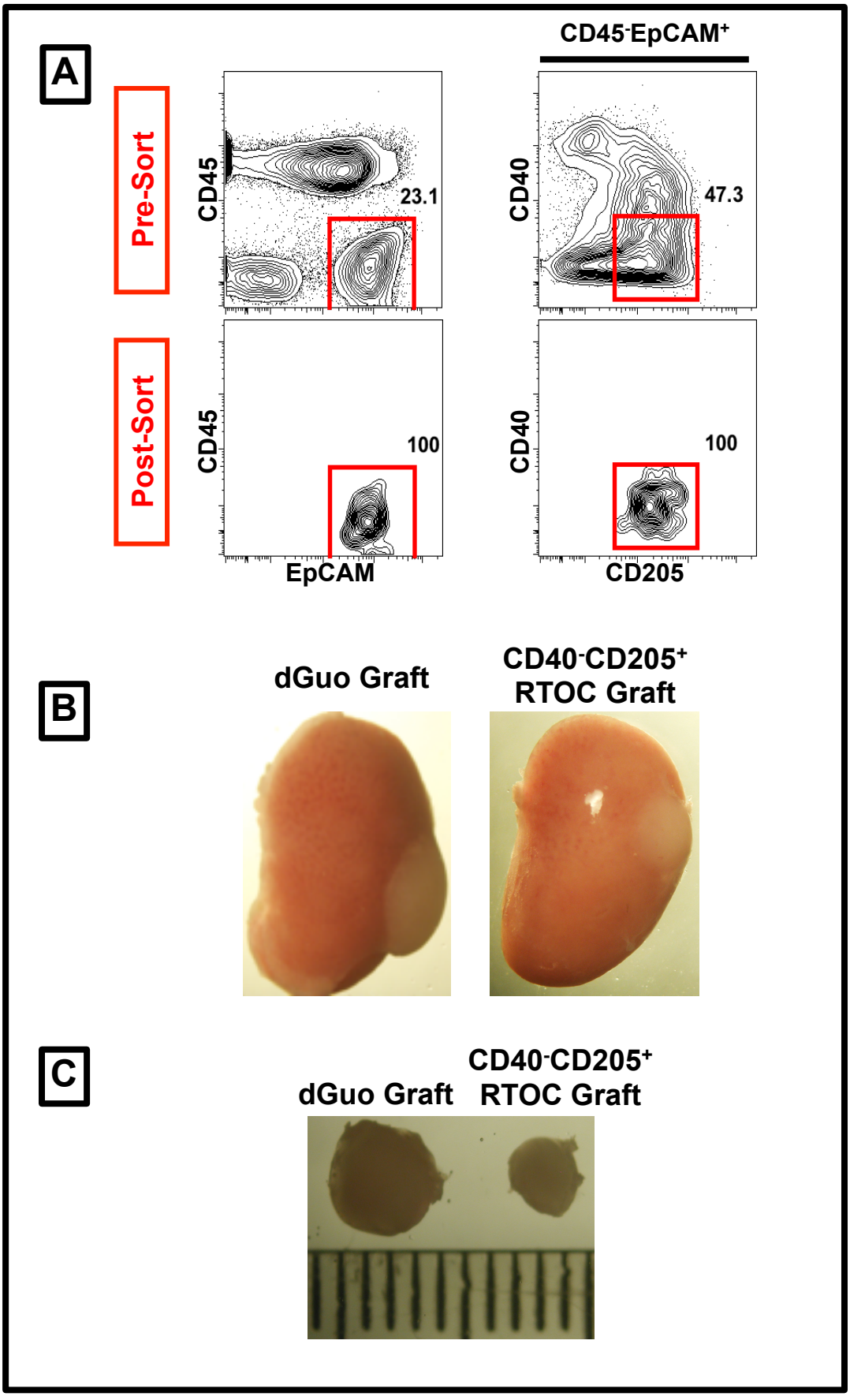

A
CD45-EpCAM+
Pre-Sort
Post-Sort
CD45
23.1
CD40
47.3
CD45
100
CD40
100
EpCAM
CD205
B
dGuo Graft
CD40-CD205+
RTOC Graft
C
dGuo Graft
CD40-CD205+
RTOC Graft

Figure 4.5. Kidney capsule transplantation of $CD40^{-}CD205^{+}$ RTOCs

Thymus of E15 wild type embryos was dissected, and fresh thymus lobes were disaggregated for cell sorting. Cells were stained with CD45, EpCAM, CD40, and CD205 antibodies. The $CD40^{-}CD205^{+}$ subset of epithelial cells within $CD45^{-}EpCAM^{+}$ cells were sorted. After sorting, purity was checked (A). The sorted cells were used to form reaggregate thymus organ cultures (RTOCs). After 4 to 5 days in culture, RTOCs were grafted under the kidney capsule of wild type or nude mice. 5-day dGuo treated E15 FTOCs were also grafted as a control. After 8 weeks, mice were sacrificed for analysis (B and C)

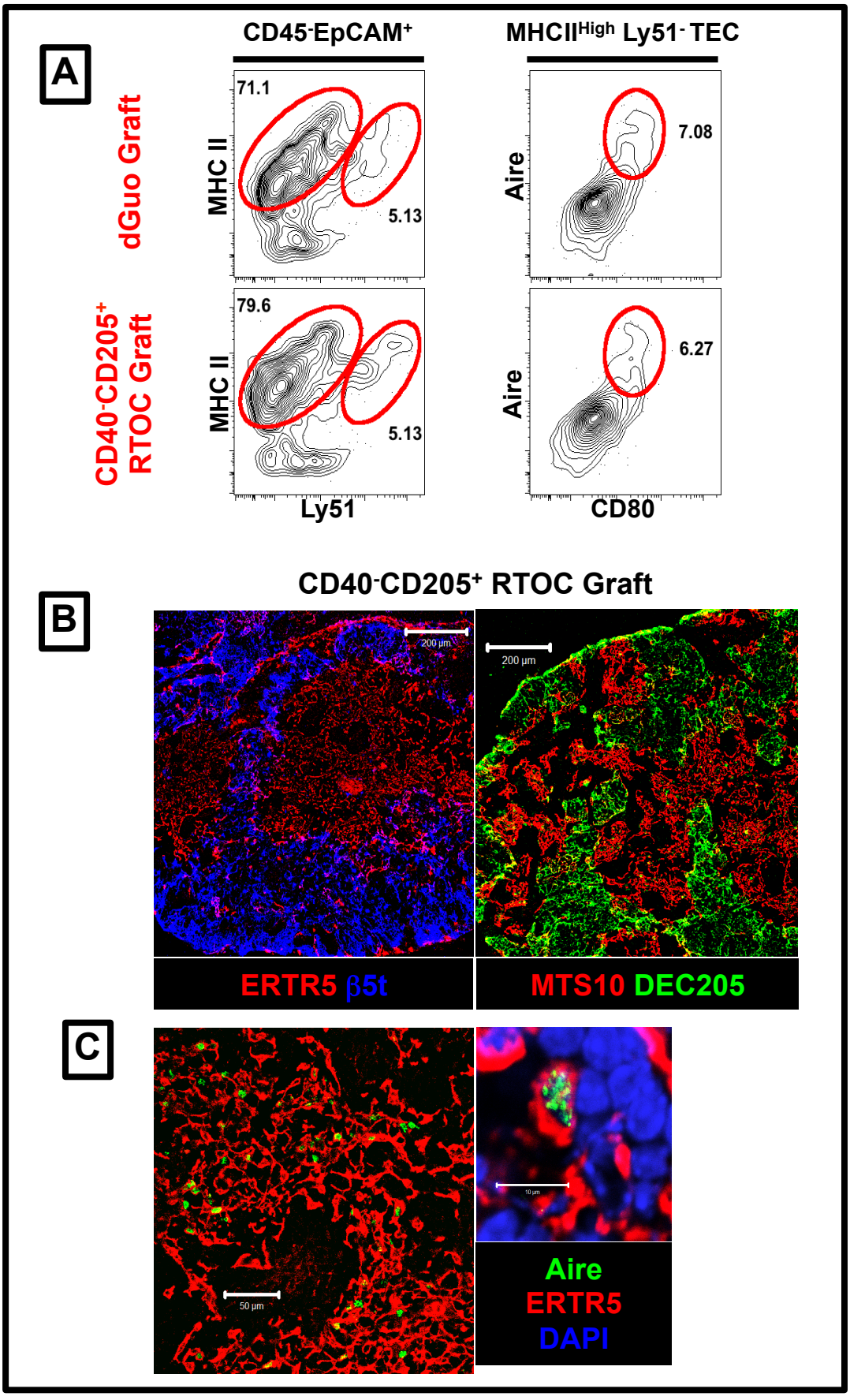

A
CD45-EpCAM+
MHCIIHigh Ly51- TEC
dGuo Graft
CD40-CD205+ RTOC Graft
71.1
5.13
79.6
5.13
MHC II
Ly51
7.08
6.27
Aire
CD80
B
CD40-CD205+ RTOC Graft
200 µm
200 µm
ERTR5 β5t
MTS10 DEC205
C
50 µm
10 µm
Aire
ERTR5
DAPI

Figure 4.6. Analysis of epithelial cells within grafted tissue by FACS and confocal.

(A) Cells were isolated from the harvested grafts and stained with CD45, EpCAM, Ly51, MHC class II, CD80 and Aire antibodies for FACS analysis. The epithelial cells gated on $CD45^{-}EpCAM^{+}$ were divided into two populations in the context of Ly51 expression. $Ly51^{-}MHCII^{+}$ TECs were further gated to check CD80 and Aire expression.

(B) Frozen sections of $CD40^{-}CD205^{+}$ RTOC graft were stained for ERTR5/β5t (left) and MTS10/CD205 (right) . Bar indicates a scale of 200μm.

(C) Frozen sections of $CD40^{-}CD205^{+}$ RTOC graft were stained for Aire, ERTR5, and DAPI. Bar indicates a scale of 50μm (left), and 10μm (right).

Secondly, the ability of TECs differentiated from $CD40^{-}CD205^{+}$ progenitors to provide microenvironments for normal T-cell development was analyzed. Figure 4.7 shows a similar proportion of DN, DP and SP thymocytes in $CD40^{-}CD205^{+}$ RTOC grafts (Figure 4.7. B) to that seen in control dGuo FTOC grafts (Figure 4.7. A). There was no statistically significant difference of the proportions of developing thymocyte subsets in $CD40^{-}CD205^{+}$ RTOC grafts and dGuo grafts (DN: p value=0.5315, DP: p value=0.1436, SP4: p value=0.5534, SP8: p value=0.8900) (Figure 4.8. A). TCR expression level of thymocytes was also comparable between $CD40^{-}CD205^{+}$ RTOC grafts and control grafts: the low level of TCR expression was observed in most of DPs, together with a high level of TCR expression in SP thymocytes (Figure 4.7. A and B). TCRβ high SP4 thymocytes were further checked for the expression of the maturation markers CD69 and HSA. The less mature ($CD69^{+}HSA^{+}$) and more mature ($CD69^{-}HSA^{-}$) SP4 thymocytes were found in both $CD40^{-}CD205^{+}$ RTOC grafts (Figure 4.7. B) and dGuo grafts (Figure 4.7. A).

A subset of SP4 thymocytes highly expressing TCR gives rise to Tregs, and this non-conventional T-cell subset is identified by the expression of CD25 and FoxP3. As one of the roles of mTEC in T cell development is to produce regulatory T cells, the presence of Tregs in RTOCs reveals the presence of functionally competent mTEC. We found both the presence of Tregs in $CD40^{-}CD205^{+}$ RTOC grafts (Figure 4.7. B) and the correct localization of Tregs within medullary regions (Figure 4.8. B), demonstrating a functional medulla within RTOC grafts. Moreover, the correct positioning of DP thymocytes, SP thymocytes, and Tregs is crucial because the chemokine-mediated migration of thymocytes within thymus relies on the precise signal provided by TECs (Lei et al., 2011). Figure 4.8. B shows the correct positioning of DP thymocytes within the cortex (pink) and the medulla resident SP4 thymocytes (blue), SP8 thymocytes (red), and Tregs (blue: surface staining for CD4, green: intracellular staining

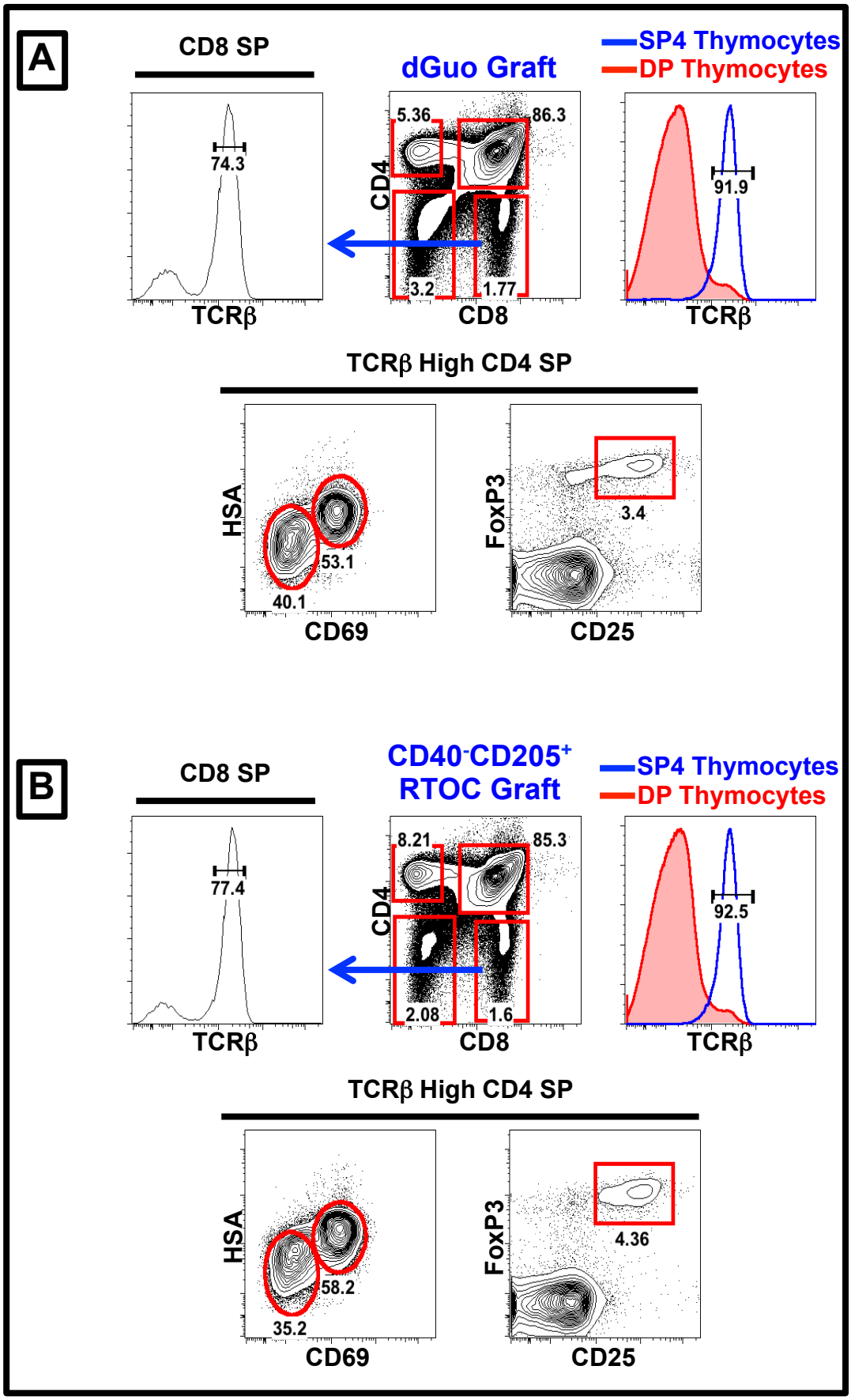

A
CD8 SP
dGuo Graft
SP4 Thymocytes
DP Thymocytes
74.3
TCRβ
5.36
86.3
CD4
3.2
1.77
CD8
91.9
TCRβ
TCRβ High CD4 SP
HSA
53.1
40.1
CD69
FoxP3
3.4
CD25
B
CD8 SP
CD40-CD205+
RTOC Graft
SP4 Thymocytes
DP Thymocytes
77.4
TCRβ
8.21
85.3
CD4
2.08
1.6
CD8
92.5
TCRβ
TCRβ High CD4 SP
HSA
58.2
35.2
CD69
FoxP3
4.36
CD25

Figure 4.7. Analysis of T-cell development within CD40^{-}CD205^{+} RTOCs

Cells were isolated from the harvested grafts. Thymocytes were stained with antibodies of cell surface marker including CD4, CD8, CD25, CD69, HSA, and TCRβ for FACS analysis. Thymocytes were also analysed for intracellular Foxp3 expression within TCRβ high CD4 SP population. The contour plot of thymocytes illustrates the profile of CD4 and CD8. CD4 single positive (SP4) and CD8 single positive (SP8) thymocytes were further gated to explore the TCRβ expression level. TCRβ high CD4 SP cells were gated to analyze the profile of CD69, HSA, CD25, and FoxP3 expression. (A= dGuo graft, B= CD40^{-}CD205^{+} RTOC graft).

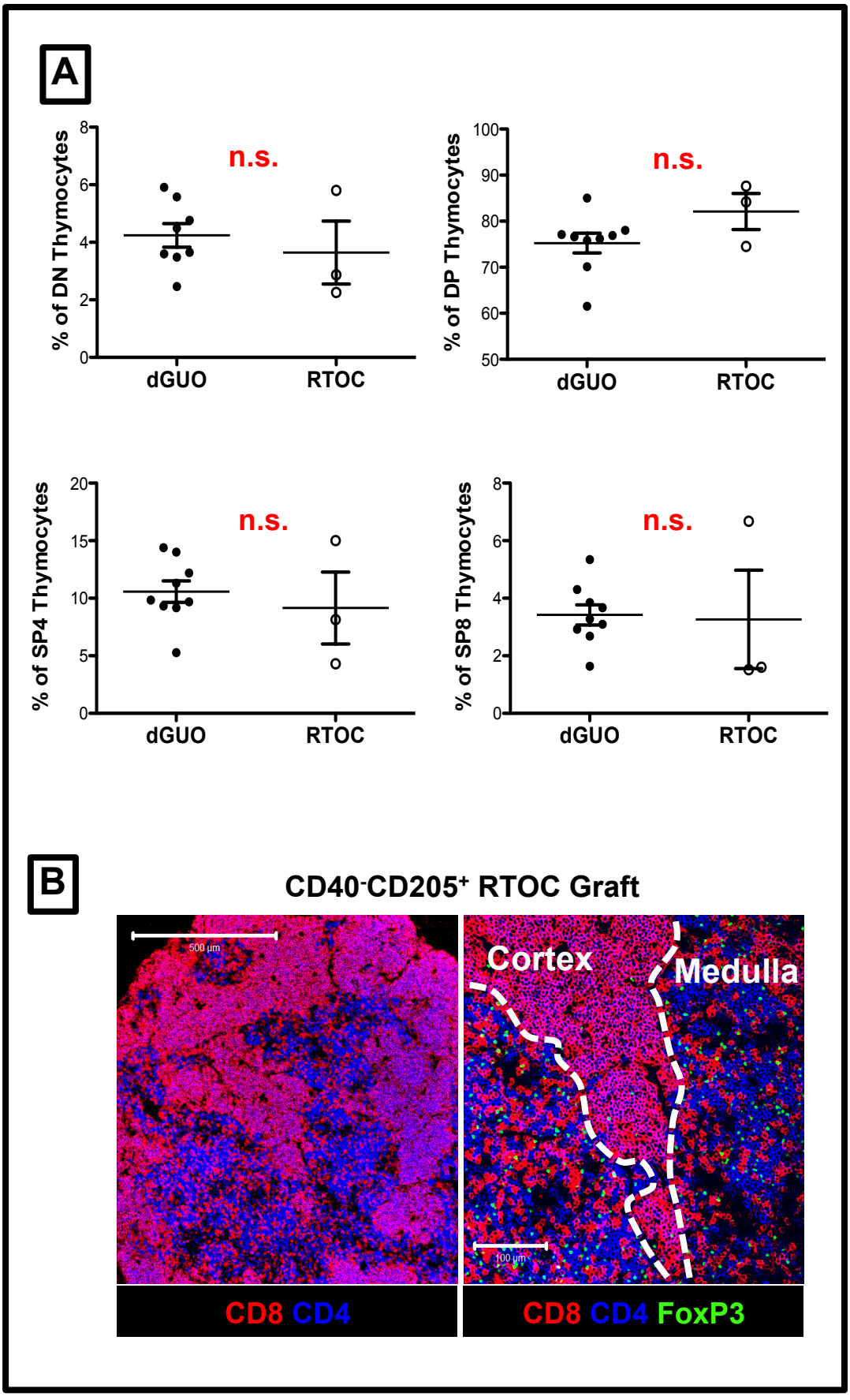

A
% of DN Thymocytes
n.s.
dGUO
RTOC
% of DP Thymocytes
n.s.
dGUO
RTOC
% of SP4 Thymocytes
n.s.
dGUO
RTOC
% of SP8 Thymocytes
n.s.
dGUO
RTOC
B
CD40-CD205+ RTOC Graft
500 µm
Cortex
Medulla
100 µm
CD8 CD4
CD8 CD4 FoxP3

Figure 4.8. Localization of developing thymocytes within CD40^{-}CD205^{+} RTOC

(A) Graph shows the percentage of DN, DP, SP4, and SP8 in dGuo grafts and CD40^{-}CD205^{+} RTOC graft. Each point represents one graft. The bar indicates the calculated mean value and the error bar represents the standard error of the mean. Level of significance, which was calculated using an unpaired T test, was shown (* = $P < 0.05$, ** = $P < 0.01$, *** = $P < 0.001$). P value greater than 0.05 considered as non-significant (n.s.).

(B) Frozen sections of CD40^{-}CD205^{+} RTOC graft were stained for CD4, CD8 and FoxP3. Bar indicates a scale of 500μm (left) and 100μm (right). White dashed line represents corticomedullary junction.

for FoxP3), demonstrating that mTECs derived from $CD205^+$ cTEC are efficient to induce chemotaxis.

Lastly, we tested whether T cells produced by $CD40^-CD205^+$ RTOC grafts were functional. To trace T cells produced by $CD40^-CD205^+$ RTOC grafts, we grafted the RTOCs under the kidney capsule of nude mice. Since T cells are absent in nude mice, if there are any T cells in the periphery of nude mice, those should be generated from the grafted tissue. Functional T cells should be able to egress with complete T-cell development and then migrate into secondary lymphoid tissues to fight viral and bacterial infections. Therefore, we examined T cells in secondary lymphoid tissues such as spleen and lymph node of grafted nude mice. Within TCRβ high cells from spleen and lymph node, $CD25^+FoxP3^+$ Tregs as well as both $CD4^+$ T cells and $CD8^+$ T cells were found in $CD40^-CD205^+$ RTOC grafted nude mice (Figure 4.9. B). In the spleen of RTOC grated nude mice, $CD4^+$ T cells comprise 43.2% of total TCRβ high cells and 11% of total TCRβ high cells is composed of $CD8^+$ T cells. Similarly, 54% of $CD4^+$ T cells and 17.7% of $CD8^+$ T cells were found within TCRβ high cells of lymph node. Moreover, 19.8% of spleen and 20.4% of lymph node within total TCRβ high $CD4^+$ T cells were Treg subset. The dGuo grafted nude mice showed the similar profile of TCRβ high $CD4^+$ T cells, $CD8^+$ T cells and Tregs in secondary lymphoid tissues with RTOC grafted nude mice. Collectively, immature $CD40^-CD205^+$ cTECs are capable of differentiation into an mTEC population and mTECs generated from the immature cTEC can contribute to the production of functional T cells.

4.2.1.4. Signals Important In $CD40^{High}CD205^-$ TEC Development

To examine the signals controlling the development of the mTEC compartment of embryonic mice, we analyzed emergence of the $CD40^{High}CD205^-$ mTEC subset in a panel of gene deficient mice. To begin, given the role of RANK in early embryonic TEC development,

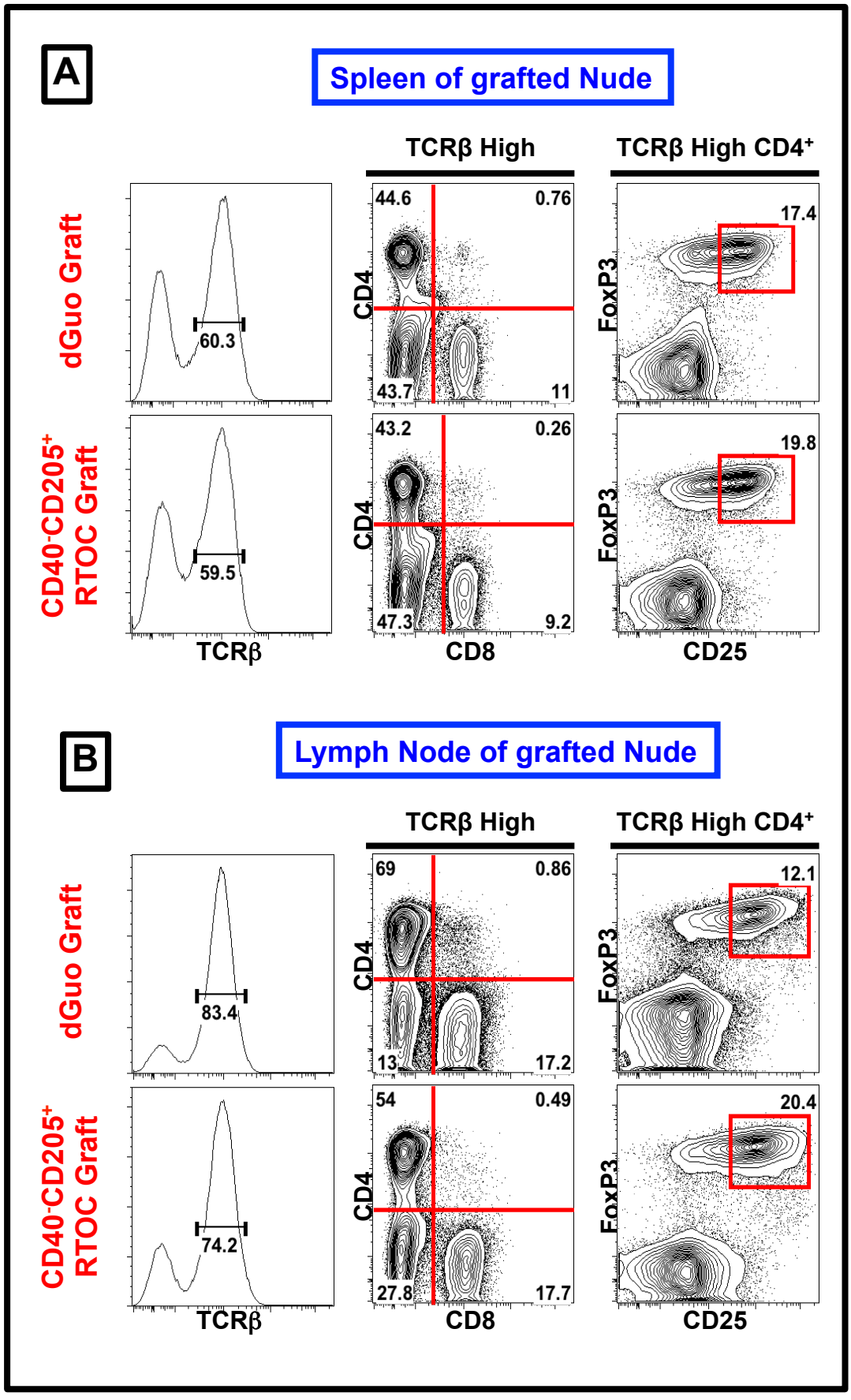

A
Spleen of grafted Nude
TCRβ High
TCRβ High CD4+
dGuo Graft
CD40-CD205+ RTOC Graft
60.3
59.5
TCRβ
44.6
0.76
43.7
11
43.2
0.26
47.3
9.2
CD4
CD8
17.4
19.8
FoxP3
CD25
B
Lymph Node of grafted Nude
83.4
74.2
69
0.86
13
17.2
54
0.49
27.8
17.7
12.1
20.4

Figure 4.9. Presence of peripheral T cells in dGuo or CD40^{-}CD205^{+} RTOC grafted nude mice

Lymphocytes were isolated from spleen (A) and lymph node (B) of dGuo or CD40^{-} CD205^{+} RTOC grafted nude mice. Cells were stained with antibodies of cell surface marker including CD4, CD8, CD25 and TCRβ for FACS analysis. Cells were also analysed for intracellular FoxP3 expression within TCRβ high CD4^{+} population. The contour plot of TCRβ^{High} cells illustrates the profile of CD4 and CD8 expression. TCRβ high CD4^{+} cells were further gated to analyze the profile of CD25 and FoxP3 expression.

we investigated E15 TEC of RANK$^{-/-}$ mice. We assumed if RANK plays a role in cTEC development or in a differentiation from cTEC into mTEC, a defect in the cTEC population and/or a loss of CD40^{High}CD205^{-} mTEC population would be found in RANK$^{-/-}$ embryos. CD40^{High}CD205^{-} mTECs were found in E15 RANK$^{-/-}$ thymus. However, the percentage of CD40^{High}CD205^{-} mTECs in E15 RANK$^{-/-}$ (2.59%, Figure 4.10. B) was about half of that seen in E15 wild type thymus (4.68%, Figure 4.10.A). We also examined E15 TEC of OPG$^{-/-}$ mice. Osteoprotegerin (OPG) is a soluble decoy receptor for the ligand of RANK and the regulation of RANK/RANKL signal by OPG is important in physiological bone turn over (Weitzmann, 2013). However, the role of OPG in TEC development has not been investigated yet. Hence, we explored embryonic TEC development in OPG$^{-/-}$ mice. CD40^{High}CD205^{-} mTECs were present in E15 OPG$^{-/-}$ like in E15 RANK$^{-/-}$. However, the proportion of CD40^{High}CD205^{-} mTECs in E15 OPG$^{-/-}$ (7.56%, Figure 4.10. C) was approximately twice the percentage of CD40^{High}CD205^{-} mTECs in E15 wild type (4.68%, Figure 4.10.A). The percentage difference of the CD40^{High}CD205^{-} mTEC population between E15 wild type and E15 RANK$^{-/-}$ is statistically significant (p value=0.0002). Also, the percentage of CD40^{High}CD205^{-} mTEC population in E15 OPG$^{-/-}$ is significantly higher than that of the mTEC population in E15 wild type (p value<0.0001) (Figure 4.10. E). Our data shows that the size of CD40^{High}CD205^{-} mTEC population is RANK-dosage dependent but a differentiation from CD40^{Int}CD205^{+} cTEC to CD40^{High}CD205^{-} mTEC does not require RANK signaling. Overall, this suggests that RANK signaling might be involved in the proliferation of CD40^{High}CD205^{-} mTECs rather than the differentiation from cTEC into mTEC.

It is known that RANK is highly expressed on mTECs compared to cTECs but the level of LTβR expression on mTECs is comparable to that of cTECs (Hikosaka et al., 2008). Hence, it is unclear which phenotypic properties of LTβR$^{-/-}$ mice are related to the absence of

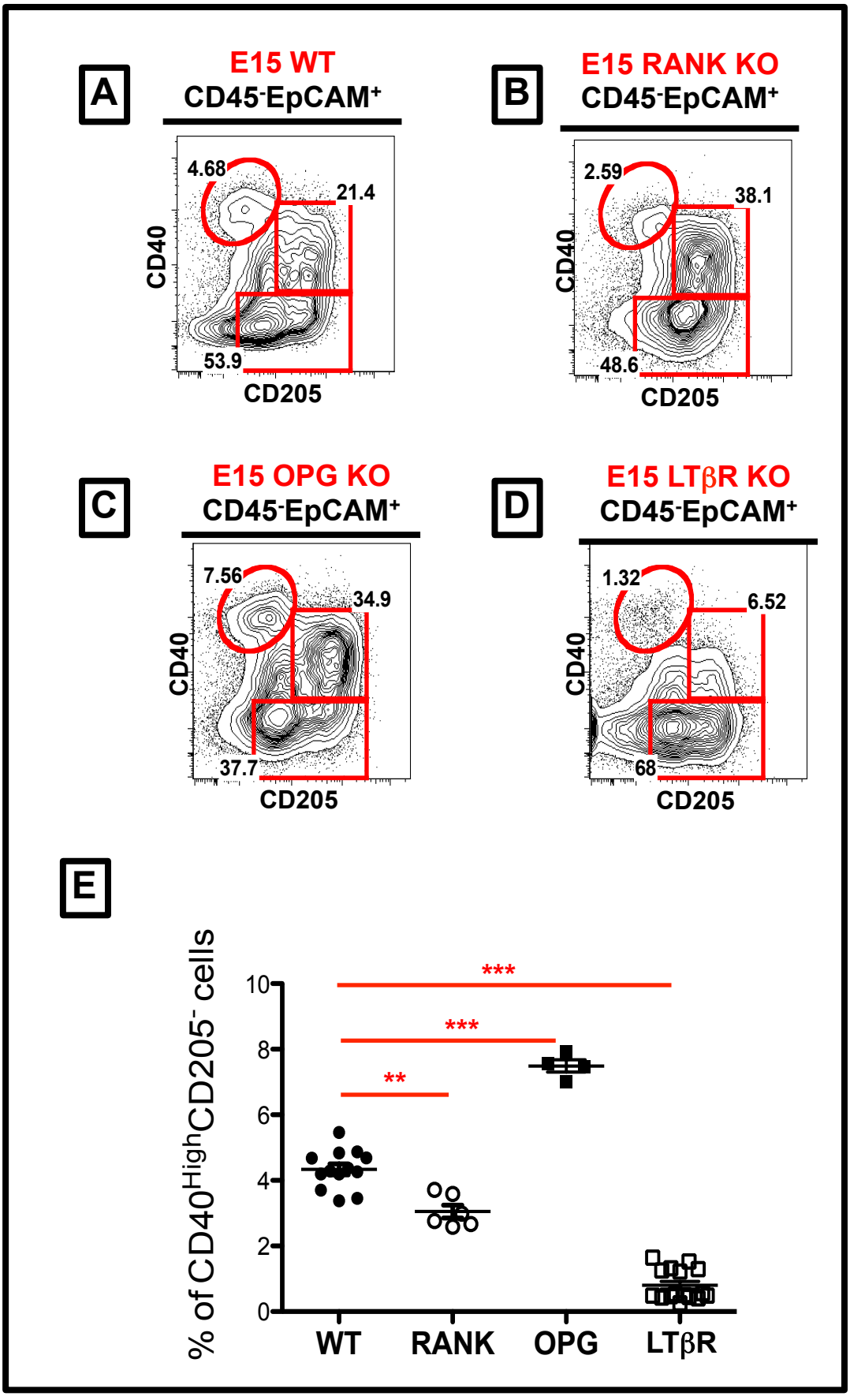

A
E15 WT
CD45-EpCAM+
4.68
21.4
53.9
CD40
CD205
B
E15 RANK KO
CD45-EpCAM+
2.59
38.1
48.6
CD40
CD205
C
E15 OPG KO
CD45-EpCAM+
7.56
34.9
37.7
CD40
CD205
D
E15 LTβR KO
CD45-EpCAM+
1.32
6.52
68
CD40
CD205
E
% of CD40HighCD205- cells
10
8
6
4
2
0
***
***
**
WT
RANK
OPG
LTβR

Figure 4.10. TEC development in RANK KO, OPG KO, and LTβR KO embryos.

Cells from embryonic thymus of wild type (A), RANK KO (B), OPG KO (C), and LTβR KO (D) mice at the age of E15 were stained for CD40 and CD205 in addition to CD45 and EpCAM. Pre-gated $CD45^{-}EpCAM^{+}$ cells were plotted CD40 versus CD205. Percentage of cells within the gated area is shown. The contour plots illustrate the profile of CD40 and CD205 expression on E15 TECs in different strains.

Graph E shows the percentage of $CD40^{High}CD205^{-}$ TECs in different strains at the age of E15. Each point represents one embryo. The bar indicates the calculated mean value and the error bar represents the standard error of the mean. Level of significance, which was calculated using an unpaired T test, was shown (* = $P < 0.05$, ** = $P < 0.01$, *** = $P < 0.001$). P value greater than 0.05 considered as non-significant (n.s.).

LTβR expression in either mTECs or cTECs. The previously reported defects in LTβR$^{-/-}$ mice were mostly involved in adult TEC, including the absent involucrin^{+} mTECs and the lower frequency of CCL21^{+} mTECs (Lkhagvasuren et al., 2013; White et al., 2010). Therefore, we next examined whether a loss of LTβR expression on TEC has effect on cTEC development and/or a differentiation from CD40^{Int}CD205^{+} cTEC to CD40^{High}CD205^{-} mTEC in embryo. Surprisingly, the proportion of CD40^{High}CD205^{-} mTEC in E15 LTβR$^{-/-}$ (1.32%, Figure 4.10. D) was even lower than the percentage of CD40^{High}CD205^{-} mTECs in E15 RANK$^{-/-}$ (2.59%, Figure 4.10. B). The statistical analysis of difference between E15 wild type and E15 LTβR$^{-/-}$ in CD40^{High}CD205^{-} mTEC population shows significant reduction (p value<0.0001) (Figure 4.10. E). Mouri *et el* demonstrated that LTβR signaling promotes RANK expression on embryonic TECs (Mouri et al., 2011). The lower percentage of CD40^{High}CD205^{-} mTECs in E15 LTβR$^{-/-}$ compared to E15 wild type and E15 RANK$^{-/-}$ thymus could be caused from a cumulative effect, if RANK signaling is responsible for the proliferation of CD40^{High}CD205^{-} mTECs and RANK expression relies on LTβR signal.

To determine whether a loss of LTβR expression on TECs has effects on the induction of RANK expression in embryonic TEC, we stimulated E14 LTβR$^{-/-}$ thymus lobes with agonistic RANK antibodies for 1 day. Upon 1-day RANK stimulation, the proportion of CD40^{High}CD205^{-} mTEC subset within E14 wild type total TEC population was doubled (Untreated: 12.8%, Stimulated: 23%) (Figure 4.11. A) and the increase was statistically significant (p value=0.0003) (Figure 4.11. D). Even though the statistically significant increase was found in the CD40^{High}CD205^{-} mTEC subset of E14 LTβR$^{-/-}$ TECs upon 1-day RANK stimulation (p value=0.0024) (Figure 4.11. D), the percentage of CD40^{High}CD205^{-} mTEC subset in E14 LTβR$^{-/-}$ (Untreated: 3.21%, Stimulated: 6.45%) (Figure 4.11. B) was much lower than in E14 wild type (Untreated: 12.8%, Stimulated: 23%) (Figure 4.11. A).

Our data indicates that the acquisition of RANK expression on embryonic TECs might be independent on LTβR signaling, but it may promote RANK expression resulting in higher levels of proliferation, or LTβR might have a role in mTEC proliferation, which is unrelated to the role of RANK in the proliferation of $CD40^{High}CD205^{-}$ mTEC subset.

Mice with defects in several genes, intrinsically critical for T-cell development, show how developing thymocytes affect TEC organization and proliferation at different stages. For example, CD3ε transgene expression causes the complete block of T-cell development at DN stages and consequently leads to a failure in developing normal thymic architecture due to the lack of crosstalk with thymocytes (Roberts et al., 2009). We explored whether the initial acquisition of RANK expression on embryonic TECs requires signaling from developing thymocytes. E14 CD3εtg26 thymus lobes were cultured for 1 day in the absence or presence of agonistic RANK antibodies and then the response was examined as an indicator of RANK expression on E14 CD3εtg26 TECs. Upon 1-day RANK stimulation, the $CD40^{High}CD205^{-}$ mTEC population expanded from 1.54% (Untreated) to 16.6% (Stimulated) (Figure 4.11. C) and the expansion was statistically significant (p value<0.0001) (Figure 4.10. E). Overall, this finding suggests that the acquisition of RANK expression by embryonic TECs does not require signals from developing thymocytes.

4.2.2. Role Of Wnt5a In TEC Development

4.2.2.1. Wnt5a Expression Within Embryonic Thymus Of Wild Type Mice

It is well known that RANK plays a major role in osteoclastgenesis (Simonet et al., 1997). Maeda *et al* demonstrated that Wnt5a/Ror2 signal induces RANK expression on osteoclast precursors and mice deficient either Wnt5a or RoR2 have defects in osteoclastogenesis (Maeda et al., 2012). However, the mechanism inducing RANK expression

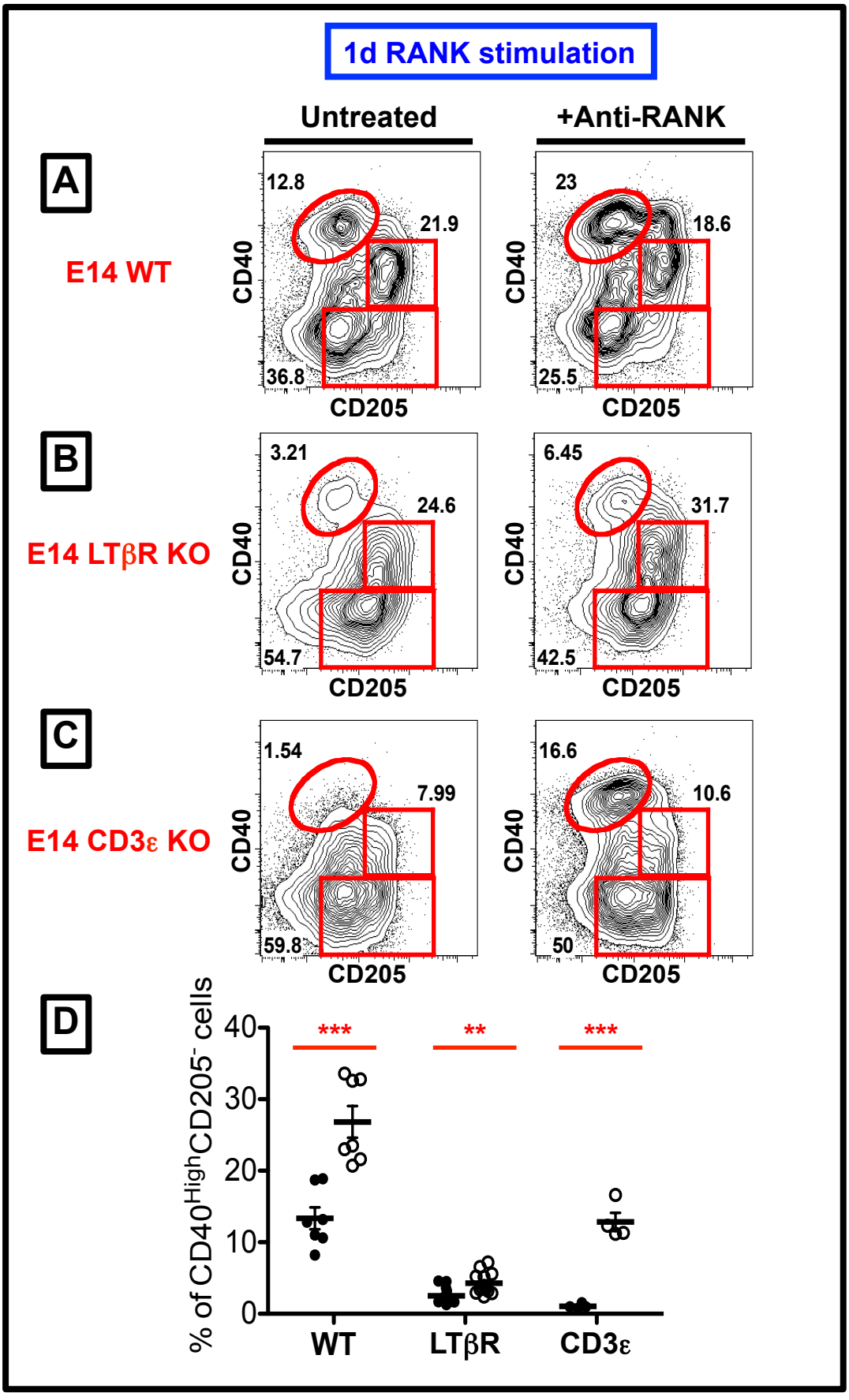

1d RANK stimulation
Untreated
+Anti-RANK
A
E14 WT
12.8
21.9
36.8
23
18.6
25.5
CD40
CD205
B
E14 LTβR KO
3.21
24.6
54.7
6.45
31.7
42.5
C
E14 CD3ε KO
1.54
7.99
59.8
16.6
10.6
50
D
% of CD40HighCD205- cells
40
30
20
10
0
***
**
***
WT
LTβR
CD3ε

Figure 4.11. 1-day RANK stimulation of E14 TECs in different strains.

Embryonic thymus of wild type (A), LTβR KO (B), and CD3ε (C) mice at the age of E14 were cultured for 1-day without/with agonistic RANK antibody. After 1-day culture, tissues were harvested for FACS analysis. Cells were isolated and stained with CD45, EpCAM, CD205, and CD40 antibodies. Pre-gated $CD45^{-}EpCAM^{+}$ cells were plotted CD40 versus CD205. Percentage of cells within the gated area is shown. The contour plots illustrate the profile of CD40 and CD205 expression on 1-day cultured E14 TECs in different strains.

Graph D shows the percentage of $CD40^{High}CD205^{-}$ cells within $CD45^{-}EpCAM^{+}$ after 1-day culture without (black dot) or with (white dot) agonistic RANK in different strains at the age of E14. The bar indicates the calculated mean value and the error bar represents the standard error of the mean. Level of significance, which was calculated using an unpaired T test, was shown (* = $P < 0.05$, ** = $P < 0.01$, *** = $P < 0.001$). P value greater than 0.05 considered as non-significant (n.s.).

on TECs is still elusive. Therefore, whether Wnt5a/Ror2 signal plays also similar role in the acquisition of RANK expression on TECs was investigated in this study.

Firstly, we examined whether Wnt5a and its receptors are expressed in embryonic thymus of wild type mice. Embryonic TEC ($CD45^-EpCAM^+$) at the age from E12 to E15 and E12 total mesenchyme ($CD45^-EpCAM^-$) were sorted and used to compare relative mRNA expression. High level of Wnt5a expression was found in E12 total mesenchyme but low Wnt5a expression was detected in TECs throughout embryonic stages (Figure 4.12. A). There are three subsets within E12 $GP38^+$ total mesenchyme in terms of PDGFRα and Ly51 expression: $PDGFR\alpha^+Ly51^-$ (74.3%), $PDGFR\alpha^-Ly51^-$ (13%), and $PDGFR\alpha^+Ly51^+$ (7.83%) mesenchyme (Figure 4.12. B). Wnt5a expression in embryonic TECs, mesenchyme subsets, and thymocytes was further investigated and compared with Wnt4 expression (Figure 4.12. C), whose expression in TECs has been reported previously (Balciunaite et al., 2002). Wnt5a mRNA expression was predominantly detectable in E12 total mesenchyme and the $PDGFR\alpha^+Ly51^-$ mesenchyme subset, while embryonic TECs and other mesenchyme subsets had lower levels of Wnt5a mRNA. Wnt4 mRNA expression was only found in TECs and gradually increased from E12 to E15 of gestation (Figure 4.12. C). In addition, E12 thymocytes ($CD45^+EpCAM^-$), E12 total mesenchyme ($CD45^-EpCAM^-$), and E12 total TEC ($CD45^-EpCAM^+$) from wild type were sorted and processed for mRNA analysis. Quantitative RT-PCR was carried out to determine the expression of known receptors for Wnt5a including receptor tyrosine kinase-like orphan receptor2 (Ror2), receptor-like tyrosine kinase (Ryk), Frizzled2 (Fz2), Frizzled3 (Fz3), Frizzled7 (Fz7), and Frizzled8 (Fz8) (Kikuchi et al., 2012). All of the above receptors were found to be expressed in both E12 total mesenchyme and E12 TEC but not in E12 thymocytes (Figure 4.13).

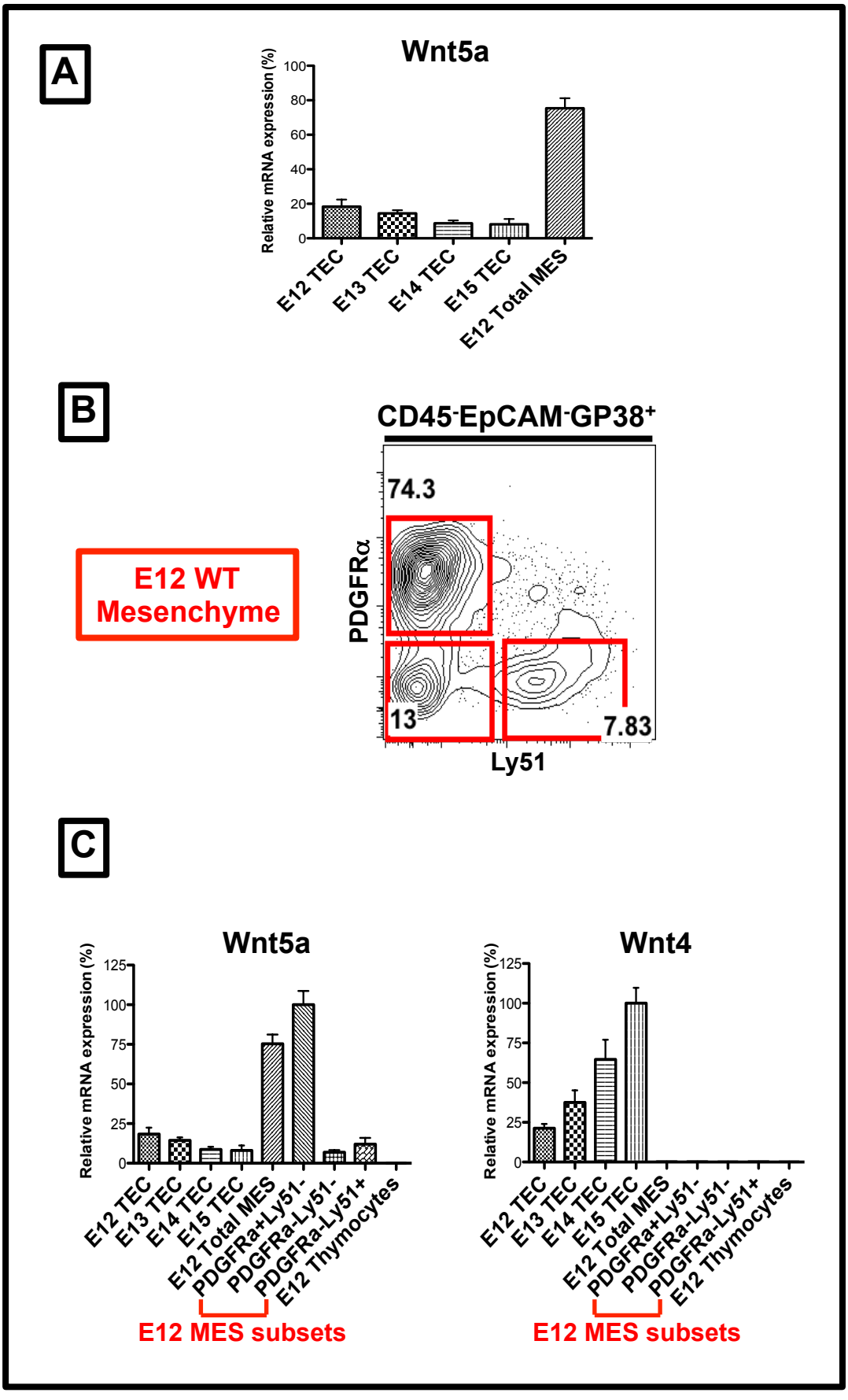

A
Wnt5a
Relative mRNA expression (%)
100
80
60
40
20
0
E12 TEC
E13 TEC
E14 TEC
E15 TEC
E12 Total MES
B
CD45-EpCAM-GP38+
74.3
13
7.83
PDGFRα
Ly51
E12 WT Mesenchyme
C
Wnt5a
Relative mRNA expression (%)
125
100
75
50
25
0
E12 TEC
E13 TEC
E14 TEC
E15 TEC
E12 Total MES
PDGFRa+Ly51-
PDGFRa-Ly51-
PDGFRa-Ly51+
E12 Thymocytes
E12 MES subsets
Wnt4
Relative mRNA expression (%)
125
100
75
50
25
0
E12 TEC
E13 TEC
E14 TEC
E15 TEC
E12 Total MES
PDGFRa+Ly51-
PDGFRa-Ly51-
PDGFRa-Ly51+
E12 Thymocytes
E12 MES subsets

Figure 4.12. Wnt5a expression in WT TEC and mesenchyme subsets

(A) Embryonic TEC ($CD45^{-}EpCAM^{+}$) at different age from E12 to E15 and E12 mesenchyme ($CD45^{-}EpCAM^{-}$) were sorted and used to compare relative mRNA expression. Relative expression of Wnt5a was normalized to the housekeeping gene, β-actin.

(B) E12 embryonic thymus was dissected and disaggregated for FACS analysis. Cells were isolated and stained with CD45, EpCAM, GP38, PDGFRα and Ly51 antibodies. Pre-gated $CD45^{-}EpCAM^{-}GP38^{+}$ cells were further plotted PDGFRα versus Ly51. Percentage of cells within the gated area is shown. The contour plots illustrate the profile of PDGFRα and Ly51 expression on mesenchyme ($CD45^{-}EpCAM^{-}GP38^{+}$) at the age of E12.

(C) Embryonic TEC ($CD45^{-}EpCAM^{+}$) at different age from E12 to E15, E12 total mesenchyme ($CD45^{-}EpCAM^{-}$), E12 mesenchyme subsets ($PDGFR\alpha^{+}Ly51^{-}$, $PDGFR\alpha^{-}Ly51^{-}$, $PDGFR\alpha^{-}Ly51^{+}$), and E12 thymocytes ($CD45^{+}EpCAM^{-}$) were sorted and used to compare relative mRNA expression. Relative expression of Wnt5a and Wnt4 was normalized to the housekeeping gene, β-actin.

(A and C) The bar indicates the mean of triplicate and the error bar represents the standard error of the mean. The data shown is the representative of two independent experiments.

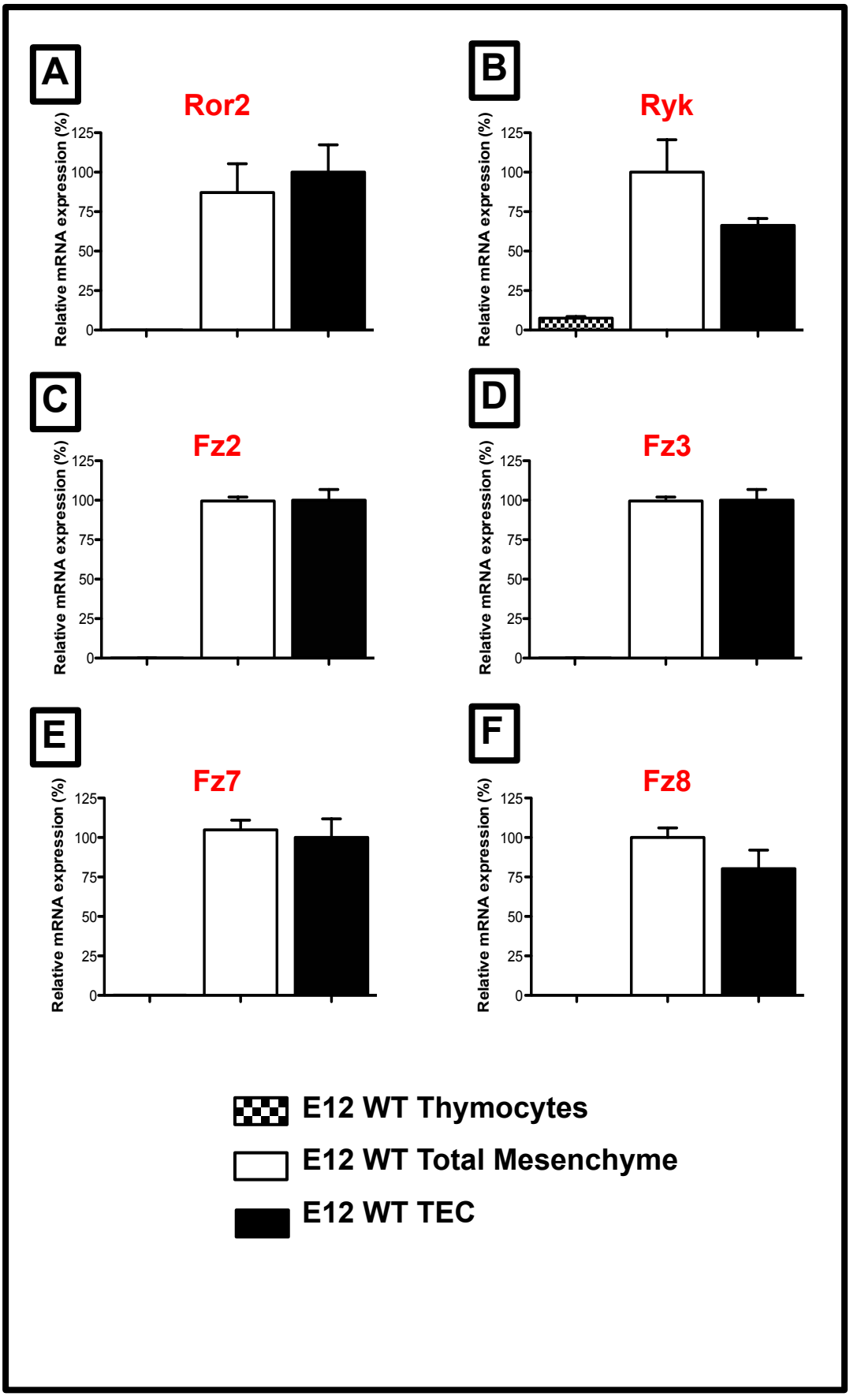

A
Ror2
Relative mRNA expression (%)
125
100
75
50
25
0
B
Ryk
Relative mRNA expression (%)
125
100
75
50
25
0
C
Fz2
Relative mRNA expression (%)
125
100
75
50
25
0
D
Fz3
Relative mRNA expression (%)
125
100
75
50
25
0
E
Fz7
Relative mRNA expression (%)
125
100
75
50
25
0
F
Fz8
Relative mRNA expression (%)
125
100
75
50
25
0
E12 WT Thymocytes
E12 WT Total Mesenchyme
E12 WT TEC

Figure 4.13. Expression of receptors for Wnt5a in E12 TEC and E12 mesenchyme (Wild Type)

E12 thymocytes ($CD45^{+}EpCAM^{-}$), E12 total mesenchyme ($CD45^{-}EpCAM^{-}$), and E12 TECs ($CD45^{-}EpCAM^{+}$) were sorted and used to compare relative mRNA expression. Relative expression of receptor tyrosine kinase-like orphan receptor2 (Ror2), receptor-like tyrosine kinase (Ryk), Frizzled2 (Fz2), Frizzled3 (Fz3), Frizzled7 (Fz7), and Frizzled8 (Fz8) was normalized to the housekeeping gene, β-actin. The bar indicates the mean of triplicate and the error bar represents the standard error of the mean. The data shown is the representative of two independent experiments.

4.2.2.2. TEC Development In Wnt5a KO Mice

Based on RT-PCR analysis of Wnt5a and its receptors in wild type mice, we hypothesized that Wnt5a produced by mesenchyme will bind Ror2 on TECs and Wnt5a-Ror2 signaling induces RANK expression on embryonic TECs. To test the idea, we analyzed the embryonic TECs of $Wnt5a^{-/-}$. $Wnt5a^{-/-}$ mice are embryonically lethal and have multiple defects including limb abnormalities, cranial defects, dwarfism, and intestinal elongation defects (Yamaguchi et al., 1999). Figure 4.14. A shows a picture of a E18 $Wnt5a^{-/-}$ embryo (right), indicating limb abnormalities, cranial defects, and dwarfism.

Firstly, the expression of surface markers including CD40, CD205, MHC class II, and LTβR by E15 $Wnt5a^{-/-}$ TECs was investigated. Pre-gated $CD45^{-}EpCAM^{+}$ TECs were analyzed for MHC class II versus CD40 expression, and four subsets were found in both E15 wild type and E15 $Wnt5a^{-/-}$: $CD40^{-}MHCII^{-}$ (WT: 17.5%, $Wnt5a^{-/-}$: 20.3%), $CD40^{-}MHCII^{Low}$ (WT: 32.8%, $Wnt5a^{-/-}$: 28.9%), $CD40^{Low}MHCII^{Low}$ (WT: 33.4%, $Wnt5a^{-/-}$: 31.5%), and $CD40^{High}MHCII^{High}$ (WT: 12.1%, $Wnt5a^{-/-}$: 13.8%). Moreover, LTβR expression on both $CD205^{-}$ mTECs and $CD205^{+}$ cTECs was detected in E15 $Wnt5a^{-/-}$ like in E15 wild type. Furthermore, not only $CD40^{Int}CD205^{+}$ cTECs but also $CD40^{High}CD205^{-}$ mTECs were observed in E15 $Wnt5a^{-/-}$. Collectively, the expression of all the surface makers was normal in E15 $Wnt5a^{-/-}$ thymus (Figure 4.14. B).

To check RANK expression on TEC, we cultured E14 $Wnt5a^{-/-}$ thymus lobe in the absence or presence of agonistic RANK antibodies for 1 day. Then, the up-regulation of MHC class II and CD40 expression was investigated. As a negative control, E14 $RANK^{-/-}$ thymus lobes were also cultured in the same conditions and the difference in the percentage of $CD40^{High}MHCII^{High}$ TECs between untreated and stimulated samples was investigated (Figure 4.15. B). In E14 $RANK^{-/-}$ thymuses, the proportion of $CD40^{High}MHCII^{High}$ TECs within

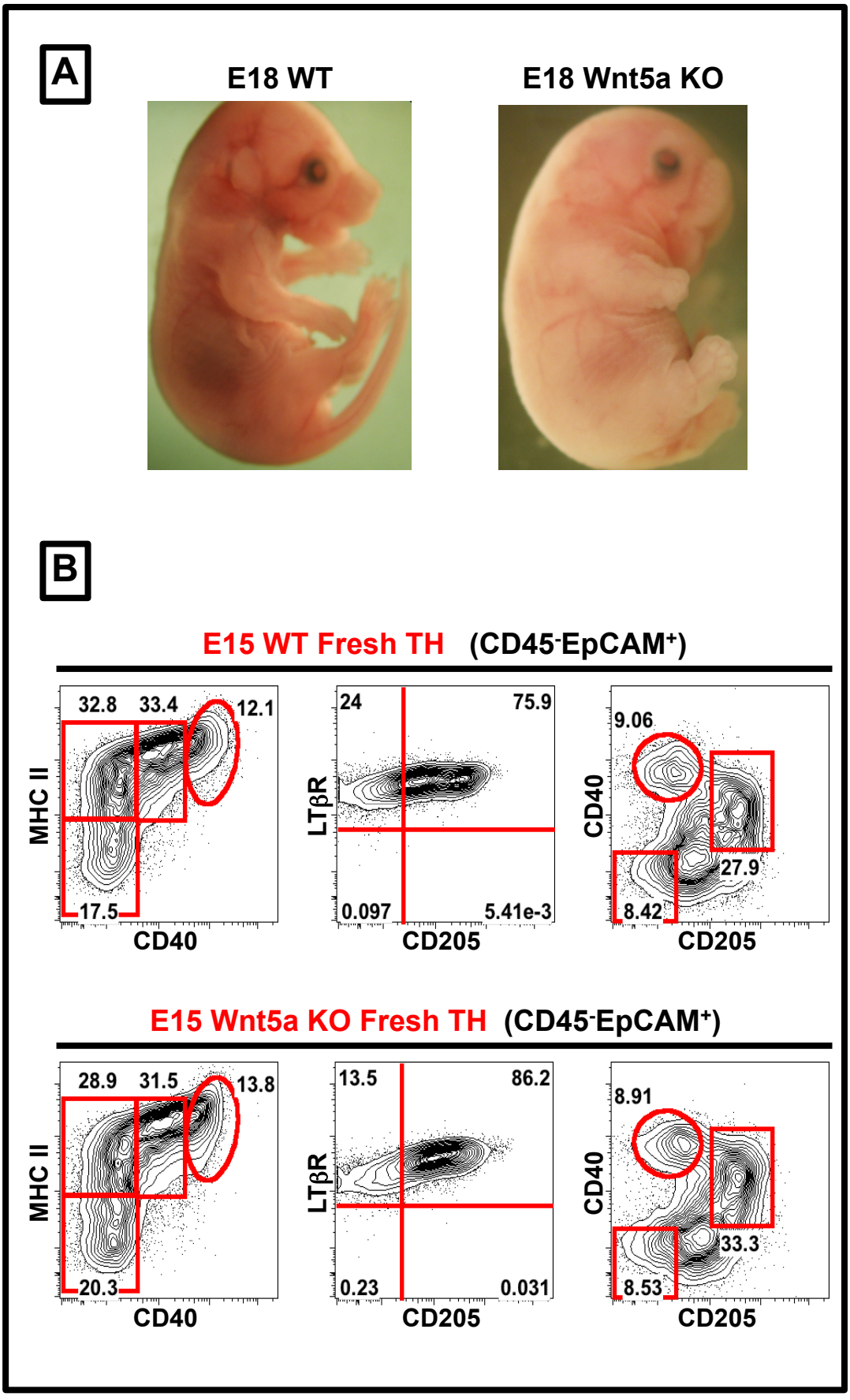

A
E18 WT
E18 Wnt5a KO
B
E15 WT Fresh TH (CD45-EpCAM+)
32.8
33.4
12.1
17.5
MHC II
CD40
24
75.9
0.097
5.41e-3
LTβR
CD205
9.06
27.9
8.42
CD40
CD205
E15 Wnt5a KO Fresh TH (CD45-EpCAM+)
28.9
31.5
13.8
20.3
MHC II
CD40
13.5
86.2
0.23
0.031
LTβR
CD205
8.91
33.3
8.53
CD40
CD205

Figure 4.14. TEC development in Wnt5a KO embryos.

(A) The picture shows wild type embryo (left) and Wnt5a KO embryo (right) at the age of E18.

(B) Cells from embryonic thymus of wild type and Wnt5a KO mice at the age of E15 were stained for CD40, CD205, MHC class II, and LTβR in addition to CD45 and EpCAM. Pre-gated $CD45^{-}EpCAM^{+}$ cells were plotted MHCII versus CD40, LTβR versus CD205, and CD40 versus CD205. Percentage of cells within the gated area is shown. The contour plots illustrate the profile of CD40, CD205, MHC class II, and LTβR expression on E15 TECs in wild type and Wnt5a KO mice.

total TECs did not increase upon 1-day RANK stimulation (Untreated: 3.28%, Stimulated: 2.9%) (Figure 4.15. B). Contrastingly, the $CD40^{High}MHCII^{High}$ TEC population expanded from 8.04% (Untreated) to 24.7% (Stimulated) upon 1-day RANK stimulation in E14 wild type (Figure 4.15. A). An increase in the percentage of the $CD40^{High}MHCII^{High}$ TEC subset (Untreated: 12.4%, Stimulated: 24.8%) was also observed in E14 $Wnt5a^{-/-}$ mice (Figure 4. 15. C). Moreover, we sorted TECs from E15 wild type, E15 $Wnt5a^{+/-}$, and E15 $Wnt5a^{-/-}$ thymuses. Then, the sorted cells were processed for mRNA and quantitative RT-PCR was carried out to analyze expression of RANK. RANK expression was found in all three samples (Figure 4.15. D). RANK expression by embryonic TECs of $Wnt5a^{-/-}$ therefore confirmed data obtained from the anti-RANK stimulation experiment. Overall, our data argues against the hypothesis that Wnt5a might be a key regulator in the induction of RANK expression on embryonic TECs.

Next, whether Wnt5a deficient mice have any defect in the late embryonic TEC development was investigated. Both $Ly51^{-}$ mTECs and $Ly51^{+}$ cTECs were observed in E18 $Wnt5a^{-/-}$ thymus ($Ly51^{-}$ mTEC: 8.25%, $Ly51^{+}$ cTEC: 62.6%), as found in E18 wild type ($Ly51^{-}$ mTEC: 7.13%, $Ly51^{+}$ cTEC: 57.7%), and E18 $Wnt5a^{+/-}$ mice ($Ly51^{-}$ mTEC: 7.35%, $Ly51^{+}$ cTEC: 57.8%) (Figure 4.16. A). We further analyzed the CD80 and Aire expression within $MHCII^{High}Ly51^{-}$ mTEC. We detected 19% of $CD80^{+}Aire^{+}$ cells within $MHCII^{High}Ly51^{-}$ mTECs of E18 $Wnt5a^{-/-}$ mice (Figure 4.16. A). Then, we explored the histology of E18 $Wnt5a^{-/-}$ thymus lobes to check the presence of $Aire^{+}$ mTECs. MTS10 were used to classify mTECs and stained with Aire antibodies. An $Aire^{+}$ mTEC subset (red: surface staining for MTS10, green: intracellular staining for Aire) was found in frozen thymic sections of E18 $Wnt5a^{-/-}$ mice (Figure 4.16. B). The presence of mature mTEC subset expressing Aire within E18 $Wnt5a^{-/-}$ mice was confirmed via flow cytometry and confocal

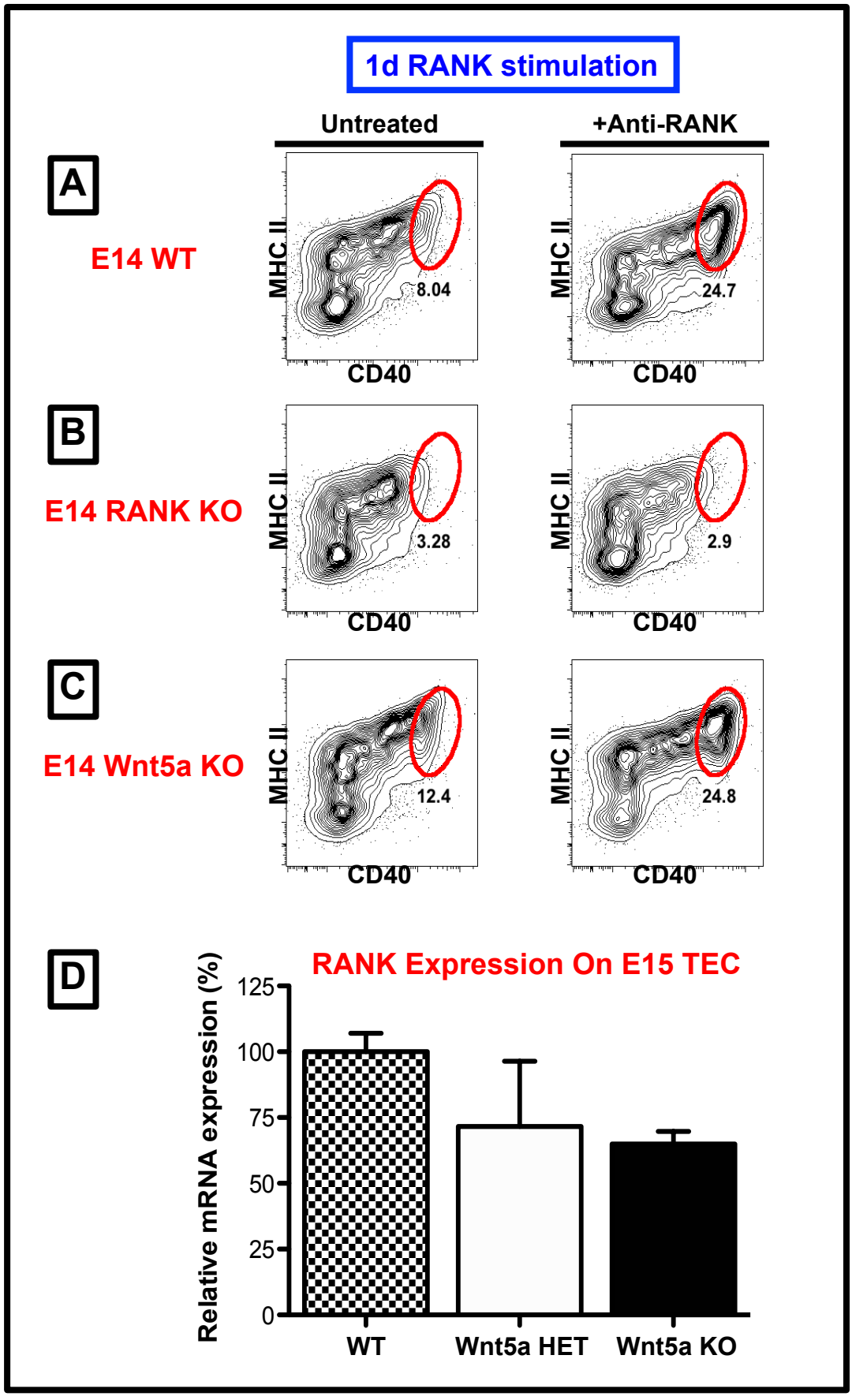

1d RANK stimulation
Untreated
+Anti-RANK
A
E14 WT
MHC II
CD40
8.04
24.7
B
E14 RANK KO
3.28
2.9
C
E14 Wnt5a KO
12.4
24.8
D
RANK Expression On E15 TEC
Relative mRNA expression (%)
125
100
75
50
25
0
WT
Wnt5a HET
Wnt5a KO

Figure 4.15. RANK expression by embryonic TECs in Wnt5a KO mice

Embryonic thymus of WT (A), RANK KO (B), and Wnt5a KO (C) mice at the age of E14 were cultured for 1-day without/with agonistic RANK antibody. After 1-day culture, tissues were harvested for FACS analysis. Cells were isolated and stained with CD45, EpCAM, MHC class II, and CD40 antibodies. Pre-gated $CD45^{-}EpCAM^{+}$ cells were plotted MHC class II versus CD40. Percentage of cells within the gated area is shown. The contour plots illustrate the profile of MHC class II and CD40 expression on 1-day cultured E14 TECs in different strains.

(D) TECs ($CD45^{-}EpCAM^{+}$) from E15 wild type (patterned bar), E15 Wnt5a HET (white bar), and E15 Wnt5a KO (black bar) were sorted and used to compare relative mRNA expression. Relative expression of RANK was normalized to the housekeeping gene, β-actin. The bar indicates the mean of triplicate and the error bar represents the standard error of the mean. The data shown is the representative of two independent experiments.

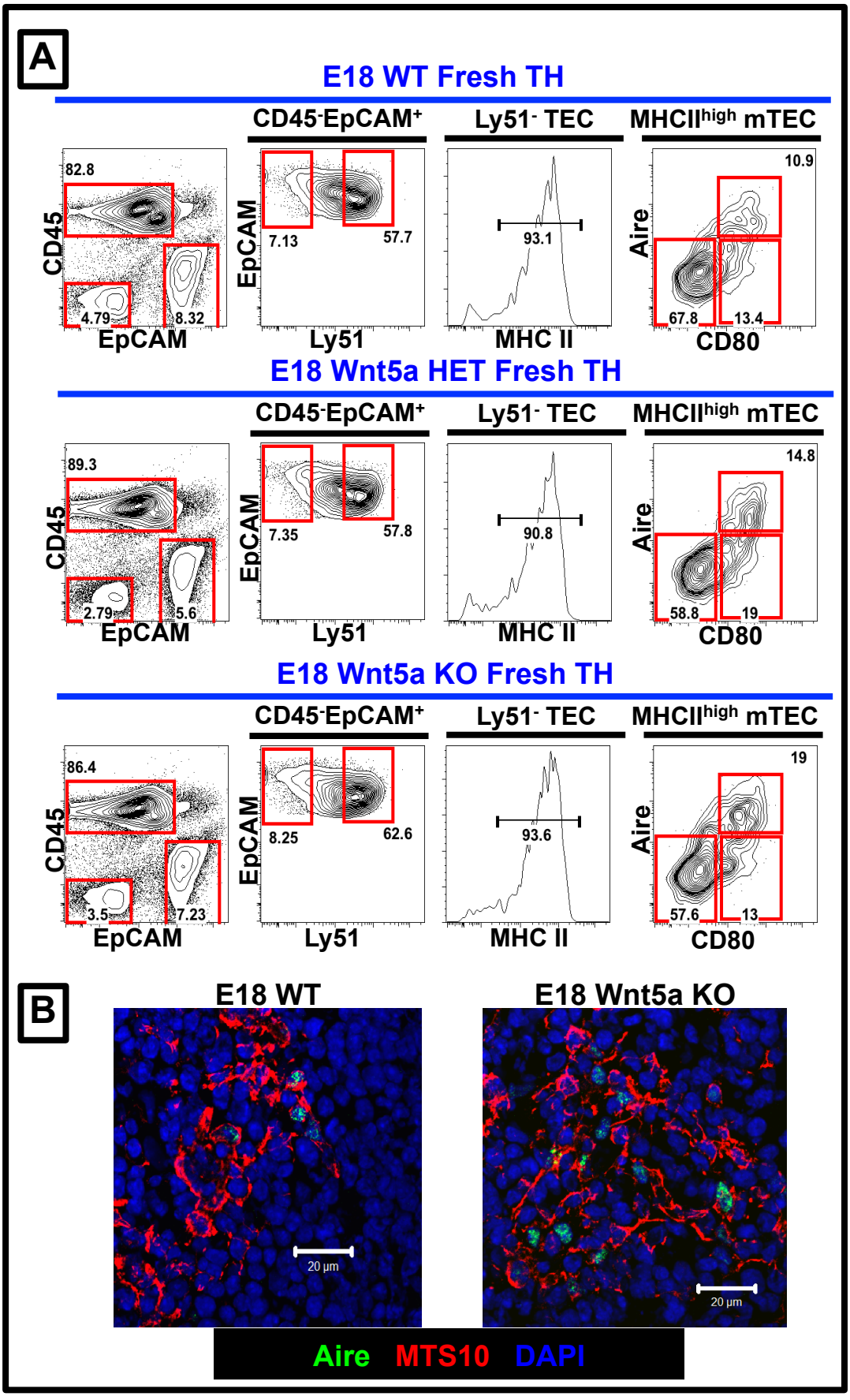

A
E18 WT Fresh TH
CD45-EpCAM+
Ly51- TEC
MHCIIhigh mTEC
82.8
CD45
4.79
8.32
EpCAM
EpCAM
7.13
57.7
Ly51
93.1
MHC II
10.9
Aire
67.8
13.4
CD80
E18 Wnt5a HET Fresh TH
CD45-EpCAM+
Ly51- TEC
MHCIIhigh mTEC
89.3
CD45
2.79
5.6
EpCAM
EpCAM
7.35
57.8
Ly51
90.8
MHC II
14.8
Aire
58.8
19
CD80
E18 Wnt5a KO Fresh TH
CD45-EpCAM+
Ly51- TEC
MHCIIhigh mTEC
86.4
CD45
3.5
7.23
EpCAM
EpCAM
8.25
62.6
Ly51
93.6
MHC II
19
Aire
57.6
13
CD80
B
E18 WT
E18 Wnt5a KO
20 µm
20 µm
Aire MTS10 DAPI

Figure 4.16. Embryonic TEC development in E18 Wnt5a KO Mice.

(A) Cells were isolated from E18 wild type (top), E18 Wnt5a HET (middle), and E18 Wnt5a KO (bottom). Cells were then stained with CD45, EpCAM, Ly51, MHC class II, CD80 and Aire antibodies for FACS analysis. The epithelial cells gated on $CD45^{-}EpCAM^{+}$ were divided into two populations in the context of Ly51 expression. $Ly51^{-}MHCII^{+}$ TECs were further gated to check CD80 and Aire expression.

(B) Frozen thymic sections of E18 wild type (left) and E18 Wnt5a KO (right) were stained for Aire, MTS10, and DAPI. Bar indicates a scale of 20μm.

microscopy, demonstrating normal embryonic TEC development. Absolute numbers of total cells (Figure 4.17. A), thymocytes (Figure 4.17. B), cTEC (Figure 4.17. C), total mTEC (Figure 4.17. D), $CD80^{-}Aire^{-}$ mTEC (Figure 4.17. E), $CD80^{+}Aire^{-}$ mTEC (Figure 4.17. F), and $CD80^{+}Aire^{+}$ mTEC (Figure 4.17. G) per thymus lobe in E18 $Wnt5a^{-/-}$ mice were calculated and compared with that seen in E18 $Wnt5a^{+/-}$ animals, the latter used as a control due to the limited availability of littermate wild type controls. Total cells (p value=0.8898), thymocytes (p value=0.9301), cTEC (p value=0.0513), total mTEC (p value=0.3303), $CD80^{-}Aire^{-}$ mTEC (p value=0.3361), and $CD80^{-}Aire^{+}$ mTEC (p value=0.1043) had no statistically significant difference between KO and HET embryos. However, the cell number of $CD80^{+}Aire^{-}$ mTEC subset in E18 $Wnt5a^{-/-}$ thymuses was slightly decreased and the decrease was statistically significant (p value=0.0489).

4.2.2.3. T-Cell Development In Wnt5a KO Mice

The analysis of cellularity and histology showed the normal TEC development in Wnt5a deficient embryos. Next, any possible effect of Wnt5a on the T-cell development was analyzed. Since $Wnt5a^{-/-}$ mice are embryonic lethal, we cultured E17 $Wnt5a^{-/-}$ thymus for 5 days to allow further T-cell development. $Wnt5a^{-/-}$ FTOC (DN: 2.89%, DP: 80.5%, SP4: 5.96%, SP8: 6.27%) had a similar profile of developing thymocytes to wild type FTOC (DN: 3.76%, DP: 74.5%, SP4: 9.67%, SP8: 7.1%). DN thymocytes were further examined for the presence of a non-conventional T-cell subset, γδT cells. In $Wnt5a^{-/-}$ FTOC, γδT cells comprise 47.7% of $CD4^{-}CD8^{-}$ cells, as observed in wild type FTOC (43.7%) (Figure 4.18. A). Moreover, TCR expression level of thymocytes in FTOC was also comparable between $Wnt5a^{-/-}$ and wild type mice: the low level of TCR expression in most of DPs and the high level of TCR expression in SP4s (Figure 4.18. A). SP thymocytes start to appear at late embryonic stage (White et al., 2008) and the histology analysis of E18 wild type thymus

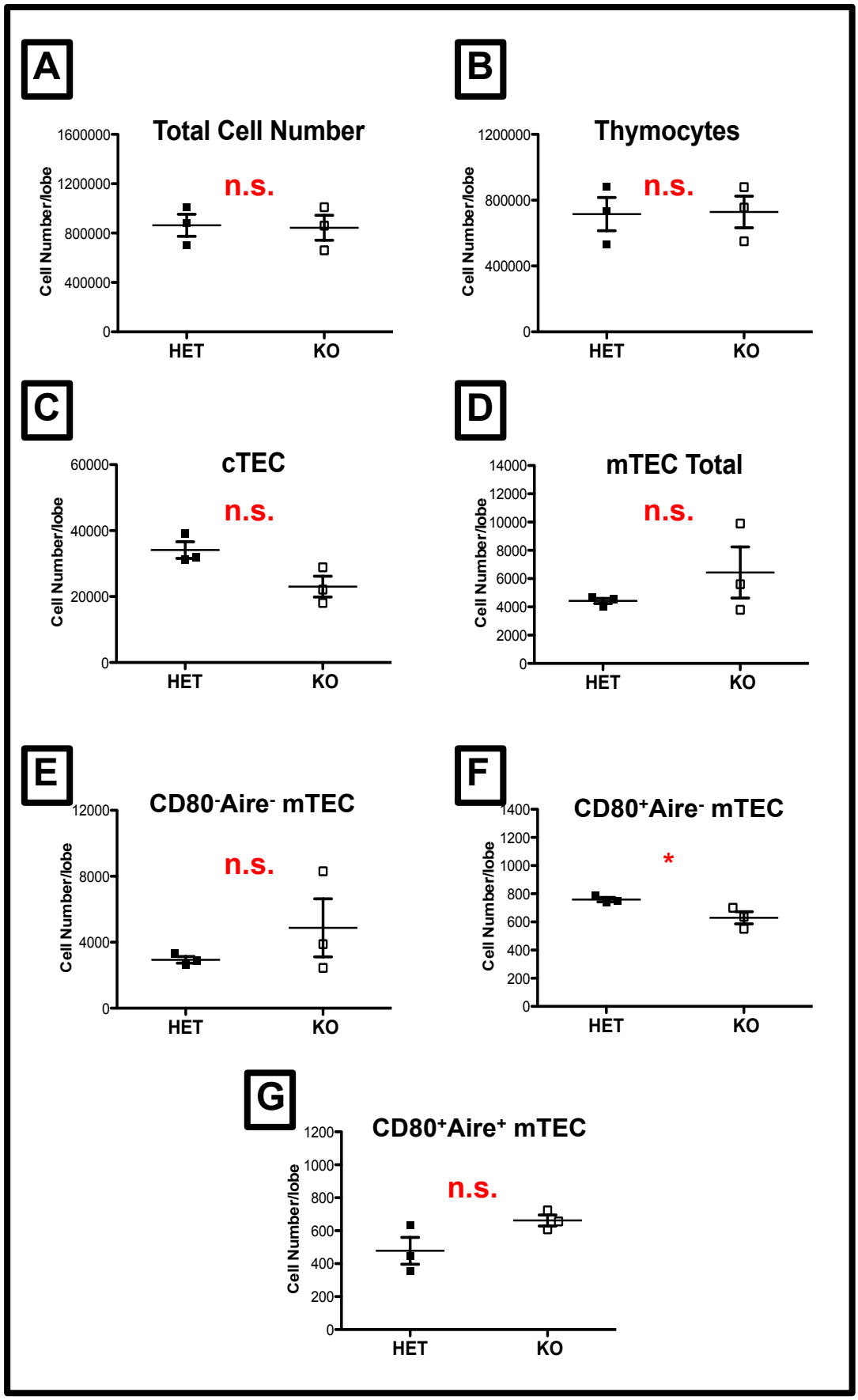

A
Total Cell Number
n.s.
Cell Number/lobe
1600000
1200000
800000
400000
0
HET
KO
B
Thymocytes
n.s.
Cell Number/lobe
1200000
800000
400000
0
HET
KO
C
cTEC
n.s.
Cell Number/lobe
60000
40000
20000
0
HET
KO
D
mTEC Total
n.s.
Cell Number/lobe
14000
12000
10000
8000
6000
4000
2000
0
HET
KO
E
CD80-Aire- mTEC
n.s.
Cell Number/lobe
12000
8000
4000
0
HET
KO
F
CD80+Aire- mTEC
*
Cell Number/lobe
1400
1200
1000
800
600
400
200
0
HET
KO
G
CD80+Aire+ mTEC
n.s.
Cell Number/lobe
1200
1000
800
600
400
200
0
HET
KO

Figure 4.17. Quantification of TEC subsets in Wnt5a KO embryos

Graphs shows the absolute number of total cells (A), thymocytes (B), cTEC (C), mTEC total (D), $CD80^{-}Aire^{-}$ mTEC (E), $CD80^{+}Aire^{-}$ mTEC (F), and $CD80^{+}Aire^{+}$ mTEC (G) per lobe in E18 Wnt5a HET and E18 Wnt5a KO. Each point represents one embryo. The bar indicates the calculated mean value and the error bar represents the standard error of the mean. Level of significance, which was calculated using an unpaired T test, was shown (* = $P < 0.05$, ** = $P < 0.01$, *** = $P < 0.001$). P value greater than 0.05 considered as non-significant (n.s.).

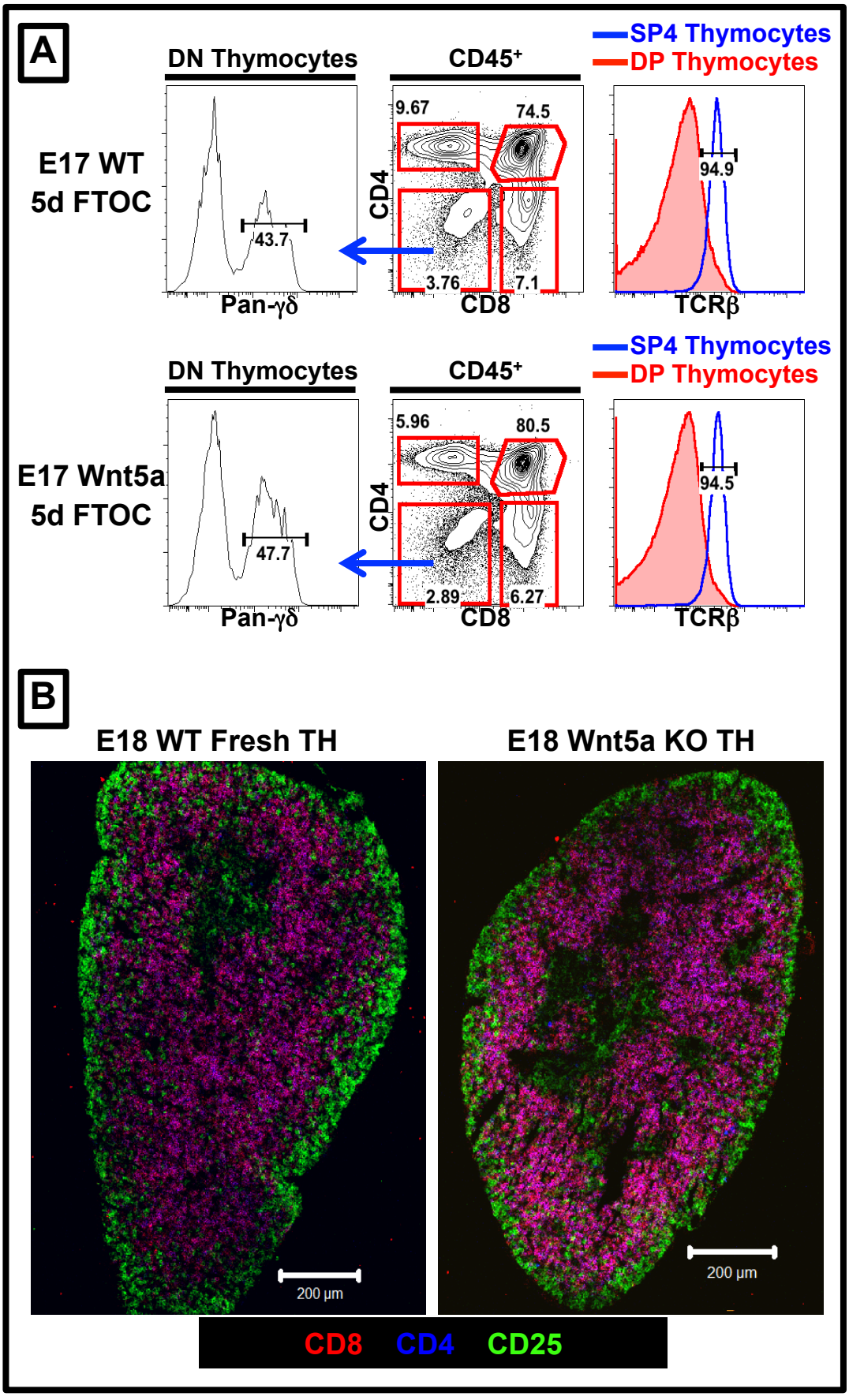

A
DN Thymocytes
CD45+
SP4 Thymocytes
DP Thymocytes
E17 WT
5d FTOC
9.67
74.5
43.7
3.76
7.1
94.9
CD4
CD8
Pan-γδ
TCRβ
E17 Wnt5a
5d FTOC
5.96
80.5
47.7
2.89
6.27
94.5
B
E18 WT Fresh TH
E18 Wnt5a KO TH
200 µm
200 µm
CD8 CD4 CD25

Figure 4.18. FACS and confocal analysis of T-cell development in Wnt5a KO embryos.

(A) Embryonic thymus of wild type and Wnt5a KO at the age of E17 was dissected and was placed in fetal thymic organ culture (FTOC) for 5 days. After culture, thymocytes were isolated for FACS analysis. Cells were stained with antibodies of cell surface marker including CD4, CD8, CD45, Pan-γδ, and TCRβ. The contour plot of $CD45^+$ thymocytes illustrates the profile of CD4 and CD8 expression. Double positive (DP, red) and CD4 single positive (SP4, blue) thymocytes were further gated to explore the TCRβ expression level. Double negative (DN) thymocytes were also further gated to check the presence of Pan-$\gamma\delta^+$ subset.

(B) Frozen thymic sections of E18 wild type (left) and E18 Wnt5a KO (right) mice were stained for CD4, CD8 and CD25. Bar indicates a scale of 200μm.

showed $CD25^+$ DN thymocytes (green) in subcapsular zone and DP thymocytes (pink) in the center of the thymus (Figure 4.18 B left). Similarly, $CD25^+$ DN thymocytes were resident in the subcapsular zone and DP thymocytes were localized in the center, confirming the correct positioning of thymocytes in embryonic thymus of $Wnt5a^{-/-}$ (Figure 4.18 B right). Collectively, not only embryonic TEC development but also T-cell development was normal in $Wnt5a^{-/-}$ embryo.

4.3. Discussion

4.3.1. Serial Development Of cTEC And mTEC

The thymus provides a specialized microenvironment for T cell development. There are two major cell populations in thymus: thymic epithelial cells and thymocytes. Thymocytes require signals from TEC for their survival and development. Also, the development of thymic epithelium is dependent upon signals from developing thymocytes. Distinct compartments of thymic epithelium drive different stages in the process of T-cell development, and sequential migration within thymus allows thymocytes to become self-tolerant T cells.

Due to interdependency between TECs and developing thymocytes, the block of T cell development at early stages leads to the failure of developing normal thymic architecture including both cortex and medulla (Mombaerts et al., 1992; Roberts et al., 2009; Shinkai et al., 1992). However, arrest at later stages, such as the $CD4^+CD8^+$ stage of T cell development causes impaired medulla development while cortex development appears normal (Palmer et al., 1993). This suggests that signals from SP thymocytes are required mostly for mTEC development but not necessary for the cTEC development. When we considered both the ordered migration of thymocytes within the thymus and the requirement of distinct thymocyte subsets for cTEC and mTEC development, we hypothesized that cTEC and mTEC might not

simultaneously emerge. Additionally, we showed that the acquisition of cTEC lineage occurs prior to the emergence of mTEC lineage. cTECs expressing CD205 appear first and then cTEC undergo maturation by acquiring an intermediate level of CD40 expression (Figure 4.1. B). Following their maturation, some of the $CD40^{Int}CD205^{+}$ TECs differentiate into $CD40^{High}CD205^{-}$ mTEC. In addition to CD205 expression, cTEC and mTEC can be distinguished according to CD40 expression level; CD40 expression level of mature mTEC is higher than that of mature cTEC (Shakib et al., 2009). This leads to the assumption that immature mTEC would express an intermediate level of CD40 combined with lack of CD205 expression. However, a transition subset between TEC progenitor and mature mTEC, whose phenotype is $CD40^{Int}CD205^{-}$, was not found at any stage. Hence, we proposed a serial developmental pathway rather than synchronous cTEC/mTEC lineage commitment.

The potential of progenitors to give rise to both cTEC and mTEC was proven via clonal analysis (Rossi et al., 2006). However, developmental stages from such bipotent progenitors to mature lineage-committed cTEC and mTEC still remained unclear. In order to test for a serial developmental TEC pathway, we analyzed the ability of embryonic TEC expressing the cTEC marker CD205 to undergo maturation upon RANK stimulation. We assumed that if an mTEC progenitor resided within the $CD205^{+}$ population, the maturation induced by an mTEC regulator could be detectable in these cells. The earliest stage that we can investigate is E11 of gestation because $CD205^{+}$ cTECs emerge at the age of E11 (Figure 4.1. B). We found that both $CD205^{-}$ TECs and $CD205^{+}$ TECs are capable of responding to RANK stimulation from E12 onwards (Figure 4.3.). This indicates the presence of both $CD205^{-}RANK^{+}$ TEC and $CD205^{+}RANK^{+}$ TEC populations at the developmental stage of E12. The finding that the $CD205^{+}RANK^{+}$ TEC subset contains mTEC progenitors therefore supports a model of a serial TEC development. However, the presence of $CD205^{-}RANK^{+}$

TEC leads to the idea that there might be either another mTEC development pathway, which is separate from a serial TEC development or that the $CD205^{-}RANK^{+}$ TEC population has already gone through a stage where cells co-express the cTEC CD205 and the mTEC marker RANK.

Our hypothesis that mTEC can develop from TEC expressing cTEC markers was tested with another approach, the ectopic transplant of immature CD205-expressing TEC. $CD40^{-}CD205^{+}$ TECs from E15 thymus were purified and used to form RTOC. $CD40^{-}CD205^{+}$ RTOCs were grafted under the kidney capsule of syngeneic adult wild type mice for analysis of their further development in vivo (Figure 4.5.). We found that $CD40^{-}CD205^{+}$ TECs could differentiate into an mTEC population, including the $Aire^{+}$ mTEC subset. mTECs generated from $CD40^{-}CD205^{+}$ TECs were not only phenotypically normal but also able to help produce functional T cells (Figure 4.6 to Figure 4.9.). Collectively, our data supports a serial model of TEC development, arguing against the synchronous model of TEC development in which both cTEC and mTEC are simultaneously developed from progenitors via independent pathway. In this model, TEC progenitors initially acquire the expression of cTEC specific genes. With the persistent expression of cTEC marker, TECs start to express a key regulator of mTEC development, RANK. Then, $CD205^{+}RANK^{+}$ TEC turn off the expression of cTEC markers becoming the mTEC population, whose phenotype is $CD205^{-}RANK^{+}$. Ohigashi *et al* and Ribeiro *et al* provided additional evidence demonstrating that mTECs, including $Aire^{+}$ mTEC subset, can originate from TEC expressing cTEC markers β5t and IL-7 (Ohigashi et al., 2013; Ribeiro et al., 2013). In the thymus of β5t fate-reporter mice, not only cTECs but also almost all of mTECs showed hallmarks of prior β5t expression, confirming that mTECs pass through a stage phenotypically defined as cTECs (Ohigashi et al., 2013). IL-7 is highly expressed in cTECs (Alves et al., 2009). Ribeiro *et al* proved the presence of a cell population

responding to RANK within IL-7^+ cTECs and the competence of IL-7^+ cTECs to give rise to mTECs (Ribeiro et al., 2013). Overall, these findings support a serial developmental pathway rather than a synchronous model of TEC development. Nevertheless, several questions still need to be answered.

First, what signal triggers the down-regulation of cTEC marker expression to generate the mTEC lineage? In addition, which cell population provides such signals? Regarding the latter, since the absence of SP thymocytes leads to the loss of medulla, SP thymocytes could be suggested as one of candidate cell populations. However, the presence of mTECs including the $Aire^+$ subset at the E16 of gestation was shown prior to the initial emergence of SP thymocytes (White et al., 2008). In other words, SP thymocytes are not required for the initial differentiation of mTEC from cTECs. The reason why mice lacking SP thymocytes still have impaired medulla could be because the signals from SP thymocytes are more important for the survival and proliferation of mTEC rather than their initial differentiation (White et al., 2008).

RANKL is expressed on $CD3^-CD4^+$ LTi cells and LTi cells appear in the thymus before SP thymocytes emerge (White et al., 2008). Therefore, we investigated whether a transition from $CD40^{Int}CD205^+$ cTECs to $CD40^{High}CD205^-$ mTECs is dependent upon RANK signals. The phenotypical analysis of embryonic TEC in $RANK^{-/-}$ (Figure 4.10. B) and $OPG^{-/-}$ mice (Figure 4.10. C) showed that the development of $CD40^{High}CD205^-$ mTECs from $CD40^{Int}CD205^+$ cTECs is independent of RANK signaling, but indicated that the size of the $CD40^{High}CD205^-$ mTEC subset is rather RANK-dosage dependent, suggesting its role in proliferation.

The percentage of the $CD40^{High}CD205^-$ mTEC subset within E15 total TEC was much lower in $LT\beta R^{-/-}$ mice compared to wild type and $RANK^{-/-}$ mice (Figure 4.10. D). It is

assumed that this might be due to the role of LTβR signaling in the induction of RANK expression, thus impaired RANK expression in LTβR$^{-/-}$ mice would cause the lower proliferation of the CD40^{High}CD205^{-} mTEC subset. However, RANK expression on TECs of E14 LTβR$^{-/-}$ was comparable to that of WT (Figure 4. 11. B). Then, LTβR may have an independent role of RANK in TEC development or in maintaining RANK expression instead of inducing initial expression on TECs. In conclusion, RANK and LTβR signals are not responsible for the differentiation of CD40^{High}CD205^{-} mTECs from CD40^{Int}CD205^{+} cTECs.

4.3.2. Role Of Wnt5a In TEC Development

Even though we showed that RANK is not involved in the transition from CD40^{Int}CD205^{+} cTECs to CD40^{High}CD205^{-} mTECs in this chapter, RANK is still important for the generation of Aire expressing mTECs (White et al., 2008). Therefore, if we understand how RANK expression is controlled, it would be helpful to study TEC development. RANK/RANKL interactions between osteoclast progenitors and osteoblast lineage cells are crucial for the generation of osteoclasts. Maeda *et al* uncovered a role of Wnt5a/Ror2 signal in inducing RANK expression in osteoclast precursors (Maeda et al., 2012). There are two different types of Wnt signals: a β-cantenin dependent canonical pathway and a non-canonical (Kikuchi et al., 2012). The non-canonical pathway is further classified into Ca^{2+}-dependent and JNK-dependent Wnt signals. In bone, Wnt5a secreted by osteoblast lineage cells binds to Ror2 on osteoclast precursor. The Wnt5a/Ror2 signal, which is dependent upon JNK, induces RANK expression on osteoclast precursor (Maeda et al., 2012). This finding led us to the idea that the same mechanism might control the RANK expression on TECs. We found Wnt5a expression in thymic mesenchyme and Ror2 expression on TECs (Figure 4.12. and 4.13.), suggesting that Wtn5a produced by mesenchyme may bind to Ror2 on early embryonic TECs to induce RANK expression on embryonic TECs. Hence, we expected to see impaired RANK

expression on TECs in Wnt5a deficient mice. However, RANK expression on TECs in Wnt5a$^{-/-}$ embryos appeared normal (Figure 4.15.). Moreover, other TNFRSFs such as CD40 and LTβR are also normally expressed by TECs in Wnt5a$^{-/-}$ embryos (Figure 4.14.). Also, mTEC maturation including acquisition of Aire expression occurred normally in Wnt5a deficient embryos, which also showed no defects in T-cell development (Figure 4.18.). Thus, although Wnt5a$^{-/-}$ mice are embryonic lethal due to severe problems in many organs, both TEC development and T-cell development appears normal, ruling out a role for this molecule in embryonic thymus development and function.

CHAPTER 5. General Discussion

5.1. Background And Overall Aims Of Study

Conventional and non-conventional T cells play major roles in adaptive immune responses and the production of the T cells is dependent on thymus microenvironments created by thymic epithelium (Anderson et al., 2006). Therefore, damaged or dysregulated development of thymic epithelium leads to impaired generation of thymic microenvironments and consequently causes a reduction in naïve T-cell production. Importantly, the process of ageing causes a reduction in thymic size and function. However, the signals triggering thymic atrophy are still not clear (George and Ritter, 1996). Moreover, the thymus is vulnerable to external insults including chemotherapy, radiation, and infection (Dudakov et al., 2012; van den Brink et al., 2004). The diminution of functional thymus tissue caused by ageing and/or additional insults results in higher chances of autoimmune disorders and immune deficiency diseases. Additionally, genetic disorders such as diGeorge syndrome and severe combined immunodeficiency (SCID) have severe problems in T-cell mediated immune responses (Fischer et al., 2013; Markert et al., 1999).

To recover T-cell mediated immune responses, bone-marrow transplantation has been studied as a potential curative therapy. However, immune rejection is the one of most practical issues for this therapy (van den Brink et al., 2004). Moreover, the ageing thymus represents a barrier to stem cell transplantation as suboptimal T-cell reconstitution because of thymus atrophy may occur in elderly patients. Hence, recent research has focused on restoring thymic function by reconstituting thymic epithelium. Most recent studies have succeeded in generating thymic epithelium from pluripotent stem cells including ES cells and iPS cells (Parent et al., 2013; Sun et al., 2013). However, due to several problems, such studies are still not complete in terms of their use as future therapeutic strategies. For example, T cells produced by grafted thymic tissues, which were generated from ES cells, were not fully

functional; peripheral T cells were generated with lower TCR diversity and lower levels of TCR activation-associated proliferation (Parent et al., 2013; Sun et al., 2013). This might be because only expression of FoxN1 was used to check thymic epithelium lineage specification from pluripotent cells. In order to promote the efficacy of functional T-cell production by grafted thymic tissues, other TEC progenitor markers besides FoxN1 and a better understanding of TEC development would be helpful.

Therefore, the ultimate goal of this study is to re-establish functionally competent thymic microenvironments in vivo from in-vitro derived TEC progenitors for future clinical applications. In more detail, the aims of this thesis were to:

-Classify the phenotype of thymic epithelial progenitor cells.

-Investigate TEC developmental pathways in embryonic development.

-Identify accessible cell lines that generate thymic tissues in vivo.

Chapter 3 summarizes the phenotype of putative TEC progenitors, and shows the differential expression of several surface markers between TECs and other type of epithelial cells in early embryos. It also demonstrates the capability of iPS cells to generate thymic tissues in vivo. Chapter 4 focuses on the potential of phenotypically defined TEC progenitors to generate both cTEC and mTEC lineages, and shows that mTEC including $Aire^{+}$ subset, are generated from cells expressing hallmarks of the cTEC lineage.

5.2. Summary Of TEC Development

5.2.1. Identification of TEC Progenitors

It is well known that FoxN1 expression is crucial for TEC development (Nehls et al., 1994). Finding such a vital role of FoxN1 in controlling TEC development has led to a huge

advance in the understanding of adaptive immune system. However, there is no other definitive TEC progenitor marker that can be used.

Parathyroid organogenesis is most closely related to thymus organogenesis. At early embryonic stages, not only the anatomical location but also the phenotype between two organs is very close. Therefore, distinguishing between parathyroid and thymus lineage-committed cells in early embryos is vital for identifying TEC progenitors. In this study, the expression of five surface markers was explored to discriminate TECs from parathyroid epithelial cells in early embryos. Some of the markers were expressed within both tissues and the rest were either thymus-specific or parathyroid-specific at around E12-E13. MTS24, an antibody that recognizes Plet-1, which is known as a possible TEC progenitor marker, defined both TECs and parathyroid epithelial cells. Neither TECs nor the epithelial cells of parathyroid express PD-L2. As demonstrated earlier, FoxN1 dependent PD-L1 expression was only found within the TEC population but not in parathyroid epithelium. Also, CD205 expression was found to be expressed by TEC but not parathyroid epithelium. Unexpectedly, parathyroid epithelial cells expressed low levels of CD40 that also marks TEC development at later stages. In other words, a non-lymphoid organ (parathyroid) expresses one of TNFRSF members that have major roles in immune responses and lymphoid organogenesis. The possible role of CD40 in either parathyroid organogenesis or function is not clear. Perhaps importantly we analyzed the expression only in embryos but not in postnatal stages. Thus, it is worth checking whether CD40 expression persisted on parathyroid epithelial cells through postnatal stages. Based on the findings from this study and previous studies, we suggest that the phenotype of TECs at early embryonic stage is $CD40^{-}CD205^{+}PD\text{-}L1^{+}PD\text{-}L2^{-}MTS24^{+}Gcm2^{-}FoxN1^{+}IL\text{-}7^{+}CCL21^{-}CCL25^{+}$ (Figure 5.1. A green) and that of parathyroid

epithelial cells is CD40^{Low}CD205^{-}PD-L1^{-}PD-L2^{-}MTS24^{+}Gcm2^{+}FoxN1^{-}IL-7^{-}CCL21^{+}CCL25^{-} (Figure 5.1. A red).

In addition to those five surface markers, the expression of other several markers was also explored to allow a better identification of TEC progenitors. We propose a putative phenotype of TEC progenitor at E11 of gestation, a stage known to contain bipotent TEC progenitors: CD205$^{-/+}$Claudin-3,4^{+}Ly51^{-}VCAM-1^{-}Integrin-α6^{+}LTβR^{+}ICAM-1$^{-/+}$ (Figure 5.1. B). The heterogeneity according to the expression of those markers was found at later embryonic stages. At E17, there is an mTEC population whose phenotype is CD205^{-}Claudin-3,4^{+}Ly51^{Low}VCAM-1^{High}Integrin-α6^{+}LTβR^{+}ICAM-1^{+} and a cTEC population whose phenotype is CD205^{+}Claudin-3,4$^{-/+}$Ly51^{High}VCAM-1$^{Low/High}$Integrin-α6^{+}LTβR^{+}ICAM-1^{+} (Figure 5.1. B). Integrin-α6, LTβR, and ICAM-1 expression does not allow discrimination between mTECs and cTECs at the age of E17. Moreover, TECs acquire expression of Integrin-α6 LTβR, and ICAM-1 early in embryonic stages and expression persists until the late embryonic stage. In contrast, the expression of other markers, namely CD205, Claudin-3,4, Ly51, and VCAM-1, shows heterogeneity between early embryonic TEC and late embryonic TEC and also between mTECs and cTECs at E17. In conclusion, the TEC progenitors with the same phenotype at E11 according to the markers used in this study were not found at E17. This suggests that TEC progenitors are present at later stage but with a different phenotype from earlier stage. Or we have not yet found the markers that identify TEC progenitors at both early and late embryonic stage.

5.2.2. Serial Model OF TEC Development

The capability of bipotent progenitors to give rise to both cTEC and mTEC is well established. However, the stages between progenitor and lineage-committed TECs are not elucidated yet. Until recently, it has been thought that cTEC and mTEC lineage diverge from

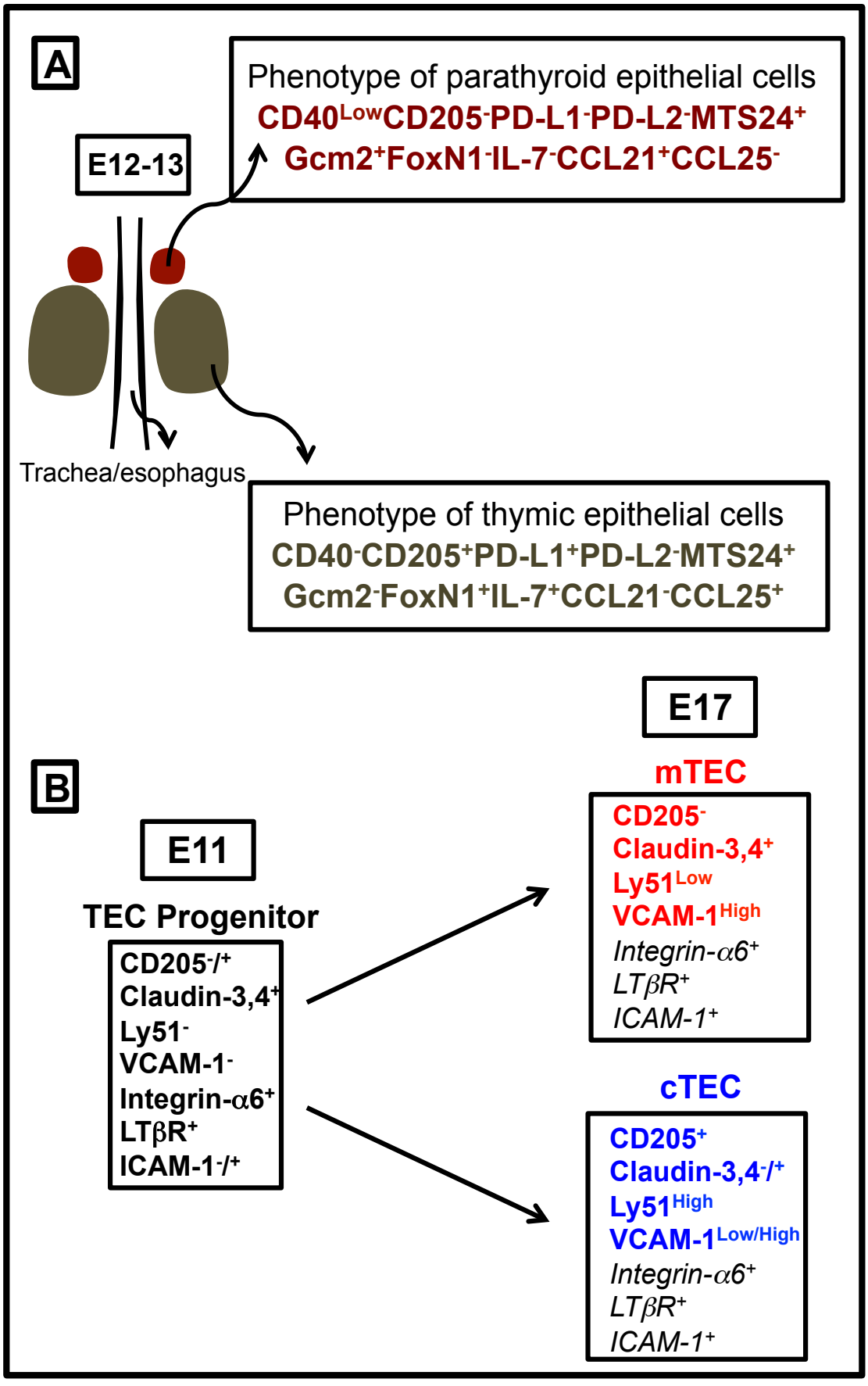

A
Phenotype of parathyroid epithelial cells
CD40LowCD205-PD-L1-PD-L2-MTS24+
Gcm2+FoxN1-IL-7-CCL21+CCL25-
E12-13
Trachea/esophagus
Phenotype of thymic epithelial cells
CD40-CD205+PD-L1+PD-L2-MTS24+
Gcm2-FoxN1+IL-7+CCL21-CCL25+
B
E11
TEC Progenitor
CD205-/+
Claudin-3,4+
Ly51-
VCAM-1-
Integrin-α6+
LTβR+
ICAM-1-/+
E17
mTEC
CD205-
Claudin-3,4+
Ly51Low
VCAM-1High
Integrin-α6+
LTβR+
ICAM-1+
cTEC
CD205+
Claudin-3,4-/+
Ly51High
VCAM-1Low/High
Integrin-α6+
LTβR+
ICAM-1+

Figure 5.1. Phenotype of TEC progenitor in early embryo

(A) Differential expression of surface markers and genes between TECs and parathyroid epithelial cells at E12-13.

(B) The phenotype of TEC progenitors at E11 (left)

The phenotype of mTEC (red) and cTEC (blue) at E17 (right)

bipotent progenitors in a binary process, simultaneously from the same developmental stage. However, we reveal in this study the developmental relationship between cTEC and mTEC lineage, based on the phenotypical and functional analysis.

We propose a new serial model of TEC development in terms of CD205 and RANK expression. TEC progenitors acquire the $CD205^+$ cTEC phenotype at E11. Then in a transition between E11 and E12, the TEC population obtains RANK expression becoming a cTEC/mTEC transitional subset. Around E14, the $CD205^+RANK^+$ TECs turn off cTEC marker expression, developing into an mTEC subset which phenotype is $CD205^-RANK^+$. According to our model, the emergence of the cTEC population is followed by the appearance of the mTEC subset. Moreover, the TEC population defined by cTEC markers is the origin of mTEC (Figure 3.2.).

Ohigashi *et al* and Ribeiro *et al* provided additional evidence supporting our serial model of TEC development (Ohigashi et al., 2013; Ribeiro et al., 2013). Ohigashi *et al* demonstrated that not only cTECs but also mTECs including $Aire^+$ subset were positive for cTEC marker β5t in β5t fate-reporter mice (Ohigashi et al., 2013). This indicates that almost all the mTEC population transverses a phenotypically defined cTEC stage. Moreover, Ribeiro *et al* also showed that $CD80^+$ mTEC population could be derived from $IL\text{-}7^+$ cTECs in IL-7 reporter mice (Ohigashi et al., 2013). Unlike the data presented by Ohigashi *et al,* Ribeiro *et al* highlighted the $IL\text{-}7^-$ TECs in embryo can also develop into $CD80^+$ mTEC population, suggesting more than one mTEC developmental pathways: cTEC-dependent and cTEC-independent (Ribeiro et al., 2013). Also, a possibility of alternative mTEC lineage might be present has been raised from this study and previous research. In this study, RANK-responsive $CD205^-$ TECs were found at E12. It is not clear whether this $CD205^-RANK^+$ TEC population at E12 is generated from $CD205^+RANK^+$ cTECs, or whether this subset develops

via a pathway, which is independent of a cTEC/mTEC transitional subset (Figure 3.2.). Moreover, the finding by Nowell *et el* supports the idea of an alternative pathway of mTEC lineage development. Nowell *et al* found $K5^{high}$Claudin-$3,4^{high}$ mTECs in E13 nude embryos (Nowell et al., 2011), suggesting that there might be a mTEC lineage which is FoxN1 and cTEC independent. However, further investigation is required to confirm the alternative mTEC lineage.

There are a few unresolved questions that remain in our model. It is not clear which TEC population gives rise to functional $CD205^{+}RANK^{-}$ cTECs. Whether the all cTECs must pass through a cTEC/mTEC transitional step like mTECs would be a determinant. If it does, a cTEC/mTEC transitional subset would be a bipotent progenitor that can develop into both $CD205^{+}RANK^{-}$ cTEC and $CD205^{-}RANK^{+}$ mTEC. If this is not the case, some of the $CD205^{+}RANK^{-}$ cTECs at E12 would maintain their phenotype and the rest would become a cTEC/mTEC transitional subset, which may then be mTEC progenitors. Or, cTECs could be originated via those two pathways, resulting in a possible heterogeneity based on developmental pathways. Lastly, all the data shown in this study is from embryonic thymus. Therefore, it is not clear how postnatal TEC development is different from and/or similar to embryonic TEC development. Checking both the presence of $CD205^{+}$ TECs in adult thymus and the bipotency of the population would be helpful to understand thymic atrophy and ultimately regenerate thymic tissue in the elderly.

5.3. Thymus Regeneration

In order to restore T-cell mediated immune responses, we have developed strategies to generate thymic tissue in vivo. iPS cells, which were generated from mouse embryonic fibroblasts, were used in this study. In a variety of 'proof-of-principle' experiments, we confirmed that the thymus tissue generated from iPS cells is functional. It had a normal

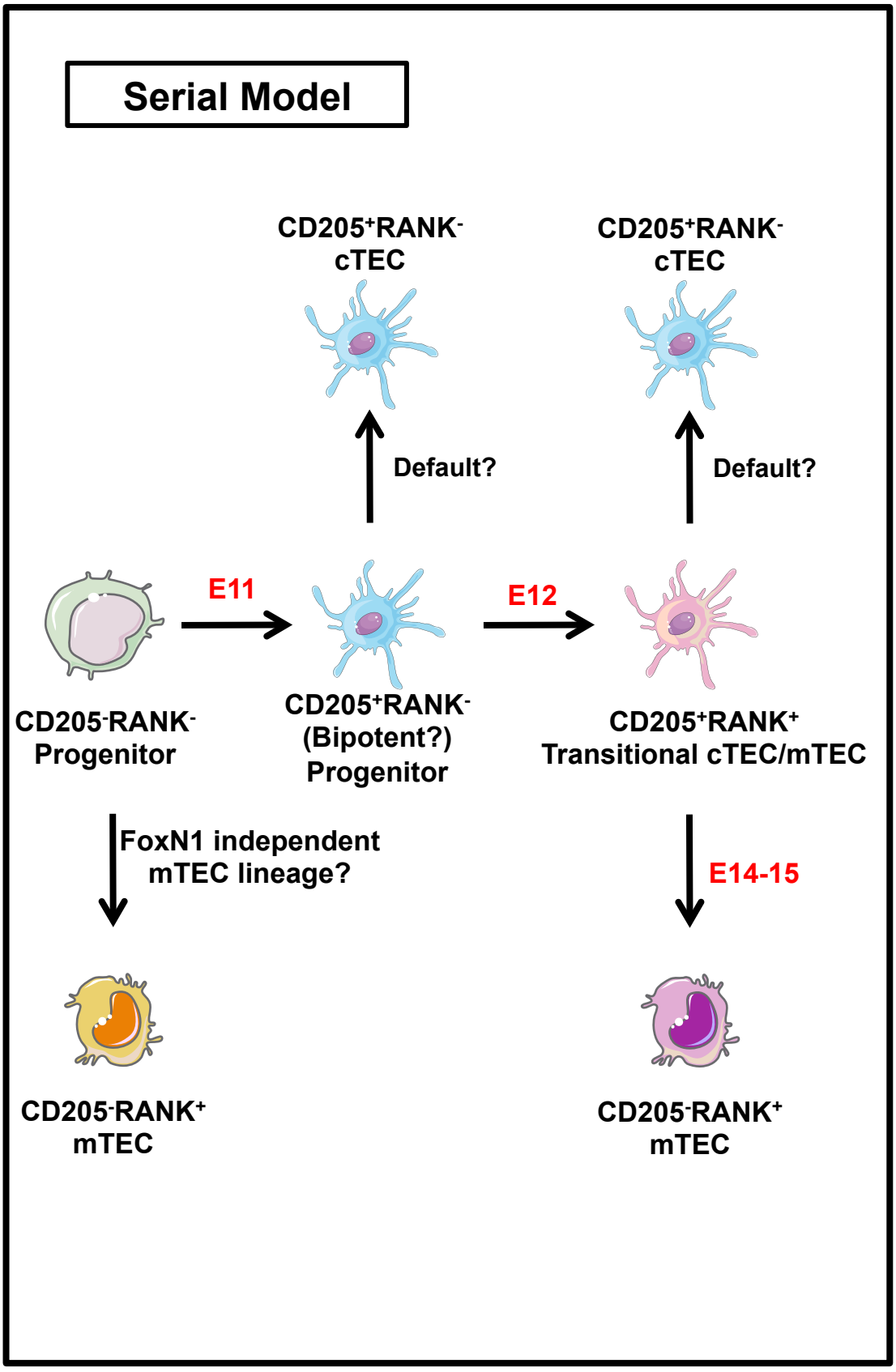

Serial Model
CD205+RANK-
cTEC
CD205+RANK-
cTEC
Default?
Default?
E11
E12
CD205-RANK-
Progenitor
CD205+RANK-
(Bipotent?)
Progenitor
CD205+RANK+
Transitional cTEC/mTEC
FoxN1 independent
mTEC lineage?
E14-15
CD205-RANK+
mTEC
CD205-RANK+
mTEC

Figure 5.2. Serial model of thymic epithelial cell development

In this serial model, TEC progenitors acquire cTEC marker CD205 expression at E11 and then the $CD205^+$ cTECs become a cTEC/mTEC transitional subset by up-regulating RANK expression at E12. Around E14-E15, the $CD205^+RANK^+$ TECs turn off CD205 expression, developing into mTEC population.

histology of thymic epithelium and a normal cellularity including conventional and non-conventional T-cell subsets. Then, the T cells produced by iPS chimera thymus were checked for their functional abilities. In order for T cells to be functional, they must migrate into secondary lymphoid tissues such as lymph node and spleen and then be activated upon stimulation. The presence of T cells within the secondary lymphoid tissues was confirmed and they were able to respond to in-vitro stimulation. More importantly, the presence of $Aire^{+}$ mTECs and $CD25^{+}FoxP3^{+}$ Tregs ensures the self-tolerance of T cells produced by iPS chimera thymus. For future work, the expression of both Aire-dependent and Aire-independent TRAs on mTECs can be further investigated to allow more robust self-tolerance TCR repertoire.

5.4. Concluding Remarks And Future Works

Our strategy to reconstitute thymic tissue involves in three steps. The first step is to reprogram somatic cells such as fibroblasts and adipocytes back to pluripotent state, generating iPS cells. The second step is to recapitulate thymus organogenesis either in vivo or in vitro, developing TEC progenitors from the iPS cells. The last step is to generate thymic tissues from the in-vitro derived TEC progenitors to provide microenvironments for T-cell production in vivo by transplanting the TEC progenitors (Figure 5.3.). This strategy of reconstituting thymic epithelium may also applicable to patients with diGeorge syndrome.

In this study, we have confirmed the capability of iPS cells formed form mouse embryonic fibroblasts to generate thymic tissues in vivo and we suggest a putative phenotype of TEC progenitor in embryo. Especially, we have demonstrated the competence of embryonic $CD205^{+}$ TEC as a progenitor population. For future therapeutic strategies, it may be interesting to generate iPS cells from adult and aged mouse fibroblasts and then to check the capability of these cell lines to develop functional thymus in vivo. Next, the signals

essential for the generation of $FoxN1^{+}CD205^{+}$ TEC progenitor from iPS cells in vitro have to be also explored. Recent studies have demonstrated that the sequential regulation of RA, TGFβ, Wnt3a, BMP4, Fgf8b, and Shh signals leads to the induction of FoxN1 and EpCAM expression from hESCs in vitro (Parent et al., 2013; Sun et al., 2013). Prior to the transplantation of TEC progenitors, confirming the expression of CD205, Claudin-3,4, Integrin-α6, LTβR, and ICAM-1 on in-vitro derived TEC progenitors might increase the efficacy of T-cell production because the expression of those markers were found on E11 embryonic TECs.

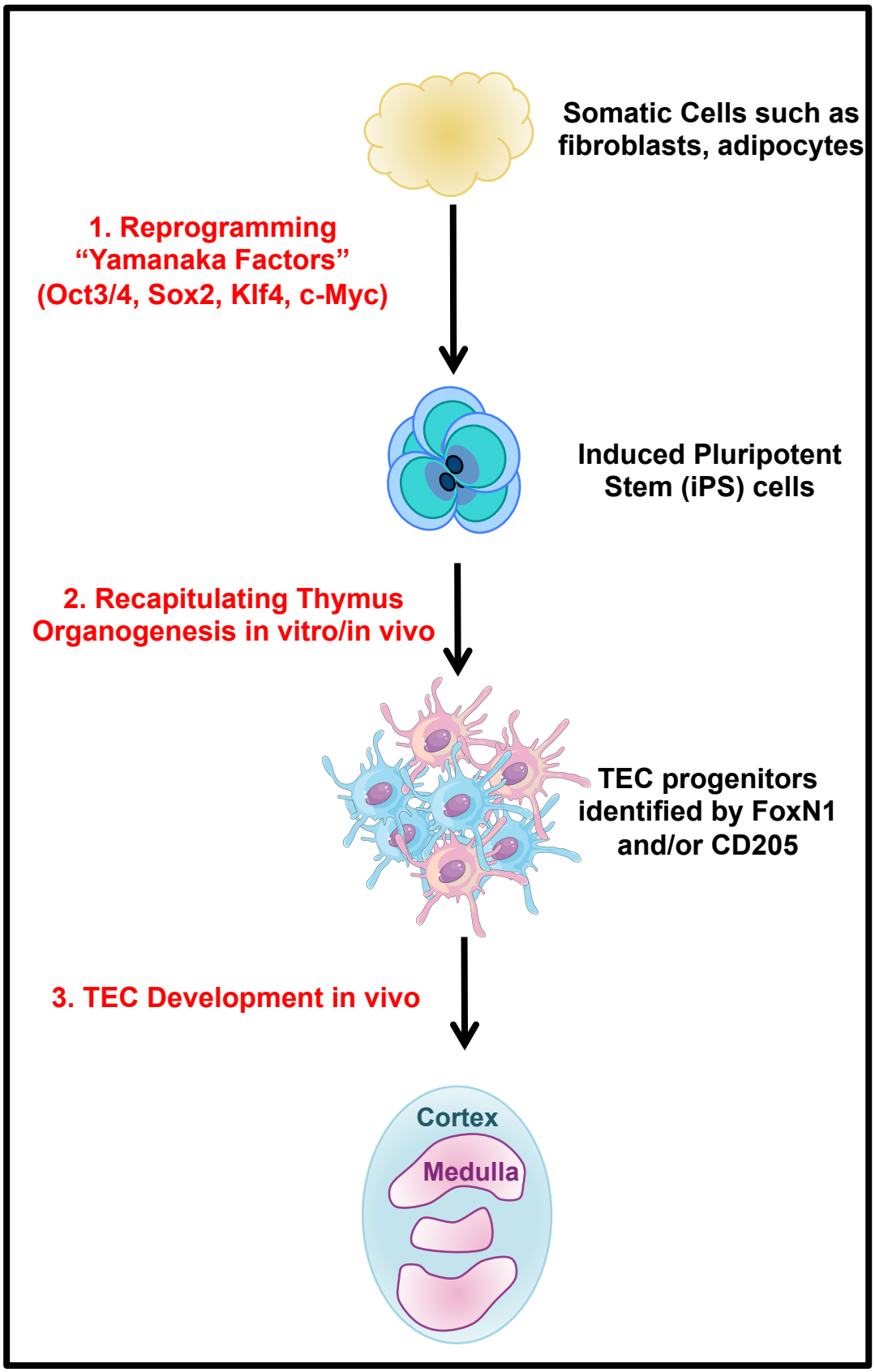

Somatic Cells such as fibroblasts, adipocytes
1. Reprogramming "Yamanaka Factors" (Oct3/4, Sox2, Klf4, c-Myc)
Induced Pluripotent Stem (iPS) cells
2. Recapitulating Thymus Organogenesis in vitro/in vivo
TEC progenitors identified by FoxN1 and/or CD205
3. TEC Development in vivo
Cortex
Medulla

Figure 5.3. Strategy to reconstitute thymic epithelium

Our strategy to combat thymus atrophy involves three steps: generating iPS cells from somatic cells, mimicking thymus organogenesis either in vivo or in vitro, and developing thymic epithelium in vivo.

Papers arising from this thesis

1. Alves NL, Takahama Y, Ohigashi I, Ribeiro AR, **Baik S**, Anderson G, Jenkinson WE. Serial progression of cortical and medullary thymic epithelial microenvironments. Eur J Immunol. 2014 Jan;44(1):16-22.

2. **Baik S**, Jenkinson EJ, Lane PJ, Anderson G, Jenkinson WE. Generation of both cortical and Aire(+) medullary thymic epithelial compartments from CD205(+) progenitors. Eur J Immunol. 2013 Jan;43:589-594.

3. Desanti GE, Cowan JE, **Baik S**, Parnell SM, White AJ, Penninger JM, Lane PJ, Jenkinson EJ, Jenkinson WE, Anderson G. Developmentally regulated availability of RANKL and CD40 ligand reveals distinct mechanisms of fetal and adult cross-talk in the thymus medulla. J Immunol. 2012 Dec 15;189(12):5519-26.

CHAPTER 6. Reference

Abramson, J., Giraud, M., Benoist, C., and Mathis, D. (2010). Aire's partners in the molecular control of immunological tolerance. Cell *140*, 123-135.

Adkins, B., Gandour, D., Strober, S., and Weissman, I. (1988). Total lymphoid irradiation leads to transient depletion of the mouse thymic medulla and persistent abnormalities among medullary stromal cells. J Immunol *140*, 3373-3379.

Aichinger, M., Wu, C., Nedjic, J., and Klein, L. (2013). Macroautophagy substrates are loaded onto MHC class II of medullary thymic epithelial cells for central tolerance. The Journal of experimental medicine *210*, 287-300.

Akiyama, T., Maeda, S., Yamane, S., Ogino, K., Kasai, M., Kajiura, F., Matsumoto, M., and Inoue, J. (2005). Dependence of self-tolerance on TRAF6-directed development of thymic stroma. Science *308*, 248-251.

Akiyama, T., Shimo, Y., Yanai, H., Qin, J., Ohshima, D., Maruyama, Y., Asaumi, Y., Kitazawa, J., Takayanagi, H., Penninger, J.M.*, et al.* (2008). The tumor necrosis factor family receptors RANK and CD40 cooperatively establish the thymic medullary microenvironment and self-tolerance. Immunity *29*, 423-437.

Allende, M.L., Dreier, J.L., Mandala, S., and Proia, R.L. (2004). Expression of the sphingosine 1-phosphate receptor, S1P1, on T-cells controls thymic emigration. The Journal of biological chemistry *279*, 15396-15401.

Alves, N.L., Richard-Le Goff, O., Huntington, N.D., Sousa, A.P., Ribeiro, V.S., Bordack, A., Vives, F.L., Peduto, L., Chidgey, A., Cumano, A.*, et al.* (2009). Characterization of the thymic IL-7 niche in vivo. Proceedings of the National Academy of Sciences of the United States of America *106*, 1512-1517.

Anderson, G., Jenkinson, W.E., Jones, T., Parnell, S.M., Kinsella, F.A., White, A.J., Pongrac'z, J.E., Rossi, S.W., and Jenkinson, E.J. (2006). Establishment and functioning of intrathymic microenvironments. Immunological reviews *209*, 10-27.

Anderson, K.L., Moore, N.C., McLoughlin, D.E., Jenkinson, E.J., and Owen, J.J. (1998). Studies on thymic epithelial cells in vitro. Developmental and comparative immunology *22*, 367-377.

Ara, T., Itoi, M., Kawabata, K., Egawa, T., Tokoyoda, K., Sugiyama, T., Fujii, N., Amagai, T., and Nagasawa, T. (2003). A role of CXC chemokine ligand 12/stromal cell-derived factor-1/pre-B cell growth stimulating factor and its receptor CXCR4 in fetal and adult T cell development in vivo. J Immunol *170*, 4649-4655.

Aschenbrenner, K., D'Cruz, L.M., Vollmann, E.H., Hinterberger, M., Emmerich, J., Swee, L.K., Rolink, A., and Klein, L. (2007). Selection of Foxp3+ regulatory T cells specific for self antigen expressed and presented by Aire+ medullary thymic epithelial cells. Nature immunology *8*, 351-358.

Aw, D., Silva, A.B., and Palmer, D.B. (2010). The effect of age on the phenotype and function of developing thymocytes. Journal of comparative pathology *142 Suppl 1*, S45-59.

Aw, D., Taylor-Brown, F., Cooper, K., and Palmer, D.B. (2009). Phenotypical and morphological changes in the thymic microenvironment from ageing mice. Biogerontology *10*, 311-322.

Baik, S., Jenkinson, E.J., Lane, P.J., Anderson, G., and Jenkinson, W.E. (2013). Generation of both cortical and Aire(+) medullary thymic epithelial compartments from CD205(+) progenitors. European journal of immunology *43*, 589-594.

Balciunaite, G., Ceredig, R., Fehling, H.J., Zuniga-Pflucker, J.C., and Rolink, A.G. (2005). The role of Notch and IL-7 signaling in early thymocyte proliferation and differentiation. European journal of immunology *35*, 1292-1300.

Balciunaite, G., Keller, M.P., Balciunaite, E., Piali, L., Zuklys, S., Mathieu, Y.D., Gill, J., Boyd, R., Sussman, D.J., and Hollander, G.A. (2002). Wnt glycoproteins regulate the expression of FoxNI, the gene defective in nude mice. Nature immunology *3*, 1102-1108.

Banchereau, J., and Steinman, R.M. (1998). Dendritic cells and the control of immunity. Nature *392*, 245-252.

Basset, C., Holton, J., O'Mahony, R., and Roitt, I. (2003). Innate immunity and pathogen-host interaction. Vaccine *21 Suppl 2*, S12-23.

Bendelac, A. (1995). Positive selection of mouse NK1+ T cells by CD1-expressing cortical thymocytes. The Journal of experimental medicine *182*, 2091-2096.

Benlagha, K., Kyin, T., Beavis, A., Teyton, L., and Bendelac, A. (2002). A thymic precursor to the NK T cell lineage. Science *296*, 553-555.

Bennett, A.R., Farley, A., Blair, N.F., Gordon, J., Sharp, L., and Blackburn, C.C. (2002). Identification and characterization of thymic epithelial progenitor cells. Immunity *16*, 803-814.

Blackburn, C.C., and Manley, N.R. (2004). Developing a new paradigm for thymus organogenesis. Nature reviews. Immunology *4*, 278-289.

Bleul, C.C., and Boehm, T. (2001). Laser capture microdissection-based expression profiling identifies PD1-ligand as a target of the nude locus gene product. European journal of immunology *31*, 2497-2503.

Bleul, C.C., and Boehm, T. (2005). BMP signaling is required for normal thymus development. Journal of Immunology *175*, 5213-5221.

Bleul, C.C., Corbeaux, T., Reuter, A., Fisch, P., Monting, J.S., and Boehm, T. (2006). Formation of a functional thymus initiated by a postnatal epithelial progenitor cell. Nature *441*, 992-996.

Boehm, T., Scheu, S., Pfeffer, K., and Bleul, C.C. (2003). Thymic medullary epithelial cell differentiation, thymocyte emigration, and the control of autoimmunity require lympho-epithelial cross talk via LTbetaR. The Journal of experimental medicine *198*, 757-769.

Bonilla, F.A., and Oettgen, H.C. (2010). Adaptive immunity. The Journal of allergy and clinical immunology *125*, S33-40.

Bryant, P., and Ploegh, H. (2004). Class II MHC peptide loading by the professionals. Current opinion in immunology *16*, 96-102.

Burkly, L., Hession, C., Ogata, L., Reilly, C., Marconi, L.A., Olson, D., Tizard, R., Cate, R., and Lo, D. (1995). Expression of relB is required for the development of thymic medulla and dendritic cells. Nature *373*, 531-536.

Calderon, L., and Boehm, T. (2011). Three chemokine receptors cooperatively regulate homing of hematopoietic progenitors to the embryonic mouse thymus. Proceedings of the National Academy of Sciences of the United States of America *108*, 7517-7522.

Carlson, C.M., Endrizzi, B.T., Wu, J., Ding, X., Weinreich, M.A., Walsh, E.R., Wani, M.A., Lingrel, J.B., Hogquist, K.A., and Jameson, S.C. (2006). Kruppel-like factor 2 regulates thymocyte and T-cell migration. Nature *442*, 299-302.

Chaplin, D.D. (2003). 1. Overview of the immune response. The Journal of allergy and clinical immunology *111*, S442-459.

Conway, S.J., Henderson, D.J., and Copp, A.J. (1997). Pax3 is required for cardiac neural crest migration in the mouse: evidence from the splotch (Sp2H) mutant. Development *124*, 505-514.

Cordier, A.C., and Haumont, S.M. (1980). Development of thymus, parathyroids, and ultimo-branchial bodies in NMRI and nude mice. The American journal of anatomy *157*, 227-263.

Cordier, A.C., and Heremans, J.F. (1975). Nude mouse embryo: ectodermal nature of the primordial thymic defect. Scandinavian journal of immunology *4*, 193-196.

Cowan, J.E., Parnell, S.M., Nakamura, K., Caamano, J.H., Lane, P.J., Jenkinson, E.J., Jenkinson, W.E., and Anderson, G. (2013). The thymic medulla is required for Foxp3+ regulatory but not conventional CD4+ thymocyte development. The Journal of experimental medicine *210*, 675-681.

Crompton, T., Outram, S.V., Buckland, J., and Owen, M.J. (1998). Distinct roles of the interleukin-7 receptor alpha chain in fetal and adult thymocyte development revealed by analysis of interleukin-7 receptor alpha-deficient mice. European journal of immunology *28*, 1859-1866.

de Oliveira Otto, M.C., Nettleton, J.A., Lemaitre, R.N., L, M.S., Kromhout, D., Rich, S.S., M, Y.T., Jacobs, D.R., and Mozaffarian, D. (2013). Biomarkers of dairy Fatty acids and risk of cardiovascular disease in the multi-ethnic study of atherosclerosis. Journal of the American Heart Association *2*, e000092.

Deindl, S., Kadlecek, T.A., Brdicka, T., Cao, X., Weiss, A., and Kuriyan, J. (2007). Structural basis for the inhibition of tyrosine kinase activity of ZAP-70. Cell *129*, 735-746.

Delves, P.J., and Roitt, I.M. (2000a). The immune system. First of two parts. The New England journal of medicine *343*, 37-49.

Delves, P.J., and Roitt, I.M. (2000b). The immune system. Second of two parts. The New England journal of medicine *343*, 108-117.

Derbinski, J., Gabler, J., Brors, B., Tierling, S., Jonnakuty, S., Hergenhahn, M., Peltonen, L., Walter, J., and Kyewski, B. (2005). Promiscuous gene expression in thymic epithelial cells is regulated at multiple levels. The Journal of experimental medicine *202*, 33-45.

Dudakov, J.A., Hanash, A.M., Jenq, R.R., Young, L.F., Ghosh, A., Singer, N.V., West, M.L., Smith, O.M., Holland, A.M., Tsai, J.J*., et al.* (2012). Interleukin-22 drives endogenous thymic regeneration in mice. Science *336*, 91-95.

Eberl, G., Lees, R., Smiley, S.T., Taniguchi, M., Grusby, M.J., and MacDonald, H.R. (1999). Tissue-specific segregation of CD1d-dependent and CD1d-independent NK T cells. J Immunol *162*, 6410-6419.

Emre, Y., Irla, M., Dunand-Sauthier, I., Ballet, R., Meguenani, M., Jemelin, S., Vesin, C., Reith, W., and Imhof, B.A. (2013). Thymic epithelial cell expansion through matricellular protein CYR61 boosts progenitor homing and T-cell output. Nature communications *4*, 2842.

Epstein, J.A., Li, J., Lang, D., Chen, F., Brown, C.B., Jin, F., Lu, M.M., Thomas, M., Liu, E., Wessels, A., and Lo, C.W. (2000). Migration of cardiac neural crest cells in Splotch embryos. Development *127*, 1869-1878.

Farr, A.G., and Anderson, S.K. (1985). Epithelial heterogeneity in the murine thymus: fucose-specific lectins bind medullary epithelial cells. J Immunol *134*, 2971-2977.

Fischer, A., Hacein-Bey-Abina, S., and Cavazzana-Calvo, M. (2013). Gene therapy of primary T cell immunodeficiencies. Gene *525*, 170-173.

Fontenot, J.D., Gavin, M.A., and Rudensky, A.Y. (2003). Foxp3 programs the development and function of CD4+CD25+ regulatory T cells. Nature immunology *4*, 330-336.

Fugmann, S.D., Lee, A.I., Shockett, P.E., Villey, I.J., and Schatz, D.G. (2000). The RAG proteins and V(D)J recombination: complexes, ends, and transposition. Annual review of immunology *18*, 495-527.

Futterer, A., Mink, K., Luz, A., Kosco-Vilbois, M.H., and Pfeffer, K. (1998). The lymphotoxin beta receptor controls organogenesis and affinity maturation in peripheral lymphoid tissues. Immunity *9*, 59-70.

Gabler, J., Arnold, J., and Kyewski, B. (2007). Promiscuous gene expression and the developmental dynamics of medullary thymic epithelial cells. European journal of immunology *37*, 3363-3372.

George, A.J., and Ritter, M.A. (1996). Thymic involution with ageing: obsolescence or good housekeeping? Immunology today *17*, 267-272.

Gill, J., Malin, M., Hollander, G.A., and Boyd, R. (2002). Generation of a complete thymic microenvironment by MTS24(+) thymic epithelial cells. Nature immunology *3*, 635-642.

Gill, J., Malin, M., Sutherland, J., Gray, D., Hollander, G., and Boyd, R. (2003). Thymic generation and regeneration. Immunological reviews *195*, 28-50.

Godfrey, D.I., Izon, D.J., Tucek, C.L., Wilson, T.J., and Boyd, R.L. (1990). The phenotypic heterogeneity of mouse thymic stromal cells. Immunology *70*, 66-74.

Godfrey, D.I., Kennedy, J., Suda, T., and Zlotnik, A. (1993). A developmental pathway involving four phenotypically and functionally distinct subsets of CD3-CD4-CD8- triple-negative adult mouse thymocytes defined by CD44 and CD25 expression. J Immunol *150*, 4244-4252.

Goldrath, A.W., and Bevan, M.J. (1999). Selecting and maintaining a diverse T-cell repertoire. Nature *402*, 255-262.

Gordon, J., Bennett, A.R., Blackburn, C.C., and Manley, N.R. (2001). Gcm2 and Foxn1 mark early parathyroid- and thymus-specific domains in the developing third pharyngeal pouch. Mechanisms of development *103*, 141-143.

Gordon, J., and Manley, N.R. (2011). Mechanisms of thymus organogenesis and morphogenesis. Development *138*, 3865-3878.

Gordon, J., Wilson, V.A., Blair, N.F., Sheridan, J., Farley, A., Wilson, L., Manley, N.R., and Blackburn, C.C. (2004). Functional evidence for a single endodermal origin for the thymic epithelium. Nature immunology *5*, 546-553.

Gossens, K., Naus, S., Corbel, S.Y., Lin, S., Rossi, F.M., Kast, J., and Ziltener, H.J. (2009). Thymic progenitor homing and lymphocyte homeostasis are linked via S1P-controlled expression of thymic P-selectin/CCL25. The Journal of experimental medicine *206*, 761-778.

Gray, D.H., Seach, N., Ueno, T., Milton, M.K., Liston, A., Lew, A.M., Goodnow, C.C., and Boyd, R.L. (2006). Developmental kinetics, turnover, and stimulatory capacity of thymic epithelial cells. Blood *108*, 3777-3785.

Green, M.D., Chen, A., Nostro, M.C., d'Souza, S.L., Schaniel, C., Lemischka, I.R., Gouon-Evans, V., Keller, G., and Snoeck, H.W. (2011). Generation of anterior foregut endoderm from human embryonic and induced pluripotent stem cells. Nature biotechnology *29*, 267-272.

Gruver, A.L., Hudson, L.L., and Sempowski, G.D. (2007). Immunosenescence of ageing. The Journal of pathology *211*, 144-156.

Guermonprez, P., Valladeau, J., Zitvogel, L., Thery, C., and Amigorena, S. (2002). Antigen presentation and T cell stimulation by dendritic cells. Annual review of immunology *20*, 621-667.

Gui, J.G., Zhu, X.K., Dohkan, J.I., Cheng, L.L., Barnes, P.F., and Su, D.M. (2007). The aged thymus shows normal recruitment of lymphohematopoietic progenitors but has defects in thymic epithelial cells. International immunology *19*, 1201-1211.

Guy, C.S., and Vignali, D.A. (2009). Organization of proximal signal initiation at the TCR:CD3 complex. Immunological reviews *232*, 7-21.

Hamazaki, Y., Fujita, H., Kobayashi, T., Choi, Y., Scott, H.S., Matsumoto, M., and Minato, N. (2007). Medullary thymic epithelial cells expressing Aire represent a unique lineage derived from cells expressing claudin. Nature immunology *8*, 304-311.

Hare, K.J., Jenkinson, E.J., and Anderson, G. (1999). CD69 expression discriminates MHC-dependent and -independent stages of thymocyte positive selection. J Immunol *162*, 3978-3983.

Harman, B.C., Jenkinson, W.E., Parnell, S.M., Rossi, S.W., Jenkinson, E.J., and Anderson, G. (2005). T/B lineage choice occurs prior to intrathymic Notch signaling. Blood *106*, 886-892.

Harty, J.T., Tvinnereim, A.R., and White, D.W. (2000). CD8+ T cell effector mechanisms in resistance to infection. Annual review of immunology *18*, 275-308.

Heino, M., Peterson, P., Sillanpaa, N., Guerin, S., Wu, L., Anderson, G., Scott, H.S., Antonarakis, S.E., Kudoh, J., Shimizu, N.*, et al.* (2000). RNA and protein expression of the murine autoimmune regulator gene (Aire) in normal, RelB-deficient and in NOD mouse. European journal of immunology *30*, 1884-1893.

Heng, T.S., Goldberg, G.L., Gray, D.H., Sutherland, J.S., Chidgey, A.P., and Boyd, R.L. (2005). Effects of castration on thymocyte development in two different models of thymic involution. J Immunol *175*, 2982-2993.

Hetzer-Egger, C., Schorpp, M., Haas-Assenbaum, A., Balling, R., Peters, H., and Boehm, T. (2002). Thymopoiesis requires Pax9 function in thymic epithelial cells. European journal of immunology *32*, 1175-1181.

Hikosaka, Y., Nitta, T., Ohigashi, I., Yano, K., Ishimaru, N., Hayashi, Y., Matsumoto, M., Matsuo, K., Penninger, J.M., Takayanagi, H.*, et al.* (2008). The cytokine RANKL produced by positively selected thymocytes fosters medullary thymic epithelial cells that express autoimmune regulator. Immunity *29*, 438-450.

Hince, M., Sakkal, S., Vlahos, K., Dudakov, J., Boyd, R., and Chidgey, A. (2008). The role of sex steroids and gonadectomy in the control of thymic involution. Cellular immunology *252*, 122-138.

Hollander, G.A., Wang, B., Nichogiannopoulou, A., Platenburg, P.P., van Ewijk, W., Burakoff, S.J., Gutierrez-Ramos, J.C., and Terhorst, C. (1995). Developmental control point in induction of thymic cortex regulated by a subpopulation of prothymocytes. Nature *373*, 350-353.

Hozumi, K., Negishi, N., Tsuchiya, I., Abe, N., Hirano, K., Suzuki, D., Yamamoto, M., Engel, J.D., and Habu, S. (2008). Notch signaling is necessary for GATA3 function in the initiation of T cell development. European journal of immunology *38*, 977-985.

Hulstaert, F., Hannet, I., Deneys, V., Munhyeshuli, V., Reichert, T., De Bruyere, M., and Strauss, K. (1994). Age-related changes in human blood lymphocyte subpopulations. II. Varying kinetics of percentage and absolute count measurements. Clinical immunology and immunopathology *70*, 152-158.

Ikawa, T., Hirose, S., Masuda, K., Kakugawa, K., Satoh, R., Shibano-Satoh, A., Kominami, R., Katsura, Y., and Kawamoto, H. (2010). An essential developmental checkpoint for production of the T cell lineage. Science *329*, 93-96.

Janeway, C.A., Jr. (1999). T-cell development: a role for self-peptides in positive selection. Current biology : CB *9*, R342-345.

Jenkinson, W.E., Bacon, A., White, A.J., Anderson, G., and Jenkinson, E.J. (2008). An epithelial progenitor pool regulates thymus growth. J Immunol *181*, 6101-6108.

Jenkinson, W.E., Jenkinson, E.J., and Anderson, G. (2003). Differential requirement for mesenchyme in the proliferation and maturation of thymic epithelial progenitors. The Journal of experimental medicine *198*, 325-332.

Jenkinson, W.E., Nakamura, K., White, A.J., Jenkinson, E.J., and Anderson, G. (2012). Normal T cell selection occurs in CD205-deficient thymic microenvironments. PloS one *7*, e53416.

Jenkinson, W.E., Rossi, S.W., Parnell, S.M., Agace, W.W., Takahama, Y., Jenkinson, E.J., and Anderson, G. (2007). Chemokine receptor expression defines heterogeneity in the earliest thymic migrants. European journal of immunology *37*, 2090-2096.

Jiang, W., Swiggard, W.J., Heufler, C., Peng, M., Mirza, A., Steinman, R.M., and Nussenzweig, M.C. (1995). The receptor DEC-205 expressed by dendritic cells and thymic epithelial cells is involved in antigen processing. Nature *375*, 151-155.

Kajiura, F., Sun, S., Nomura, T., Izumi, K., Ueno, T., Bando, Y., Kuroda, N., Han, H., Li, Y., Matsushima, A.*, et al.* (2004). NF-kappa B-inducing kinase establishes self-tolerance in a thymic stroma-dependent manner. J Immunol *172*, 2067-2075.

Kane, L.P., Lin, J., and Weiss, A. (2000). Signal transduction by the TCR for antigen. Current opinion in immunology *12*, 242-249.

Kearns, N.A., Genga, R.M., Ziller, M., Kapinas, K., Peters, H., Brehm, M.A., Meissner, A., and Maehr, R. (2013). Generation of organized anterior foregut epithelia from pluripotent stem cells using small molecules. Stem cell research *11*, 1003-1012.

Keir, M.E., Butte, M.J., Freeman, G.J., and Sharpe, A.H. (2008). PD-1 and its ligands in tolerance and immunity. Annual review of immunology *26*, 677-704.

Kikuchi, A., Yamamoto, H., Sato, A., and Matsumoto, S. (2012). Wnt5a: its signalling, functions and implication in diseases. Acta Physiol (Oxf) *204*, 17-33.

Kim, J.M., Rasmussen, J.P., and Rudensky, A.Y. (2007). Regulatory T cells prevent catastrophic autoimmunity throughout the lifespan of mice. Nature immunology *8*, 191-197.

Kincade, P.W., Owen, J.J., Igarashi, H., Kouro, T., Yokota, T., and Rossi, M.I. (2002). Nature or nurture? Steady-state lymphocyte formation in adults does not recapitulate ontogeny. Immunological reviews *187*, 116-125.

Kishimoto, H., and Sprent, J. (1997). Negative selection in the thymus includes semimature T cells. The Journal of experimental medicine *185*, 263-271.

Klein, L., Hinterberger, M., Wirnsberger, G., and Kyewski, B. (2009). Antigen presentation in the thymus for positive selection and central tolerance induction. Nature reviews. Immunology *9*, 833-844.

Koch, U., Fiorini, E., Benedito, R., Besseyrias, V., Schuster-Gossler, K., Pierres, M., Manley, N.R., Duarte, A., Macdonald, H.R., and Radtke, F. (2008). Delta-like 4 is the essential, nonredundant ligand for Notch1 during thymic T cell lineage commitment. The Journal of experimental medicine *205*, 2515-2523.

Kurobe, H., Liu, C., Ueno, T., Saito, F., Ohigashi, I., Seach, N., Arakaki, R., Hayashi, Y., Kitagawa, T., Lipp, M.*, et al.* (2006). CCR7-dependent cortex-to-medulla migration of positively selected thymocytes is essential for establishing central tolerance. Immunity *24*, 165-177.

Ladi, E., Yin, X., Chtanova, T., and Robey, E.A. (2006). Thymic microenvironments for T cell differentiation and selection. Nature immunology *7*, 338-343.

Lai, L., Cui, C., Jin, J., Hao, Z., Zheng, Q., Ying, M., Boyd, R., and Zhao, Y. (2011). Mouse embryonic stem cell-derived thymic epithelial cell progenitors enhance T-cell reconstitution after allogeneic bone marrow transplantation. Blood *118*, 3410-3418.

Le Lievre, C.S., and Le Douarin, N.M. (1975). Mesenchymal derivatives of the neural crest: analysis of chimaeric quail and chick embryos. Journal of embryology and experimental morphology *34*, 125-154.

Lei, Y., Ripen, A.M., Ishimaru, N., Ohigashi, I., Nagasawa, T., Jeker, L.T., Bosl, M.R., Hollander, G.A., Hayashi, Y., Malefyt Rde, W.*, et al.* (2011). Aire-dependent production of XCL1 mediates medullary accumulation of thymic dendritic cells and contributes to regulatory T cell development. The Journal of experimental medicine *208*, 383-394.

Lewis, J.M., Girardi, M., Roberts, S.J., Barbee, S.D., Hayday, A.C., and Tigelaar, R.E. (2006). Selection of the cutaneous intraepithelial gammadelta+ T cell repertoire by a thymic stromal determinant. Nature immunology *7*, 843-850.

Liang, S.C., Latchman, Y.E., Buhlmann, J.E., Tomczak, M.F., Horwitz, B.H., Freeman, G.J., and Sharpe, A.H. (2003). Regulation of PD-1, PD-L1, and PD-L2 expression during normal and autoimmune responses. European journal of immunology *33*, 2706-2716.

Liston, A., Lesage, S., Wilson, J., Peltonen, L., and Goodnow, C.C. (2003). Aire regulates negative selection of organ-specific T cells. Nature immunology *4*, 350-354.

Liu, C., Saito, F., Liu, Z., Lei, Y., Uehara, S., Love, P., Lipp, M., Kondo, S., Manley, N., and Takahama, Y. (2006). Coordination between CCR7- and CCR9-mediated chemokine signals in prevascular fetal thymus colonization. Blood *108*, 2531-2539.

Liu, J., Pan, B., Zeng, L.Y., and Xu, K.L. (2013). [Administration of high dose dexamethasone impairs the function of thymus cells]. Zhongguo shi yan xue ye xue za zhi / Zhongguo bing li sheng li xue hui = Journal of experimental hematology / Chinese Association of Pathophysiology *21*, 1271-1274.

Liu, Z., Yu, S., and Manley, N.R. (2007). Gcm2 is required for the differentiation and survival of parathyroid precursor cells in the parathyroid/thymus primordia. Developmental biology *305*, 333-346.

Livak, F., Tourigny, M., Schatz, D.G., and Petrie, H.T. (1999). Characterization of TCR gene rearrangements during adult murine T cell development. J Immunol *162*, 2575-2580.

Lkhagvasuren, E., Sakata, M., Ohigashi, I., and Takahama, Y. (2013). Lymphotoxin beta receptor regulates the development of CCL21-expressing subset of postnatal medullary thymic epithelial cells. J Immunol *190*, 5110-5117.

Mackall, C.L., Punt, J.A., Morgan, P., Farr, A.G., and Gress, R.E. (1998). Thymic function in young/old chimeras: substantial thymic T cell regenerative capacity despite irreversible age-associated thymic involution. European journal of immunology *28*, 1886-1893.

MacLennan, I.C., Toellner, K.M., Cunningham, A.F., Serre, K., Sze, D.M., Zuniga, E., Cook, M.C., and Vinuesa, C.G. (2003). Extrafollicular antibody responses. Immunological reviews *194*, 8-18.

Macleod, A.S., and Havran, W.L. (2011). Functions of skin-resident gammadelta T cells. Cellular and molecular life sciences : CMLS *68*, 2399-2408.

Maeda, K., Kobayashi, Y., Udagawa, N., Uehara, S., Ishihara, A., Mizoguchi, T., Kikuchi, Y., Takada, I., Kato, S., Kani, S.*, et al.* (2012). Wnt5a-Ror2 signaling between osteoblast-lineage cells and osteoclast precursors enhances osteoclastogenesis. Nature medicine *18*, 405-412.

Manley, N.R. (2000). Thymus organogenesis and molecular mechanisms of thymic epithelial cell differentiation. Seminars in immunology *12*, 421-428.

Markert, M.L., Boeck, A., Hale, L.P., Kloster, A.L., McLaughlin, T.M., Batchvarova, M.N., Douek, D.C., Koup, R.A., Kostyu, D.D., Ward, F.E.*, et al.* (1999). Transplantation of thymus tissue in complete DiGeorge syndrome. The New England journal of medicine *341*, 1180-1189.

Matloubian, M., Lo, C.G., Cinamon, G., Lesneski, M.J., Xu, Y., Brinkmann, V., Allende, M.L., Proia, R.L., and Cyster, J.G. (2004). Lymphocyte egress from thymus and peripheral lymphoid organs is dependent on S1P receptor 1. Nature *427*, 355-360.

Mazzucchelli, R.I., Warming, S., Lawrence, S.M., Ishii, M., Abshari, M., Washington, A.V., Feigenbaum, L., Warner, A.C., Sims, D.J., Li, W.Q.*, et al.* (2009). Visualization and identification of IL-7 producing cells in reporter mice. PloS one *4*, e7637.

McCaughtry, T.M., Wilken, M.S., and Hogquist, K.A. (2007). Thymic emigration revisited. The Journal of experimental medicine *204*, 2513-2520.

McIntyre, B.A., Alev, C., Mechael, R., Salci, K.R., Lee, J.B., Fiebig-Comyn, A., Guezguez, B., Wu, Y., Sheng, G., and Bhatia, M. (2013). Expansive Generation of Functional Airway Epithelium From Human Embryonic Stem Cells. Stem cells translational medicine.

Mebius, R.E., and Kraal, G. (2005). Structure and function of the spleen. Nature reviews. Immunology *5*, 606-616.

Medzhitov, R., and Janeway, C.A., Jr. (1997). Innate immunity: impact on the adaptive immune response. Current opinion in immunology *9*, 4-9.

Metzger, T.C., Khan, I.S., Gardner, J.M., Mouchess, M.L., Johannes, K.P., Krawisz, A.K., Skrzypczynska, K.M., and Anderson, M.S. (2013). Lineage tracing and cell ablation identify a post-aire-expressing thymic epithelial cell population. Cell reports *5*, 166-179.

Min, H., Montecino-Rodriguez, E., and Dorshkind, K. (2004). Reduction in the developmental potential of intrathymic T cell progenitors with age. J Immunol *173*, 245-250.

Min, H., Montecino-Rodriguez, E., and Dorshkind, K. (2006). Reassessing the role of growth hormone and sex steroids in thymic involution. Clin Immunol *118*, 117-123.

Misslitz, A., Pabst, O., Hintzen, G., Ohl, L., Kremmer, E., Petrie, H.T., and Forster, R. (2004). Thymic T cell development and progenitor localization depend on CCR7. The Journal of experimental medicine *200*, 481-491.

Mitchell, J. (1973). Lymphocyte circulation in the spleen. Marginal zone bridging channels and their possible role in cell traffic. Immunology *24*, 93-107.

Mombaerts, P., Iacomini, J., Johnson, R.S., Herrup, K., Tonegawa, S., and Papaioannou, V.E. (1992). RAG-1-deficient mice have no mature B and T lymphocytes. Cell *68*, 869-877.

Mondino, A., Khoruts, A., and Jenkins, M.K. (1996). The anatomy of T-cell activation and tolerance. Proceedings of the National Academy of Sciences of the United States of America *93*, 2245-2252.

Mouri, Y., Yano, M., Shinzawa, M., Shimo, Y., Hirota, F., Nishikawa, Y., Nii, T., Kiyonari, H., Abe, T., Uehara, H.*, et al.* (2011). Lymphotoxin signal promotes thymic organogenesis by eliciting RANK expression in the embryonic thymic stroma. J Immunol *186*, 5047-5057.

Muller, S.M., Terszowski, G., Blum, C., Haller, C., Anquez, V., Kuschert, S., Carmeliet, P., Augustin, H.G., and Rodewald, H.R. (2005). Gene targeting of VEGF-A in thymus epithelium disrupts thymus blood vessel architecture. Proceedings of the National Academy of Sciences of the United States of America *102*, 10587-10592.

Murata, S., Sasaki, K., Kishimoto, T., Niwa, S., Hayashi, H., Takahama, Y., and Tanaka, K. (2007). Regulation of CD8+ T cell development by thymus-specific proteasomes. Science *316*, 1349-1353.

Naito, T., Tanaka, H., Naoe, Y., and Taniuchi, I. (2011). Transcriptional control of T-cell development. International immunology *23*, 661-668.

Nedjic, J., Aichinger, M., Emmerich, J., Mizushima, N., and Klein, L. (2008). Autophagy in thymic epithelium shapes the T-cell repertoire and is essential for tolerance. Nature *455*, 396-400.

Nehls, M., Kyewski, B., Messerle, M., Waldschutz, R., Schuddekopf, K., Smith, A.J., and Boehm, T. (1996). Two genetically separable steps in the differentiation of thymic epithelium. Science *272*, 886-889.

Nehls, M., Pfeifer, D., Schorpp, M., Hedrich, H., and Boehm, T. (1994). New member of the winged-helix protein family disrupted in mouse and rat nude mutations. Nature *372*, 103-107.

Nishikawa, Y., Hirota, F., Yano, M., Kitajima, H., Miyazaki, J., Kawamoto, H., Mouri, Y., and Matsumoto, M. (2010). Biphasic Aire expression in early embryos and in medullary thymic epithelial cells before end-stage terminal differentiation. The Journal of experimental medicine *207*, 963-971.

Nitta, T., Murata, S., Sasaki, K., Fujii, H., Ripen, A.M., Ishimaru, N., Koyasu, S., Tanaka, K., and Takahama, Y. (2010). Thymoproteasome shapes immunocompetent repertoire of CD8+ T cells. Immunity *32*, 29-40.

Nowell, C.S., Bredenkamp, N., Tetelin, S., Jin, X., Tischner, C., Vaidya, H., Sheridan, J.M., Stenhouse, F.H., Heussen, R., Smith, A.J., and Blackburn, C.C. (2011). Foxn1 regulates lineage progression in cortical and medullary thymic epithelial cells but is dispensable for medullary sublineage divergence. PLoS genetics *7*, e1002348.

Ohigashi, I., Zuklys, S., Sakata, M., Mayer, C.E., Zhanybekova, S., Murata, S., Tanaka, K., Hollander, G.A., and Takahama, Y. (2013). Aire-expressing thymic medullary epithelial cells originate from beta5t-expressing progenitor cells. Proceedings of the National Academy of Sciences of the United States of America *110*, 9885-9890.

Olsen, N.J., Olson, G., Viselli, S.M., Gu, X., and Kovacs, W.J. (2001). Androgen receptors in thymic epithelium modulate thymus size and thymocyte development. Endocrinology *142*, 1278-1283.

Paessens, L.C., Singh, S.K., Fernandes, R.J., and van Kooyk, Y. (2008). Vascular cell adhesion molecule-1 (VCAM-1) and intercellular adhesion molecule-1 (ICAM-1) provide co-stimulation in positive selection along with survival of selected thymocytes. Molecular immunology *45*, 42-48.

Palmer, D.B., Viney, J.L., Ritter, M.A., Hayday, A.C., and Owen, M.J. (1993). Expression of the alpha beta T-cell receptor is necessary for the generation of the thymic medulla. Developmental immunology *3*, 175-179.

Parent, A.V., Russ, H.A., Khan, I.S., LaFlam, T.N., Metzger, T.C., Anderson, M.S., and Hebrok, M. (2013). Generation of functional thymic epithelium from human embryonic stem cells that supports host T cell development. Cell stem cell *13*, 219-229.

Parkin, J., and Cohen, B. (2001). An overview of the immune system. Lancet *357*, 1777-1789.

Peters, H., Neubuser, A., Kratochwil, K., and Balling, R. (1998). Pax9-deficient mice lack pharyngeal pouch derivatives and teeth and exhibit craniofacial and limb abnormalities. Genes & development *12*, 2735-2747.

Petrie, H.T. (2003). Cell migration and the control of post-natal T-cell lymphopoiesis in the thymus. Nature reviews. Immunology *3*, 859-866.

Petrie, H.T., and Zuniga-Pflucker, J.C. (2007). Zoned out: functional mapping of stromal signaling microenvironments in the thymus. Annual review of immunology *25*, 649-679.

Pfaffl, M.W. (2001). A new mathematical model for relative quantification in real-time RT-PCR. Nucleic acids research *29*, e45.

Pfister, O., Della Verde, G., Liao, R., and Kuster, G.M. (2013). Regenerative therapy for cardiovascular disease. Translational research : the journal of laboratory and clinical medicine.

Plotkin, J., Prockop, S.E., Lepique, A., and Petrie, H.T. (2003). Critical role for CXCR4 signaling in progenitor localization and T cell differentiation in the postnatal thymus. J Immunol *171*, 4521-4527.

Podack, E.R. (1995). Functional significance of two cytolytic pathways of cytotoxic T lymphocytes. Journal of leukocyte biology *57*, 548-552.

Porritt, H.E., Rumfelt, L.L., Tabrizifard, S., Schmitt, T.M., Zuniga-Pflucker, J.C., and Petrie, H.T. (2004). Heterogeneity among DN1 prothymocytes reveals multiple progenitors with different capacities to generate T cell and non-T cell lineages. Immunity *20*, 735-745.

Prockop, S., and Petrie, H.T. (2000). Cell migration and the anatomic control of thymocyte precursor differentiation. Seminars in immunology *12*, 435-444.

Revest, J.M., Suniara, R.K., Kerr, K., Owen, J.J., and Dickson, C. (2001). Development of the thymus requires signaling through the fibroblast growth factor receptor R2-IIIb. J Immunol *167*, 1954-1961.

Ribeiro, A.R., Rodrigues, P.M., Meireles, C., Di Santo, J.P., and Alves, N.L. (2013). Thymocyte selection regulates the homeostasis of IL-7-expressing thymic cortical epithelial cells in vivo. J Immunol *191*, 1200-1209.

Roberts, N.A., Desanti, G.E., Withers, D.R., Scott, H.R., Jenkinson, W.E., Lane, P.J., Jenkinson, E.J., and Anderson, G. (2009). Absence of thymus crosstalk in the fetus does not preclude hematopoietic induction of a functional thymus in the adult. European journal of immunology *39*, 2395-2402.

Roberts, N.A., White, A.J., Jenkinson, W.E., Turchinovich, G., Nakamura, K., Withers, D.R., McConnell, F.M., Desanti, G.E., Benezech, C., Parnell, S.M.*, et al.* (2012). Rank signaling links the development of invariant gammadelta T cell progenitors and Aire(+) medullary epithelium. Immunity *36*, 427-437.

Rodewald, H.R. (2008). Thymus organogenesis. Annual review of immunology *26*, 355-388.

Rossi, F.M., Corbel, S.Y., Merzaban, J.S., Carlow, D.A., Gossens, K., Duenas, J., So, L., Yi, L., and Ziltener, H.J. (2005). Recruitment of adult thymic progenitors is regulated by P-selectin and its ligand PSGL-1. Nature immunology *6*, 626-634.

Rossi, S.W., Chidgey, A.P., Parnell, S.M., Jenkinson, W.E., Scott, H.S., Boyd, R.L., Jenkinson, E.J., and Anderson, G. (2007a). Redefining epithelial progenitor potential in the developing thymus. European journal of immunology *37*, 2411-2418.

Rossi, S.W., Jenkinson, W.E., Anderson, G., and Jenkinson, E.J. (2006). Clonal analysis reveals a common progenitor for thymic cortical and medullary epithelium. Nature *441*, 988-991.

Rossi, S.W., Kim, M.Y., Leibbrandt, A., Parnell, S.M., Jenkinson, W.E., Glanville, S.H., McConnell, F.M., Scott, H.S., Penninger, J.M., Jenkinson, E.J.*, et al.* (2007b). RANK signals from CD4(+)3(-) inducer cells regulate development of Aire-expressing epithelial cells in the thymic medulla. The Journal of experimental medicine *204*, 1267-1272.

Sambandam, A., Maillard, I., Zediak, V.P., Xu, L., Gerstein, R.M., Aster, J.C., Pear, W.S., and Bhandoola, A. (2005). Notch signaling controls the generation and differentiation of early T lineage progenitors. Nature immunology *6*, 663-670.

Samelson, L.E. (2002). Signal transduction mediated by the T cell antigen receptor: the role of adapter proteins. Annual review of immunology *20*, 371-394.

Schlenner, S.M., Madan, V., Busch, K., Tietz, A., Laufle, C., Costa, C., Blum, C., Fehling, H.J., and Rodewald, H.R. (2010). Fate mapping reveals separate origins of T cells and myeloid lineages in the thymus. Immunity *32*, 426-436.

Schlenner, S.M., and Rodewald, H.R. (2010). Early T cell development and the pitfalls of potential. Trends in immunology *31*, 303-310.

Shakib, S., Desanti, G.E., Jenkinson, W.E., Parnell, S.M., Jenkinson, E.J., and Anderson, G. (2009). Checkpoints in the development of thymic cortical epithelial cells. J Immunol *182*, 130-137.

Shinkai, Y., Rathbun, G., Lam, K.P., Oltz, E.M., Stewart, V., Mendelsohn, M., Charron, J., Datta, M., Young, F., Stall, A.M., and et al. (1992). RAG-2-deficient mice lack mature lymphocytes owing to inability to initiate V(D)J rearrangement. Cell *68*, 855-867.

Shores, E.W., Van Ewijk, W., and Singer, A. (1994). Maturation of medullary thymic epithelium requires thymocytes expressing fully assembled CD3-TCR complexes. International immunology *6*, 1393-1402.

Simonet, W.S., Lacey, D.L., Dunstan, C.R., Kelley, M., Chang, M.S., Luthy, R., Nguyen, H.Q., Wooden, S., Bennett, L., Boone, T.*, et al.* (1997). Osteoprotegerin: a novel secreted protein involved in the regulation of bone density. Cell *89*, 309-319.

Smith-Garvin, J.E., Koretzky, G.A., and Jordan, M.S. (2009). T cell activation. Annual review of immunology *27*, 591-619.

Sommer, C.A., Stadtfeld, M., Murphy, G.J., Hochedlinger, K., Kotton, D.N., and Mostoslavsky, G. (2009). Induced pluripotent stem cell generation using a single lentiviral stem cell cassette. Stem Cells *27*, 543-549.

Spence, P.J., and Green, E.A. (2008). Foxp3+ regulatory T cells promiscuously accept thymic signals critical for their development. Proceedings of the National Academy of Sciences of the United States of America *105*, 973-978.

Starr, T.K., Jameson, S.C., and Hogquist, K.A. (2003). Positive and negative selection of T cells. Annual review of immunology *21*, 139-176.

Streckfuss-Bomeke, K., Jende, J., Cheng, I.F., Hasenfuss, G., and Guan, K. (2013). Efficient Generation of Hepatic Cells from Multipotent Adult Mouse Germ-Line Stem Cells Using an OP9 Co-Culture System. Cellular reprogramming.

Su, D., Ellis, S., Napier, A., Lee, K., and Manley, N.R. (2001). Hoxa3 and pax1 regulate epithelial cell death and proliferation during thymus and parathyroid organogenesis. Developmental biology *236*, 316-329.

Sun, X., Xu, J., Lu, H., Liu, W., Miao, Z., Sui, X., Liu, H., Su, L., Du, W., He, Q.*, et al.* (2013). Directed differentiation of human embryonic stem cells into thymic epithelial progenitor-like cells reconstitutes the thymic microenvironment in vivo. Cell stem cell *13*, 230-236.

Taub, D.D., and Longo, D.L. (2005). Insights into thymic aging and regeneration. Immunological reviews *205*, 72-93.

Terszowski, G., Muller, S.M., Bleul, C.C., Blum, C., Schirmbeck, R., Reimann, J., Pasquier, L.D., Amagai, T., Boehm, T., and Rodewald, H.R. (2006). Evidence for a functional second thymus in mice. Science *312*, 284-287.

Tsai, P.T., Lee, R.A., and Wu, H. (2003). BMP4 acts upstream of FGF in modulating thymic stroma and regulating thymopoiesis. Blood *102*, 3947-3953.

Turvey, S.E., and Broide, D.H. (2010). Innate immunity. The Journal of allergy and clinical immunology *125*, S24-32.

Uehara, S., Hayes, S.M., Li, L., El-Khoury, D., Canelles, M., Fowlkes, B.J., and Love, P.E. (2006). Premature expression of chemokine receptor CCR9 impairs T cell development. J Immunol *176*, 75-84.

Ueno, T., Saito, F., Gray, D.H., Kuse, S., Hieshima, K., Nakano, H., Kakiuchi, T., Lipp, M., Boyd, R.L., and Takahama, Y. (2004). CCR7 signals are essential for cortex-medulla migration of developing thymocytes. The Journal of experimental medicine *200*, 493-505.

van den Brink, M.R., Alpdogan, O., and Boyd, R.L. (2004). Strategies to enhance T-cell reconstitution in immunocompromised patients. Nature reviews. Immunology *4*, 856-867.

Van Vliet, E., Melis, M., Foidart, J.M., and Van Ewijk, W. (1986). Reticular fibroblasts in peripheral lymphoid organs identified by a monoclonal antibody. The journal of histochemistry and cytochemistry : official journal of the Histochemistry Society *34*, 883-890.

Van Vliet, E., Melis, M., and Van Ewijk, W. (1984). Monoclonal antibodies to stromal cell types of the mouse thymus. European journal of immunology *14*, 524-529.

Vicari, A.P., Figueroa, D.J., Hedrick, J.A., Foster, J.S., Singh, K.P., Menon, S., Copeland, N.G., Gilbert, D.J., Jenkins, N.A., Bacon, K.B., and Zlotnik, A. (1997). TECK: a novel CC chemokine specifically expressed by thymic dendritic cells and potentially involved in T cell development. Immunity *7*, 291-301.

von Andrian, U.H., and Mempel, T.R. (2003). Homing and cellular traffic in lymph nodes. Nature reviews. Immunology *3*, 867-878.

von Boehmer, H., and Fehling, H.J. (1997). Structure and function of the pre-T cell receptor. Annual review of immunology *15*, 433-452.

Wang, C.R., Hashimoto, K., Kubo, S., Yokochi, T., Kubo, M., Suzuki, M., Suzuki, K., Tada, T., and Nakayama, T. (1995). T cell receptor-mediated signaling events in CD4+CD8+ thymocytes undergoing thymic selection: requirement of calcineurin activation for thymic positive selection but not negative selection. The Journal of experimental medicine *181*, 927-941.

Wang, J.H., and Reinherz, E.L. (2012). The structural basis of alphabeta T-lineage immune recognition: TCR docking topologies, mechanotransduction, and co-receptor function. Immunological reviews *250*, 102-119.

Wei, Q., and Condie, B.G. (2011). A focused in situ hybridization screen identifies candidate transcriptional regulators of thymic epithelial cell development and function. PloS one *6*, e26795.

Weih, F., Carrasco, D., Durham, S.K., Barton, D.S., Rizzo, C.A., Ryseck, R.P., Lira, S.A., and Bravo, R. (1995). Multiorgan inflammation and hematopoietic abnormalities in mice with a targeted disruption of RelB, a member of the NF-kappa B/Rel family. Cell *80*, 331-340.

Weitzmann, M.N. (2013). The Role of Inflammatory Cytokines, the RANKL/OPG Axis, and the Immunoskeletal Interface in Physiological Bone Turnover and Osteoporosis. Scientifica *2013*, 125705.

White, A.J., Nakamura, K., Jenkinson, W.E., Saini, M., Sinclair, C., Seddon, B., Narendran, P., Pfeffer, K., Nitta, T., Takahama, Y.*, et al.* (2010). Lymphotoxin signals from positively selected thymocytes regulate the terminal differentiation of medullary thymic epithelial cells. J Immunol *185*, 4769-4776.

White, A.J., Withers, D.R., Parnell, S.M., Scott, H.S., Finke, D., Lane, P.J., Jenkinson, E.J., and Anderson, G. (2008). Sequential phases in the development of Aire-expressing medullary thymic epithelial cells involve distinct cellular input. European journal of immunology *38*, 942-947.

Wu, L., Gabriel, C.L., Parekh, V.V., and Van Kaer, L. (2009). Invariant natural killer T cells: innate-like T cells with potent immunomodulatory activities. Tissue antigens *73*, 535-545.

Wucherpfennig, K.W., Gagnon, E., Call, M.J., Huseby, E.S., and Call, M.E. (2010). Structural biology of the T-cell receptor: insights into receptor assembly, ligand recognition, and initiation of signaling. Cold Spring Harbor perspectives in biology *2*, a005140.

Xing, Y., and Hogquist, K.A. (2012). T-cell tolerance: central and peripheral. Cold Spring Harbor perspectives in biology *4*.

Yamaguchi, T.P., Bradley, A., McMahon, A.P., and Jones, S. (1999). A Wnt5a pathway underlies outgrowth of multiple structures in the vertebrate embryo. Development *126*, 1211-1223.

Yamanaka, S., and Takahashi, K. (2006). [Induction of pluripotent stem cells from mouse fibroblast cultures]. Tanpakushitsu kakusan koso. Protein, nucleic acid, enzyme *51*, 2346-2351.

Yamashita, I., Nagata, T., Tada, T., and Nakayama, T. (1993). Cd69 Cell-Surface Expression Identifies Developing Thymocytes Which Audition for T-Cell Antigen Receptor-Mediated Positive Selection. International immunology *5*, 1139-1150.

Yano, M., Kuroda, N., Han, H., Meguro-Horike, M., Nishikawa, Y., Kiyonari, H., Maemura, K., Yanagawa, Y., Obata, K., Takahashi, S.*, et al.* (2008). Aire controls the differentiation program of thymic epithelial cells in the medulla for the establishment of self-tolerance. The Journal of experimental medicine *205*, 2827-2838.

Yokosuka, T., and Saito, T. (2009). Dynamic regulation of T-cell costimulation through TCR-CD28 microclusters. Immunological reviews *229*, 27-40.

Zamisch, M., Moore-Scott, B., Su, D.M., Lucas, P.J., Manley, N., and Richie, E.R. (2005). Ontogeny and regulation of IL-7-expressing thymic epithelial cells. J Immunol *174*, 60-67.

Zhu, J., and Paul, W.E. (2008). CD4 T cells: fates, functions, and faults. Blood *112*, 1557-1569.

Zhu, X., Gui, J., Dohkan, J., Cheng, L., Barnes, P.F., and Su, D.M. (2007). Lymphohematopoietic progenitors do not have a synchronized defect with age-related thymic involution. Aging cell *6*, 663-672.

Zook, E.C., Zhang, S., Gerstein, R.M., Witte, P.L., and Le, P.T. (2013). Enhancing T lineage production in aged mice: a novel function of foxn1 in the bone marrow niche. J Immunol *191*, 5583-5593.

Zuniga-Pflucker, J.C., and Lenardo, M.J. (1996). Regulation of thymocyte development from immature progenitors. Current opinion in immunology *8*, 215-224.